Charles University

Faculty of Science

Institute of Geology and Paleontology

Study program Geology

Doctoral thesis

Roland Nádaskay

Analysis of depositional controls and provenance of the Upper Paleozoic and Mesozoic deposits and its implication for tectonosedimentary evolution of the northern Bohemian Massif

Analýza provenience a faktorů řídících ukládání svrchního paleozoika a mezozoika a její využití při interpretaci tektonosedimentárního vývoje severní části Českého masivu

Supervisor:

Mgr. Karel Martínek, Ph.D.

Advisors:

Prof. RNDr. Stanislav Opluštil, Ph.D.

Mgr. Kateřina Schöpfer, Ph.D.

Praha, 2021

Prohlášení

Prohlašuji, že jsem předkládanou disertační práci zpracoval samostatně a že jsem uvedl všechny použité informační zdroje a literaturu. Tato práce ani její podstatná část nebyla předložena k získání jiného nebo stejného akademického titulu.

V Praze, 4. března 2021

Podpis

Prohlášení školitele o podílu studenta na publikacích, které jsou součástí doktorské práce

Z pozice školitele studenta Mgr. Rolanda Nádaskayho prohlašuji, že student se podílel na pracích, které předložil jako součást jeho disertační práce, následujícím podílem:

Appendix 1*:* Schöpfer, K., **Nádaskay**, **R.**, Martínek, K. (submitted): Evaluation of climatic and tectonic imprints in fluvial successions of an early Permian depositional system (Asselian Vrchlabí Fm., Krkonoše Piedmont Basin, Czech Republic). Journal of Sedimentary Research.

Celkový podíl **45 %** – účast na definování tématu, získání ½ terénních sedimentologických dat a úcast na jejich popisu a interpretaci, pořízení gamaspektrometrických profilů, korelace vrtných a gamaspektrometrických křivek (konstrukce korelačních panelů), účast na interpretaci a závěrech

Appendix 2*:* **Nádaskay**, **R.**, Kochergina, Y.V., Čech, S., Švábenická, L., Valečka, J., Erban, V., Halodová, P., Čejková, B. (2019): Integrated stratigraphy of an offshore succession influenced by intense siliciclastic supply: Implications for Coniacian tectonosedimentary evolution of the West Sudetic area (NW Bohemian Cretaceous Basin, Czech Republic). Cretaceous Research, 102, 127–159.

Celkový podíl **60 %** – definování tématu, terénní práce (revize profilů z dipl. práce), účast na odběru vzorků na chemické analýzy, práce na vrtném profilu (podrobný sedimentologický popis, měření RFA/XRF), popis a interpretace naměřených dat (sedimentologie, prvková geochemie, stabilní izotopy, karotážní křivky), integrace a interpretace dat, závěry

Appendix 3*:* **Nádaskay**, **R.**, Žák, J., Sláma, J., Sidorinová, T., Valečka, J. (2019): Deciphering the Late Paleozoic to Mesozoic tectonosedimentary evolution of the northern Bohemian Massif from detrital zircon geochronology and heavy mineral provenance. International Journal of Earth Sciences, 108, 2653–2681.

Celkový podíl **60 %** – definování tématu, odběr vzorků v terénu, integrace dat a účast na jejich interpretaci, příprava diskusní části a závěrů

Mgr. Karel Martínek, Ph.D.

školitel

Abstract

Lifespan of sedimentary basins may be terminated by processes leading to 'contingent fate', independent from the basin type. It is typically represented by basin inversion which is a process when a formerly extensional basin undergoes shortening accommodated by fault reactivation in typically compressional regime. Compressive forces transmitted from the orogenic front towards distant foreland regions are capable of reactivating basement faults and controlling basin development. This mechanism for basin inversion has been widely discussed for the foreland area of Alpine Orogen in Europe, with the Elbe and Tornquist zones given as typical examples of repeatedly (from Late Paleozoic onwards) reactivated crustal-scale faults. The Bohemian Massif forms an extensive, proximal part of the Alpine foreland. It is a widely regarded notion that it experienced complex intra-plate tectonosedimentary evolution since until the termination of Variscan Orogeny practically until the present-day. This thesis examines the post-Variscan, Late Paleozoic to Late Cretaceous tectonosedimentary evolution of the northern Bohemian Massif as a case example of complex intra-plate movements in the Alpine foreland of central Europe. Sedimentological, stratigraphic and provenance data from the Permian, Jurassic and Upper Cretaceous sedimentary successions are integrated to interpret controls on deposition of stratigraphic successions (by analysis of accommodation/supply ratio, transgressive–regressive cycles, etc.), direction of sediment dispersal and source areas and to provide time constraints on their possible shifts. The main issue this thesis addresses is whether the basins formed diachronously in the northern Bohemian Massif between the Permian and the Late Cretaceous, but were later completely destructed by subsequent tectonic processes, their fill recycled into younger basins. This could have happened over a relatively short time span – as in the case of basin formation and deformation resulting from multiple reactivations of NW–SE faults (e.g., Lusatian Fault, Elbe Zone) during the Late Paleozoic. The evolution of fluvio-lacustrine system of Vrchlabí Fm. of the Krkonoše Piedmont Basin records extensional phase of an extensive basin complex, succeeded by formation of transtensional basins tectonically discordant to the previous generation. Alternativelly, inversion processes are exemplified by mid-Cretaceous inversion of the hypothetic Lusatian Basin and redeposition of its fill into the successor Bohemian Cretaceous Basin. The latter contains large amount of Paleo-/Mesoprozerozoic, Baltica-derived zircons that ended up on the Bohemain Massif presumably after multi-phase recycling of deposits extending between Scandinavian and N Bohemia. At last, they were recycled from sedimentary cover of unroofing Lusatian Block, particulary during late Turonian–Coniacian period of tectonic acceleration. As a result, a time-slice reconstruction of paleogeographic and tectonosedimentary evolution of the northern Bohemian Massif is used to demonstrate that periods of basin development and deposition (early Permian, late early Permian to Early Triassic, Middle Jurassic–Early Cretaceous, Late Cretaceous) were interrupted by major depositional gaps (Middle Triassic–Early Jurassic, mid-Cretaceous). The Mesozoic depositional episodes occured when major NW–SE fault zones were reactivated due to stress transfer from the North Atlantic Rift during Jurassic to Early Cretaceous, overridden by the far-field effect of convergence of Iberia, Africa, and Europe during Late Cretaceous. This phenomenon is well-known from a number of basins ('marginal troughs') of central Europe, recently interpreted as 'intraplate foreland basins'.

Preface

My postgraduate tenure at the Institute of Geology and Paleontology (IGP), Charles University, Prague, started in October 2013. In its initial phase, my doctoral thesis was focused primarily on interpreting climate vs. tectonic impact on non-marine depositional systems by integrating sedimentological analysis and sequence stratigraphy in fluvio-lacustrine setting. The early Permian succession of the Vrchlabí Formation of the Krkonoše Piedmont Basin was selected by my supervisor, Dr. Karel Martínek, as a pilot case study. After joining the Czech Geological Survey in June 2014 (full-time since Oct. 2015), the focus of my Ph.D. thesis was expanded, with IGP's consent, to incorporate certain aspects of the Bohemian Cretaceous Basin in order to comply with my department's Mesozoic-oriented agenda. As a result, this thesis, submitted in partial fulfilment of Charles University's requirements for the Ph.D. degree, presents a synthesis of tectonosedimentary development of the West Sudetic area (northeastern Bohemian Massif, Czechia) between the Late Paleozoic and Mesozoic (Pennsylvanian–Late Cretaceous). Individual chapters represent three mandatory papers – two of them published in journals with IF (Cretaceous Research, International Journal of Earth Sciences) by autumn 2019, third as a manuscript submitted to the Journal of Sedimentary Research. The manuscript was reviewed by the end of 2020; major revisions were recommended by the journal's editor to be done by the half of March 2021.

Preliminary and partial results were presented on a number of conferences, seminars and workshops:

2014   Central European Meeting of Sedimentary Geology, Olomouc, Czechia

   5th IAS International Summer School of Sedimentology 2014, Beijing and Luanping, China

2015   31st IAS Meeting of Sedimentology, Kraków, Poland

   Open congress of Czech and Slovak geological societies, Mikulov, Czechia

   Sediment provenance analysis short course, Göttingen, Germany

2016   8th International Siberian Early Career GeoScientists Conference, Novosibirsk, Russia

2017   10th International Symposium on the Cretaceous, Vienna, Austria

   GeoBremen 2017, Bremen, Germany

2018   GeoBonn 2018, Bonn, Germany

2019   UNCE PhD Student Conference 2019, Charles University, Prague, Czechia

   17th Meeting of the Central European Tectonic Groups, Rozdrojovice, Czechia

2020   Conference "Paleozoikum 2020", Brno, Czechia

Acknowledgements

Table of contents

Introduction

Lifespan of sedimentary basins is estimated to vary from <1 m.y. for trench basins to >100 m.y. for passive-margin and intracratonic basins (Woodcock 2004; Allen et al. 2015). Life cycle of sedimentary basin may be terminated by processes leading to, on one hand, a 'consequent fate', i.e., predetermined by the tectonic setting of the particular basin class, or, on the other hand, a 'contingent fate'. The latter is independent from the basin type and is typically represented by basin inversion, i.e., far-field shortening of extensional basins. This contrasts with consequent fate, represented for instance by accretion of trench-basin fill (Woodcock 2004) or orogenic deformation of orogen-related basins.

The basin inversion is defined as a process when a basin, formerly established by extension of continental crust, undergo shortening that is accommodated by reactivation of extant faults and fractures across a wide range of scales (Turner and Williams 2004). The shortening is mainly accommodated by compression, but transpression and strike-slip deformation may also generate subsiding areas and uplifts within a basin (Allen and Allen 2005; Kley et al. 2008). In this process, external horizontal rather than isostatic vertical forces are required for inversion (Lowell 1995). The inversion is dependent on pre-existing basin configuration in the initial subsidence (usually during extensional phase) and the resolution of compressional forces in the later shortening phase. The inversion manifests itself as reactivation of faults in a reverse sense, i.e., turning of normal faults to thrusts, and the uplift of formerly subsiding areas and vice versa subsidence of former highs (Voigt et al. 2009). The basin inversion generates distinctive deformational architecture, and it is implicated strongly in sedimentary basin exhumation (Turner and Williams 2004). It means that basin compartments, depocenters/sub-basins and intrabasinal highs, whose formation reflects fragmentation of a basin as a result of inversion, may be uplifted and eroded, the eroded sediments being redeposited in adjoining depocentres (Voigt et al. 2009).

Compressive forces appear to be transmitted backward from the lead edge of an underthrusted foreland plate to invert rather remote regions and basins that are carried on that plate (Lowell 1995). Generally, such forces are sufficient to reactivate inherited basement faults, to generate intraplate compressional structures, and to exert control over basin development even in relatively distant foreland of active orogens (e.g., Hayward and Graham 1989; Ziegler 1990a; Ziegler et al. 1995, 1998; Marshak and Paulsen 1996; van der Pluijm et al. 1997; Cloetingh et al. 2007). Thus, they may represent a significant part of the mechanism for basin inversion of foreland area underthrusted along the Alpine system in Europe (Lowell 1995). The evolution of

inverted basins, which are now recognized as representing compressionally/transpressionally deformed extensional and/or transtensional hanging-wall basins, has been the subject of debate for substantial part of the 20th century until present. Particular question is the origin of stresses which controlled their post-rift deformation (Ziegler et al. 1995). Reactivation of basement faults, basin formation and inversion has been discussed in context of the Alpine Orogen and its foreland area in northwestern, western and parts of the eastern Europe (north of the Alpine-Carpathian Belt) and the southern North Sea (an area further referred to as 'central Europe' for short; e.g., Ilies 1974, 1975; Ziegler 1975, 1983; Sengör 1976; Ziegler et al. 1995).

The intra-plate compressional structures have played an important role in the tectonic framework of central Europe not only in context of the Alpine orogenic cycle, but practically since the termination of the Variscan Orogeny. The most obvious examples of the crustal-scale faults within the central Europe that are interpreted to be repeatedly reactivated during the Late Paleozoic, Mezosoic and Cenozoic are the Elbe Zone (sensu Scheck et al. 2002; e.g., Scheck and Bayer 1999; Kossow and Krawczyk 2002; Mazur and Scheck-Wenderoth 2005; Scheck-Wenderoth and Lamarche 2005) and the Torquist Zone, or the Trans-European Suture Zone in a broader sense (e.g., Pożaryski and Brochwicz-Lewinski 1978; Pegrum 1984; Erlström et al. 1997; Hakenberg and Świdrowska 2001; Mogensen 1995; Mogensen and Korstgård 2003). A number of tectonic zones of rather local significance, some of them parallel to the Elbe Zone, are accessible to surface geological analyses within well-exposed basement regions such as Osning Zone, Harz Mts., Pays-de-Bray Anticline, Scania as well as the Bohemian Massif. Others are concealed beneath the thick Cenozoic deposits of the North Sea Basin, the Alpine-Carpathian Foredeep, or overprinted by elements of the European Cenozoic Rift System (ECRIS; Ziegler 1994).

The Bohemian Massif in the central Europe, where the study area of this thesis is located, forms a significant part of the northern foreland of Alpine orogenic belt. The Variscan basement north of the Alps recorded several phases of intraplate tectonic deformation from the late Carboniferous onwards that resulted from diverse geodynamic processes and related far-field plate-boundary forces (e.g., Ziegler 1990a; Brink et al. 1992; Mattern 2001; Ventura and Lisker 2003; Nielsen et al. 2005, 2007; Kley and Voigt 2008; Reicherter et al. 2008; Coubal et al. 2015; Meier et al. 2016).

The intraplate deformation was preceded by a continuum of late orogenic to early post-orogenic processes – from late-orogenic extension and destruction of the Variscan orogenic plateau, cessation of the marine foreland basin (Late Devonian to early Carboniferous in age) and the development of extensional ('intermontane') continental basins within the eroded orogen's interior accompanied by paleorelief inversion during the early Pennsylvanian (e.g., Dewey and Burke 1973; Lorenz and Nicholls 1976, 1984; Dewey 1988; Ménard and Molnar 1988; Burg et al.

1994; Henk 1997; Dörr and Zulauf 2010; Žák et al. 2018; Vacek and Žák 2019). Therefore, subsequent tectonic processes took place after the main, Mississippian–early Pennsylvanian phase ('Sudetic' phase sensu Stille 1924) of the Variscan Orogeny in Europe. The Pennsylvanian–Permian extensional basin system that formed within the Bohemian Massif ('Pilsen–Trutnov Basin Complex' sensu Cháb et al. 2008) records its late orogenic to early post-orogenic tectonosedimentary history. Several unconformities within the sedimentary record of the Pilsen–Trutnov Basin Complex (e.g., Opluštil et al. 2016) indicate several periods of non-deposition or erosion as a result of tectonic reactivation of basement faults governed by late orogenic and later intraplate compressive forces. The latter, as supported by several lines of evidence (e.g., Arthaud and Matte 1977; Mattern 1995a, 2001; Uličný et al. 2002), resulted in formation of basin structures discordant to older ones that were partly or completely inverted.

Despite the Mesozoic, particularly the period between the Triassic and the Early Cretaceous, having been traditionally viewed as 'period of quiescence' in the geological history of Bohemian Massif, a number of papers pointed out that basement faults of the Bohemian Massif may have been reactivated during this time (Jindrich 1971; Malkovský 1976, 1980, 1987; Schröder 1987; Nachtmann and Wagner 1987; Martínek et al. 2008). As already mentioned, the intra-plate deformation of the Bohemian Massif was driven by vertical crustal motions in the Alpine foreland. These motions involved exhumation and surface uplift generated by compression as well as subsidence and basin development, the latter represented by formation of extensional grabens or transtensional to pull-apart basins along strike-slip faults (e.g., Betz et al. 1987; Lake and Karner 1987; Liboriussen et al. 1987; Norling and Bergström 1987; Tucker and Arter 1987; van Wijhe 1987; Guillocheau et al. 2000; Voigt et al. 2006; Uličný et al. 2009a,b). These basins are interpreted to form in coincidence with global sea-level changes and marine transgressive–regressive cycles at different scales (e.g., Pieńkowski et al. 2008; Voigt et al. 2008, and references therein), but the intraplate stress fields themselves are able to cause short-term, relative sea-level variations (e.g., Cloethingh et al. 1985; Cloethingh 1986). In this regard, a number of studies pointed to a rather complex picture of interaction between the eustatic sea-level changes and intra-plate crustal deformations during the Mesozoic, particularly the Jurassic (e.g., Hallam 2001; Nielsen 2003; Zimmermann et al. 2015; Krajewski et al. 2016) and the mid-/Late Cretaceous (Laurin and Uličný 2004; Voigt et al. 2006; Uličný et al. 2009b, 2014; Wilmsen et al. 2010; Janetschke and Wilmsen 2015; Dölling et al. 2018). Although the post-Variscan intra-plate deformation is generally well-known from the Mesozoic basins of the central Europe (e.g., Kockel 1986, 2003; Mortimore 1986, 2018; Mortimore and Pomerol 1997; Mortimore et al. 1998; von Eynatten et al. 2008; Krzywiec and Stachowska 2016; Krzywiec et al. 2018; Voigt et al. 2021), its sedimentary response in basins of the Bohemian Massif remains relatively underexplored –

though, in recent years, several papers touched on the issue (e.g., Uličný et al. 2009b; Nádaskay and Uličný 2014; Niebuhr 2018; Niebuhr et al. 2020). For instance, Hofmann et al. (2018), based on earlier assumption of Voigt (1994, 2009), suggested that formation of the Late Jurassic to Early Cretaceous basin in the northern Bohemian Massif may have preceded the Bohemian Cretaceous Basin, as inferred from presumed recycling of the Middle Jurassic sandstones.

Aims and goals of the thesis

In this thesis, I focus on examining the post-Variscan, Late Paleozoic to Late Cretaceous tectonosedimentary evolution of the northern Bohemian Massif as a case example of complex intraplate movements in the Alpine foreland of central Europe. Sedimentological, stratigraphic and provenance data from the Upper Cretaceous as well as from the underlying Jurassic and Permian successions are integrated to interpret the controls on deposition of stratigraphic sequences, direction of sediment dispersal and source areas and to provide time constraints on their possible shifts. Individual chapters expand on previous studies focused primarily on the Permian (**Chapter 1**; Uličný et al. 2002; Martínek et al. 2006) and the Late Cretaceous (**Chapter 2**, Voigt 1994, 2009; Hofmann et al. 2013, 2018). Resulting interpretations are placed into a broader context of intra-plate tectonic movements in the basin development, inversion, and rapid recycling during the Late Paleozoic–Mesozoic (**Chapter 3**). The main questions to be answered are as follows:

(1) Does fluvio-lacustrine fill of the Vrchlabí Fm. (Krkonoše Piedmont Basin) record a marked tectonic process? Is it possible to distinguish climatic and tectonic control on deposition of the formation through correlation of individual contrasting parts of its depositional system?

(2) What happened in the northern Bohemian Massif between the inversion of the W–E/oriented complex of the Pennsylvanian–Permian basins in western/central Bohemia and Sudetes, and the mid-Cretaceous onset of deposition in the Bohemian Cretaceous Basin? Was pre-Cretaceous deposits, for instance Jurassic, originally deposited over subtle portions of the West Sudetes, where their present-day erosion remnants are found, or did they actually cover a substantial part of the northern Bohemian Massif?

(3) Is it possible that basins formed diachronously in the northern Bohemian Massif during the Late Jurassic to Early Cretaceous and the Late Cretaceous? Is it possible that the earlier generation of basins was destructed by subsequent tectonic processes and their fill recycled into younger basins over a relatively short time span?

(4) Does depositional record of the NW Bohemian Cretaceous Basin, particularly the critical interval of late Turonian–Coniacian, provide clues to decipher sequence of precursor events of the basin inversion? Does tectonic acceleration during this time interval and subsequent inversion of the Bohemian Cretaceous Basin correlate with other basins of central Europe?

Table 1. Schematic summary of partial issues resolved by this thesis, in a stratigraphic order from oldest to youngest. Presumed major controls on deposition as well as geotectonic context is listed.

Where? Field area	When? Age	Presumed major controls on deposition	Wider geotectonic context
Chapter 1: Deposition of the Vrchlabí Fm., Krkonoše Piedmont Basin (E Bohemia)	early Permian, Asselian, ca. 298.9–297.5 Ma	tectonic subsidence, climate forcing (transition from humid to arid climate)	Collapse of the Variscan Orogen, crustal extension, formation of extensive 'intermontane' graben system
Introductory discussion and Chapter 3 (marginally) Outliers of Permian deposits along the Lusatian Fault (N Bohemia)	early Permian, Sakmarian–Artinskian, ca. 293.5–286 Ma	tectonic subsidence	Strike-slip reactivation of the NW–SE oriented ('Sudetic') Variscan Faults in the Bohemian Massif, formation of transtensional basins
Chapter 3: Remnants of Jurassic deposits along the Lusatian Fault (N Bohemia)	late Middle to Late Jurassic, Callovian–Tithonian, ca. 165–152 Ma	tectonic subsidence, eustatic sea-level changes	Doming and later extension (rifting) in the North Sea area; Flooding of the Variscan Europe (Callovian transgression), N/NE Bohemian Massif transgressed as late as of Oxfordian Reactivation of the NW–SE faults in the N/NE Bohemian Massif
Chapter 2: Upper Turonian to Coniacian deposits of the Lužice–Jizera sub-basin, Bohemian Cretaceous Basin (Lusatian Mts., N Bohemia)	late Turonian–Coniacian, ca. 91–86.3 Ma	tectonic subsidence, elevated siliciclastic supply, eustatic sea-level changes	Thrusting in the nascent Alpine-Carpathian Belt (Eoalpine Orogeny), preceding the 'Laramide' phase (Campanian–Maastrichtian) Incipient inversion of the BCB (terminated by Campanian) overlapping with inversion of basins north of the Bohemian Massif ('Subhercynian' phase of Alpine foreland deformation
Chapter 3: Permian, Jurassic and Upper Cretaceous along the Lusatian Fault (N Bohemia)	early Permian to Late Cretaceous (Santonian), ca. 293.5–83.6 Ma	listed above	Multiple events of tectonic reactivation of basement faults as a result of diverse geodynamic processes Several phases of basin formation and subsequent deformation

Geology of the northern Bohemian Massif with emphasis on the Late Paleozoic–Mesozoic sedimentary basins

The northern Bohemian Massif, an area approximately between Meißen (Germany), Liberec (Czechia) and Kłodzko (Poland) as defined in this thesis (Fig. 1a), represents geologically intricate territory at the junction of several principal basement units – Saxothuringian, Lugian and Teplá–Barrandian. These are formed by Variscan lithosphere with extensively reworked crustal components of Neoproterozoic (Cadomian) and Early Paleozoic age (e.g., Edel and Weber 1995; Franke 2000, 2006; Winchester et al. 2006; Schulmann et al. 2009; Nance et al. 2010; Kroner and Romer 2013). As evident from any small-scale geological map of the area (e.g., Kozdrój et al. 2001; Asch 2005; Cháb et al. 2007; Fig. 1), these units form a complex mosaic of uplifted basement rocks whose age spans from Late Proterozoic to Mississippian, intruded by igneous rocks of Late Proterozoic–early Cambrian, Cambrian–Ordovician and Mississppian in age. More detailed description and discussion of the basement areas is provided by **Chapter 3** of this thesis.

The basement units are overlain by sedimentary successions, Late Paleozoic to Cenozoic in age (Fig. 2). In this thesis, Pennsylvanian–Permian, Jurassic and, in particular, Late Cretaceous sedimentary successions are examined.
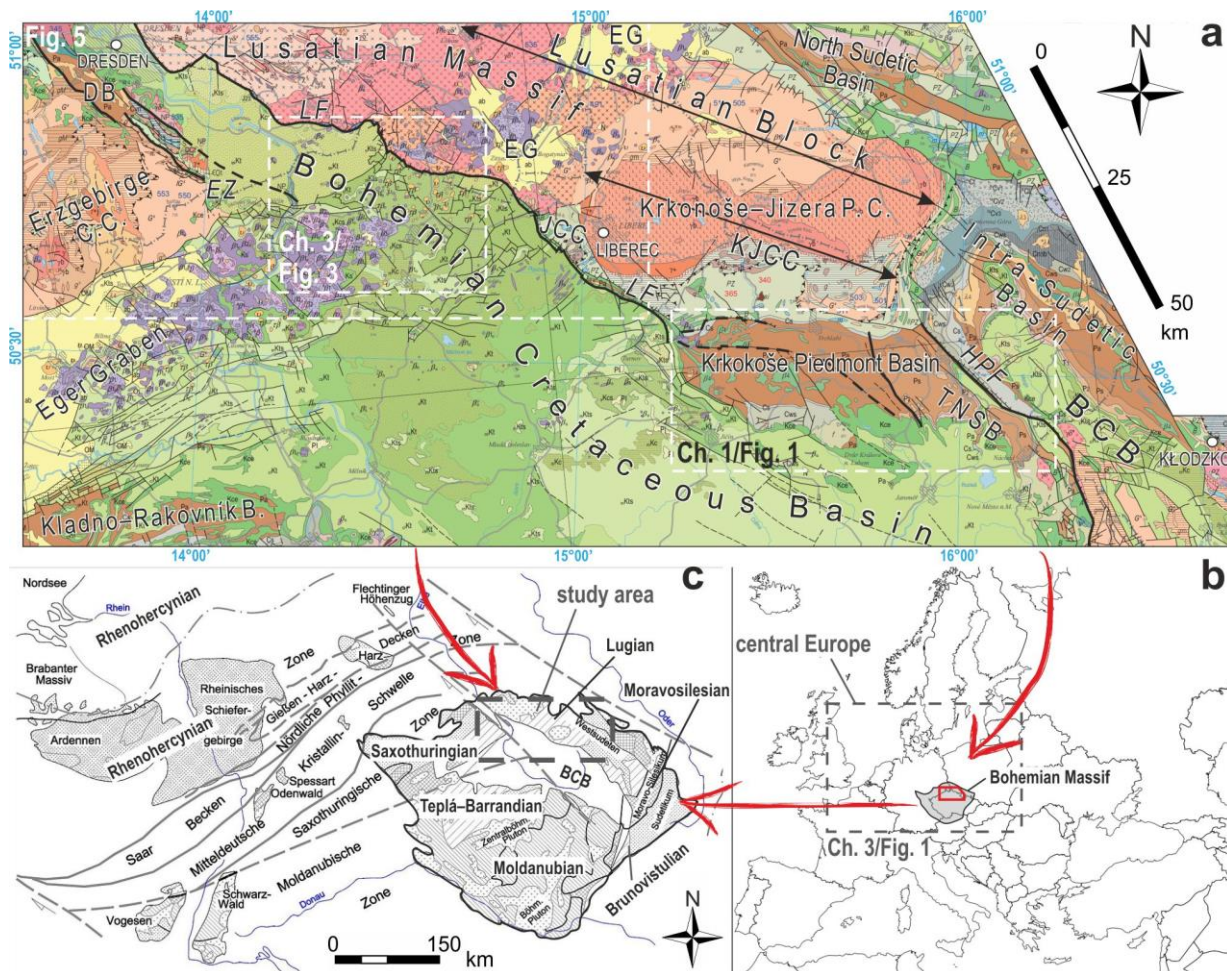
Figure 1. (a) Overview geological map of the study area located in the northern Bohemian Massif between Meißen/Dresden (Saxony, Germany), Liberec (Czechia) and Kłodzko (Poland), with extent of the resolved regions indicated. Based on the Geological map of the Czech Republic 1:500 000 (Cháb et al. 2007; detailed explanations therein). Relevant geological units discussed further in the text are labelled. Thick lines mark major relevant faults. Abbreviations: BCB – Bohemian Cretaceous Basin; DB – Döhlen Basin; EZ – Elbe Zone; HPF – Hronov–Poříčí Fault; JCC – Ještěd Crystalline Complex; KJCC – Krkonoše–Jizera Crystalline Complex; LF – Lusatian Fault; TNSB – Trutnov–Náchod sub-basin. The volcano-sedimentary complexes of the Eger Graben (EG), an incipient rift and part of the ECRIS, Oligocene–Miocene in age (Rajchl et al. 2009), post-date geological units and tectonic structures relevant to this thesis. **(b)** An overview map displaying approximate extent of the 'central Europe', a broader area discussed in this thesis, with position of the Bohemian Massif and the study area in its northern part. **(c)** Bohemian Massif (with the study area indicated) and neighboring Variscan basement areas and their relation to the main structural zones of the Variscan Orogen in Europe[1].

Late Paleozoic continental successions

The Late Paleozoic continental successions of the Bohemian Massif represent, in terms of their tectonic setting, components of post-orogenic intra-continental extensional/transtensional basin system developed at ca. 320–280 Ma (Mattern 2001; Uličný et al. 2002; Opluštil et al. 2016). Geographically they are situated in two distinct areas: the central and western Bohemain basins and the basins of Lugicum (Fig. 3), described in detail within the **chapters 1** and **3**. The Late

---

[1] "Gliederung der Variszidenin Mitteleuropa nach Kossmat 1927, verändert nach Franke & Hoffmann 1997, Oncken 1997, 1998" by Jo Weber. Available online at: https://en.wikipedia.org/wiki/File:Gliederung_der_Variszidenin_Mitteleuropa.jpg
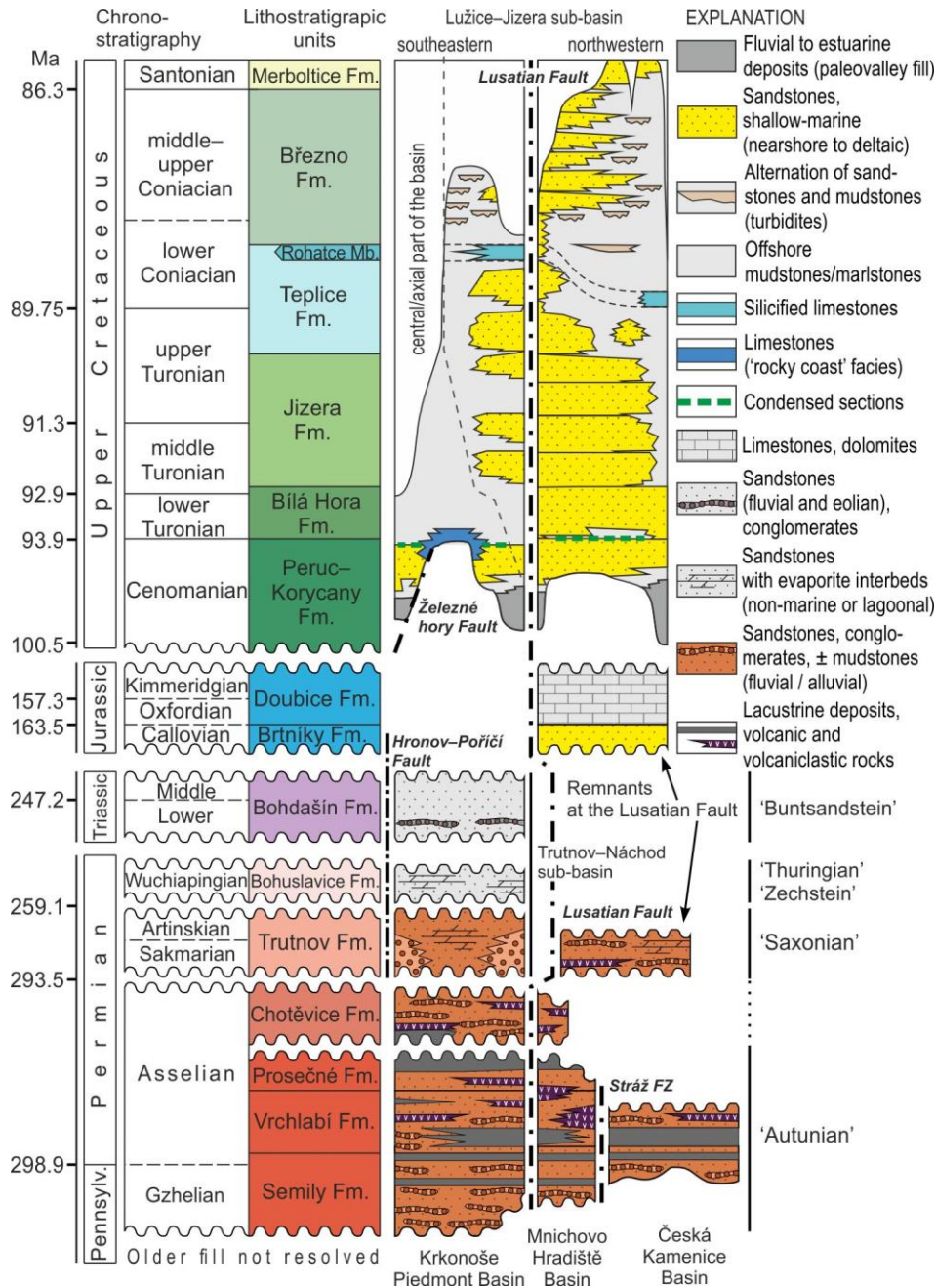
Figure 2. Schematic juxtaposition of sedimentary basins within the study area with respect to their stratigraphic age and tectonic relationships.

Paleozoic basins of the Lugian area include the Intra-Sudetic, Krkonoše Piedmont, Mnichovo Hradiště, Česká Kamenice and Orlice basins. The Krkonoše Piedmont and Česká Kamenice basins are the target of this thesis, and are, therefore, described in a greater detail.

(1) Krkonoše Piedmont Basin (KPB) forms an eastern promontory of the basin system developed between western/central Bohemia and central Silesia ('Pilsen–Trutnov Basin Complex' sensu Cháb et al. 2008). The KPB is filled with ca. 1800 m of Pennsylvanian (Moscovian/Kasimovian) to Lower Triassic non-marine deposits. The infill comprise several unconformities (Pešek 2001; Opluštil et al. 2016; Martínek et al. 2017) that imply complex tectonosedimentary evolution with presumed multiple changes in basin geometry, shift of
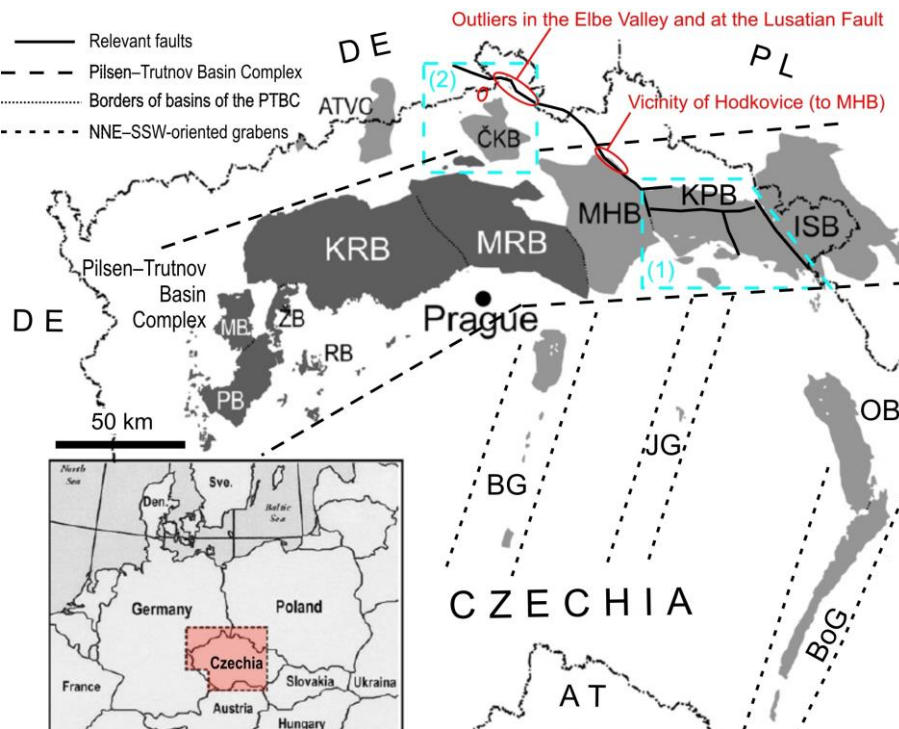
Figure 3. Late Paleozoic continental basins in the Czech territory (Opluštil et al. 2013, amended); geographic groups (1, 2) indicated. Abbreviations: ATVC – Altenberg–Teplice Volcanic Complex, BG – Blanice Graben, BoG – Boskovice Graben, ČKB – Česká Kamenice Basin, ISB – Intra-Sudetic Basin, JG – Jihlava Graben, KRB – Kladno–Rakovník Basin, MB – Manětín Basin, MHB – Mnichovo Hradiště Basin, MRB – Mšeno–Roudnice Basin, OB – Orlice Basin, PB – Pilsen Basin, RB – Radnice Basin, ŽB – Žihle Basin. For complete nomenclature of Carboniferous–Permian basins of Czechia see Opluštil and Pešek (1998).

depocenters and source areas over time (Martínek 2008; Martínek and Štolfová 2009; Opluštil et al. 2016). Based on the well-constrained hiatuses (each lasting up to ca. 1.5 Myr; Opluštil et al. 2016), the middle Pennsylvanian to early Permian lifespan of the basin can be divided into at least three depositional cycles (Fig. 4). Presumably during the Saale tectonic phase, i.e., between the 'Autunian' (Asselian–Sakmarian) and 'Saxonian' (Sakmarian–Kungurian; Opluštil et al. 2016), the KPB experienced inversion accompanied by pervasive brittle deformation and coeval formation of the Trutnov–Náchod Sub-basin (TNSB), a structure governed by dextral slip on NW–SE trending strike-slip faults (Uličný et al. 2002). Although, the TNSB is associated with the KPB (e.g., Pešek 2001), it represents a structurally distinct tectonic element that is superimposed on the older strata in the KPB.

(2) Česká Kamenice Basin (ČKB) is completely concealed beneath younger deposits, with subcrop area about 300 km^2 according to Pešek (2001). A handful of deep boreholes that reached the pre-Pennsylvanian basement allows for interpretation that the basin is divided into three sub-basins (Fig. 5): (1) Česká Kamenice Basin s. s.; (2) Srbská Kamenice sub-basin; (3) Kravaře sub-basin. The most complete succession was drilled by borehole Vf-1 (Holub et al. 1984) within the main depocenter; it recorded up to 620 m thick succession of alternating mudstones, sandstones, and conglomerates with intercalations of basic to intermediate volcanic and volcaniclastic rocks,

17

Gzhelian–Asselian in age (Kučera and Pešek 1982; Vejlupek et al. 1986). The basin fill comprise three gray- and/or varicolored fine-grained horizons, uppermost of them correlated with the Rudník Mb. (as defined in the Mnichovo Hradiště and Krkonoše Piedmont basins; Fig. 4) – which is supported by presence of Autunian-age sporomorphs (Vejlupek 1986).

The Carboniferous–Permian deformed outliers along the Lusatian Fault, only several tens of meters long and with a reduced stratigraphic range, composed of alternating sandstones and conglomerates with intercalations of volcanic and volcaniclastic rocks (e.g., Fediuk et al. 1958). It has been assumed that they once formed a single depositional space with the ČKB (cf. Malkovský 1987 after J. Dvořák 1962; Klein and Opletal 1971, Fig. 6). However, recent borehole data (Nádaskay et al. 2019) revealed a different depositional pattern, suggesting that the Permian outliers along the Lusatian fault may represent remnants of a separate basin post-dating the ČKB, i.e., late Autunian to Saxonian (Sakmarian–Artinskian) in age (see discussion further in this thesis).
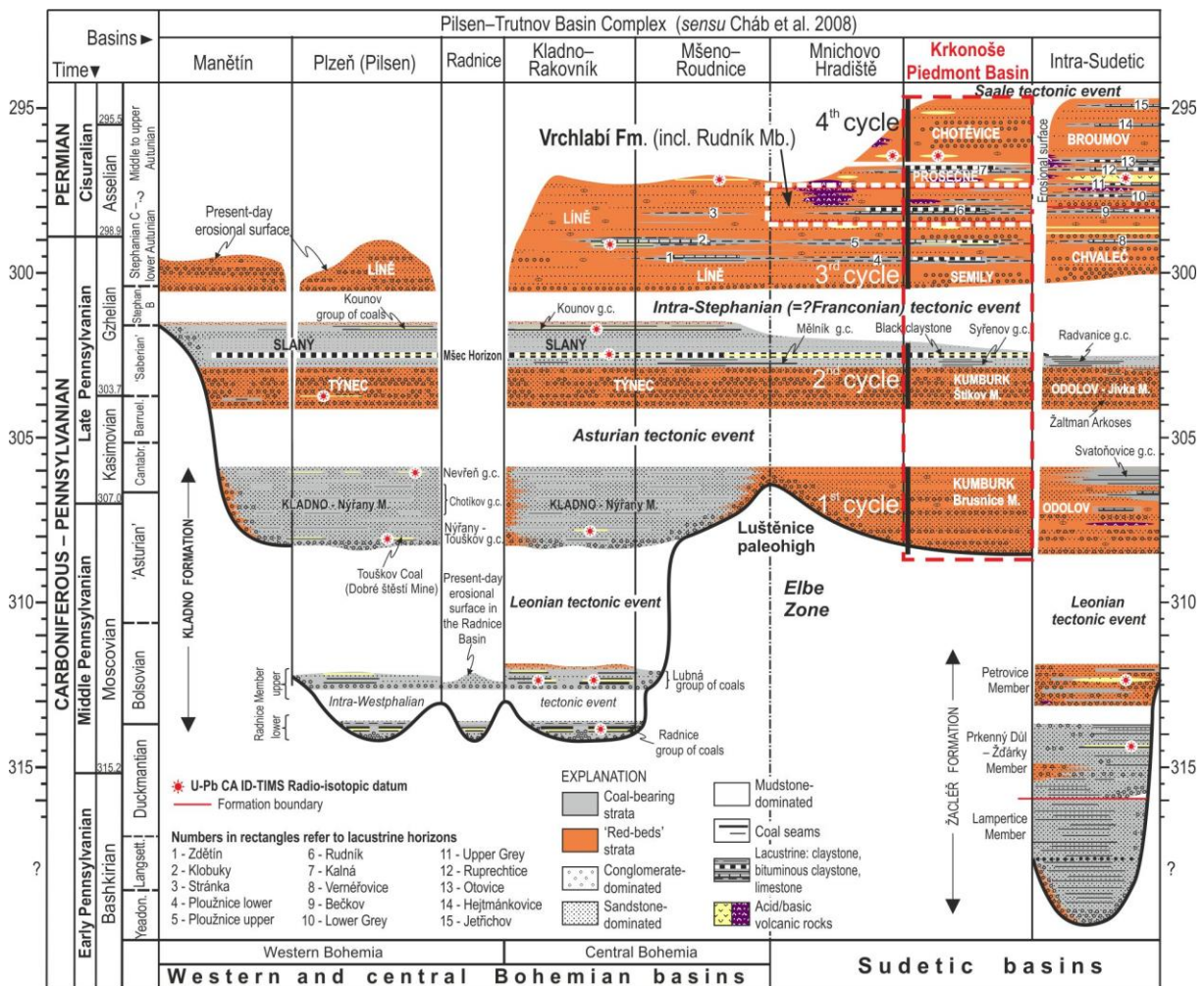
Figure 4. Tectonostratigraphic model of the 'Pilsen–Trutnov Basin Complex' (PTBC; sensu Cháb et al. 2008) calibrated by the most recent high-precision (TIMS) radioisotopic data of Opluštil et al. (2016) from both flanks of the basin system, i.e. central/western Bohemian and Lugian. Dated samples are indicated by asterisk. Post-Asselian fill of the KPB (Trutnov, Bohuslavice and Bohdašín formations) excluded. Česká Kamenice Basin is not shown here as part of the PTBC because of its present-day relatively detached position to the north off the basin system; this is interpreted as a result of Permian- and Cretaceous-age tectonic deformation (Uličný et al. 2009a).

Jurassic marine successions

The Jurassic deposits of the northern Bohemian Massif are exposed, or were exposed in the past, at several locations (Fig. 5; overview in Voigt 2009 and Valečka 2019) in northern Bohemia/Czechia and Saxony. They are preserved along the Lusatian Fault as several blocks up to a few tens of meters in along-strike length, intensely deformed and tilted in a similar fashion to the Permian deposits that accompany them (Fig. 6; Opletal et al. 2006; Valečka et al. 2006). The Jurassic deposits are composed of quartzose and dolomitic sandstones at the base (Brtníky Fm.), interpreted as representing near-shore deposits locally recycling material from the ?Permian red beds (Eliáš 1981). This basal unit is overlain conformably by fossiliferous dolomitic limestones and dolomites (Doubice Fm.), interpreted to be deposited in hemipelagic, offshore environment (Eliáš 1981; Valečka 2019). They were paleontologically dated at Oxfordian–Tithonian (Holcová and Holcová 2016 for more details). In addition, pebbles of Jurassic carbonates and cherts embedded within the Upper Cretaceous as well as fragments of Jurassic ammonites and presumably redeposited ooliths are found at several localities (e.g., Voigt 2009; Valečka 2019).

There is no direct evidence on the original tectonic setting of the Middle–Upper Jurassic deposits; this issue is a matter of discussion (cf. Malkovský 1987; Voigt 2009) continued by this thesis.

The Bohemian Cretaceous Basin

The northern and northeastern Bohemian Massif is extensively overlain by the ca. 14,600 km^2 Bohemian Cretaceous Basin (BCB). For position of the BCB within the central Europe and the Bohemian Massif, respectively, see Figs. 1 and 2 in **Chapter 3** (p. 160 and 162). Geological setting and stratigraphy of the BCB is summarized by, e.g., Voigt 1994; Herčík et al. 2003; Voigt et al. 2008, Čech 2011; more details also availabe in **chapters 2** and **3**.).

The BCB formed as a result of mid-Cretaceous reactivation of the Variscan basement faults during early phases of the Alpine Orogeny (e.g., Voigt et al. 2008) and was filled during Cenomanian to Santonian by up to 1 km thick coarse marine siliciclastic successions, concentrated along the most intensely subsiding, tectonically driven basin margins bordered by uplifted basement blocks (e.g., Voigt et al. 2008; Uličný et al. 2009b). The deposition may have continued until the Campanian (Klein et al. 1979). The infill of the BCB was inverted and overprinted by multiple deformation events, the main phase of basin inversion occurred after 86–85 Ma (Voigt et al. 2008). It is estimated that at least about 500 m of the basin fill was removed by inversion and erosion (Uličný et al. 2009a), but more recent evidence suggest much more (see discussion). The post-depositional deformation involved displacement along intrabasinal strike-slip faults and reverse/thrust faults at the basin margins (e.g., Coubal et al. 2015; and references therein). The post-Cretaceous geological evolution of the Lusatian Massif and its vicinity was
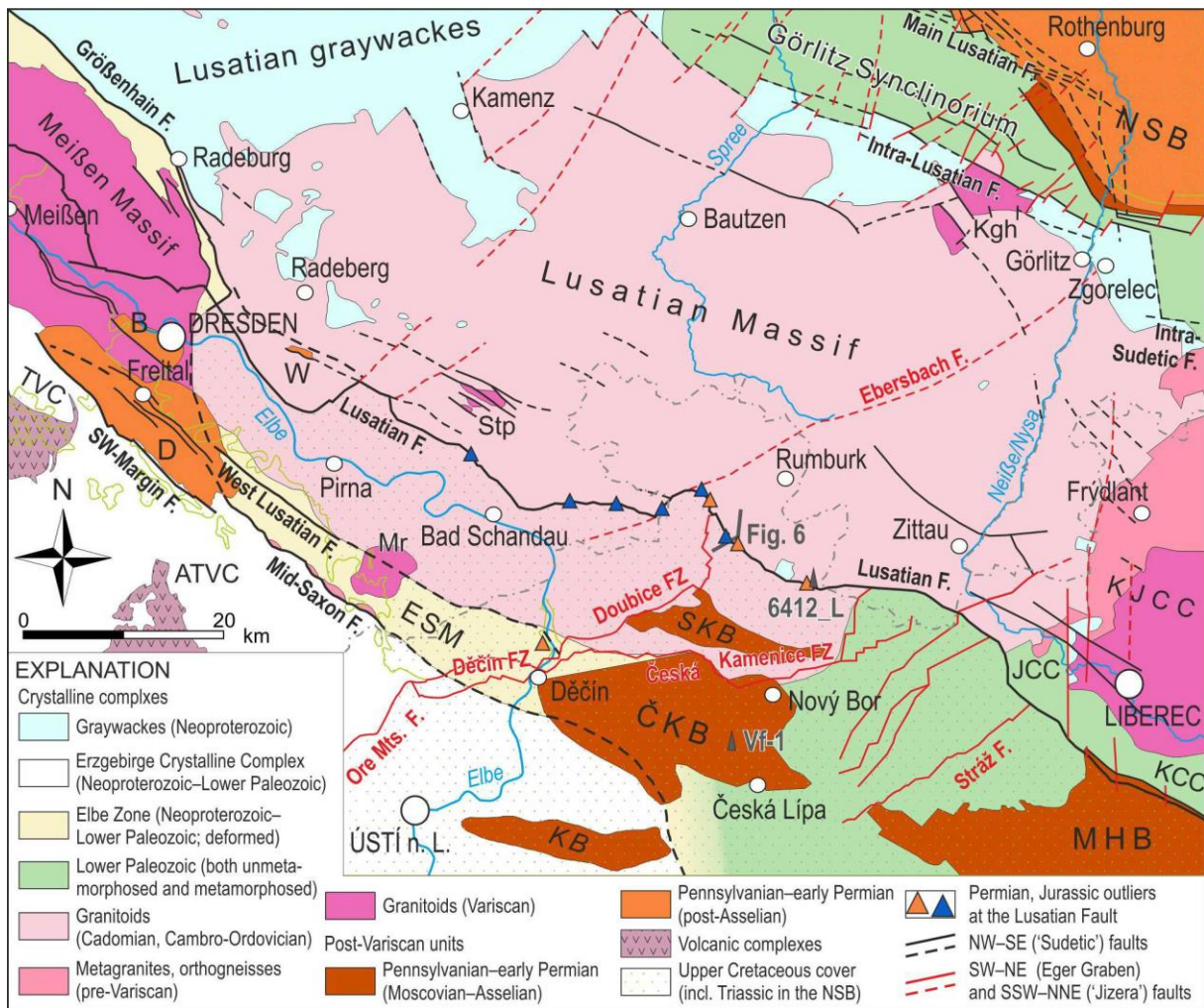
Figure 5. Geological map of the pre-Cenozoic basement of northwestern portion of the study area in the northern Bohemian Massif, an area spanning between Meißen (Saxony, Germany) and Liberec (Czechia). Abbreviations: ATVC – Altenberg–Teplice Volcanic Complex; ČKB – Česká Kamenice Basin (KB – Kravaře sub-basin; SKB – Srbská Kamenice sub-basin); D – Döhlen Basin (B – Briesnitz sub-basin; W – Weißig sub-basin); ESM – Elbe Slate Mts.; JCC – Ještěd Crystalline Complex; Kgh – Königshain massif; KJCC – Krkonoše–Jizera Crystalline Complex; MHB – Mnichovo Hradiště Basin; Mr – Markersbach massif; NSB – North Sudetic Basin; Stp – Stolpen massif; TVC – Tharandt Volcanic Complex. Interpreted borders of the ČKB (+ SKB, KB) after B. Mlčoch (unpublished). Boreholes 6412_L and Vf-1 as well as geological section presented in Fig. 6 are indicated.

dominated by crustal extension and continental intraplate volcanism, and related basin formation (see summary by Tietz and Büchner (2015). In the NW part of the BCB, the Lužice–Jizera sub-basin (LJSB) was one of the main tectonically controlled depocenters. The preserved infill of the sub-basin reaches up to 1 km and is subdivided into six formations, Cenomanian to Santonian in age (Fig. 2):

(1) The basal Peruc–Korycany Fm. comprises two contrasting units. The lower to middle Cenomanian Peruc Mb., not exposed in the study area, includes fluvial to estuarine sandstones and conglomerates with mudstone/claystone intercalations filling paleovalleys in the pre-Late Cretaceous basement (Uličný et al. 2009a). In contrast, the upper Cenomanian Korycany Mb. covers virtually the entire NW BCB, mostly in subcrop. It comprises quartzose and argillaceous

20

sandstones and conglomerates of an average thickness of 30–70 m (up to between 80–130 m along the Lusatian Fault). The member is interpreted to record widespread shallow-marine environment after filling up of the fluvial–estuarine paleovalleys (Uličný et al. 2009a).

(2) The <u>Bílá Hora Fm.</u> (lower–middle Turonian) in the NW part of the BCB is characterized by a relatively constant thickness (ca. 80–120 m) and monotonous facies development. Its basal part is formed by ca. 15 m thick sequence of marlstones, passing upwards to partly silicified quartzose sandstones with intercalations of conglomerates (e.g., Valečka 1979).

(3) The <u>Jizera Fm.</u> (middle–upper Turonian) is lithologically more varied and thicker (up to 420 m near the Lusatian Fault) and is formed by quartzose sandstones and conglomerates arranged into several tens of meters thick coarsening-upward cycles (e.g., Valečka 1989).

The Bílá Hora and Jizera formations were deposited under similar conditions in terms of sedimentary processes and tectonic activity (e.g., Uličný et al. 2009b) – individual sequences within both formations record progradation-dominated nearshore to deltaic environment. Deposition of the Bílá Hora Fm. marks the onset of Turonian transgression, one of the major transgressive events in central Europe (e.g., Klein et al. 1979; Valečka and Skoček 1991; Voigt et al. 2008) that flooded most of the pre-Cenomanian intrabasinal highs and significantly widened the epicontinental marine realm. The clastic material was delivered from two uplifted source areas located northeast and west of the LJSB – the 'West Sudetic Island' and 'Most–Teplice elevation', respectively (e.g., Uličný et al. 2009b; and references therein). From the early middle Turonian onwards, the latter was drowned and the West Sudetic Island remained the dominant source area for this part of the basin (Uličný et al. 2009b).

(4) The <u>Teplice Fm.</u> (upper Turonian–lower Coniacian) is formed by well-sorted fine-grained sandstones in its lower (Turonian) part, locally argillaceous and with a rare conglomeratic layers, interpreted as relatively shallow-water, tide-modified prograding nearshore sandbodies (Valečka et al. 2006). Basinward, they pinch out and are overlain by a sequence of lower–middle Coniacian offshore mudstones and marlstones (Čech and Švábenická 1992).

(5) The <u>Březno Fm.</u> (uppermost lower–upper Coniacian) covers substantial part of the NW BCB (**chapters 2** and **3**) where it fills the deepest part of the LJSB, reaching a thickness of about 450 m (Čech et al. 1987). The formation comprises three lithofacies (Valečka 1979): quartzose sandstones of variable grain-size arranged into coarsening-upward cycles, mudstone-dominated facies, and a heterolithic ('flyschoid') facies formed by alternation of fine- to medium-grained sandstones and mudstones. Nádaskay and Uličný (2014) connected these facies into a single progradational nearshore to deltaic depositional system. The quartzose sandstones represent the delta front facies, while heterolithic facies represents gravity flow-dominated prodelta and the mudstone-dominated facies represent offshore deposits.

Deposition of the Teplice and Březno formations took part during a period of gradual deepening of the basin, coinciding with a series or marine transgressions around the Turonian–Coniacian boundary and during the early Coniacian (Uličný et al. 2009b, 2014). The most salient feature of the Coniacian deposition is presumed acceleration of subsidence, compensated by gradually increasing siliciclastic supply from the uplifted West Sudetic Island.

(6) The Merboltice Fm. (Santonian) is the least extensive formation of the BCB, only preserved as relics within the Eger Graben. It is predominantly formed by fine-grained arkosic or quartzose sandstones with feldspar admixture (Valečka and Slavík 1985), interpreted as deposited in relatively shallow-water, probably deltaic environment (Voigt et al. 2008).
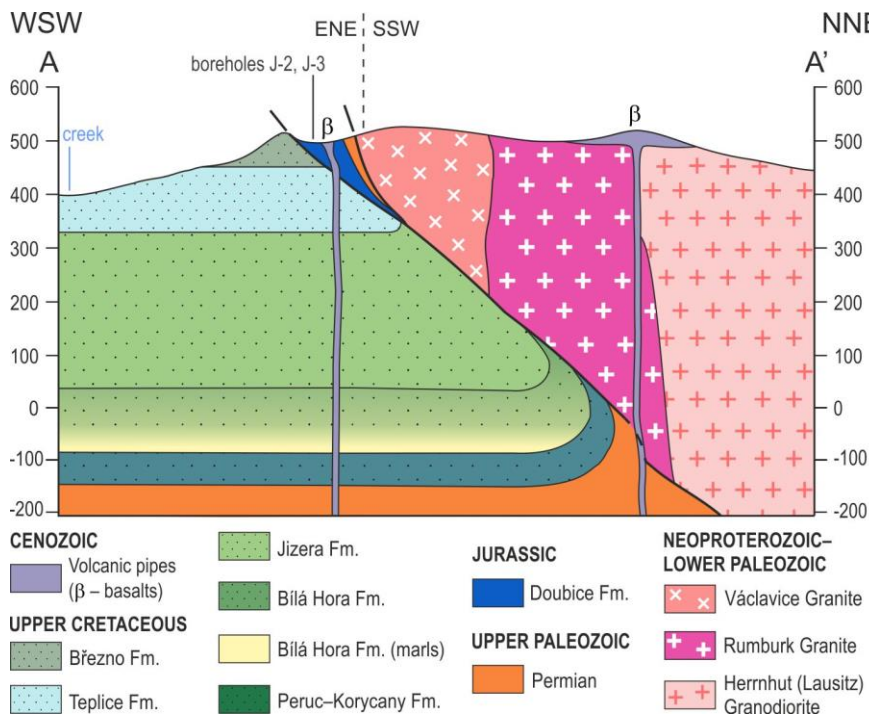
Figure 6. Simplified geological section at the boundary between the Bohemian Cretaceous basin and Lusatian Massif (amended after Klein and Opletal 1971). The section is located between Doubice and Krásná Lípa municipalities in the northern Bohemia (for approximate location see Fig. 5) Distance between A and A' is ca. 3,5 km. Details to boreholes J-2 and J-3 in Eliáš (1981).

Methods

The methods employed within individual case studies (**chapters 1** to **3**) had been chosen in order to analyze the sedimentary succession and to decipher its provenance and tectonosedimentary record. Common denominator of all the chapters is the conventional sedimentological analysis of selected representative sections, both in ourcrop and in core. Other methods were selected with respect to partial goals of the individual chapters.

Analysis of lithofacies and architectural elements

Sedimentological interpretations, as presented by **chapters 1** to **3** are based on investigating facies and architectures in outcrop and palaeocurrent measurements. In **chapters 2** and **3**, this is complemented by detailed sandstone petrography performed on thin sections.

The description of non-marine lithofacies (**Chapter 1**) follows a widely applied scheme by Miall (1977); it considers lithology, grain size, sorting and clast roundness, texture, bedding,

sedimentary structures, and the 'facies shape'. The architectural elements, i.e., geometric arrangement of facies assemblages, are defined by geometries and bounding surfaces, using the methodology of Bridge (1993). Lithofacies of marine Upper Cretaceous (**Chapter 2**) are defined in roughly the same fashion, based on combination of lithology (grain-size) and diagnostic sedimentary structures, following lithofacies definitions by Nádaskay and Uličný (2014) and Uličný et al. (2009b). In **Chapter 3**, lithofacies are not resolved in detail; instead, basic lithologic description of individual samples together is provided in overview table together with interpreted depositional environment (based on own data and literature).

Correlation of facies of the depositional system: Well-logs, gammaspectrometry, XRF

In addition to conventional sedimentological logs, well-logs, spectral gamma-ray logs and XRF curves were employed in order to better facilitate the correlation of contrasting lithofacies of the depositional system (Fig. 7), e.g., fluvial to alluvial, deltaic and lacustrine, or proximal shallow-marine (nearshore, deltaic) to distal (prodelta, offshore).

A number of spectral gamma-ray logs were obtained in outcrop to constrain the stratigraphic position of key sections through their correlation to well-logs (see **Chapter 1**; non-marine Krkonoše Piedmont Basin). This approach, when applied to complex sedimentary systems, such as fluvio-lacustrine or fluvio-deltaic/estuarine, allows for correlation of key stratigraphic surfaces with much higher resolution. Gamma-ray (GR) logs reflect summary concentrations of main radiogenic elements (K, Th and U) and are used as a proxy for clay mineral content (Rider 1996). Basic principle of this method is the same when rendered as both outcrop gammaspectrometry and geophysical well-log. Within sedimentary formations, the increase of clay mineral content is usually interpreted as decreasing grain size and vice versa. The outcrop GR-logs bridged few km long distances between two neighbouring boreholes and were used as primary data for constructing stratigraphic cross-sections. Together with sedimentological outcrop data, the basin-scale correlations provided information on large-scale depositional architecture of fluvial deposits of the Vrchlabí Fm. and their relationship to lacustrine facies in the central part of the basin.

Well-logs were used as lithological proxy for correlation of individual facies of the depositional system (**chapters 1** and **2**) and to better visualise spatial and temporal transitions of facies within the depositional system. The most extensively used type of well-logs were gamma-ray (GR) logs; additionaly, resisitvity (RES) and density/neutron (NL) logs were employed in **chapter 2**. Summary concentrations of main radiogenic elements (K, Th and U) reflected by the GR represent a proxy of clay mineral content, extrapolated as reflecting sediment grain size. For more details to well-logs and their specifics, e.g., typical well-log signatures of studied lithofacies see Fig. 5 in **Chapter 1** and Fig. 4 in **Chapter** , p. 75 and 112, respectively.

The handheld XRF analyzer was employed to aquire element concentrations as recored by core section presented in **Chapter 2**. Results were presented (see Fig. 10 in **Chapter 2**, p. 126) as curves of $CaCO_3$ and element ratios (Si in proportion to Al, Ti, Zr) in order to analyze bioproductivity and siliciclastic signal, respectively. Variations is both are assumed to result from interplay of sea-level changes (notably independent on local processes, i.e., eustatic) and siliciclastic supply; variations in the latter can be, in turn, related to tectonic reactivation of the source area. To interpret controls on deposition as recorded by the analyzed core section, the acquired XRF curves were correlated to well-logs from the same borehole, which allowed their correlation within a broader area.
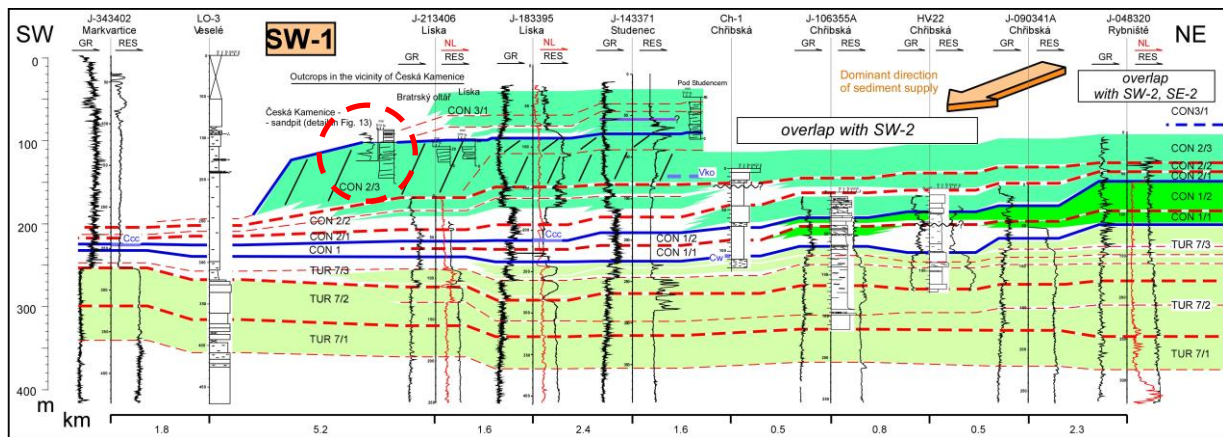
Figure 7. An example of the correlation cross-section, located in northern Lužice–Jizera sub-basin of the BCB, based on geophysical well-logs (GR, RES and NL) complemented by outcrop lithological sections as well as by field gamma-ray curve (in red circle). Thick blue lines represent interpreted maximum transgressive surfaces (MTS; sensu Helland-Hansen and Martinsen 1996) that separate individual stratigraphic sequences (their proximal, sandstone-dominated parts in green). Taken from Nádaskay and Uličný (2014).

Evaluating controls on stratigraphic record

Deposition of stratigraphic sequences is governed by interplay (Fig. 8) of sediment influx, rate of change of sediment accommodation (i.e., eustasy and sea-floor subsidence/uplift) and [basin] physiography. In general, eustasy and sea-floor subsidence/uplift determine the timing of sequence boundaries, whereas sediment flux and physiography are most effective in determining the stratal architecture between those bounding surfaces (Posamentier and Allen 1993).

The eustatic sea-level changes are globally significant (independent on the basin setting) and generated by remote plate-tectonic processes linked to sea-floor spreading, continental drift and orogeny (e.g., Burgess et al. 1997; Kominz 2001; Rovere et al. 2016), or by climate change driven by variations in insolation as a result of Milankovitch cycles (e.g., Miller et al. 2005; Boulila et al. 2018). In this case, sea-level rise/fall may be achieved through accretion/melting of polar ice caps – so far, the glacio-eustasy (e.g., Miller et al. 2003), or combination of aquifer-eustatic and glacio-eustatic forcing (Wendler and Wendler 2016), has been discussed as a possible driving mechanism behind the Late Cretaceous global sea-level changes. Besides orbital forcing, the
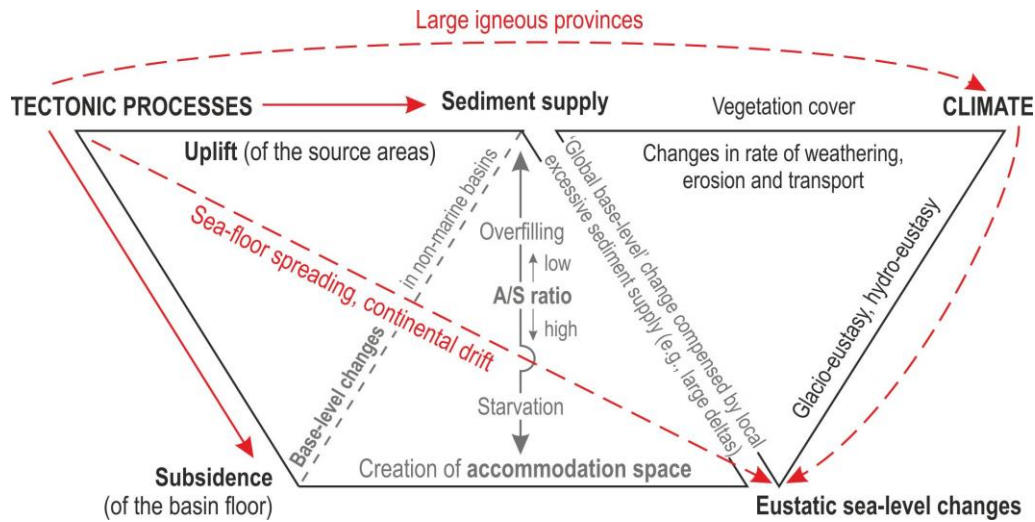
Figure 8. Schematic relationship between the controls on stratigraphic record, i.e., subsidence, sediment supply and eustatic sea-level changes – their interplay generates processes (inner triangle, in gray) with direct control over deposition of the stratigraphic sequences and their cyclic repetition. Endogenous / tectonic processes and climate represent 'superior' driving mechanisms. Red arrows indicate impact of tectonic processes on other controls (dashed – global, no dash – local tectonic processes). 'Starvation' refers to increasing A/S ratio (increase in creation of accommodation), while 'overfilling' refers to decreasing A/S ratio (increase in sediment supply).

climate change can be triggered by endogenous processes as well. For instance, by intraplate volcanism releasing quantity of greenhouse gases to the atmosphere that, in turn, may cause increase in hydrological cycling (e.g., Xu et al. 2017). Climate change can also enhance weathering and runoff, and, thus, increase an amount of sediment delivered into the basin(s) (e.g., Ruffell et al. 2016).

Since sea-level changes played no role in the Krkonoše Piedmont Basin (KPB), a continental interior, 'intermontane' basin, this thesis (**Chapter 1**) attempts to assess the changes in large-scale fluvial architectures in reaction to [local] base-level changes. The latter are caused by varying rate of creation of accommodation space (by tectonic subsidence, climate-induced lake expansion) in proportion to sediment supply (Fig. 8), which may be, in turn, dependent on the vegetation (e.g., Leeder et al. 1998). It is important to note that the interplay of accommodation and supply can also lead to deposition of small-scale cycles that result from autogenic processes, e.g., the intrinsic behaviour of fluvial system type (e.g., Ventra and Nichols 2014). To qualitatively express the magnitude of base-level changes over the studied time interval, we employ the A/S [accommodation/sediment supply] ratio of Martinsen et al. (1999). The A/S ratio is a simple tool to interpret stratigraphic interactions within the non-marine depositional systems—in this case, between riverine and lacustrine part of depositional system of the Vrchlabí Fm.—as a measure of: (1) accommodation, the most remarkably reflected by lake expansion; (2) sediment supply, reflected by variable thickness and stacking pattern of fluvial channels vs. floodplain deposits. The concept of A/S ratio as applied to the KPB is illustrated by Fig. 16 in **Chapter 1** (p. 95).

Construction of the sequence stratigraphic framework is not sought in this thesis, since the database is insufficient to track important stratigraphic surfaces across larger distances.

In case of the Bohemian Cretaceous Basin (BCB), subsurface data (well-logs) were correlated (Fig. 7) using genetic sequence-stratigraphic methodology as adapted for the BCB by Laurin and Uličný (2004) and Uličný et al. (2009b). This methodology follows the genetic sequence concept of Galloway (1989), based on tracing maximum flooding surfaces (MFS), i.e., maximum transgressive surfaces (MTS) sensu Helland-Hansen and Martinsen (1996). Details to the genetic stratigraphy as applied in the BCB are provided by **Chapter 2**. This approach allowed for defining the stratigraphic sequences, interpreted to be deposited by an interplay of sediment supply, basin-floor subsidence and eustatic sea-level changes.

Strontium isotope geochemistry

In addition to conventional stratigraphic methods, strontium isotope geochemistry was employed (**chapter 2**) to better constrain a duration of stratigraphic sequences in the NW BCB (Lužice–Jizera sub-basin), defined by combination of allo- and biostratigraphic methods, as well as to evaluate presumed increase of input siliciclastic material to the basin.

In theory, the Sr isotopic composition of seawater reflects steady-state equilibrium between various Sr sources (rock weathering, volcanism, seafloor alteration) and sinks (marine carbonates). Generally, low or decreasing $^{87}Sr/^{86}Sr$ reflects periods characterised by high seafloor activity (mantle $^{87}Sr/^{86}Sr$ lower than 0.703), whereas increasing $^{87}Sr/^{86}Sr$ reflects periods of elevated weathering rates of continental felsic rocks with high time-integrated $^{87}Sr/^{86}Sr$ (Kump 1989). A composite Phanerozoic seawater $^{87}Sr/^{86}Sr$ curve (e.g., McArthur et al. 2012) is widely applied as a chemostratigraphic tool and it can also be used to identify the influence of continental sources (e.g., Richter et al. 1992). Periodicity of Sr isotope ratio in time may indicate short time oscillations of marine carbonate Sr composition or variable input of dissolved terrestrial Sr. Elevated $^{87}Sr/^{86}Sr$ ratio in riverine waters was observed in intensely folded regions (e.g., Richter et al. 1992). The idea behind the use of Sr isotopes in this thesis has two parts: (1) to explore viability of their use as a novel chemostratigraphic tool (within framework of the BCB); (2) to verify a possibility that incipient inversion of the BCB, presumably coeval with uplift of the adjacent source area (the West Sudetic Island), could be recorded in the sedimentary record by perturbation of Sr isotope ratio (as compared to seawater $^{87}Sr/^{86}Sr$ curve for respective time interval; cf. McArthur et al. 2012).

Although the Late Cretaceous phase of the Alpine Orogeny did not directly involve the Bohemian Massif, numerous studies (e.g., Ventura and Lisker 2003; Lange et al. 2008; Ventura et al. 2009; Danišík et al. 2010; Sobczyk et al. 2015; Hofmann et al. 2018; Botor et al. 2019; Käßner

et al. 2020) have so far provided indirect evidence for tectonic reactivation and uplift of parts of the northern Bohemian Massif, which facilitates this premise.

Provenance of the sedimentary formations

Sediment provenance analysis (SPA) concern the origin, composition, transport and deposition of clastic material and, thus, plays an important role in understanding the links between basinal sedimentation, and hinterland tectonics and unroofing (Scott et al. 2014). A purpose of the SPA is to constrain the primary source areas of clastic material delivered to the basin, usually through multi-method comparison of detrital mineral spectrum with mineral composition of inferred primary source rocks. The SPA can help to determine the directions of sediment transport and dispersal (e.g., Otava and Hartley 2001; Weislogel et al. 2015; Augustsson et al. 2018), recycling of clastic material from older generations of basins (e.g., Biernacka 2012; Hofmann et al. 2018; Moecher et al. 2019) and to uncover tectonic setting and evolution of sedimentary basins (e.g., von Eynatten et al. 2008; Žák et al. 2018; Zieger et al. 2019). As such, it is an important tool for paleogeographic reconstructions (e.g., Biernacka and Józefiak 2009; Žák and Sláma 2018) as well as for interpreting geodynamic history of orogens (e.g., Becker et al. 2006; Pastor-Galán et al. 2013; Schwartz et al. 2019). However, inferring provenance from the final product, a basin fill, is not straightforward because the detrital spectrum evolves as the sediment is transported along the pathway from source to basin (Weltje and von Eynatten 2004).

The provenance of Permian, Jurassic and Upper Cretaceous deposits in the northern Bohemia (**Chapter 3**) was studied by heavy mineral analysis (HMA), i.e., matching the heavy mineral suite in the sediment to that of the potential source rock areas, and geochronology, in this case by matching zircon age distributions with age spectra of potential source rocks.

The HMA yielded a heavy mineral assemblage, identified in the individual samples. The data are presented in stratigraphic order using selected heavy mineral indexes (Fig. 7 in **Chapter 3**, p. 172): (1) the zircon–tourmaline–rutile (ZTR) index, which indicates mineralogical maturity of the studied rock; (2) the monazite–zircon (MZi) index, which reflects the relative significance of granitic material in the source; and (3) TiO_2-minerals–zircon (RZi) index, which reflects input of material derived from high-grade metamorphic rocks.

The detrital zircon geochronology was performed by ICP-MS U/Pb dating. For detailed description of instrumental measurement and calculation of zircon ages see **Chapter 3**. To match the detrital zircon ages with inferred source areas, the obtained U–Pb age spectra were divided into eight distinct groups that were interpreted in terms of their potential primary source area, either within or outside the Bohemian Massif, with implications for paleotectonic events responsible for basin formation and inversion as well as for paleogeography.

Tectonosedimentary evolution of the northen Bohemian Massif: A synthesis and discussion

Comprehensive research that integrated the methods presented above revealed that during the Late Paleozoic to late Mesozoic, the northern Bohemian Massif experienced complex intra-plate tectonosedimentary evolution that involved development of several generations of sedimentary basins in different settings. Circumstances of the basin development and inversion are summarized in following chapters with discussion of these events in a wider geotectonic context and implications for paleogeography of the central Europe between the Variscan and Alpine orogenies. The main outputs of the thesis are largely summarized by **Chapter 3** (graphical summary in Fig. 13, p. 182–185) as well.

Pennsylvanian to early/middle Permian (Rotliegend)

The first major event recorded in the central Europe since the Variscan Orogeny is the Late Viséan–Westphalian late-orogenic crustal extension and destruction of the Variscan orogenic plateau (e.g., Dewey and Burke 1973; Lorenz and Nicholls 1976, 1984; Dewey 1988). This involved a gravitational instability of thickened crust ('gravitational collapse') enhanced by changes in plate-boundary stresses (Ménard and Molnar 1988; Burg et al. 1994; Henk 1997; Dörr and Zulauf 2010). The paleorelief inversion during the early Pennsylvanian (Žák et al. 2018), related to destruction Variscan orogenic plateau, was followed by widespread extension within the Variscan orogenic belt was completed by development of continental basins in the eroded orogen's interior ('intermontane' basins; Opluštil and Cleal 2007 for overview).

As a reaction to the late-orogenic extension within the Bohemian Massif, the Pilsen–Trutnov Basin Complex (PTBC; sensu Cháb et al. 2008) was established roughly along the major crustal boundary between the Saxothuringian and Teplá–Barrandian units. Between the middle/late Pennsylvanian and early Permian, its sub-basins, one of them being the present-day Krkonoše Piedmont Basin (KPB), were gradually filled with large volumes of siliciclastic material derived from the surrounding basement uplifts. Similar lithostratigraphic development of sub-basins of the PTBC implies that they formed a single depositional space or were at least partially interconnected (e.g., Opluštil and Pešek 1998). Deposition within the PTBC was puncutated by several hiatuses (Fig. 4; Havlena and Pešek 1980; Pešek 2001; Martínek et al. 2017; Opluštil et al. 2016) interpreted as a result of episodes of tectonic reactivation of basement faults (corresponding roughly to tectonic phases of Stille 1920) governed by late orogenic and later intraplate compressive forces (e.g., Schulmann et al. 2014).

In the KPB, the hiatuses were recently constrained by dating of syndepositional volcanic products (Opluštil et al. 2016), which allows for interpreting at least four tectonosedimentary cycles during the Pennsylvanian–early/middle Permian (Fig. 4): (1st) Asturian–Cantabrian

(Brusnice Mb. of the Kumburk Fm.); (2nd) late Barruelian–Saberian (Štikov Mb. of the Kumburk Fm., Syřenov Fm.); (3rd) Stephanian C–Asselian (Semily, Vrchlabí, Prosečné fms.); presumably (4th) late Asselian–?Sakmarian (Chotěvice Fm. see discussion below), followed by (5th) Sakmarian –Artinskian ('Saxonian', Trutnov Fm.). Deposition of these cycles was governed by tectonic processes, responsible for initial arrangement of depocenters and subsidence, and by subordinate climate forcing (cf. Opluštil et al. 2013).

The Vrchlabí Fm. represents a part of the Stephanian C–Asselian depositional cycle, initiated after the Intra-Stephanian tectonic event (cf. Opluštil et al. 2016). Deposition of the Semily and Vrchlabí formations marks a formation of the new depocenter, discordant to the one(s) where the older formations were deposited (cf. Opluštil and Pešek 1998). Thick coarse-grained facies of the Semily and Vrchlabí formations (incl. those of the fluvial system analyzed in the **Chapter 1**) deposited along the basin margins indicate elevated sediment supply from neighboring high-elevation regions. The Vrchlabí Fm. shows that in the early Permian, the deposition in the eastern (Sudetic) part of the PTBC was driven by coincidence of multiple factors. At first, a notion that tectonic-driven creation of accommodation space in the earlier phases of deposition of the Vrchlabí Fm. is supported by formation of two parallel half-grabens separated by intra-basinal high (Fig. 13 in **Chapter 1**, p. 89). In the later phase, the bounding fault of the northern half-graben had become dominant, which led to downwarping of the intra-basinal high a shift of subsidence towards the northern basin margin (cf. Martínek et al. 2006). This is evidenced by marked disproportion in thickness of the formation in the north and south (350 to 200 m), with the lacustrine Rudník Mb. reaching up to 130 m in the north, but only ca. 40–60 m in the south (e.g., Prouza and Tásler 2001). Despite cyclic expansion/reduction as a result of short-term climate forcing (e.g., Martínek et al. 2006), the Rudník lake underwent northward retreat accompanied by general fining-upward trend in the fluvial system together with its gradual progradation towards north. This all suggest substantial waning of tectonic activity during deposition of the upper Vrchlabí Fm., contemporaneous with aridization towards the late Asselian – a general trend described from other Variscan intermontane basins (e.g., Roscher and Schneider 2006; Michel et al. 2015). Deposition in relatively low-gradient, low-accommodation setting and under pronounced arid climate is typical for overlying Prosečné Fm. (Blecha et al. 1999).

Provenance of the Vrchlabí Fm. reflects local sources such as the Krkonoše–Jizera Crystalline Complex (Martínek et al. 2012) as well as distant ones, e.g., crystalline complexes of the NE Moldanubian, or now eroded fill of the Devonian–Mississippian Jítrava–Hradec Basin (Martínek and Štolfová 2009). Additional distant source areas, as expected by W–E axial sediment dispersal, could have been found in western part of the Bohemian Massif (e.g., Teplá–

Barrandian Unit, Central Bohemian Plutonic Complex, etc.; Fig. 13a in **Chapter 3**, p. 182). In any case, diverse distant sources indicate substantial topography in the neighborhood of the PTBC during the early Permian. Clastic material from distant sources in the south may have been delivered by axial fluvial drainage of the Blanice and/or Jihlava grabens (Fig. 3).

From the late early Permian (late Asselian/Sakmarian) onwards, the gap in deposition points to a wide-scale tectonic uplift and inversion of the Pennsylvanian–Permian basins, associated with reactivation of the NW–SE-trending faults (Fig. 13b in **Chapter 3**, p. 182). The strike-slip reactivation of the Variscan basement faults has been reported from different parts of the Bohemian Massif – Bavaria (Mattern 1995a,b), Elbe Zone in Saxony (Mattern 1996), West Sudetes (e.g., Mastalerz and Wojewoda 1991; Uličný et al. 2002; Wojewoda 2007). However, the reactivation does not represent a single event, but a sequence of events spanning the Pennsylvanian–Permian (Mattern 2001).

The first phase, Namurian–Stephanian ('Silesian'), involved dextral movement compatible with the Late Paleozoic right-lateral shear zone between the Appalachians and the Urals (Arthaud and Matte 1977). Movement on the Elbe Zone during this phase was responsible for marked right-lateral offset of the Lusatian Massif and Saxothuringian (Mattern 1996). Additionaly, it may have driven formation of the NNE–SSW-oriented shear zones within the Bohemian Massif, formed as Riedel joints to the NW–SE fault zones with dextral slip. As noted by Brandmayr et al. (1995), the dextral shear within NW–SE-trending shear zones and sinistral shear within generally NE–SW-trending faults is consistent with the model of Arthaud and Matte (1977) and Matte (1986). Later, these shear zones may have been extensionally or transtensionally reactivated to form the NNE–SSW-oriented grabens (Blanice, Jihlava and Boskovice basins) strikingly oblique to the PTBC, formed during the latest Pennsylvanian–Permian (e.g., Opluštil et al. 2017). Since Brandmayr et al. (1995) argue that NE–SW-trending faults developed as a conjugate set after the Variscan N–S-trending convergence of Laurasia and Gondwana, the explanation for formation of the NNE–SSW-oriented grabens may be found in the far-field stress transfer from the Uralian Orogeny.

The second phase, early Permian ('Rotliegend'), is represented by sinistral strike-slip movement on the NW–SE-oriented faults responsible for formation of transtensional basins at the western margin of the Bohemian Massif (Mattern 1995a,b) as well as along the Elbe Zone – for instance, the Döhlen Basin near Dresden. The latter is interpreted as a 'strike-slip basin' (Zieger et al. 2019) or even as a 'pull-apart basin' (Hofmann et al. 2009). Recent data from the Permian outlier at the Lusatian Fault near Varnsdorf, N Bohemia (Nádaskay et al. 2019; Fig. 9), together with report of the Permian deposits in the Elbe Valley near Děčín that resemble those of the Döhlen Basin (Absolon 1979), indicate that to the southwest, the Döhlen Basin was
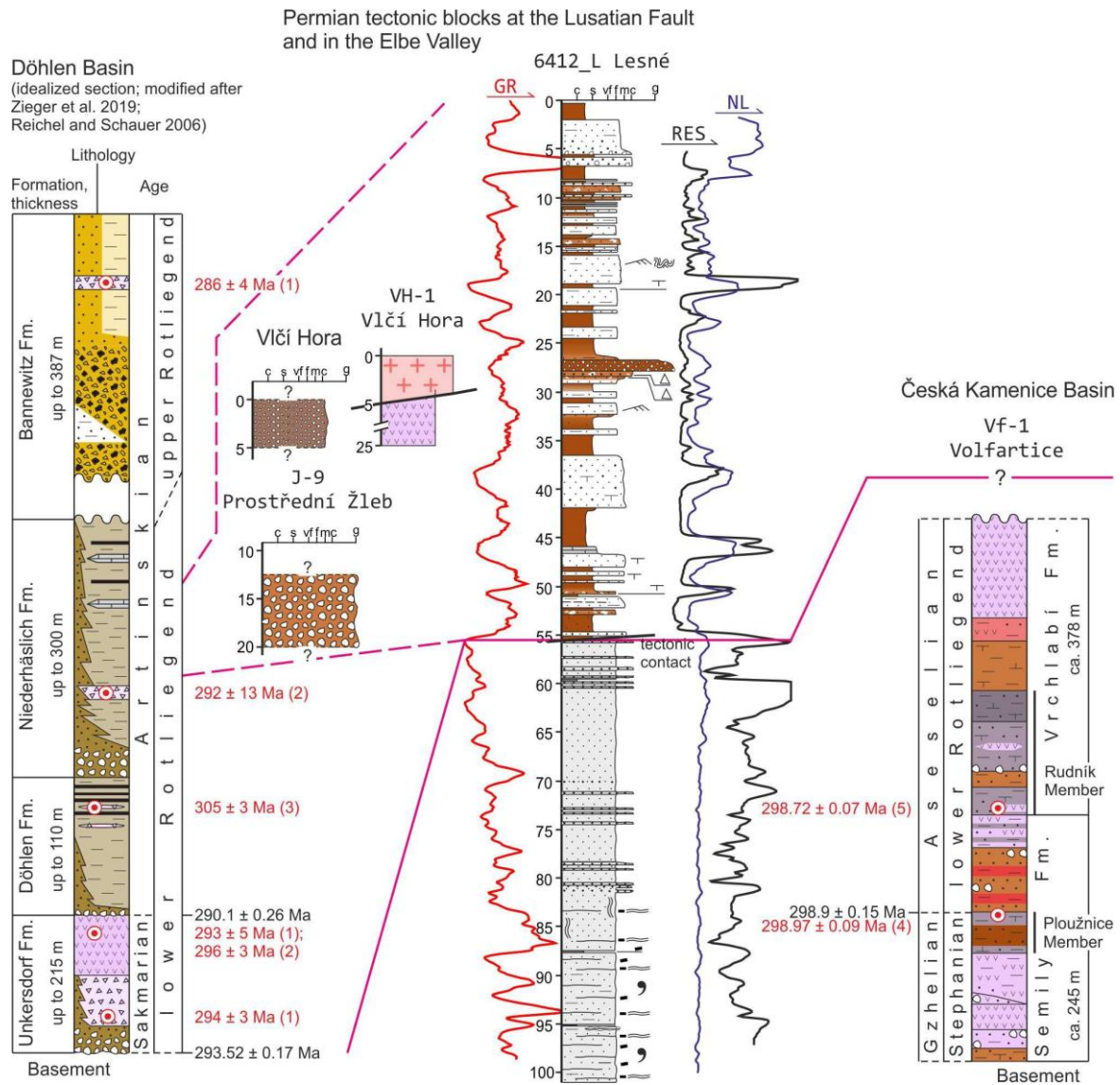
Figure 9. Correlation of the Permian at the Lusatian Fault (as recorded mainly by borehole 6412_L near Varnsdorf, N Bohemia) and in the Elbe Valley (Prostřední Žleb) with the Döhlen Basin in Saxony and Česká Kamenice Basin (ČKB) as the most proximal representative of the PTBC (sensu Cháb et al. 2008). Datums for Döhlen Basin after [1] Zieger et al. (2019), [2] Hofmann et al. (2009), [3] Hoffmann et al. (2013); for ČKB correlated from the KPB after [4] Opluštil et al. (2016 and unpublished).

neighbored by a basin of similar origin (Fig. 13b in **Chapter 3**, p. 182). This basin was later deformed and almost completely eroded as a result of the Meso-Cenozoic tectonic activity on the Lusatian Fault (Nádaskay et al., in prep.). Provenance of the Permian deposits at the Lusatian Fault (**Chapter 3**) suggest local source (Lusatian Massif) and no recycling of inverted fill of the <u>Česká Kamenice Basin</u> (ČKB) whose provenance is expected (no data so far) to be more varied (cf. Martínek and Štolfová 2009). However, at the time, the ČKB was likely located more to south, in the proximity to the Mnichovo Hradiště and Krkonoše Piedmont basins – as evidenced by similar lithofacies development (e.g., Pešek 2001). Thus, present-day spatial proximity of the ČKB and the Permian outliers at the Lusatian Fault could be an effect of later tectonic movements with strike-slip compoment. Most recent dating of syndepositional volcanic products

in the Döhlen Basin (Zieger et al. 2019) suggest that these basins may have existed sometime between 294–286 Ma (Fig. 9). The onset of deposition is, therefore, roughly coeval with onset of deposition of the Chotěvice Fm. in the KPB that unconformably overlies older lower Permian formations (Figs. 2 and 4) and comprise fluvial strata markedly coarser than those of the underlying Prosečné Fm. (Fig. 4). Arguably, deposition of the formation could have occurred as a result of incipient tectonic rearrangement of the KPB, when NW–SE faults gradually took over the W–E faults dominating in the earlier basin configuration. Whether the NW–SE-oriented (in present-day structural setting) Orlice Basin was formed by sinistral transtension during this phase, or how exactly was the sinistral strike-slip reactivation (affecting the Sudetic basins) related to the NNE–SSW-oriented basins (Boskovice Basin in this case), remains to be explored.

Presumably during the Saale phase of the Variscan orogeny, i.e., between the 'Autunian' (Asselian–Sakmarian) and 'Saxonian' (Sakmarian–Kungurian; Opluštil et al. 2016), the KPB experienced inversion accompanied by pervasive brittle deformation and coeval formation of the Trutnov–Náchod Sub-basin (TNSB), a structure governed by dextral slip on NW–SE trending strike-slip faults (Uličný et al. 2002; Martínek 2008; Fig. 13b in **Chapter 3**, p. 182). Although the TNSB use to be associated with the KPB (e.g., Pešek 2001), it represents a structurally distinct tectonic element that is superimposed on the older strata in the KPB. This is interpreted as an effect of the third phase of strike-slip reactivation of Variscan basement faults. The tectonic activity that resulted in formation of the TNSB was accompanied by generation of high-gradient topography within source areas such as the Orlice–Sněžník and Krkonoše–Jizera crystalline complexes. Danišík et al. (2010) speculate for successive unroofing and erosion of the Krkonoše–Jizera Plutonic Complex during the late early Permian ('Saxonian') based on large volumes of coarse clastics deposited in the basins south, east, and north of the Krkonoše Mts. Within the TNSB, this is evidenced by presence of alluvial-fan conglomeratic facies (Horní Město Conglomerate) in the NE flank of the basin.

Reactivation of the Sudetic faults may have been controlled during this phase by reactivation of the major NW–SE fault zones of central Europe, e.g., the Elbe Zone (sensu Scheck et al. 2002) and the Trans-European Shear Zone, that generated widsperad subsidence in the Southern Permian Basin (e.g., McCann 1998). The nature of tectonic movements in West Sudetes is consistent with the early Rotliegend (Asselian–Sakmarian) right-lateral WNW to W trending transtensional strike-slip movements that dominated in the area of the Southern Permian Basin (Gast and Gundlach 2006). The pulses of post-Variscan tectonic reorganization of central Europe led to thermal relaxation of the lithosphere as the dominant subsidence mechanism of the Late Permian to Mesozoic basin system of the northern Germany and Poland (van Wees et al. 2000; Kiersnowski and Buniak 2006) neighboring the N/NE Bohemian Massif.

Late Permian to Triassic

By the end of Permian, the Lusatian Block and its vicinity was largely planed off (e.g., Migoń and Danišík 2012), as inferred from the nature of Upper Permian ('Zechstein') deposits preserved within the TNSB and adjacent basins in Poland – non-marine siltstones, fine-grained sandstones, caliche and gypsum beds, as well as limestones, dolomites and marls of marine origin (e.g., Śliwiński 1980; Holub and Stapf 1995). The Early to (?Middle) Triassic was dominated by fluvial (Prouza et al. 1985; Kowalski 2020) to eolian (Uličný 2004) deposition of the 'Buntsandstein' facies. The subsidence during this time was generated by NE–SW-oriented dextral transtension (Kowalski 2017). At roughly the same time (ca. 250 Ma, Early Triassic), the Očkov fault of the Prague Basin, located in 'core' of the Bohemian Massif, was compressionally reactivated (Roberts et al. 2021). In accordance with other data from the interior part (Prague Basin; Glasmacher et al. 2002) as well as western boundary (Franconian Fault Zone; Hejl et al. 1997; Peterek et al. 1997) of the Bohemian Massif, Roberts et al. (2021) suggest that the Vindelician High (in boundaries similar to the Early Jurassic – as depicted in Fig. 10) experienced N–S compression at around 250 Ma. A possible cause for this otherwise poorly explored intra-plate compressional phase was likely a short-lived compression in the overriding plate caused by the subduction of the southerly Palaeotethys Ocean (Roberts et al. 2021). Following extensive Middle–Late Triassic ('Muschelkalk' and 'Keuper') marine transgressions over the Variscan Europe, the Bohemian Massif, a part of the NE–SW-extending 'Vindelician' land, was left as one of the few emerged source area in the central Europe (e.g., Ziegler et al. 1990b).

The Late Triassic to Early Cretaceous represents an enigma in the history of West Sudetic area, since the depositional record for this period is scarce (Middle–Late Jurassic) or completely missing (Late Triassic to late Middle Jurassic) within or around the West Sudetes. During the Triassic, the extension and block faulting led to the development of a series of roughly N–S-oriented grabens in central/north Germany (continued towards the Oslo Graben) along the major continent-separating suture parallel to the subsequent Mid-Atlantic Rift (e.g., Ziegler et al. 1990b). The graben system east of the Bohemian Massif acted as a feeder rift system for sediment transport from the Variscan hinterland to the subsiding foredeep in the north (McCann 1998). It was partly fed by material derived from the Bohemian Massif (e.g., Augustsson et al. 2018). The latter, or its parts, represented an emerged source area for most of the Mesozoic (cf. Paul et al. 2008, 2009; Dill and Klosa 2011; Kowal-Linka and Stawikowski 2013; Nehyba and Opletal 2016, 2017; Kowal-Linka and Walczak 2017; Kotowski et al. 2020). During this time, the Bohemian Massif, including West Sudetes, presumably experienced slowgoing peneplenization (cf. Migoń and Danišík 2012), with a significant role of deep weathering and formation of thick weathering mantles on the Paleozoic basement rocks (Migoń and Lidmar–Bergström 2001). However, since
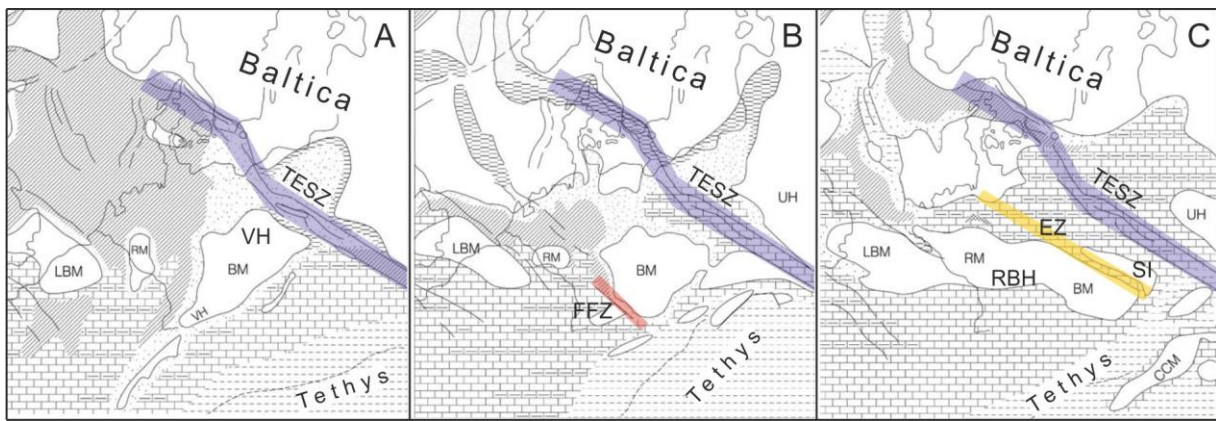
Figure 10. One of the possible scenarios of paleogeographic development of central Europe during the individual epochs of Jurassic: (A) Early; (B) Middle; (C) Late. From Pieńkowski et al. (2008), redrawn after Ziegler (1988). In this perception, the Elbe Zone (EZ)—compared to the Trans-European Shear Zone (TESZ) and Franconian Fault Zone (FFZ)—is not indicated as a major active fault zone, despite interpreted formation of conspicuous marine seaway separating the 'core' of the Bohemian Massif and the Sudetic area that presumably occurred between the Middle and Late Jurassic. Abbreviations: RBH – Rheno–Bohemian High; SI – Sudetic Island; VH – Vindelician High.

no weathering residuals from this period are reported from the Krkonoše and Jizera mts., the geological history of the northern Bohemian Massif between ca. 230–90 Ma remains unclear, as pointed out by Danišík et al. (2010).

Jurassic to Early Cretaceous

The Jurassic period in Europe was marked by significant paleogeographic changes (Fig. 10; e.g., Pieńkowski et al. 2008). The Early–Middle Jurassic uplift of the North Sea Dome and incipient extension in the area (e.g., Ziegler 1990c; Underhill and Partington 1993) significantly affected the North German Basin (e.g., Pieńkowski et al. 2008), but apparently did not affect the Bohemian Massif, a stable lithospheric block at that time.

The Bohemian Massif remained a major and coherent topographic high from Middle Triassic until at least Middle/Late Jurassic transition (Fig. 13c,d in **Chapter 3**, p. 182; e.g., Ziegler 1990b). The emergence of individual islands on this block (Fig. 10) was previously assumed as being controlled by long-term sea-level fluctuations for the most part (e.g., Ziegler 1988; Pieńkowski et al. 2008). Presence of the Jurassic deposits on southern slopes of the Bohemian Massif (e.g., Adámek 2005) and in its northern part as well as their possible remnants scattered in between those areas (e.g., Eliáš 1981), has been used as an argumet for existence of a marine seaway (termed 'Saxon strait' by Ziegler 1975) separating the 'core' of the Bohemian Massif (a part of the extensive Rheno–Bohemian High; Fig. 10c) and the Sudetic area (the 'Sudetic Island'). Possible contribution of the NW-SE-striking faults to formation of this marine seaway was brought up by Eliáš (1981) and Malkovský (1987), the latter interpreting the tectonic mechanism as wrench-fault reactivation. The Jurassic ductile reactivation is supported by reactivation of the

Rodl Fault in the southern Moldanubian at 180–170 Ma, as revealed by dating of syntectonic micas (Brandmayr et al. 1995).

The late Middle–Late Jurassic reactivation of the 'Sudetic' faults is elaborated by **Chapter 3**. Provenance of Jurassic rocks in northern Bohemia does not point to source in the Lusatian Massif, but rather suggest southerly and westerly Variscan (and reworked Cadomian) basement blocks, e.g., the Moldanubian and Teplá–Barrandian units, as major source areas. This corroborates the long-term subsidence of northern portion of the Bohemian Massif (Fig. 13b–e in **Chapter 3**, p. 182–183), already suggested by Hofmann et al. (2018). The subsidence was generated by reactivation of major Variscan strike-slip faults of the northern Bohemian Massif, i.e., Lusatian and Elbe fault zones. In long-term, the tectonic reactivation occurred during a period of gradual sea-level rise since the late Aalenian onwards (e.g., Haq 2018). Although early Oxfordian sea-level rise is implied by the paleontological data from northern Bohemia (Holcová and Holcová 2016), this period is, on the contrary, regarded as a period of sea-level fall (Norris and Hallam 1995; Haq 2018) related to global cooling event (e.g., Tremolada et al. 2006). For instance, in southern Poland and in southern part of the European Platform, the Middle–Late Jurassic boundary interval is marked by a stratigraphic gap and weathering surfaces (Pieńkowski et al. 2008). In spite of that, the onset of widespread deposition of the carbonate facies in the northern Bohemian Massif (Fig. 2) implies transgressive conditions. This strongly favor the fault-controlled mechanism of the Late Jurassic transgression that would be consistent with the major Late Jurassic phase of extensional reactivation of the Paleozoic basement, graben formation and subsidence that occurred within elements of the neighboring Mid-Polish Trough between the Oxfordian and Kimmeridgian (Gutowski et al. 2003; Krajewski et al. 2015). Furthermore, it suggests that tectonic subsidence substantially contributed to opening of the marine space between the Tethyan and Boreal seas ('Saxon strait'), though, in a paleogeographic configuration different to previously proposed models (cf. Ziegler 1975, 1990b; Eliáš 1981, and references therein). In fact, carbonate facies distribution suggest that the transgression was not limited by the Elbe and Lusatian faults, but progressed farther into the interior part of the Bohemian Massif, leaving only its core (parts of the Moldanubian and Teplá-Barrandian units) as an emerged high (Valečka 2019). In contrast to Ziegler's (1988) model (Fig. 10c), the western portion of Bohemian Massif, characterized at the time by tectonic quiescence and slow subsidence (from Jurassic until mid-Cretaceous; Hejl et al. 1997), may have been separated from the emerged Rhenish Massif by another N–S seaway, termed 'Hessian' (e.g., Meyer and Schmidt-Kaler 1989). A solitary idea that the entire Bohemian Massif was completely submerged during the Late Jurassic (Matyja and Wierzbowski 1995) cannot be completely excluded until more detailed provenance analysis of the Upper Jurassic deposits in basins surrounding the Bohemian Massif. The absence of post-

Oxfordian deposits on the passive southern margin of the Bohemian Massif (e.g., Adámek 2005) is not diagnostic, since they may have been removed by later tectonic processes. However, presence of breccia with clasts of silicified limestones with bauxite cement of presumably Kimmeridgian age in the Blansko Graben (N of Brno) suggest, according to Bosák (1978), that this part of the Bohemian Massif was exposed to tropical lateritic weathering during the Late Jurassic. Subaerial exposure of the Jurassic deposits may have been caused by marine regression (Bosák 1978) or by tectonic uplift on the graben flanks (cf. Käßner et al. 2020).

To sum up, the late Middle to Late Jurassic tectonic reactivation in the northern Bohemian Massif facilitated formation of hypothetical basin extending over the Lusatian Block and adjacent areas, as originally concieved by Voigt (1994, 2009). The formation of this basin, tentatively termed as 'Lusatian Basin' (or 'Prignitz–Lausitz Basin' sensu Voigt 2009), was corroborated by provenance analysis (Hofmann et al. 2018 and **Chapter 3**). The extensive tectonic event that affected the central Europe during the Middle–Late Jurassic and, among other effects, established the Lusatian Basin and governed transgression over vast part of the Bohemian Massif, can be explained as a result of far-field stress transfer from the initiating North Atlantic Rift (e.g., Malkovský 1987; Ziegler 1990c; Doré 1991; Erratt et al. 1999).

Not only did the Lusatian Basin exist beyond the Jurassic/Cretaceous boundary, it is likely it experienced intensified basin-floor subsidence accompanied with increasing influx of sedimentary material, too. Based on apatite fission-track (AFT) ages and thermal history modelling of the Upper Cretaceous near Dresden and Weißig Basin (Permian outlier on the Lusatian Massif; Fig. 5), Käßner et al. (2020) interpret exhumation of these units at ca. 150–120 Ma (Tithonian–Aptian). It must have occurred in extensional setting, probably on the graben flanks of the Lusatian Basin, bounded by synthetic normal faults (Käßner et al. 2020). This assumption is consistent with AFT data from neighboring Erzgebirge Crystalline Complex (Ventura and Lisker 2003) that indicate a cooling event between 160 and 130 Ma (Oxfordian–Hauterivian). Interpreted extension in the study area is coeval with general extension/subsidence trend, interrupted by minor uplift events, recorded within the neighboring Mid-Polish Trough (e.g., Gutowski et al. 2003). Additionaly, continuous piling of sediment during at least part of the Early Cretaceous is the only way to explain presenece of substantial amount of Baltica-derived zircons within the Upper Cretaceous formations of the NW Bohemian Cretaceous Basin (see **Chapter 3**).

The Early Cretaceous paleogeographic setting of central Europe (Fig. 11) seems to be the most favorable for delivery of recycled material containing the Baltica-sourced zircons from emerged basement highs in the northern Germany towards the northern Bohemian Massif (Fig. 13e in **Chapter 3**, p. 183). As demonstrated by, e.g., Vejbæk et al. (2010) and Schneider et al.

(2018; Fig. 11), area north and east of the Bohemian Massif was dominated by fluvial–lacustrine and deltaic to shallow-marine clastic depositional systems during Early Cretaceous capable of sediment transport from areas on the southern margin of Baltica to the northern Bohemian Massif. Hypothetical Early Cretaceous-aged deposits of the Lusatian Basin may have represented the eastern continuation of 'Wealden' facies, i.e., the Lower Cretaceous (Berriasian–earliest Aptian) non-marine deposits of SE England, and their counterparts in the North German Basin (Wealden-type deposits are dated here as mid–late Berriasian; Schneider et al. 2018). Marked paleogeographic changes in central Europe likely occurred in reaction to episodes of eustatic sea-level fall – minor early Berriasian and major latest Berriasian–Valanginian (e.g. Haq 2014).

Although the Middle Jurassic sandstones in the northern Germany contain significant proportion of the Baltica-sourced zircons as well (Hofmann et al. 2018), the deposits of the same age in the Lusatian Basin could not have been a source of these zircons recycled into the Upper Cretaceous – the Middle and Late Jurassic deposits in northern Bohemia are practically devoid of these zircons (Fig. 11 in **Chapter 3**, p. 178). Although Hofmann et al. (2018) correctly identified their primary Scandinavian source, they misinterpreted the process of their delivery towards the northern Bohemian Massif. Although extensive deltaic depositional system developed south of Baltica in northern Germany during the Early–Middle Jurassic, its maximum extent during the Aalenian only reached the area approximately south of Berlin, and was not capable of delivering large amounts of clastic material towards the north Bohemian Massif (Zimmermann et al. 2015; M. Franz, J. Zimmermann, pres. comm.). Therefore, the Middle Jurassic sandstones must have undergone recycling into the Lusatian Basin during the Early Cretaceous. Additionaly, deposition of the Early–Middle Jurassic nearshore–deltaic sequences was not influenced by thermal doming in the North Sea area (Zimmermann et al. 2015), which contradicts the interpretation of Hofmann et al. (2018) that the sudden Middle Jurassic input of Baltica-sourced zircons to the North German Basin during was caused by uplift of the North Sea Dome.

Circumstances around cessation of the Lusatian Basin are unknown. However, published AFT data on exhumation of basement blocks in the northern Bohemian Massif provide approximate time constraints of its inversion. Firstly, preserved thickness of the Upper Cretaceous sandstones deposited in the Lužice–Jizera sub-basin (BCB), ca. 1 km, as well as estimated erosion of additional at least 500 m (Uličný et al. 2009b), implies that from mid-Cretaceous onwards, a substantial amount of material covering the Lusatian Block was eroded and redeposited into the BCB. Danišík et al. (2010) assumed that ca. 3.6–6 km (maximum, ca. 2.6–5 km, during the Late Cretaceous, at ca. 100–75 Ma) of overburden was removed from the Krkonoše–Jizera Massif since the Permian. Similarly, Käßner et al. (2020) assume that ≥3–4 km of overburden was removed from the Lusatian Block and Kořínková et al. (2013) estimated ca. 4
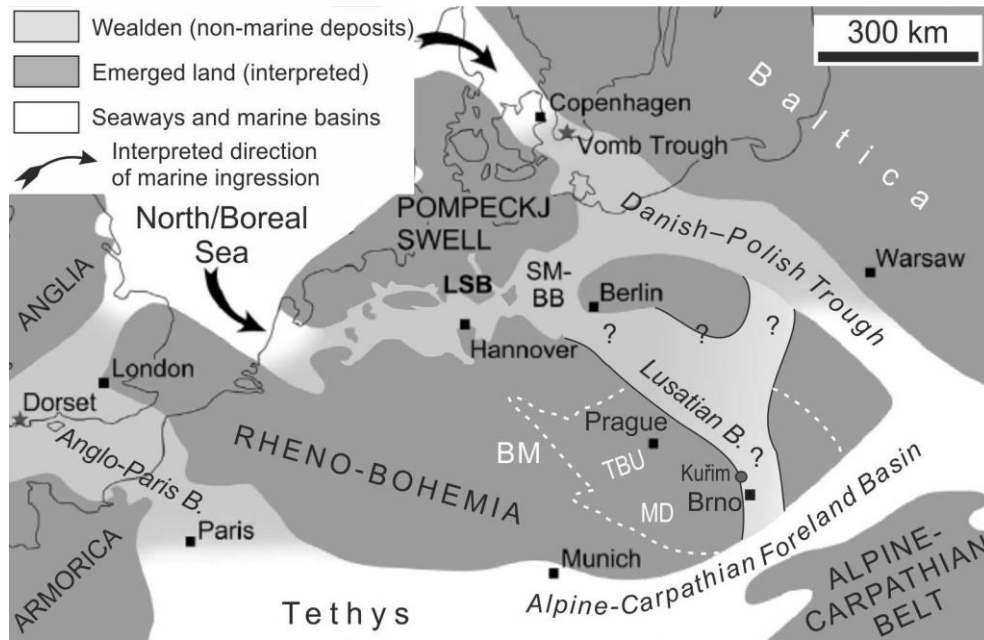
Figure 11. The Early Cretaceous paleogeography of the central Europe as compiled by Schneider et al. (2018), for the Berriasian (although the paleogeographic setting corresponds rather to the Aptian, cf. Mutterlose and Böckel 1998), amended. Lusatian Basin extetnds in the NE part of the Bohemian Massif. Kuřim, a locality with Aptian–Albian limestomes, is indicated. Abbreviations: LSB – Lower Saxony Basin; SM-BB – Südmecklenburg–Brandenburg Basin. Dashed line indicate approximate position of the present-day Bohemian Massif with its interior parts discussed in the text: MD – Moldanubian; TBU – Teplá Barrandian Unit.

km (since the Late Triassic). Part of this overburden was likely represented by the Jurassic–Lower Cretaceous sedimentary fill of the Lusatian Basin. The uplift of the Lusatian Block is dated by the AFT at early Cenomanian, ca. 97 Ma, in its southern part (Krkonoše–Jizera Massif; Danišík et al. 2010) and ca. 100–95 Ma in the northern (Lusatian Massif; Käßner et al. 2020). Thus, the final inversion of the Lusatian Basin must have taken place prior to the Albian/Cenomanian transition.

More exact answer can be found in depositional record of basins neighboring the Bohemian Massif. In the Mid-Polish Trough, the major uplift is dated as having occurred sometimes between middle and late Albian (Gutowski et al. 2003) and is recorded by conspicuous unconformity (e.g., Krzywiec et al. 2018) underlying the upper Albian transgressive sediments. The gap in deposition is constrained between the middle Albian *Hoplites dentatus* and the late Albian *Mortoniceras inflatum* ammonite zones (Leszczyński 1997), i.e., approximately between 109.5 and 104 Ma (Ogg et al. 2012). Moreover, provenance of the Albian sandstones of the 'Miechów Synclinorium' (southern Mid-Polish Trough) suggests the Svratka Crystalline Complex (W Moldanubian) and metamorphic terrains of East Sudetes as source areas (Kotowski et al. 2020). This is consistent with source areas interpreted for the Lower–Middle Triassic deposits in the Opole Basin (Silesia, E margin of the Bohemian Massif; Kowal-Linka and Stawikowski 2013; Kowal-Linka and Walczak 2017) and implies that the eastern Bohemian Massif had been uplifted at the time of middle–late Albian transgressions in the southern Mid-

Polish Trough that was supplied by clastic material recycled from the Triassic. Additionaly, it could have been supplied by recycled pre-Albian Lower Cretaceous fill of the inverted Lusatian Basin, whose primary source area had been located presumably in the Moldanubian (incl. the Svratka C. C.), possibly through fluvial drainage with easterly outflow.

Within the Lower Saxony Basin (a part of the N. German Basin) with continuous Lower Cretaceous deposits, a major regression is recorded by enhanced progradation of the Osning/Roth (Münsterland depocenter) and 'Hilssandstein' (Subhercynian depocenter) sandstones and their correlative counterparts in the Prignitz and Altmark basins during the late Aptian–early Albian. The overlying marls labelled as '*minimus* Clay' mark the middle Albian (base *Hoplites dentatus* zone) transgression following a minor depositional gap in the end of early Albian. Subsequent, more extensive transgression at the base of 'Flammenmergel' marls, slightly preceding the *Mortoniceras inflatum* zone, is already late Albian (Voigt et al. 2008). As demonstrated, the overall trend and its timing is not unlike that recorded in the Mid-Polish Trough. Thus, it is inferred that the evolution of both basins was influenced by similar mix of large-scale processes (e.g., eustasy and far-field stress transfer).

The Mesozoic depositional record of the Alpine Foreland Basin (SW margin of the Bohemian Massif) shows a major depositional gap between the upper part of Berriasian and the upper part of Albian (Gross et al. 2015, and references therein). It is possible that the Early Cretaceous inversion of the Bohemian Massif prograded in S–N direction proportionally with proximity to the nascent Alpine–Carpathian Belt, given that far-field stress transfer from this area was its driving mechanism. This event terminated deposition in the Lusatian Basin and initiated unroofing of the Lusatian Block and its re-establishment as a source area (the West Sudetic Island; Fig. 13f–h in **Chapter 3**, p. 184–185) during the late Cenomanian.

Although far outside the study area, scarce remnants of the Early Cretaceous deposits on the Bohemian Massif carry certain importance for paleogeography in terms of the upcoming mid-Cretaceous transgressions. Micrite to biomicrite limestones with Aptian–Albian microfauna transgressively deposited over granitoids of the Brno Massif near Kuřim, are interpreted to represent a vestige of initial, limited marine ingression from the Tethyan realm south of the Bohemian Massif (Krystek and Samuel 1978). Uncertain Albian-age palynomorphs reported from the lowermost paleovalley fill in the Blansko Graben (Svobodová and Brenner 1999) insinuate that transgression leading to eventual creation of the BCB set on already in the latest Early Cretaceous. To the east of Bohemian Massif, the Late Cretaceous depositional cycle starts with gradual transgressions from the late Albian through Cenomanian (e.g., Marcinowski and Radwanski 1983) as a result of the late Albian to presumably early Turonian extension (e.g., Gutowski et al. 2003).
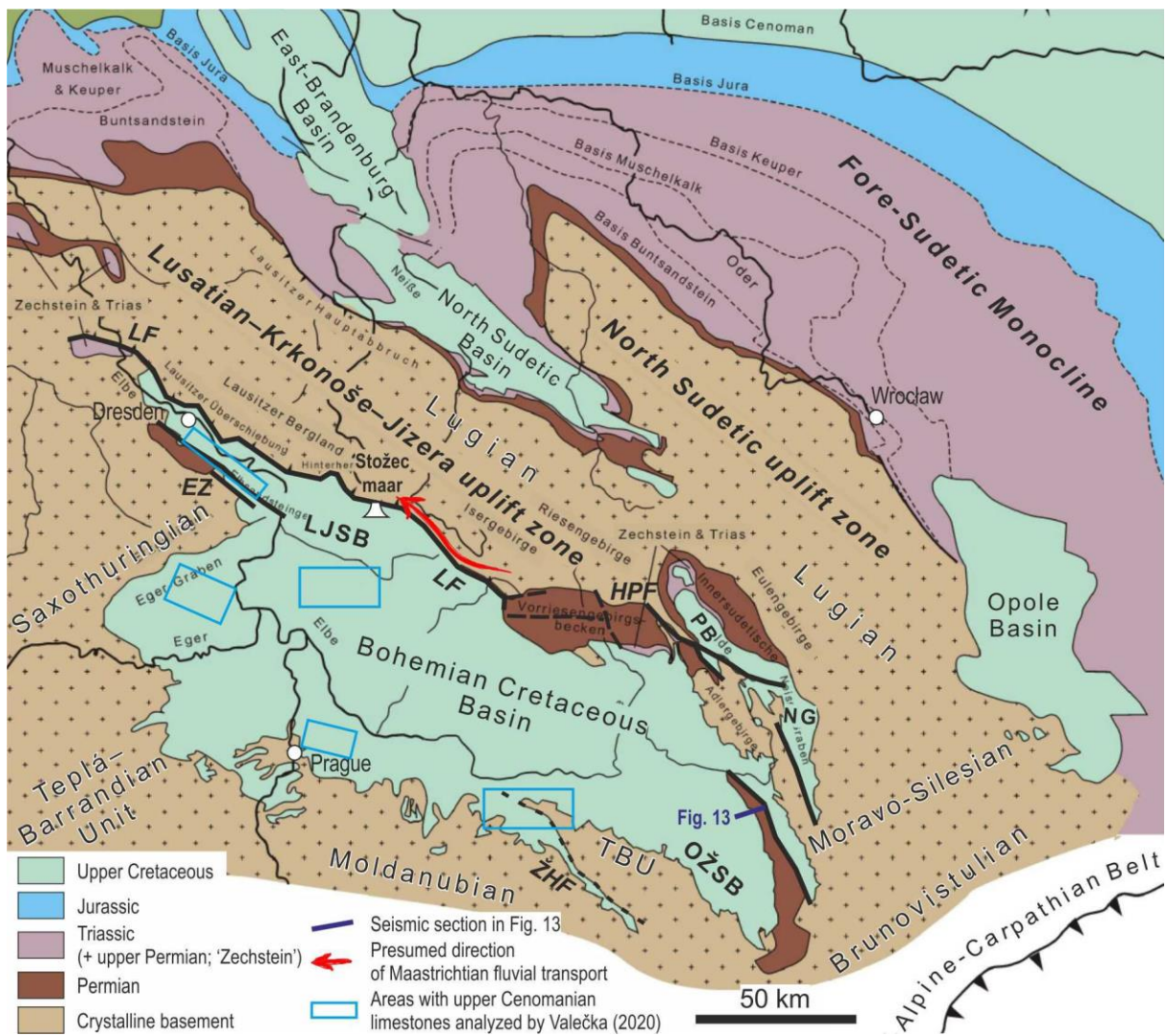
Figure 12. A simplified map showing the present day geological situation of the northern Bohemian Massif; taken from Voigt (2009), amended. The Bohemian Cretaceous Basin as well as neighboring Late Cretaceous basins are displayed in their present-day erosional boundaries. Main faults and other features discussed in the text are indicated. The term 'uplift zone' ("Antiklinalzone" sensu Voigt 2009) denotes extensive basement areas exposed to long-term generally upward-directed vertical movement during the Late Cretaceous–Cenozoic. Abbreviations: EZ – Elbe Zone; HPF – Hronov–Poříčí Fault; LF – Lusatian Fault; LJSB – Lužice–Jizera sub-basin; NG – Nysa Graben; OŽSB – Orlice–Žďár sub-basin; PB – Police Basin; ŽHF – Železné Hory Fault.

Late Cretaceous

The Late Creaceous paleogeography of central Europe (Fig. 1a in **Chapter 2**, p. 106, and Fig. 1b in **Chapter 3**, p. 160) was governed by two major factors: (1) Major eustatic sea-level changes that resulted in two distinct transgressive-regressive cycles that dramatically changed the landmass/shelf sea proportion (cf. Ziegler 1990b) in central Europe through epicontinental marine flood. The earlier of these eustatic-driven pulses, late Albian–early Coniacian, exerted significant influence on paleogeography of the Bohemian Massif. (2) Tectonic reactivation of the Variscan basement faults (e.g., the Elbe Zone). The interplay of both factors established the Bohemian Cretaceous Basin (BCB), a complex system of sub-basins (partly separated from each

other by post-Late Cretaceous tectonic processes; Fig. 12) that represented one entity in terms of paleogeography (e.g., Voigt et al. 2008), fauna (Košťák et al. 2004), marine current regime (Mitchell et al. 2010) and depositional process (e.g., Uličný 2001).

The overall trend of sea-level rise during the Cenomanian (e.g., Wilmsen et al. 2019) significantly contributed to formation of an epicontinental seaway ('Bohemian strait') in the N/NE Bohemian Massif during the late Cenomanian (Uličný et al. 2009a). Importance of rising sea-level trend during the middle Cenomanian–early Turonian is illustrated by filling of the mid-Cretaceous paleovalley system that formed across the northern Bohemian Massif and was controlled by multi-phase, long-term sea-level rise rather than by tectonic subsidence (Špičáková et al. 2014). Additionaly, the late Cenomanian and early–late Turonian sea-level fluctuations partly controlled basinwide creation of accommodation space, both in a relatively long- (first Myr) and short-term (10–100 Kyr scale; e.g., Uličný et al. 1997, 2009b, 2014). On the contratry, the long-term (ca. 5 Myr) creation of accommonation space is interpreted as resulting from tectonic layout of the basin (Uličný et al. 2009b). Moreover, accelerated subsidence during the late Turonian–Coniacian driven by incipient tectonic inversion of the BCB (e.g., Uličný et al. 2009b; Nádaskay and Uličný 2014; **Chapter 2** of this thesis), makes it uneasy to quantify the eustatic component of accommodation rate (Uličný et al. 2009b).

The tectonic processes behind the basin-floor subsidence and creation of accommodation space, at the same time generated uplift of certain basement areas that initially served as drainage divides of paleovalley systems (Uličný et al. 2009a) and later, after the late Cenomanian transgression, formed emerged highs (islands) surrounding the basin. These emerged highs are represented by the Rheno–Bohemian Massif (RBM; also termed as the Mid- or Central European Island) on the W/SW and the Sudetic Islands in the E/NE. The eastern margin of RBM, formed by parts of the Moldanubian and Teplá–Barrandian units, is interpreted as being mostly tectonically inactive and 'passively' transgressed gradually between the late Cenomanian–early Turonian (e.g., Žítt et al. 1997, 2006; Čech et al. 2005; Valečka 2020), and partly faulted, as evidenced by formation of the Orlice–Zďár sub-basin (Uličný et al. 2009b). On the contrary, the Sudetic Islands were established as faulted, uplifted blocks and, as such, played a role of principal source areas (e.g., Čech 2011). While the East Sudetic Island (ESI) has been discussed (see overview in Biernacka and Józefiak 2009) in terms of exact extent and compactness (one or more islands?), the West Sudetic Island (WSI; represented by parts of the present-day Lusatian Block), relevant for this thesis, is relatively well-constrained in space and time (e.g., Skoček and Valečka 1983; Uličný et al. 2009b; Niebuhr 2018). A development of depositional architectures and processes (e.g., Uličný 2001; Uličný et al. 2009b; Nádaskay and Uličný 2014; Čech and Uličný

2021; and **Chapter 2** of this thesis) as well as provenance data (Hofmann et al. 2018; **Chapter 3**) prove that the WSI represented a source area for the adjacent Lužice–Jizera sub-basin (LJSB).

Based largely on present-day configuration of the basement areas and their juxtaposition with erosional remnants of the Late Cretaceous basins, it was interpreted that mostly crystalline source rocks, particularly granitoids, were exposed on the WSI (e.g., Skoček and Valečka 1983). However, not only a marked disproportion between presumed source and final product (mature, well-sorted, quartzose sandstones), but chiefly provenance of the Cenomanian–Santonian sandstones of the LJSB (e.g., Hofmann et al. 2018; **Chapter 3**) suggest that basement of the Lusatian Block once had a sedimentary cover. This sedimentary cover was deposited as infill of the hypothetical Middle/Late Jurassic to Early Cretaceous Lusatian Basin. Its final inversion transpired prior to the middle/late Albian and together with consequent removal of its deposits is assumed from a depositional gap in the study area between the Late Jurassic and Cenomanian. Reworking of the sedimentary cover of Lusatian Block, suggested by Hofmann et al. (2018), has been proven (**Chapter 3**) by preesence of Paleo-/Mesoproterozoic-aged zircons found in the Upper Cretaceous that could not have been sourced from within the basement of Bohemian Massif and their primary source area can be found on the SW margin of Baltica. The Late Cretaceous paleogeographic a depositional setting of central Europe excludes direct sedimentary input from SW Baltica to the BCB. Furthermore, the Baltica-sourced zircons could not have been recycled from Jurassic deposits of the previously interpreted 'Saxon Strait' basin (cf. Ziegler 1975) separating the emerged Lusatian Block from the Rheno–Bohemian Massif, because the Middle/Late Jurassic deposits of northern Bohemia practically do not contain such zircons. If the Baltica-sourced zircons were recycled from the Middle Jurassic sandstones of northern Germany, as claimed by Hofmann et al. (2018), this had to be carried out by additional round of recycling. It is interpreted that paleogeographic situation and depositional setting (cf. Vejbæk et al. 2010; Schneider et al. 2018; Fig. 11) of central Europe during the Early Cretaceous represent the most favorable situation to deliver the Baltica-sourced zircons (see section Jurassic–Early Cretaceous). Several other lines of support exist for the basin-scale recycling: (1) the heavy mineral spectrum of Upper Cretaceous rocks is anomalously rich in zircons (up to ca. 70 %), which points to maturity of source deposits, and hence, suggest multi-phase recycling; (2) The Upper Cretaceous sandstones exhibit mineralogical maturity and sorting that, together with general lack of material derived directly from weathered granitoids (rich in kaolinite clay, kaolinized feldspar grains and rock fragments and micas), indicates a supply from older, mature sedimentary rocks, possibly in combination with further sorting by marine currents in a nearshore setting (e.g., Uličný 2001); (3) Thermochronological data indicate that surprisingly thick overburden, up to several km, was removed from in different parts of the Lusatian Block.

The latter approach revealed that ca. 3.6–6 km of overburden was removed from the SE part of Lusatian Block (Krkonoše–Jizera Massif) since Permian, with maximum erosion (ca. 2.6–5 km) at around 100–75 Ma (Cenomanian–Campanian), a time interval roughly coinciding with the existence of the BCB. In the NE part of Lusatian Block (Lusatian Massif) Käßner et al. (2020) imply removal of ca. 3–4 km of overburden; consistently, data of Ventura et al. (2009) point to a minimum denudation of 3 km of the Lusatian Block in the Late Cretaceous.

The detrital zircon spectra (Figs. 9 and 11 in **Chapter 3**, p. 176 and 178) are consistent with the termochronological data, as discussed above, as well as with the sedimentary record. The latter indicate intensified creation of accommodation in the LJSB and elevated sediment supply from the WSI since the late Turonian (e.g., Uličný et al. 2009b; Nádaskay and Uličný 2014; and **Chapter 2** of this thesis). Uplift of the source area, as revealed by the Late Cretaceous detrital zircon spectrum, may have taken place in two phases – late Cenomanian, followed by a period of decelerated tectonic activity in the early–middle Turonian, and late Turonian–Coniacian. Moreover, eastward progradation of sandstone wedges adjoining the Erzgebirge Crystalline Complex (Uličný et al. 2009b) and interpreted contribution from the late-Variscan crustally-derived Saxothuringian granites point to temporary emergence of an additional source area – the Most–Teplice High (present-day eastern Erzgebirge Mts.). Further stratigraphic trends in the heavy mineral spectra (**Chapter 3**) indicate that during the late Turonian–Coniacian, the erosion of the WSI reached pre-Jurassic rocks. Moreover, increasing complexity of clay minerals in younger deposits (Štaffen 2002) may indicate contribution of diverse source rocks and could be interpreted in terms of accelerated differential uplift of individual fault-bounded blocks and variable fluvial incision within the WSI from the latest Turonian onwards (Fig. 13h–i in **Chapter 3**, p. 185; see also Sobczyk et al. 2015). Unfortunately, this record of elevated influx of clastic material cannot be abstracted from marine Sr isotope curve (**Chapter 2**).

A removal of substantial part of deposits of the Lusatian Basin is interpreted to take place by the end of Coniacian, as signalized by the Santonian increased input from granitic rocks (Fig. 11 in **Chapter 3**, p. 178) of rapidly uplifting Krkonoše–Jizera Massif. This Santonian 'event' marks the onset of subsequent phase of the inversion when the basin became substantially narrowed with the main depocenter shifted to near the Lusatian Fault, reactivated as a reverse fault (Fig. 13i in **Chapter 3**, p. 185). Additionaly, a seaway between the West and East Sudetic islands was closed (Leszczyński 2018) and the deposition eventually ended purportedly later during the Santonian (e.g., Voigt et al. 2008). The end of deposition is also constrained at early–middle Campanian by emplacement of the oldest ultramafic dykes in the northern Bohemian, dated at ca. 79–77 Ma (Pivec et al. 1998; Skála et al. 2015) – as originally conceived by Klein et al. (1979). Timing of final inversion of the BCB is supported by AFT data as well. For instance, data

of Ventura et al. (2009) imply uplift of the Lusatian Massif after ca. 94 (around Cenomanian/Turonian boundary) with most ages between ca. 89 and 72 Ma (early Coniacian to Campanian/Maastrichtian boundary), while Käßner et al. (2020) suggest that the major part of basin inversion occurred around 80 Ma (middle Campanian). Farther south (Krkonoše–Jizera Massif), the inversion is interpreted to take place between ca. 90 and 75 Ma (Turonian/Coniacian boundary to late Campanian; Danišík et al. 2010).

As implied above, the most intriguing episode of the lifetime of BCB occurred over 15 Myr during the Coniacian–Campanian, with substantial part of depositional record of the Santonian–Campanian age removed by later tectonic and erosional processes. While sedimentological works (Skoček and Valečka 1983; Uličný et al. 2009b) estimated few hundreds of meters of inverted basin fill to be removed, most recent data show that 2–3 km (AFT; Käßner et al. 2020) or ca. 3 km (vitrinite reflectance; Danigel et al. 2019) of the Late Cretaceous deposits may have been removed from the Lusatian Block. This is in accord with earlier assumption of Danišík et al. (2010) that ca. 3.6 km of deposits have been eroded since the Turonian.

A remaining Late Cretaceous history of the Bohemian Massif until Eocene (oldest deposits preserved within the Eger Graben) is veiled. However, recent reseach of maar diatremes cross-cutting infill of the BCB and dated as Maastrichtian (Wenger et al., in prep.; E. Wenger, O. Tietz, pres. comm.) revealed that these diatremes comprise 'exotic' sedimentary material formed by well-rounded quartzite boulders (likely derived from Ještěd or Železné Hory crystalline complexes) embedded within reddish fine-grained matrix (reworked Permian). Tentatively, this sediment is interpreted as a remnant of Maastrichtian fluvial system that—being active during an overall uplift of northern part of the Bohamian Massif that did not facilitate sediment preservation—would not leave a trace if its deposits are not trapped within the maar structure. A thalweg of this fluvial drainage may have been tectonically predefined by the Lusatian Fault (Fig. 12), similar to the Cenomanian fluvial system (Uličný et al. 2009a).

The Bohemian Cretaceous Basin was established, and later destructed, by intra-plate deformational processes that were of regional scale and involved vast region of the pre-Mesozoic basement in the Alpine foreland. This is implied by a broader picture of central European basins, where gradual deformation of basin margins was accompanied by basement-involved thrusting and deep erosion of uplifted flanks. Similar processes as inferred above for the BCB, were documented in the Mid-Polish Trough as well as north German basins (e.g., Krzywiec and Stachowska 2016; Krzywiec et al. 2018; von Eynatten et al. 2008; Voigt et al. 2021). The main phase of the Late Cretaceous intra-plate shortening used to be placed between the late Turonian and Campanian (ca. 86–70 Ma; e.g., Ziegler et al. 1995; Vejbæk and Andersen 2002; Kockel 2003; Voigt et al. 2004; Krzywiec 2006), interpreted as reflecting continental collision in the Alps (e.g.,
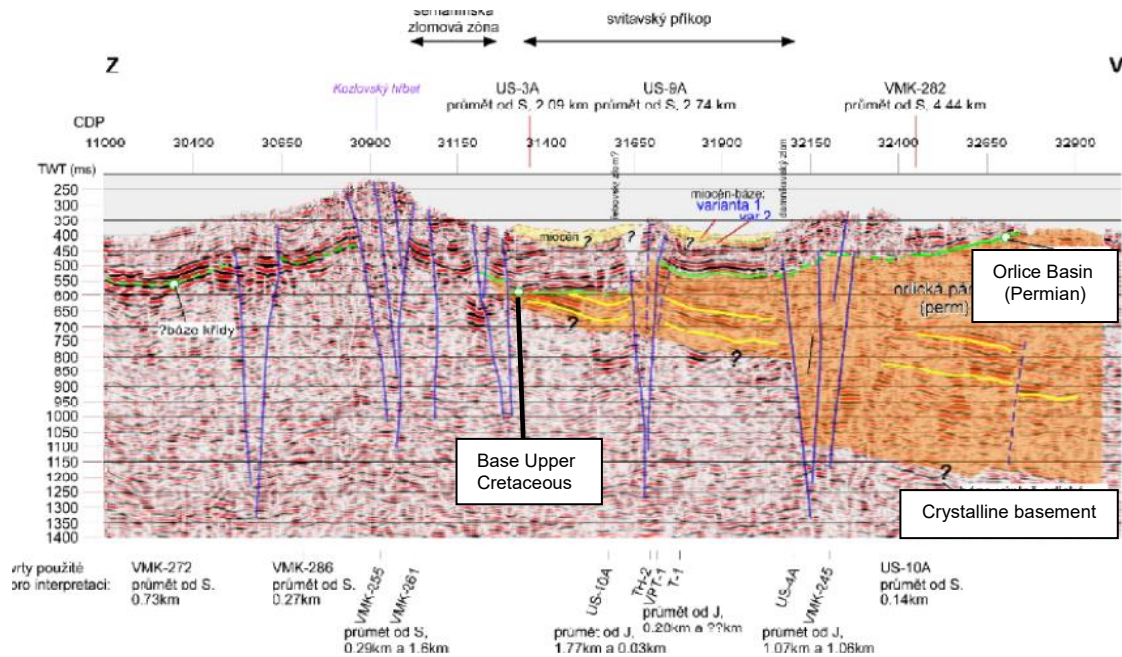
Figure 13. Preliminary interpretation (Uličný et al. 2015) of the reflexion seismic section RBSP/2011 – A, whose acquisition was funded by Czech Geol. Survey project "Re-evaluation of groundwater resources". The section is located on the present-day SE margin of the BCB, at the boundary of the Vysoké Mýto 'syncline' and the Permian Orlice Basin (in orange). The interpreted flower structures indicate presence of strike-slip faults trending perpendicular to the section (i.e., in generally N–S direction). Note that Upper Cretaceous deposits does not thicken towards the strike-slip faults, as would be expected in transtensional/pull-apart basins; a brittle deformation, thus, post-dates the Late Cretaceous depositional processes.

Marotta et al. 2001; Ziegler 1990a; Ziegler et al. 1995), partucularly its 'Laramide' (Campanian–Maastrichtian) phase or its precursor events. Alternatively, coeval convergence of Africa–Iberia–Europe is offered as an explanation (Kley and Voigt 2008). However, these processes commenced, as recently suggested by Voigt et al. (2021), relatively synchronously at ca. 95 Ma (late Cenomanian), five million years earlier than commonly assumed.

This notion suggest that in case of the BCB, the acceleration of basin-floor subsidence, together with elevated sediment supply resulting from coeval uplift of the basin margin, does not really mark the onset of inversion, but rather its substantial acceleration. The onset of inversion could be placed into the late Cenomanian. In the light of new data on the compressional deformation of Alpine foreland, it is possible to revisit the concept of Uličný (2001) and Uličný et al. (2009a,b) that the BCB was established as a transtensional basin system formed by reactivation of major NW–SE-trending strike-slip faults. In this concept, the 'Lusatian Fault Zone' and 'Labe–Železné Hory Fault Zone' are interpreted as basin's principal displacement zones responsible for formation of individual 'pull-apart sub-basins' (Uličný 2001). However, several factors testify against this concept.

So far, there is no evidence for syndepositional activity of large-scale, NW–SE-oriented strike-slip fault systems (cf. Coubal et al. 2015). Although features associated with strike-slip

faults have recently been interpreted (Fig. 13; Uličný et al. 2015) on seismic sections from eastern part of the BCB, they may have been generated by post-depositional deformation. The Lusatian Fault must have been active during the Late Cretaceous, as evidenced by large amount of Cenomanian–Coniacian sandstones deposited in the adjacent LJSB. Creation of accommodation space for these deposits cannot be explained in terms of eustatic sea-level rise only (e.g., Uličný et al. 2009b). An evidence of lateral movement on the Lusatian Fault has been reported (Coubal et al. 2015), but these movements occurred during at least three Cenozoic–Quaternary phases, and were rather subtle, counting few hundreds of meters. However, there is no evidence for the Late Creatceous strike-slip regime on the Lusatian Fault (cf. Coubal et al. 2015). Furthermore, a SE continuation of the Lusatian Fault beyond the Krkonoše Piedmont Basin (KPB), as proposed by Uličný (2001) and Uličný et al. (2009b), is largely speculative. It is interpreted that the Lusatian Fault terminates in the NW tip of the KPB whose western margin is deformed as a fold structure termed Koberovy 'flexure' (Prouza et al. 2013). Instead, major brittle tectonic structures are W–E-oriented faults that governed subsidence of the KPB during the early Permian (Fig. 13 in **Chapter 1**, p. 89), represented by present-day Škodějov and Kundratice–Javorník faults. These faults may have accommodated W–E offset of the major NW–SE-trending tectonic structures reactivated in the area during the Late Cretraceous, i.e., the Lusatian and Hronov–Poříčí faults.

At the present-day southern tectonic margin of the BCB, the Železné Hory Fault (ŽHF) does not propagate farther NW to join the Elbe Zone – at least this is not evidenced by changes in thickness of the Upper Cretaceous. The interpretation of Uličný (2001) and Uličný et al. (2009b) that the ŽHF and Elbe Zone form one, large-scale tectonic structure (labelled as 'Labe–Železné Hory Fault Zone'), a southern principal displacement zone to the Lusatian Fault, is probably incorrect. Moreover, a present-day marked tectonic boundary between the Upper Cretaceous and Železné Hory Mts. crystalline basement was formed by multiphase reactivation of the ŽHF as thrust and strike-slip fault most likely during the Cenozoic (cf. Coubal et al. 2019).

A presence of abundant local highs in the pre-Cretaceous paleorelief in marginal as well as axial part of the basin, that existed until early/middle Turonian, indicate that the basement morphology significantly influenced deposition of the basal marine Korycany Mb., with highest thickness in the narrow, marginal nearshore zone off the axial part of the basin (Valečka 2020). This implies, according to Valečka (2020), a leading role of late Cenomanian eustatic sea-level rise in flooding of NE portion of the Bohemian Massif. Exceptionall large thickness (ca. 100–125 m) of the Korycany Mb. is known from a narrow area in the LJSB – proximity of this thick package of coarse siliciclastic deposits (sandstones, conglomerates in places) to the Lusatian Fault indicates that unlike in the rest of BCB, deposition of the Korycany Mb. in this area was partly controlled by tectonic subsidence. In general, thickness of the Korycany Mb. accumulated during
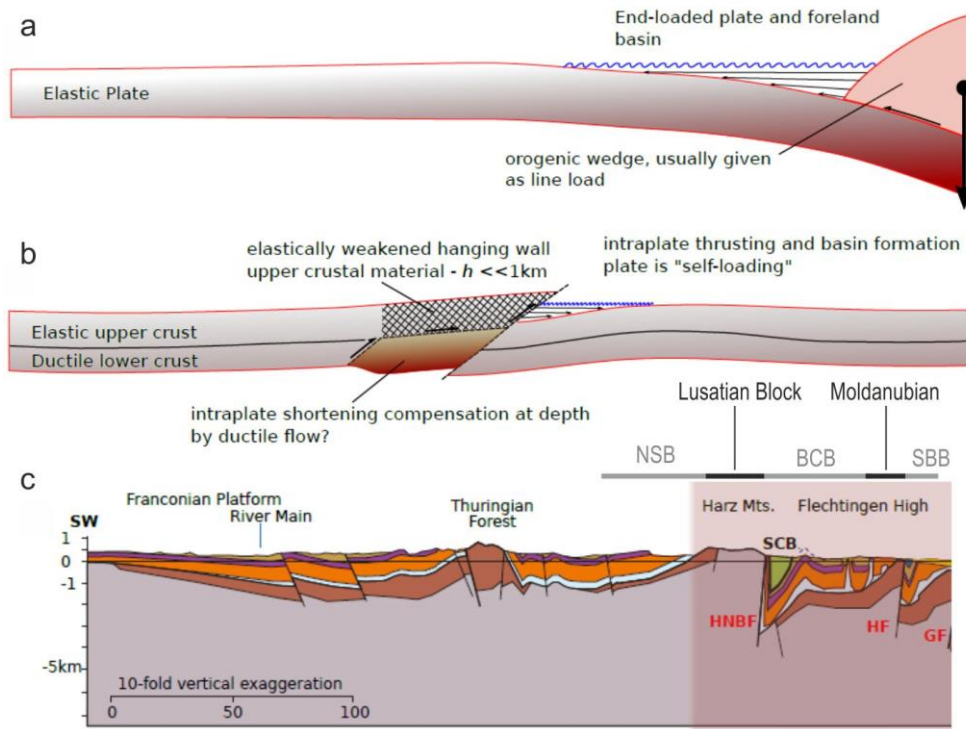
Figure 14. Schematic depiction of deformation mechanism leading to formation of foreland basins (from Hindle and Kley 2020): **(a)** By edge-load on the end of a plate typical of subduction zones; **(b)** By intraplate deformation-associated flexural basin from this paper with an assumed elastically weakened hanging wall and a basement thrust transecting most or all of the elastic crust and possible local weakening of the rest of the lithosphere.
(c) Interpreted deformation of a broader vicinity of the Harz Mts. with adjacent Subhercynian Basin. Comparable position of Late Cretaceous basin and uplifted basement areas in the Bohemian Massif added to demonstrate the same deformational mechanism of the Bohemian Cretaceous (BCB) and its vicinity (from Hindle and Kley 2020, amended). NSB – North Sudetic Basin; SBB – South Bohemian basins.

ca. 1–1.5 Myr is low, implying low subsidence rate ca. 0.1 mm/year (Valečka 2020). Such subsidence rate does not support rapid initital subsidence, typical for transtensional basins (Gölke et al. 1994). Instead, low initial subsidence and rather localized influence of tectonic activity on basin-floor subsidence (e.g., in the LJSB), followed by accelerated tectonic activity – with a number of consequences such as intensified basin-floor subsidence, elevated sediment supply, narrowing of depocenters, etc. (Uličný et al. 2009b; Niebuhr et al. 2020)

All the listed arguments call for finding a different explanation of formation of the BCB. A structural setting and evolution of infill (Voigt et al. 2006; von Eynatten et al. 2008) of the Subhercynian Basin adjacent to Harz Mts. in northern Germany makes this basin a more 'simple' counterpart to the BCB, both being elements of a wider system of intraplate basins formed across central Europe in compressional setting during the Late Cretaceous. Structural modeling of formation and inversion of the Subhercynian Basin, rendered by Hindle and Kley (2020), suggest that its subsidence and geometry can be well explained by a combination of elastic flexure and rigid tilting of lithosphere that has been tectonically segmented by basement thrusting (Fig. 14). Therefore, Hindle and Kley (2020) propose calling the Subhercynian Basin as an 'intraplate

foreland basin', since this term conveys the compressional nature of the subsidence, the tectonic setting and the basin's likely depositional evolution, and also the fact that it will contain large amounts of the eroded product of adjacent basement uplifts and their sedimentary cover. Based on the arguments above, the explanation of Hindle and Kley (2020) is ushered for the BCB as well. It is necessary to mention that the term 'flexural foreland basin' ("flexurelle Vorlandbecken") has already been used to describe the mechanism of formation of the BCB (Niebuhr et al. 2020).

The end of Late Cretaceous inversion, as noted by Voigt et al. (2021), is not easy to pinpoint, although unconformities of late Campanian to Paleogene age on inverted structures indicate slow decline of uplift rates. Continuity of this process is exemplified in the Bohemian Massif by South Bohemian basins (present-day České Budějovice and Třeboň basins; S of Prague). These basins were established by the Late Cretaceous Alpine tectonic reactivation of the NW–SE and NE–SW to NNE–SSW faults (Fuchs and Matura 1976) during the late Turonian–Coniacian (cf. Knobloch 1985) parallel with accelerated inversion of the BCB. Filling of the South Bohemian basins continued throught the Cenozoic with several hiatuses, possibly indicating pulses of compressional reactivation of shear zones in the Moldanubian basement.

References

Absolon, A. (1979): Permské slepence v údolí Labe u Děčína. – Geologický průzkum, 2, 58.

Adámek, J. (2005): The Jurassic floor of the Bohemian Massif in Moravia – geology and paleogeography. Bulletin of Geosciences, 80, 291–305.

Allen, P.A., Allen, J.R. (2005): Basin Analysis: Principles and Applications. 2nd edition. Blackwell Publishing, Malden, Oxford, Victoria.

Allen, P.A., Eriksson, P.G., Alkmim, F.F., Betts, P.G., Catuneanu, O., Mazumder, R., Meng, Q., Young, G.M. (2015): Classification of basins, with special reference to Proterozoic examples. In: Mazumder, R., Eriksson, P.G. (eds.): Precambrian Basins of India: Stratigraphic and Tectonic Context. Geological Society, London, Memoirs, 43, p. 5–28.

Arthaud, F., Matte, P. (1977): Late Paleozoic strike-slip faulting in southern Europe and northern Africa: result of a right-lateral shear zone between the Appalachians and the Urals. Geological Society of America Bulletin, 88, 1305–1320.

Asch, K. (2005): IGME 5000: 1:5 Million International Geological Map of Europe and Adjacent Areas – final version for the internet. Die Bundesanstalt für Geowissenschaften und Rohstoffe, Hannover.

Augustsson, C., Voigt, T., Bernhart, K., Kreißler, M., Gaupp, R., Gärtner, A., Hofmann, M., Linnemann, U. (2018): Zircon size-age sorting and source-area effect: The German Triassic Buntsandstein Group. Sedimentary Geology, 375, 218–231.

Becker, T.P., Thomas, W.A., Gehrels, G.E. (2006): Linking late Paleozoic sedimentary provenance in the Appalachian Basin to the history of Alleghanian deformation. American Journal of Science, 306, 777–779.

Betz, D., Führer, F., Greiner, G., Plein, E. (1987): Evolution of the Lower Saxony Basin. Tectonophysics, 137, 127–170.

Biernacka, J. (2012): Provenance of Upper Cretaceous quartz-rich sandstones from the North Sudetic Synclinorium, SW Poland: constraints from detrital tourmaline. Geological Quarterly, 56, 315–332.

Biernacka, J., Józefiak, M. (2009): The Eastern Sudetic Island in the Early-to-Middle Turonian: evidence from heavy minerals in the Jerzmanice sandstones, SW Poland. Acta Geologica Polonica, 59, 545–565.

Blecha, M., Martínek, K., Mihaljevič, M. (1999): Sedimentary and geochemical record of the ancient Kalná Lake, Lower Permian, Krkonoše Piedmont Basin, Czech Republic. Acta Universitatis Carolinae – Geologica, 43, 657–665.

Bosák, P. (1978): Rudická plošina v Moravském krasu – část III. Petrografie a diageneze karbonátů a silicitů jurského reliktu u Olomučan. Acta Musei Moraviae, Scientiae naturales, 63, 7–28.

Botor, D., Anczkiewicz, A.A., Mazur, S., Siwecki, T. (2019): Post-Variscan thermal history of the Intra-Sudetic Basin (Sudetes, Bohemian Massif) based on apatite fission track analysis. International Journal of Earth Sciences, 108, 2561–2576.

Boulila, S., Laskar, J., Haq, B.U., Galbrun, B., Hara, N. (2018): Long-term cyclicities in Phanerozoic sea-level sedimentary record and their potential drivers. Global and Planetary Change, 165, 128–136.

Brandmayr, M., Dallmeyer, R.D., Handler, R., Wallbrecher, E. (1995): Conjugate shear zones in the southern Bohemian Massif (Austria): implications for Variscan and Alpine tectonothermal activity. Tectonophysics, 248, 97–116.

Bridge, J.S. (2003): Rivers and floodplains. Blackwell, Oxford.

Brink, H.J., Dürschner, H., Trappe, H. (1992): Some aspects of the late and post-Variscan development of the northwestern German Basin. Tectonophysics, 207, 65–95.

Burg, J.P., van den Driessche, J., Brun, J.P. (1994): Syn- to post-thickening extension in the Variscan Belt of Western Europe: modes and structural consequences. Géologie de la France, 3, 33–51.

Burgess, P.M., Gurnis, M., Moresi, L., (1997): Formation of sequences in the cratonic interior of North America by interaction between mantle, eustatic, and stratigraphic processes. Geological Society of America Bulletin, 109, 1515–1535.

Čech, S. (2011): Palaeogeography and stratigraphy of the Bohemian Cretaceous Basin (Czech Republic) – An overview. Geologické výzkumy na Moravě a ve Slezsku, 18, 18–21.

Čech, S., Hercogová, J., Knobloch, E., Pacltová, B., Pokorný, V., Sajverová, E., Slavík, J., Švábenická, L., Valečka, J. (1987): Svrchní křída ve vrtu Volfartice Vf-1. Sborník Geologických věd, Geologie, 42, 113–159.

Čech, S., Švábenická, L. (1992): Macrofossils and nannofossils of the type locality of the Březno Formation (Turonian–Coniacian, Bohemia). Věstník Ústředního ústavu geologického, 67, 311–326.

Čech, S., Hradecká, L., Svobodová, M., Švábenická, L. (2005): Cenomanian and Cenomanian-Turonian boundary in the southern part of the Bohemian Cretaceous Basin, Czech Republic. Bulletin of Geosciences, 80, 321–354.

Čech, S., Uličný, D. (2021): The Turonian-Coniacian stage boundary in an expanded siliciclastic succession: Integrated stratigraphy in deltaic through offshore facies, Bohemian Cretaceous Basin. Cretaceous Research, 117, 104576.

Cháb, J., Stráník, Z., Eliáš, M. (2007): Geological map of the Czech Republic 1:500 000. Czech Geological Survey, Prague.

Cháb, J., Breitr, K., Fatka, O., Hladil, J., Kalvoda, J., Šimůnek, Z., Štorch, P., Vašíček, Z., Zajíc, J., Zapletal, J. (2008): Stručná geologie základu Českého masivu a jeho karbonského a permského pokryvu. Vydavatelství České geologické služby, Praha.

Cloetingh, S. (1986): Intraplate stresses: a new tectonic mechanism for fluctuations of relative sea level. Geology, 14, 617–620.

Cloetingh, S., McQueen, H., Lambeck, K. (1985): On a tectonic mechanism for regional sea level variations. Earth and Planetary Science Letters, 75, 157–166.

Cloetingh, S., Ziegler, P.A., Bogaard, P.J.F., Andriessen, P.A.M., Artemieva, I.M., Bada, G., van Balen, R.T., Beekman, F., Ben-Avraham, Z., Brun, J.P., Bunge, H.P., Burov, E.B., Carbonell, R., Faccenna, C., Friedrich, A., Gallart, J., Green, A.G., Heidbach, O., Jones, A.G., Matenco, L., Mosar, J., Oncken, O., Pascal, C., Peters, G., Sliaupa, S., Soesoo, A., Spakman, W., Stephenson, R.A., Thybo, H., Torsvik, T., de Vicente, G., Wenzel, F., Wortel, M.J.R. (2007): TOPO-EUROPE: the geoscience of coupled deep Earth-surface processes. Global and Planetary Change, 58, 1–118.

Coubal, M., Málek, J., Adamovič, J., Štěpančíková, P. (2015): Late Cretaceous and Cenozoic dynamics of the Bohemian Massif inferred from the paleostress history of the Lusatian Fault Belt. Journal of Geodynamics, 87, 26–49.

Coubal, M., Zelenka, P., Stemberk, J. (2019): Projevy alpínské kinematické aktivity železnohorského zlomu v křehkém porušení okolí jeho jihovýchodní části. Zprávy o geologických výzkumech, 52, 141–146.

Danigel, M., Voigt, T., Ustaszewski, K. (2019): Thermal maturity of Cretaceous deposits in the marginal trough of the Bohemian Cretaceous Basin – evidence for deep burial during Late Cretaceous inversion of Central Europe. Geophysical Research Abstracts, 21, EGU2019-17371.

Danišík, M., Migoń, P., Kuhlemann, J., Evans, N.J., Dunkl, I., Frisch, W. (2010): Thermochronological constraints on the long-term erosional history of the Karkonosze Mts., Central Europe. Geomorphology, 117, 78–89.

Dewey, J.F., Burke, K. (1973): Tibetan, Variscan and Precambrian basementreactivation: products of continental collision. Journal of Geology, 81, 683–692.

Dewey, J.F. (1988): Extensional collapse of orogens. Tectonics, 7, 1123–1139.

Dill, H.G., Klosa, D. (2011): Heavy mineral-based provenance analysis of Mesozoic continental-marine sediments at the western edge of the Bohemian Massif, SE Germany: with special reference to Fe–Ti minerals and the crystal morphology of heavy minerals. International Journal of Earth Sciences, 100, 1497–1513.

Doré, A.G. (1991): The structural foundation and evolution of Mesozoic seaways between Europe and the Arctic. Palaeogeography, Palaeoclimatology, Palaeoecology, 87, 441–492.

Dölling, B., Dölling, M., Hiss, M., Berensmeier, M., Püttmann, T. (2018): Upper Cretaceous shallow-marine deposits of the southwestern Münsterland (northwest Germany) influenced by synsedimentary tectonics. Cretaceous Research, 87, 261–276.

Dörr, W., Zulauf, G. (2010): Elevator tectonics and orogenic collapse of a Tibetan-style plateau in the European Variscides: the role of the Bohemian shear zone. International Journal of Earth Sciences, 99, 299–325.

Edel, J.B., Weber, K. (1995): Cadomian terranes, wrench faulting and thrusting in the central Europe Variscides: geophysical and geological evidence. Geologische Rundschau, 84, 412–432.

Eliáš, M. (1981): Facies and paleogeography of the Jurassic of the Bohemian Massif. Sborník geologických věd, Geologie, 35, 75–144.

Erlström, M., Thomas, S.A., Deeks, N., Sivhed, U. (1997): Structure and tectonic evolution of the Tornquist Zone and adjacent sedimentary basins in Scania and the southern Baltic Sea area. Tectonophysics, 271, 191–215.

Erratt, D., Thomas, G.M., Wall, G.R.T. (1999): The evolution of the Central North Sea Rift. Geological Society, London, Petroleum Geology Conference Series, 5, 63–82.

Fediuk, F., Losert, J., Röhlich, P., Šilar, J. (1958): Geologické poměry území podél lužické poruchy ve Šluknovském výběžku. Rozpravy ČSAV, Řada matematicko-přírodovědná, 68, 1–42.

Franke, W. (2000): The mid-European segment of the Variscides: tectonostratigraphic units, terrane boundaries and plate tectonic evolution. In: Franke, W., Haak, V., Oncken, O., Tanner, D. (eds.): Orogenic Processes: Quantification and Modelling in the Variscan Belt. Geological Society, London, Special Publications, 179, p. 35–61.

Franke, W. (2006): The Variscan orogen in Central Europe: construction and collapse. In: Gee, D.G., Stephenson, R.A. (eds.): European Lithosphere Dynamics. Geological Society, London, Memoirs, 32, p. 333–343.

Fuchs, G., Matura, A. (1976): Zur Geologie des Kristallins der südlichen Böhmischen Masse. Jahrbuch der Geologischen Bundesanstalt, 119, 1–43.

Galloway, W.E. (1989): Genetic stratigraphic sequences in basin analysis I: Architecture and genesis of flooding-surface bounded depositional units. Bulletin of the American Association of Petroleum Geologists, 73, 125–142.

Gast, R., Gundlach, T. (2006): Permian strike slip and extensional tectonics in Lower Saxony, Germany. Zeitschrift der Deutschen Gesellschaft für Geowissenschaften, 157, 41–56.

Glasmacher, U.A., Mann, U., Wagner, G.A. (2002): Thermotectonic evolution of the Barrandian, Czech Republic, as revealed by apatite fission-track analysis. Tectonophysics, 359, 381–402.

Gölke, M., Cloetingh, S., Fuchs, K. (1994): Finite-element modelling of pull-apart basin formation. Tectonophysics, 240, 45–57.

Gross, D., Sachsenhofer, R., Rech, A., Sageder, S., Geissler, M., Schnitzer, S., Troiss, W. (2015): The Trattnach Oil Field in the North Alpine Foreland Basin (Austria). Austrian Journal of Earth Sciences, 108, 151–171.

Guillocheau, F., Robin, C., Allemand, P., Bourquin, S., Braulta, N., Dromart, G., Friedenberg, R., Garcia, J.-P., Gaulier, J.-M., Gaumet, F., Grosdoy, B., Hanot, F., Le Strat, P., Mettraux, M., Nalpas, T., Prijac, C., Rigollet, C., Serrano, O., Grandjean, G. (2000): Meso-Cenozoic geodynamic evolution of the Paris Basin: 3D stratigraphic constraints. Geodinamica Acta, 13, 189–246.

Gutowski, J., Krzywiec, P., Pożaryski, W. (2003): From Extension to Inversion – Sedimentary Record of Mesozoic Tectonic Evolution within the Marginal Fault Zone, SE Mid-Polish Trough. Geolines, 16, 38–39.

Hakenberg, M., Świdrowska, J. (2001): Cretaceous basin evolution in the Lublin area along the Teisseyre-Tornquist Zone (SE Poland). Annales Societatis Geologorum Poloniae, 71, 1–20.

Hallam A. (2001): A review of the broad pattern of Jurassic sea-level changes and their possible causes in the light of current knowledge. Palaeogeography, Palaeoclimatology, Palaeoecology, 167, 23–37.

Haq, B.U. (2014): Cretaceous eustasy revisited. Global and Planetary Change, 113, 44–58.

Haq, B.U. (2018): Jurassic Sea-Level Variations: A Reappraisal. GSA Today, 28, 4–10.

Havlena, V., Pešek, J. (1980): Stratigrafie, paleogeografie a základní strukturní členění limnického permokarbonu Čech a Moravy. Sborník Příroda Plzeň, 34, 1–144.

Hayward, A.B., Graham, R.H. (1989): Some geometrical characteristic of inversion. In: Cooper, M.A., Williams, G.D. (eds.): Inversion tectonics. Geological Society, London, Special Publications, 44, p. 17–39.

Hejl, E., Coyle, D., Lal, N., van den Haute, P., Wagner, P.A. (1997): Fission-track dating of the western border of the Bohemian massif: thermochronology and tectonic implications. Geologische Rundschau, 86, 210–219.

Helland-Hansen, W., Martinsen, O.J. (1996): Shoreline trajectories and sequences: Description of variable depositional-dip scenarios. Journal of Sedimentary Research, 66, 670–688.

Henk, A. (1997): Gravitational orogenic collapse versus plate boundary stresses – a numerical modeling approach to the Permo-Carboniferous evolution of Central Europe. Geologische Rundschau, 86, 39–55.

Herčík, F., Herrmann, Z., Valečka, J. (2003): Hydrogeology of the Bohemian Cretaceous Basin. Czech Geological Survey, Prague.

Hindle, D., Kley, J. (2020): The Subhercynian Basin: An example of an intraplate foreland basin due to a broken plate, Solid Earth Discuss. [preprint], https://doi.org/10.5194/se-2020-185, in review, 2020.

Hoffmann, U., Breitkreuz, C., Breiter, K., Sergeev, S., Stanek, K., Tichomirowa, M. (2013): Carboniferous—Permian volcanic evolution in Central Europe—U/Pb ages of volcanic rocks in Saxony (Germany) and northern Bohemia (Czech Republic). International Journal of Earth Sciences, 102, 73–99.

Hofmann, M., Linnemann, U., Gerdes, A., Ullrich, B., Schauer, M. (2009): Timing of dextral strike-slip processes and basement exhumation in the Elbe Zone (Saxo-Thuringian Zone): the final pulse of the Variscan Orogeny in the Bohemian Massif constrained by LA-SF-ICP-MS U–Pb zircon data. In: Murphy, J. B., Keppie, J. D., Hynes, A. J. (eds.): Ancient Orogens and Modern Analogues. Geological Society, London, Special Publications, 327, 197–214.

Hofmann, M., Linnemann, U., Voigt, T. (2013): The Upper Cretaceous section at Schmilka in Saxony (Elbsandsteingebirge, Germany): syntectonic sedimentation and inverted zircon age populations revealed by LA-ICP-MS U/Pb data. Geologica Saxonica, 59, 101–130.

Hofmann, M., Voigt, T., Bittner, L., Gärtner, A., Zieger, J., Linnemann, U. (2018): Reworked Middle Jurassic sandstones as a marker for Upper Cretaceous basin inversion in Central Europe – a case study for the U–Pb detrital zircon record of the Upper Cretaceous Schmilka section and their implication for the sedimentary cover of the Lausitz. International Journal of Earth Sciences, 107, 913–932.

Holcová, K., Holcová, M. (2016): Calcareous nannoplankton in the Upper Jurassic marine deposits of the Bohemian Massif: new data concerning the Boreal–Tethyan communication corridor. Geological Quarterly, 60, 624–636.

Holub, V., Chaloupský, J., Čadková, Z., Čech, S., Hercogová, J., Jetel, J., Knobloch, E., Rybářová, L., Schovánková, D., Slavík, J., Švábenická, L., Valečka, J., Valín, F., Vejlupek, M. (1984): Strukturní vrt Vf-1 Volfartice. Závěrečná zpráva. Unpublished report, Czech Geological Survey, Prague.

Holub, V.M., Stapf, K.R.G., 1995. Eine kuestennahe, sandige Zechstein-Sabkha in NE-Boehmen mit dolomitisierten Calcretes, Spelaeolithen und Grainstones. Neues Jahrbuch für Geologie und Paläontologie, 3, 129–165.

Illies, H. (1974): Intra-Plattentektonik in Mitteleuropa und der Rheingraben. Oberrheinische geologische Abhandlungen, 23, 1–24.

Illies, H. (1975): Intraplate tectonics in stable Europe as related to plate tectonics in the Alpine system. Geologische Rundschau, 64, 677–699.

Janetschke, N., Nieburh, B., Wilmsen, M. (2015): Inter-regional sequence-stratigraphical synthesis of the Plänerkalk, Elbtal and Danubian Cretaceous groups (Germany): Cenomanian–Turonian correlations around the Mid-European Island. Cretaceous Research, 56, 530–549.

Jindrich, V. (1971): New views in tectonic significance of platform sediments in the Bohemian Massif, Czechoslovakia. Geological Society of America Bulletin, 82, 763–768.

Käßner, A., Stanek, K.P., Lapp, M. (2020): Post-Variscan tectonic and landscape evolution of the Elbe Fault Zone and the Lusatian Block based on apatite fission-track data and geomorphologic constraints. Geomorphology, 355, 106860.

Kiersnowski, H., Buniak, A. (2006): Evolution of the Rotliegend Basin of northwestern Poland. Geological Quarterly, 50, 119–138.

Klein, V., Opletal, M. (1971): Geologický řez bez kvartéru ZJZ–SSV, M-33-41-B-d (Chřibská). Unpublished material, Ústřední ústav geologický, Praha.

Klein, V., Müller, V., Valečka, J. (1979): Lithofazielle und Paläogeographische Entwicklung des Böhmischen Kreidebeckens. In. Wiedmann, J. (ed.): Aspekte Des Kreide Europas. IUGS Series A, 6, p. 435–446.

Kley, J., Voigt T. (2008): Late Cretaceous intraplate thrusting in Central Europe: Effect of Africa-Iberia-Europe convergence, not alpine collision. Geology, 36, 839–842.

Kley, J., Franzke, H.-J., Jähne, F., Krawczyk, C., Lohr, T., Reicherter, K., Scheck-Wenderoth, M., Sippel, J., Tanner, D., van Gent, H., the SPP Structural Geology Group (2008): Strain and Stress. In: Littke, R., Bayer, U., Gajewski, D., Nelskamp, S. (eds.): Dynamics of Complex Intracontinental Basins. The Central European Basin System. Springer, Berlin, Heidelberg, p. 97–121.

Knobloch, E. (1985): Paläobotanisch-biostratigraphische Charakteristik der Klikov-Schichtenfolge (Oberturon–Santon) in Südböhmen. Sborník geologických věd, Geologie, 40, 101–145.

Kockel, F. (1986): Upper Cretaceous biostratigraphy – the key to the understanding of inversion tectonics in NW-Germany. Annales de la Société géologique de Belgique, 109, 357–361.

Kockel, F. (2003): Inversion structures in Central Europe: expressions and reasons, an open discussion. Netherlands Journal of Geosciences, 82, 351–366.

Kominz, M.A. (2001): Sea Level Variations Over Geologic Time. In: Steele, J.H., Thorpe, S., Turekian, K. (eds.): Encyclopedia of Ocean Sciences (2nd Edition). Academic Press.

Kořínková, D., Adamovič, J., Svojtka, M., Filip, J. (2013). Reconstruction of low time-temperature history of the crystalline blocks and sedimentary rocks along Lusatian Faul,Bohemian Massif. Abstract, 11th Meeting of the Central European Tectonic Studies Groups (CeTeG), Várgesztes, Hungary.

Kossow, D., Krawczyk, C.M. (2002): Structure and quantification of processes controlling the evolution of the inverted NE-German Basin. Marine and Petroleum Geology, 19, 601–618.

Košťák, M., Čech, S., Ekrt, B., Mazuch, M., Wiese, F., Voigt, S., Wood, C. (2004): Belemnites of the Bohemian Cretaceous Basin in a global context. Acta geologica Polonica, 54, 511–533.

Kotowski, J., Nejbert, K., Olszewska-Nejbert, D. (2020): Tourmalines as a Tool in Provenance Studies of Terrigenous Material in Extra-Carpathian Albian (Uppermost Lower Cretaceous) Sands of Miechów Synclinorium, Southern Poland. Minerals, 2020, 10.

Kowalski, A. (2017): Fault geometry and evidence of depocentre migration within a transtensional intra-basinal high – a case study from the Łaczna Anticline (Intrasudetic Synclinorium, SW Poland). Geological Quarterly, 61, 779–794.

Kowalski, A. (2020): Triassic palaeogeography of NE Bohemian Massif based on sedimentological record in the Wleń Graben and the Krzeszów Brachysyncline (SW Poland). Annales Societatis Geologorum Poloniae, 90: 125–148.

Kowal-Linka, M., Stawikowski, W. (2013): Garnet and tourmaline as provenance indicators of terrigenous material in epicontinental carbonates (Middle Triassic, S Poland). Sedimentary Geology, 291, 27–47.

Kowal-Linka, M., Walczak, K. (2017): Peridotite-derived detrital pyropes versus high-pressure felsic granulite-derived pyrope-almandine garnets from the Lower Triassic deposits of the NE foreland of the Bohemian Massif (S Poland, Central Europe). Sedimentary Geology, 374,179–201.

Kozdrój, W., Krentz, O., Opletal, M. (2001): Commentson the Geological Map Lausitz–Jizera–Karkonosze (without Cenozoic sediments) 1:100 000. Sächsisches Landesamt für Umwelt und Geologie, Freiberg, Państwowy Instytut Geologiczny, Warszawa, Český geologický ústav, Praha.

Krajewski, M., Olchowy, P., Felisiak, I. (2016): Late Jurassic facies architecture of the Złoczew Graben: implications for evolution of the tectonic-controlled northern peri-Tethyan shelf (Upper Oxfordian–Lower Kimmeridgian, Poland). Facies, 62.

Kroner, U., Romer, R.L. (2013): Two plates — many subduction zones: the Variscan orogeny reconsidered. Gondwana Research, 24, 298–329.

Krystek, I., Samuel, O. (1978): Výskyt kriedy karpatského typu severně od Brna (Kuřim). Geologické Práce, Správy GÚDŠ, 71, 93–110.

Krzywiec, P. (2006): Triassic-Jurassic evolution of the Pomeranian segment of the Mid-Polish Trough—basement tectonics and subsidence patterns. Geological Quarterly, 50, 139–150.

Krzywiec, P., Stachowska, A. (2016): Late Cretaceous inversion of the NW segment of the Mid-Polish Trough: how marginal troughs were formed, and does it matter at all? Zeitschrift der Deutschen Gesellschaft für Geowissenschaften, 167, 107–119.

Krzywiec, P., Stachowska, A., Stypa, A. (2018): The only way is up – On Mesozoic uplifts and basin inversion events in SE Poland. In: Kilhams, B., Kukla, P.A., Mazur, S., McKie, T., Mijnlieff, H.F., van Oijk, K. (eds.): Mesozoic Resource Potential in the Southern Permian Basin. Geological Society, London, Special Publications, 469, p. 33–57.

Kučera, M., Pešek, J. (1982): Geology of the Česká Kamenice Basin and vicinity. Acta Universitatis Carolinae Geologica, 3, 285–295.

Kump, L.R. (1989): Alternative modeling approaches to the geochemical cycles of carbon, sulfur, and strontium isotopes. American Journal of Science, 289, 390–410.

Lake, S.D., Karner, G.D. (1987): The structure and evolution of the Wessex Basin, southern England: an example of inversion tectonics. Tectonophysics, 137, 347–378.

Lange, J.-M., Tonk, C., Wagner, G.A. (2008): Apatitspaltspurdaten zur postvariszischen thermotektonischen Entwicklung des sächsischen Grundgebirges – erste Ergebnisse. Zeitschrift der Deutschen Gesellschaft für Geowissenschaften, 159, 123–132.

Laurin, J., Uličný, D. (2004): Controls on a shallow-water hemipelagic carbonate system adjacent to a siliciclastic margin: Example from late Turonian of Central Europe. Journal of Sedimentary Research, 74, 697–717.

Leeder, M.R., Harris, T., Kirkby, M.J. (1998): Sediment supply and climate change: implications for basin stratigraphy. Basin Research, 10, 7–18.

Leszczyński, K. (1997): The Lower Cretaceous depositional architecture and sedimentary cyclicity in the Mid-Polish Trough. Geological Quarterly, 41, 509–520.

Leszczyński, S. (2018): Integrated sedimentological and ichnological study of the Coniacian sedimentation in North Sudetic Basin, SW Poland. Geological Quarterly, 62, 767–816.

Liboriussen, J., Ashton, P., Tygesen, T. (1987): The tectonic evolution of the Fennoscandian border zone in Denmark. Tectonophysics, 137, 21–29.

Lorenz, V., Nicholls, I.A. (1976): The Permocarboniferous Basin and Range Province of Europe. An application of plate tectonics. In: Falke, H. (ed.): The Continental Permian in Central, West, and South Europe. D. Reidel Publishing Company, Dordrecht, p. 313–342.

Lorenz, V, Nicholls, I.A. (1984): Plate and intraplate processes of Hercynian Europe during the Late Paleozoic. Tectonophysics, 107, 25–56.

Lowell, J.D. (1995): Mechanics of basin inversion from worldwide examples. In: Buchanan, J.G, Buchanan, P.G. (eds.): Basin Inversion. Geological Society, London, Special Publications, 88, p. 39–57.

Malkovský, M. (1976): Saxonische Tektonik der Böhmischen Masse. Geologische Rundschau, 65, 127–143.

Malkovský, M. (1980): Saxon tectogenesis of the Bohemian Massif. Sborník geologických věd, Geologie, 34, 67–101.

Malkovský, M. (1987): The Mesozoic and Tertiary basins of the Bohemian Massif and their evolution. Tectonophysics, 137, 31–42.

Marcinowski, R., Radwanski, A. (1983): The Mid-Cretaceous transgression onto the Central Polish Uplands (marginal part of the Central European Basin). Zitteliana, 10, 65–95.

Marotta, A.M., Bayer, U., Scheck, M., Thybo, H. (2001): The stress field below the NE German basin: effects induced by the Alpine collision. Geophysical Journal International, 144, 8–12.

Marshak, S., Paulsen, T. (1996): Midcontinent U.S. fault and fold zones: a legacy of Proterozoic intracratonic extensional tectonism? Geology, 24, 151–154.

Martínek, K. (2008): Climatic, tectonic and provenance record of the Permian non-marine deposits of the Krkonoše Piedmont Basin. Unpublished PhD. thesis, Charles University, Prague.

Martínek, K., Svojtka, M., Filip, J. (2008): Multiphase cooling and exhumation of the Krkonoše Piedmont Basin during Mesozoic – Cenozoic basin inversion based on apatite fission track analysis. Abstracts of the 33 International Geological Congress, Oslo, Norway.

Martínek, K., Blecha, M., Daněk, V., Franců, J., Hladíková, J., Johnová, R., Uličný, D. (2006): Record of palaeoenvironmental changes in a Lower Permian organic-rich lacustrine succession: integrated sedimentological and geochemical study of the Rudník Member, Krkonoše Piedmont Basin, Czech Republic. Palaeogeography, Palaeoclimatology, Palaeoecology, 230, 85–128.

Martínek, K., Štolfová, K. (2009): Provenance study of Permian non-marine sandstones and conglomerates of the Krkonoše Piedmont Basin (Czech Republic): exotic marine limestone pebbles, heavy minerals and garnet composition. Bulletin of Geosciences, 84, 555–568.

Martínek, K., Verner, K., Buriánek, D., Žáček, V. (2012): Zdrojové horniny detritických biotitů spodněpermských pískovců severního okraje podkrkonošské pánve. Zprávy o geologických výzkumech, 46, 45–50.

Martínek, K., Pešek, J., Opluštil, S. (2017): Significant hiatuses in the terrestrial Late Variscan Central and Western Bohemian basins (Late Pennsylvanian–Early Cisuralian) and their possible tectonic and climatic links. Geologica Carpathica, 68, 269–281.

Martinsen, O.J., Ryseth, A.L.F., Helland–Hansen, W., Flesche, H., Torkildsen, G., Idil, S. (1999): Stratigraphic base level and fluvial architecture: Ericson sandstone (Campanian), rock springs uplift, SW Wyoming, USA. Sedimentology, 46, 235–263.

Mastalerz, K., Wojewoda, J. (1991): Geodynamic regime of the Sudetes as interpreted from contrasting palaeoenvironmental indicators: Lower Permian and Upper Cretaceous. Seminar proceeding. Bautzen, 1991. Available online at: http://www.jw.ing.uni.wroc.pl/nauka/publikacje/PDF/PDF%20abstrakty/1991%20a%20Mastalerz%20&%20Wojewoda.pdf

Matte, P. (1986): Tectonics and plate tectonics model for the Variscan belt of Europe. Tectonophysics, 126, 329–374.

Mattern, F.(1995a): Late Carboniferous to Lower Triassic shear sense reversals at strike-slip faults in eastern Bavaria. Zentralblatt für Geologie und Paläontologie, Teil I, Geologie, 1993, 1471–1490.

Mattern, F. (1995b): The fault (s) of the 'Fränkische Linie' (NE Bavaria), interpreted as a Rotliegend sinistral extensional strike-slip duplex. Zentralblatt für Geologie und Paläontologie, Teil I, Geologie, 1993, 1491–1504.

Mattern, F. (1996): The Elbe zone at Dresden – a Late Paleozoic pull-apart intruded shear zone. Zeitschrift der Deutschen Gesellschaft für Geowissenschaften, 147, 57–80.

Mattern, F. (2001): Permo-Silesian movements between Baltica and Western Europe: tectonics and 'basin families'. Terra Nova, 13, 368–375.

Matyja, B.A., Wierzbowski, A. (1995): Biogeographic differentiation of the Oxfordian and Early Kimmeridgian ammonite faunas of Europe, and its stratigraphic consequences. Acta Geologica Polonica, 45, 1–8.

Mazur, S., Scheck-Wenderoth, M. (2005): Constraints on the tectonic evolution of the Central European Basin System revealed by seismic reflection profiles from Northern Germany. Netherlands Journal of Geosciences, 84, 389–401.

McArthur, J.M., Howarth, R.J., Shields, G.A. (2012): Strontium Isotope Stratigraphy. In: Gradstein, F.M., Ogg, J.G., Schmitz, M., Ogg, G. (eds.): The Geologic Time Scale 2012. Elsevier.

McCann,T. (1998): The Rotliegend of the NE German Basin: background and prospectivity. Petroleum Geoscience, 4, 17–27.

Meier, T., Soomro, R.A., Viereck, L., Lebedev, S., Behrmann, J.H., Weidle, C., Cristiano, L., Hanemann, R. (2016): Mesozoic and Cenozoic evolution of the Central European lithosphere. Tectonophysics, 692, 58–73.

Ménard, G., Molnar, P. (1988): Collapse of a Hercynian Tibetan Plateau into a late Palaeozoic European Basin and Range province. Nature, 334, 235–237.

Meyer, R.K.F., Schmidt-Kaler H. (1989): Paläogeographischer Atlas des süddeutschen Oberjura (Malm). Geologisches Jahrbuch, Reihe A, 115, 1–77.

Miall, A.D. (1977): Lithofacies Types and Vertical Profile Models in Braided River Deposits: A Summary. In: Miall, A.D. (ed.): Fluvial Sedimentology – Memoir 5, p. 597–604.

Michel, L.A., Tabor, N.J., Montañez, I.P., Schmitz, M.D., Davydov, V.I. (2015): Chronostratigraphy and Paleoclimatology of the Lodève Basin, France: Evidence for a pan-tropical aridification event across the Carboniferous–Permian boundary. Palaeogeography, Palaeoclimatology, Palaeoecology, 430, 118–131.

Migoń, P., Lidmar-Bergström, K. (2001): Weathering mantles and their significance for geomorphological evolution of central and northern Europe since the Mesozoic. Earth-Science Reviews, 56, 285–324.

Migoń, P., Danišík, M. (2012): Erosional history of the Karkonosze Granite Massif – constraints from adjacent sedimentary basins and thermochronology. Geological Quarterly, 56, 440–454.

Miller, K.G., Sugarman,P.J., Browning, J.V., Kominz, M.A., Hernandez, J.C., Olsson, R.K., Wright J.D., Feigenson, M.D. (2003): Late Cretaceous chronology of large, rapid sea-level changes: Glacioeustasy during the greenhouse world. Geology, 31, 585–588.

Miller, K.G, Kominz, M.A., Browning, J.V., Wright, J.D., Mountain, G.S., Katz, M.E., Sugarman, P.J., Cramer, B.S., Christie-Blick, N., Pekar, S.F. (2005): The Phanerozoic Record of Global Sea-Level Change. Science, 25, 1293–1298.

Mitchell, A.J., Uličný, D., Hampson, G.J., Allison, P.A., Gorman, G.J., Pigott, M.D., Wells, M.R., Pain, C.C. (2010). Modelling tidal current-induced bed shear stress and palaeocirculation in an epicontinental seaway: the Bohemian Cretaceous Basin, Central Europe. Sedimentology, 57, 359–388.

Moecher, D.P., Kelly, E.A., Hietpas, J., Samson, S.D. (2019): Proof of recycling in clastic sedimentary systems from textural analysis and geochronology of detrital monazite: Implications for detrital mineral provenance analysis. Geological Society of America Bulletin, 131, 1115–1132.

Mogensen, T.E. (1995): Triassic and Jurassic structural development along the Tornquist Zone, Denmark. Tectonophysics, 252, 197–220.

Mogensen, T.E., Korstgård, J.A. (2003): Triassic and Jurassic transtension along part of the Sorgenfrei–Tornquist Zone in the Danish Kattegat. Geological Survey of Denmark and Greenland Bulletin, 1, 437–458.

Mortimore, R.N. (1986): Controls on Upper Cretaceous sedimentation in the South Downs with particular reference to flint distribution. In: Sieveking, G. de G., Hart, M.B. (eds.): The Scientific Study of Flint and Chert. Cambridge University Press, p. 21–42.

Mortimore, R.N. (2018): Late Cretaceous tectonosedimentary events in NW Europe. Proceedings of the Geologists' Association, 129, 392–420.

Mortimore, R.N., Pomerol, B. (1997): Upper Cretaceous tectonic phases and end Cretaceous inversion in the Chalk of the Anglo-Paris Basin. Proceedings of the Geologists' Association, 108, 231–255.

Mortimore, R.N., Wood, C.J., Pomerol, B., Ernst, G. (1998): Dating the phases of the Subhercynian tectonic epoch: Late Cretaceous tectonics and eustatics in the Cretaceous Basins of Northern Germany compared with the Anglo-Paris Basin. Zentralblatt für Geologie und Paläontologie, Teil I, 1996, 1349–1401.

Mutterlose, J., Böckel, B. (1998): The Barremian–Aptian interval in NW Germany: a review. Cretaceous Research, 19, 539–568.

Nachtmann, W., Wagner, L. (1987): Mesozoic and Early Tertiary evolution of the Alpine foreland in upper Austria and Salzburg, Austria. Tectonophysics, 137, 61–76.

Nádaskay, R., Uličný, D. (2014): Genetic stratigraphy of Coniacian deltaic deposits of the northwestern part of the Bohemian Cretaceous Basin. Zeitschrift der Deutschen Gesellschaft für Geowissenschaften, 165, 547–575.

Nádaskay, R., Valečka, J., Mlčoch, B., Tenenko, V., Kořalka, S. (2019): Závěrečná zpráva průzkumného geologického vrtu 6412_L. Resibil – Bilance vodních zdrojů ve východní části česko-saského pohraničí a hodnocení možnosti jejich dlouhodobého užívání. Výstup projektu ResiBil č. 100267011. ČGS 661280. Unpublished final report, Czech Geological Survey, Prague.

Nádaskay, R., Mlčoch, B., Valečka, J., Skácelová, Z., Horna, F., Karous, M., Kořalka, S., (in prep.): Permian deposits at the Lusatian Fault and within the Elbe Zone: discussion of their formation and subsequent deformation.

Nance, R.D., Gutierréz-Alonso, G., Keppie, J.D., Linnemann, U., Murphy, J.B., Quesada, C., Strachan, R.A., Woodcock, N.H. (2010): Evolution of the Rheic Ocean. Gondwana Research, 17, 194–222.

Nehyba, S., Opletal, V. (2016): Depositional environment and provenance of the Gresten Formation (Middle Jurassic) on the southeastern slopes of the Bohemian Massif (Czech Republic, subsurface data). Austrian Journal of Earth Sciences, 109, 262–276.

Nehyba, S., Opletal, V. (2017): Sedimentological study of the Nikolčice Formation – evidence of the Middle Jurassic transgression onto the Bohemian Massif (subsurface data). Geological Quarterly, 61, 138–155.

Niebuhr, B. (2018): Kreidesandsteine auf der Lausitz (Sachsen): Hinweise zu Paläogeographie und Inversionstektonik. Freiberger Forschungshefte C 553, Paläontologie, Stratigraphie, Fazies, 24, 51–78.

Niebuhr, B., Wilmsen, M., Voigt, T. (2020): Die Oberkreide (Cenomanium–Mittelconiacium) im Zittauer Sandsteingebirge (Deutschland, Tschechien). Zeitschrift der Deutschen Gesellschaft für Geowissenschaften, 171, 163–197.

Nielsen, L.H. (2003): Late Triassic–Jurassic development of the Danish Basin and the Fennoscandian border zone, southern Scandinavia. Geological Survey of Denmark and Greenland Bulletin, 526, 459–526.

Nielsen, S.B., Stephenson, R., Thomsen, E. (2007): Dynamics of mid-Palaeocene North Atlantic rifting linked with European intra-plate deformations. Nature, 450, 1071–1074.

Nielsen, S.B., Thomsen, E., Hansen, D.L., Clausen, O.R. (2005): Plate-wide stress relaxation explains European Palaeocene Basin inversions. Nature, 435, 195–198.

Norling, E., Bergström, J. (1987): Mesozoic and Cenozoic tectonic evolution of Scania, southern Sweden. Tectonophysics, 137, 7–19.

Norris, M.S., Hallam, A. (1995): Facies variations across the Middle–Upper Jurassic boundary in Western Europe and the relationship to sea-level changes. Palaeogeography, Palaeoclimatology, Palaeoecology, 116, 189–245.

Ogg, J.G., Hinnov L.A., Huang, C. (2012): Cretaceous. In: Gradstein, F.M., Ogg, J.G., Schmitz, M., Ogg, G. (eds.): The Geologic Time Scale 2012. Elsevier, p. 793–853.

Opletal, M., Adamová, M., Burda, J., Dušek, K., Fediuk, F., Kořán, V., Knobloch, E., Manová, M., Nekovařík, Č., Nývlt, D., Prouza, V., Rambousek, P., Šalanský, K., Valečka, J. (2006): Vysvětlivky k základní geologické mapě České republiky 1 : 25 000, 02-233 Mikulášovice, 02-214 Dolní Poustevna. Česká geologická služba, Praha.

Opluštil, S., Pešek, J. (1998): Stratigraphy, palaeoclimatology and palaeogeography of the Late Palaeozoic continental deposits in the Czech Republic. Geodiversitas, 20, 597–620.

Opluštil, S., Cleal, C. (2007): A comparative analysis of some Late Carboniferous basins of Variscan Europe, Geological Magazine, 144, 417–448.

Opluštil, S., Šimůnek, Z., Zajíc, J., Mencl, V. (2013): Climatic and biotic changes around the Carboniferous/Permian boundary recorded in the continental basins of the Czech Republic. International Journal of Coal Geology, 119, 114–151.

Opluštil, S., Schmitz, M., Kachlík, V., Štamberg, S. (2016): Re-assesment of lithostratigraphy, biostratigraphy and volcanic activity of the Late Paleozoic Intra-Sudetic, Krkonoše-Piedmont and Mnichovo Hradiště basins (Czech Republic) based on new U-Pb CA-ID-TIMS ages. Bulletin of Geosciences, 91, 399–432.

Opluštil, S., Jirásek, J., Schmitz, M., Matýsek, D. (2017): Biotic changes around the radioisotopically constrained Carboniferous-Permian boundary in the Boskovice Basin (Czech Republic). Bulletin of Geosciences 92, 95–122.

Otava, J., Hartley, A. (2001): Sediment provenance and dispersal in a deep marine foreland basin: the Lower Carboniferous Culm Basin, Czech Republic. Journal of the Geological Society, 158, 137–150.

Pastor-Galán, D., Gutiérrez-Alonso, G., Murphy, J.B., Fernández-Suárez, J., Hofmann, M., Linnemann, U. (2013): Provenance analysis of the Paleozoic sequences of the northern Gondwana margin in NW Iberia: Passive margin to Variscan collision and orocline development. Gondwana Research, 23, 1089–1103.

Paul, J., Wemmer, K., Ahrendt, H. (2008): Provenance of siliciclastic sediments (Permian to Jurassic) in the Central European Basin. Zeitschrift der Deutschen Gesellschaft für Geowissenschaften, 159, 641–650.

Paul, J., Wemmer, K., Wetzel, F. (2009): Keuper (Late Triassic) sediments in Germany: indicators of rapid uplift of Caledonian rocks in southern Norway. Norwegian Journal of Geology, 89, 193–202.

Pegrum, R.M. (1984): The extension of the Tornquist Zone in the Norwegian North Sea. Norsk Geologisk Tidsskrift, 64, 39–68.

Pešek, J. (2001): Geologie a ložiska svrchnopaleozoickych limnických pánví České Republiky. Český geologický ústav, Praha.

Peterek, A., Rauche, H., Schröder, B., Franzke, H.J., Bankwitz, P., Bankwitz, E. (1997): The late- and post-Variscan tectonic evolution of the Western Border fault zone of the Bohemian massif (WBZ). Geologische Rundschau, 86, 191–202.

Pieńkowski, G., Schudack, M., Bosák, P., Enay, R., Feldman-Olszewska, A., Golonka, J., Gutowski, J., Herngreen, J.G.F.W., Jordan. P., Krobicki, M., Lathuiliere, B., Leinfelder, R., Michalík, J., Mönnig, E., Noe-Nygaard, N., Pálfy, J., Pint, A., Rasser, M.W., Reisdorf, A.G., Schmid, D.U., Schweigert, G., Surlyk, F., Wetzel, A., Wong, T.E. (2008): Jurassic. In: McCann, T. (ed.): Geology of Central Europe, Volume 2: Mesozoic and Cenozoic. Geological Society, London, p. 823–922.

Pivec, E., Ulrych, J., Höhndorf, A., Rutšek, J. (1998): Melilititic rocks from northern Bohemia: geochemistry and mineralogy. Neues Jahrbuch für Mineralogie - Abhandlungen, 1998, 312–339.

Posamentier, H.W, Allen, G.P. (1993): Variability of the sequence stratigraphic model: effects of local basin factors. Sedimentary Geology, 86, 91–109.

Požaryski, W., Brochwicz-Lewinski, W. (1978): On the Polish Trough. Geologie en Mijnbouw, 57, 545–557.

Prouza V., Tásler R., Valín F., Holub V. (1985): Gravelly to sandy braidplain deposition in the buntsandstein-facies bohdašin formation in northeastern bohemia (Czechoslovakia). In: Mader, D. (ed.): Aspects of Fluvial Sedimentation in the Lower Triassic Buntsandstein of Europe. Lecture Notes in Earth Sciences, 4. Springer, Berlin, Heidelberg.

Prouza, V., Tásler, R. (2001): Podkrkonošská pánev. In: Pešek, J. (ed.): Geologie a ložiska svrchnopaleozoickych limnických pánví České Republiky. Český geologický ústav, Praha, p. 128–166.

Prouza, V., Coubal, M., Adamovič, J. (2013): Problematika jihovýchodního pokračování lužického zlomu v západním Podkrkonoší. Zprávy o geologických výzkumech, 46, 59–63.

Rajchl, M., Uličný, D., Grygar, R., Mach, K. (2009): Evolution of basin architecture in an incipient continental rift: the Cenozoic Most Basin, Eger Graben (Central Europe). Basin Research, 21, 269–294.

Reichel, W., Schauer, M. (2006): Das Döhlener Becken bei Dresden / Geologie und Bergbau. Sächsisches Landesamt für Umwelt und Geologie, Dresden.

Reicherter, K., Froitzheim, N., Jarosiński, M., Badura, J., Franzke, H.J., Hansen, M., Hübscher, C., Müller, R., Stackebrandt, W., Voigt, T., von Eynatten, H., Zuchiewicz, W. (2008): Alpine tectonics north of the Alps. In: McCann, T. (ed.): Geology of Central Europe, Volume 2: Mesozoic and Cenozoic. Geological Society, London, p. 999–1030.

Richter, F.M., Rowley, D.B., DePaolo, D.J. (1992): Sr isotope evolution of seawater: The role of tectonics. Earth and Planetary Science Letters, 109, 11–23.

Rider, M.H. (1996): The Geological Interpretation of Well Logs, 2nd ed. Whittles Publishing, Caithness.

Roberts, N.M.W., Žák, J., Vacek, F., Sláma, J. (2021): No more blind dates with calcite: fluid-flow vs fault-slip along the Očkov thrust, Prague Basin. Geoscience Frontiers, in press.

Roscher, M., Schneider, J.W. (2006): Permo-Carboniferous climate: Early Pennsylvanian to Late Permian climate development of central Europe in a regional and global context. In: Lucas, S.G., Cassinis, G., Schneider, J.W. (eds.): Non-Marine Permian Biostratigraphy and Biochronology. Geological Society, Special Publication 265, p. 95–136.

Rovere, A., Stocchi, P., Vacchi, M. (2016): Eustatic and Relative Sea Level Changes. Current Climate Change Reports, 2, 221–231.

Ruffell, A., Simms, M., Wignall, P. (2016). The Carnian Humid Episode of the late Triassic: A review. Geological Magazine, 153, 271–284.

Scheck, M., Bayer, U. (1999): Evolution of the Northeast German Basin – inferences from a 3D structural model and subsidence analysis. Tectonophysics, 313, 145–169.

Scheck, M., Bayer, U., Otto, V., Lamarche, J., Banka, D., Pharaoh, T. (2002): The Elbe Fault System in north central Europe – a basement-controlled zone of crustal weakness. Tectonophysics, 360, 281–299.

Scheck-Wenderoth, M., Lamarche, J. (2005): Crustal memory and basin evolution in the Central European Basin System – new insights from a 3D structural model. Tectonophysics, 397, 143–165.

Scheck-Wenderoth, M., Krzywiec, P., Zühlke, R., Maystrenko, Y., Froitzheim, N. (2008): Permian to Cretaceous tectonics. In: McCann, T. (ed.): Geology of Central Europe, Volume 2: Mesozoic and Cenozoic. Geological Society, London, p. 999–1030.

Schneider, A.C., Heimhofer, U., Heunisch, C., Mutterlöse, J. (2018): The Jurassic–Cretaceous boundary interval in non-marine strata of northwest Europe – New light on an old problem. Cretaceous Research, 87, 42–54.

Schröder, B. (1987): Inversion tectonics along the Western margin of the Bohemian Massif. Tectonophysics, 137, 93–100.

Schulmann, K., Konopásek, J., Janoušek, V., Lexa, O., Lardeaux, J.M., Edel, J.B., Štípská, P., Ulrich, S. (2009): An Andean type Palaeozoic convergence in the Bohemian Massif. Comptes Rendus - Géoscience, 341, 266–286.

Schulmann, K., Martínez Catalán, J.R., Lardeaux, J.M., Janoušek, V., Oggiano, G. (2014): The Variscan orogeny: extent, timescale and the formation of the European crust. In: Schulmann, K., Martínez Catalán, J.R., Lardeaux, J.M., Janoušek, V., Oggiano, G. (eds.): The Variscan orogeny: extent, timescale and the formation of the European crust. Geological Society of London, Special Publications 405. 1–6

Schwartz, T. M., Schwartz, R. K., Weislogel, A. L. (2019). Orogenic recycling of detrital zircons characterizes age distributions of North American Cordilleran strata. Tectonics, 38, 4320–4334.

Scott, R.A., Smyth, H.R., Morton, A.C., Richardson, N. (2014): Sediment Provenance Studies in Hydrocarbon Exploration and Production. Geological Society, London, Special Publications, 386.

Sengör, A.M.C (1976): Collision of irregular continental margins: Implications for foreland deformation of Alpine-type orogens. Geology, 4 , 779–782.

Skála, R., Ulrych, J., Ackerman, L., Krmíček, L., Fediuk, F., Balogh, K., Hegner, E. (2015): Upper Cretaceous to Pleistocene melilitic volcanic rocks of the Bohemian Massif: petrology and mineral chemistry. Geologica Carpathica, 66, 197–216.

Skoček, V., Valečka, J. (1983): Paleogeography of the Late Cretaceous Quadersandstein of Central Europe. Palaeogeography, Palaeoclimatology, Palaeoecology, 44, 71–92.

Śliwiński, W. (1980): A model for caliche formation in the continental Permian deposits of southeastern Intra-Sudetic Basin, southwestern Poland. Geologia Sudetica, 15, 83–104.

Sobczyk, A., Danišík, M., Aleksandrowski, P., Anczkiewicz, A. (2015): Post-Variscan cooling history of the central Western Sudetes (NE Bohemian Massif, Poland) constrained by apatite fission-track and zircon (U–Th)/He thermochronology. Tectonophysics, 649, 47–57.

Špičáková, L., Uličný, D., Svobodová, M. (2014): Phases of the mid-Cenomanian transgression recorded in a composite palaeovalley fill – the Horoušany quarry, Bohemian Cretaceous Basin. Zeitschrift der Deutschen Gesellschaft für Geowissenschaften, 165, 581–619.

Štaffen, Z. (2002): Chemostratigraphic determination of equivalent strata and formations in Bohemian Cretaceous Basin. Acta Montana, Seria A, 21, 77–109.

Stille, H. (1920): Alter und Art der Phasen variscischer Gebirgsbildung. Nachrichten von der Gesellschaft der Wissenschaften zu Göttingen, Mathematisch-Physikalische Klasse, 218–224.

Stille, H., 1924. Grundfragen der vergleichenden Tektonik. Bornträger, Berlin.

Svobodová, M., Brenner, G.J. (1999): Correlation of Mid-Cretaceous plant microfossils from the Raritan Formation of the Atlantic Coastal Plain with the Peruc-Korycany Formation of the Blansko Graben. Acta Palaeobotanica, Supplement 2, 199–209.

Tietz, O., Büchner, J. (2015): The landscape evolution of the Lausitz Block since the Palaeozoic – with special emphasis to the neovolcanic edifices in the Lausitz Volcanic Field (Eastern Germany). Zeitschrift der Deutschen Gesellschaft für Geowissenschaften, 166, 125–147.

Tremolada, F., Bornemann, A., Bralower, T.J., Koeberl, C., van de Schootbrugge, B., 2006. Paleoceanographic changes across the Jurassic/Cretaceous boundary: the calcareous phytoplankton response. Earth and Planetary Science Letters, 241, 361–371.

Turner, J.P., Williams, G.A. (2004): Sedimentary basin inversion and intra-plate shortening. Earth-Science Reviews, 65, 277–304.

Tucker, R.M., Arter, G. (1987): The tectonic evolution of the North Celtic Sea and Cardigan Bay Basins with special reference to basin inversion. Tectonophysics, 137, 291–307.

Uličný, D. (2001): Depositional systems and sequence stratigraphy of coarse-grained deltas in a shallow-marine, strike-slip setting: The Bohemian Cretaceous Basin, Czech Republic. Sedimentology, 48, 599–628.

Uličný, D. (2004): A drying-upward aeolian system of the Bohdašín Formation (Early Triassic), Sudetes of NE Czech Republic: record of seasonality and long-term palaeoclimate change. Sedimentary Geology, 167, 17–39.

Uličný, D., Kvaček, J., Svobodová, M., Špičáková, L. (1997): High-frequency sea-level fluctuations and plant habitats in Cenomanian fluvial to estuarine succession: Pecinov quarry, Bohemia

Uličný, D., Martínek, K., Grygar, R. (2002): Syndepositional geometry and post-depositional deformation of the Krkonoše Piedmont Basin: a preliminary model. Geolines, 14, 101–102.

Uličný, D., Špicáková, L., Grygar, R., Svobodová, M., Čech, S., Laurin, J. (2009a) Palaeodrainage systems at the basal unconformity of the Bohemian Cretaceous Basin: Roles of inherited fault systems and basement lithology during the onset of basin filling. Bulletin of Geosciences, 84, 577–610.

Uličný, D., Laurin, J., Čech, S. (2009b): Controls on clastic sequence geometries in a shallow-marine, transtensional basin: The Bohemian Cretaceous Basin, Czech Republic. Sedimentology, 56, 1077–1114.

Uličný, D., Jarvis, I., Gröcke, D.R., Čech, S., Laurin, J., Olde, K., Trabucho-Alexandre, J.P., Švábenická, L., Pedentchouk, N. (2014): A high-resolution carbon-isotope record of the Turonian stage correlated to a siliciclastic basin fill: Implications for mid-Cretaceous sea-level change. Palaeogeography, Palaeoclimatology, Palaeoecology, 405, 42–58.

Uličný, D., Špičáková, L., Cajz, V., Hronec, L. (2015): Podklady pro prostorový model hydrogeologicky významných stratigrafických rozhraní ve vybraných Hydrogeologických Rajonech. Geofyzikální Ústav AV ČR. Unpublished report. Czech Geological Survey, Prague.

Underhill, J.R., Partington, M.A. (1993): Jurassic thermal doming and deflation in the North Sea: implications of the sequence stratigraphic evidence. Geological Society, London, Petroleum Geology Conference Series, 4, 337–345.

Vacek, J., Žák, J. (2019): A lifetime of the Variscan orogenic plateau from uplift to collapse as recorded by the Prague Basin, Bohemian Massif. Geological Magazine, 156, 485–509.

Valečka, J. (1979): Paleogeografie a litofaciální vývoj severozápadní části české křídové pánve. Sborník geologických věd, Geologie, 33, 47–81.

Valečka, J. (1989): Sedimentology, stratigraphy and cyclicity of the Jizera Formation (Middle–Upper Turonian) in the Děčín area (N. Bohemia). Věstník Ústředního ústavu geologického, 64, 77–90.

Valečka, J. (2019): Jurassic pebbles in the Cretaceous sandstones of the Bohemian Basin as a possible tool for reconstruction of the Late Jurassic and Late Cretaceous palaeogeography. Volumina Jurassica, 17, 17–38.

Valečka, J. (2020): Transgresní, příbřežní vápence korycanských vrstev (cenoman) v centrální části české křídové pánve a diskuse týkající se vzniku této pánve. Zprávy o geologických výzkumech, 53, 149–159.

Valečka J., Slavík. J. (1985): Litologický a sedimentologický vývoj na křídových stratotypových lokalitách Sutiny a Merboltice. Unpublished report. Czech Geological Survey, Prague.

Valečka, J., Skoček, V. (1991): Late Cretaceous lithoevents in the Bohemian Cretaceous Basin, Czechoslovakia. Cretaceous Research, 12, 561–577.

Valečka, J., Adamová, M., Burda, J., Dušek, K., Fediuk, F., Kořán, V., Manová, M., Nekovařík, Č., Nývlt, D., Opletal, M., Prouza, V., Rambousek, P., Šalanský, K. (2006): Vysvětlivky k základní geologické mapě České republiky 1 : 25 000, 02-242 Dolní Podluží. Česká geologická služba, Praha.

van Wees, J.D., Stephenson, R.A., Ziegler, P.A., Bayer, U., McCann, T., Dadlez, R., Gaupp, R., Narkiewicz, M., Bitzer, F., Scheck, M. (2006): On the origin of the Southern Permian Basin, Central Europe. Marine and Petroleum Geology, 17, 43–59.

van Wijhe, D.H. (1987): Structural evolution of inverted basins in the Dutch offshore. Tectonophysics, 137, 171–219.

van der Pluijm, B.A., Craddock, J.P., Graham, B.R., Harris, J.H. (1997): Paleostress in cratonic North America: implications for deformation of continental interiors. Science, 277, 794–796.

Vejbæk, O.V., Andersen, C. (2002): Post mid-cretaceous inversion tectonics in the Danish Central Graben: regionally synchronous tectonic events? Bulletin of the Geological Society of Denmark, 49, 129–144.

Vejbæk, O.V., Andersen, C., Dusa, M., Herngreen, W., Krabbe, H., Leszczynski, K., Lott, G.K., Mutterlose, J., van der Molen, A.S. (2010): Cretaceous. In: Doornenbal, H., Stevenson, A. (eds.): Petroleum Geological Atlas of the Southern Permian Basin Area. EAGE Publications, Houten, p. 195–209.

Vejlupek, M., Novák, J., Schovánková, D. (1986): Geologie permokarbonu českokamenické a kravařské pánve. Sborník geologických věd, Geologie, 41, 127–165.

Ventra, D., Nichols, G.J. (2014): Autogenic dynamics of alluvial fans in endorheic basins: Outcrop examples and stratigraphic significance: Sedimentology, 61, 767–791.

Ventura, B., Lisker, F. (2003): Long-term landscape evolution of the northeastern margin of the Bohemian Massif: apatite fission-track data from the Erzgebirge (Germany). International Journal of Earth Sciences, 92, 961–700.

Ventura, B., Lisker, F., Kopp, J. (2009): Thermal and denudation history of the Lusatian Block (NE Bohemian Massif, Germany) as indicated by apatite fission-track data. In: Ventura, B., Lisker, F., Glasmacher,U.A. (eds.): Thermochronological Methods: From Palaeotemperature Constraints to Landscape Evolution Models. Geological Society, London, Special Publications, 324, 1–12.

Voigt, S., Wagreich, M., Surlyk, F., Walaszczyk, I., Uličný, D., Čech, S., Voigt T., Wiese, F., Wilmsen, M., Niebuhr, B., Reich, M., Funk, H., Michalík, J., Jagt., J.W.M., Felder, P.J., Schulp, A.S. (2008): Cretaceous. In: McCann, T. (ed.): Geology of Central Europe, Volume 2: Mesozoic and Cenozoic. Geological Society, London, p. 923–997.

Voigt, T. (1994): Faziesentwicklung und Ablagerungssequenzen am Rand eines Epikontinentalmeeres – Die Sedimentationsgeschichte der Sächsischen Kreide. Unpublished PhD. thesis, TU Bergakademie Freiberg.

Voigt, T. (2009): Die Lausitzer-Riesengebirgs-Antiklinalzone als kreidezeitliche inversionsstruktur: geologische Hinweise aus den umgebenden Kreidebecken. Zeitschrift für Geologische Wissenschaften, 37, 15–39.

Voigt, T., von Eynatten, H., Franzke, H.J. (2004): Late Cretaceous unconformities in the Subhercynian Cretaceous Basin (Germany). Acta Geologica Polonica, 54, 673–694.

Voigt, T., Wiese, F., von Eynatten, H., Franzke, H.J., Gaupp, R. (2006): Facies evolution of syntectonic Upper Cretaceous deposits in the Subhercynian Cretaceous Basin and adjoining areas (Germany). Zeitschrift der Deutschen Gesellschaft für Geowissenschaften, 157, 203–243.

Voigt, T., Reicherter, K., von Eynatten, H., Littke, R., Voigt, S., Kley, J. (2009): Sedimentation during basin inversion. In: Littke, R., Bayer, U., Gajewski, D., Nelskamp, S. (eds.): Dynamics of Complex Intracontinental Basins. The Central European Basin System. Springer, Berlin, Heidelberg, p. 211–232.

Voigt, T., Kley, J., Voigt, S. (2021): Dawn and Dusk of Late Cretaceous Basin Inversion in Central Europe, Solid Earth Discuss. [preprint], https://doi.org/10.5194/se-2020-188, in review, 2020.

von Eynatten, H., Voigt, T., Meier, A., Franzke, H.-J., Gaupp, R. (2008): Provenance of Cretaceous clastics in the Subhercynian Basin: Constraints to exhumation of the Harz Mountains and timing of inversion tectonics in Central Europe. International Journal of Earth Sciences, 97, 1315–1330.

Weislogel, A.L., Hunt, B., Lisi, A., Lovell, T., Robinson, D.M. (2015): Detrital zircon provenance of the eastern Gulf of Mexico subsurface: Constraints on Late Jurassic paleogeography and sediment dispersal of North America. IN: Anderson, T.H., Didenko, A.N., Johnson, C.L., Khanchuk, A.I., and MacDonald, J.H., Jr. (eds.): Late Jurassic Margin of Laurasia—A Record of Faulting Accommodating Plate Rotation: Geological Society of America Special Papers, 513,

Weltje, G.J., von Eynatten, H. (2004) Quantitative provenance analysis of sediments: review and outlook. Sedimentary Geology, 171, 1–11.

Wendler, J.E., Wendler, I. (2016): What drove sea-level fluctuations during the mid-Cretaceous greenhouse climate? Palaeogeography, Palaeoclimatology, Palaeoecology, 441, 412–419.

Wenger, E., Tietz, O., Büchner, J., Nádaskay, R. (in prep.): Exotic pebbles embedded in diatreme breccias from the West Sudetes – what do they reveal about the latest Cretaceous paleogeography of the northern Bohemian Massif?

Wilmsen, M., Niebuhr, B., Chellouche, P., Pürner, T., Kling, M. (2010): Facies pattern and sea-level dynamics of the early Late Cretaceous transgression: a case study from the lower Danubian Cretaceous Group (Bavaria, southern Germany). Facies, 56, 483–507.

Wilmsen, M., Niebuhr, B., Fengler, M., Püttmann, T., Berensmeier, M. (2019): The Late Cretaceous transgression in the Saxonian Cretaceous Basin (Germany): old story, new data and novel findings. Bulletin of Geosciences, 94, 71–100.

Winchester, J.A., Pharaoh, T.C., Verniers, J., Ioane, D., Seghedi, A. (2006): Palaeozoic accretion of Gondwana-derived terranes to the East European Craton: recognition of detached terrane fragments dispersed after collision with promontories. In: Gee, D.G., Stephenson, R.A. (eds.): European Lithosphere Dynamics. Geological Society, London, Memoirs, 32, 232–332.

Wojewoda, J., 2007. Perm basenu Nachodu. In: Wojewoda, J. (ed.): Review of Permian sedimentary successions of Boskovice Trough, Nachod Basin and Trutnov Basin. Sedimentologica, 1, 85–99.

Woodcock, N.H. (2004): Life span and fate of basins. Geology, 32, 685–688.

Xu, W., Ruhl, M., Jenkyns, H.C., Hesselbo, S.P., Riding, J.B., Selby, D., Naafs, B.D.A, Weijers, J.W.H., Pancost, R.D., Tegelaar E.W., Idiz, E.F. (2017): Carbon sequestration in an expanded lake system during the Toarcian oceanic anoxic event. Nature Geoscience, 10, 129–134.

Žák, J., Sláma, J. (2018): How far did the Cadomian 'terranes' travel from Gondwana during Early Paleozoic? A critical reappraisal based on detrital zircon geochronology International Geology Review 60: 313–338.

Žák, J., Svojtka, M., Opluštil, S. (2018): Topographic inversion and changes in the sediment routing systems in the Variscan orogenic belt as revealed by detrital zircon and monazite U–Pb geochronology in post-collisional continental basins. Sedimentary Geology, 377, 63–81.

Zieger, J., Bittner, L., Gärtner, A., Hofmann, M., Gerdes, A., Marko, L., Linnemann, U. (2019): U–Pb ages of magmatic and detrital zircon of the Döhlen Basin: geological history of a Permian strike-slip basin in the Elbe Zone (Germany). International Journal of Earth Sciences, 108, 887–910.

Ziegler, P.A. (1975): The geological evolution of the North Sea area in the tectonic framework of North Western Europe. Norges geologiske undersøkelse Bulletin, 316, 1–27.

Ziegler, P.A. (1983): Inverted Basins in the Alpine Foreland. In: Bally, A.W. (ed.): Seismic Expression of Structural Styles: A Picture and Work Atlas. Volume 1 – The Layered Earth, Volume 2 – Tectonics Of Extensional Provinces, & Volume 3 – Tectonics Of Compressional Provinces. AAPG Studies in Geology, 15.

Ziegler, P.A. (1988): Evolution of the Arctic-North Atlantic and the Western Tethys. AAPG, Memoirs, 43.

Ziegler, P.A. (1990a) Collision related intra-plate compression deformations in Western and Central Europe. Journal of Geodynamics, 11, 357–388.

Ziegler, P.A. (1990b): Geological Atlas of Western and Central Europe. 2nd edition. Shell International Petroleum Maatschappij B.V., The Hague.

Ziegler, P.A. (1990c): Tectonic and palaeogeographic development of the North Sea rift system. In: Blundell, D.J., Gibbs, A.D. (eds.): Tectonic evolution of the North Sea rifts. Oxford University Press, Oxford, p. 1–36.

Ziegler, P.A. (1994): Cenozoic rift system of Western and Central Europe: an overview. Geologie en Mijnbouw, 73, 99–127.

Ziegler, P.A., Cloething, S., van Wees, J.-D. (1995): Dynamics of intra-plate compressional deformation: the Alpine foreland and other examples. Tectonophysics, 252, 7–59.

Ziegler, P.A., van Wees, J.D., Cloetingh, S. (1998): Mechanical controls on collision-related compressional intraplate deformation. Tectonophysics, 300. 103–129.

Zimmermann, J., Franz, M., Heunisch, C., Luppold, F.W., Mönnig, E., Wolfgramm, M. (2015): Sequence stratigraphic framework of the Lower and Middle Jurassic in the North German Basin: Epicontinental sequences controlled by Boreal cycles. Palaeogeography, Palaeoclimatology, Palaeoecology, 440, 395–416.

Žítt, J., Nekvasilová, O., Bosák, P., Svobodová, M., Štemproková-Jírová, D., Šťastný, M. (1997): Rocky coast facies of the Cenomanian-Turonian Boundary interval at Velim (Bohemian Cretaceous Basin, Czech Republic). First Part. Věstník Českého geologického ústavu, 72, 83–102.

Žítt, J., Vodrážka, R., Hradecká, L., Svobodová, M., Zágoršek, K. (2006): Late Cretaceous environments and communities as recorded at Chrtníky (Bohemian Cretaceous Basin, Czech Republic). Bulletin of Geosciences, 81, 43–79.

Chapter 1

Evaluation of climatic and tectonic imprints in fluvial successions of an early Permian depositional system (Asselian Vrchlabí Fm., Krkonoše Piedmont Basin, Czech Republic)

by Kateřina Schöpfer, Roland Nádaskay

and Karel Martínek

"Es ist so gewiß als wunderbar, daß Wahrheit und Irrthum aus Einer Quelle entstehen; deßwegen man oft dem Irrthum nicht schaden darf, weil man zugleich der Wahrheit schadet."

"It is as certain as it is marvelous that truth and error come from one source. Therefore one often may not injure error, because at the same time one injures truth."

Johann Wolfgang Goethe:
Maximen und Reflexionen

Key words

Non-marine basin, fluvial, lacustrine, climate, tectonics, early Permian, Krkokoše Piedmont Basin

Abstract

The Krkonoše Piedmont Basin (KPB), an early post-Variscan basin (c. 310–280 Ma) located in the northern Czech Republic, contains up to 300 m thick non-marine lower Permian deposits in its southern-central part. The early Permian KPB exhibits striking similarities to other early Variscan, near equatorial basins in terms of tectonostratigraphic evolution. This work focuses on sedimentological analysis of the Vrchlabí Fm. (Asselian) in the SW part of the KPB. In the southern-central KPB, the formation consists of fluvio-deltaic deposits, which laterally pass into lacustrine deposits derived from lake Rudník in the northern part of the KPB. Fluvial deposits comprise sandstone and conglomeratic bodies interpreted as single- and multi-storey channel fills as well as various macroforms (e.g., bars) deposited by a braided fluvial system. Vertically, fluvial successions are divided into five different units that exhibit variable ratios between preserved channel fill and floodplain deposits (reflecting differing accommodation/supply ratio) and contrasting channel-fill geometries. In order to explain the observed changes in the fluvial style and to determine the controlling factors, the interaction of the fluvial system with the lacustrine basin was investigated by interpreting base-level changes of the fluvial system, as well as tracing horizons of lake expansion (allegedly a result of humid periods). In the central part of the KPB, the transition from fluvial to lacustrine deposits is represented by alternating grey sandstone and dark grey siltstone/mudstone beds, deposited either as mouth bars or bottomsets of lacustrine microdeltas. Detailed correlation of existing borehole data and newly acquired outcrop gamma-ray logs led to better understanding of lateral

60

and vertical relationships between the fluvial, the 'transitional' and the lake facies at the basin-scale. Altough initial tectonic subsidence played a substainal role during the intial deposition of the formation, the observed pattern cannot be explained merely by tectonics. The external geometries and internal architecture of fluvial channel bodies, variable degree of floodplain preservation together with inferred decelerated fault subsidence indicate that changes in fluvial style through time were significantly controlled by climate variations. This study illustrates the usefulness of an interdisciplinary approach to reconstruct a basin's early Permian stratigraphic history in a region with sparse outcrops and very limited fossil record.

Introduction

A depositional record of ancient continental fluvial successions is most basically interpreted to reflect changing rate of sediment supply vs. accommodation, both in turn reflecting the tectonic background, such as basin type and its subsidence rate and plate-tectonic setting (e.g., Martinsen et al. 1999, Arche and López-Gómez 1999; Holbrook and Schumm 1999; Catuneanu and Elango 2001; Medici et al. 2015; Scherer et al. 2015) and climatic forcing (e.g., Vandenberghe 2003; Allen et al. 2011, 2014). The interplay of accommodation and supply can also lead to deposition of small-scale cycles that result from autogenic processes, e.g., the intrinsic behaviour of fluvial system type (e.g., Ventra and Nichols 2014). Since the effects of sea-level changes on fluvial stratigraphic architectures reach their limit within c. 100 km upstream from the shoreline (e.g., Blum and Törnqvist 2000), sea-level changes do not affect basins in the continental interior.

Within extensional basins developing in the Variscan mountain range (Fig. 1a) complex fluvial-alluvial or fluvial-lacustrine systems developed in time and space, as exemplified by the post-Variscan Bohemian Carboniferous (middle–late Pensylvanian) to Permian intramontane basin system (e.g., Lojka et al. 2016; Opluštil et al. 2015, 2005; Opluštil 2005; Martínek et al. 2006a). Whereas small-scale fluvial cycles within Carboniferous formations are interpreted as resulting from channel migration in a low accommodation setting (e.g., Lojka et al. 2016), large-scale fluvial cycles seem to be governed by climate (e.g., Opluštil et al. 2015). However, no constraints on tectonic vs. climatic forcing of early Permian fluvial systems have so far been presented, though it is expected that climate played a significant role through a general shift from wetter to drier conditions around the Carboniferous–Permian boundary and a gradual aridization towards the late early to middle Permian (e.g., Opluštil et al. 2013; Martínek and Uličný 2001).

The most extensive exposures of lower Permian rocks are found in the Krkonoše Piedmont Basin (KPB; NE Czech Republic; Fig. 1b). In this basin the thickest, so far poorly studied, fluvial strata are preserved within the Vrchlabí Formation (Asselian), that laterally passes

into fossiliferous lacustrine strata of the same age that were, in contrast, intensely studied in the past (e.g., Martínek et al. 2006a; Blecha et al. 1997). In order to fill this gap, this study focuses on lower Permian (Asselian) fluvial deposits of the Vrchlabí Fm. in the southern and central KPB. Previously, individual members of the Vrchlabí Fm. were correlated only as lithofacies with low resolution (Tásler et al. 1981). The present study illustrates that high-resolution stratigraphic correlation results in better understanding of the tectonostratigraphic evolution of the KPB during early Permian times.

This paper presents the first detailed analysis of the lower Permian fluvial succession in terms of sedimentary facies, architectures and palaeocurrents of the two fluvial members of the Vrchlabí Fm., namely the Stará Paka Sandstone and the Čistá Sandstone. The depositional model is based on detailed analysis of outcrop data in combination with subsurface data permitting the correlation of time-equivalent depositional units. This approach enabled the assessment of stratigraphic juxtaposition of fluvial and lacustrine deposits of the Vrchlabí Fm. across the southern and central KPB.

This study, therefore, aims to improve the general understanding of main controls on the deposition of an early Permian fluvial system and its interaction with an extensive lake located in the northern KPB (Martínek et al. 2006a). Furthermore, we compare this depositional model and the stratigraphic evolution of the early Permian fluvial system in the KPB with published contemporary analogues in the North American–European Variscan Orogeny, e.g., the Autun, Lodéve and Saar–Nahe basins and the Cumberland Basin, Canada.

Geological setting

The Krkonoše Piedmont Basin (KPB) is a part of an extensive basin system located between western Bohemia and central Silesia (Figs. 1b, c) that formed as a result of early post-Variscan extension/transtension (middle Pennsylvanian to early Permian, ca. 310–280 Ma) within the Bohemian Massif. Several unconformities recorded within the infill of the KPB (Prouza and Tásler 2001; Opluštil et al. 2016) imply a complex tectonosedimentary evolution. Despite changes in the basin geometry during Mesozoic and Cenozoic times (Uličný et al. 2002), the formation and the original geometry of the basin was probably controlled by NE-SW trending fault zone, following the boundary, i.e. the suture zone, between the Saxothuringian and Teplá–Barrandian (Fig. 1b). Uličný et al. (2002) further inferred that the KPB existed as a half-graben with maximum subsidence located at a major NE–SW trending normal fault that constituted the northern basin margin during late Carboniferous (middle–late Pennsylvanian) and early Permian (Asselian) times. Additionally, the basin could have been segmented by number of NW–SE oriented ('Sudetic') faults.
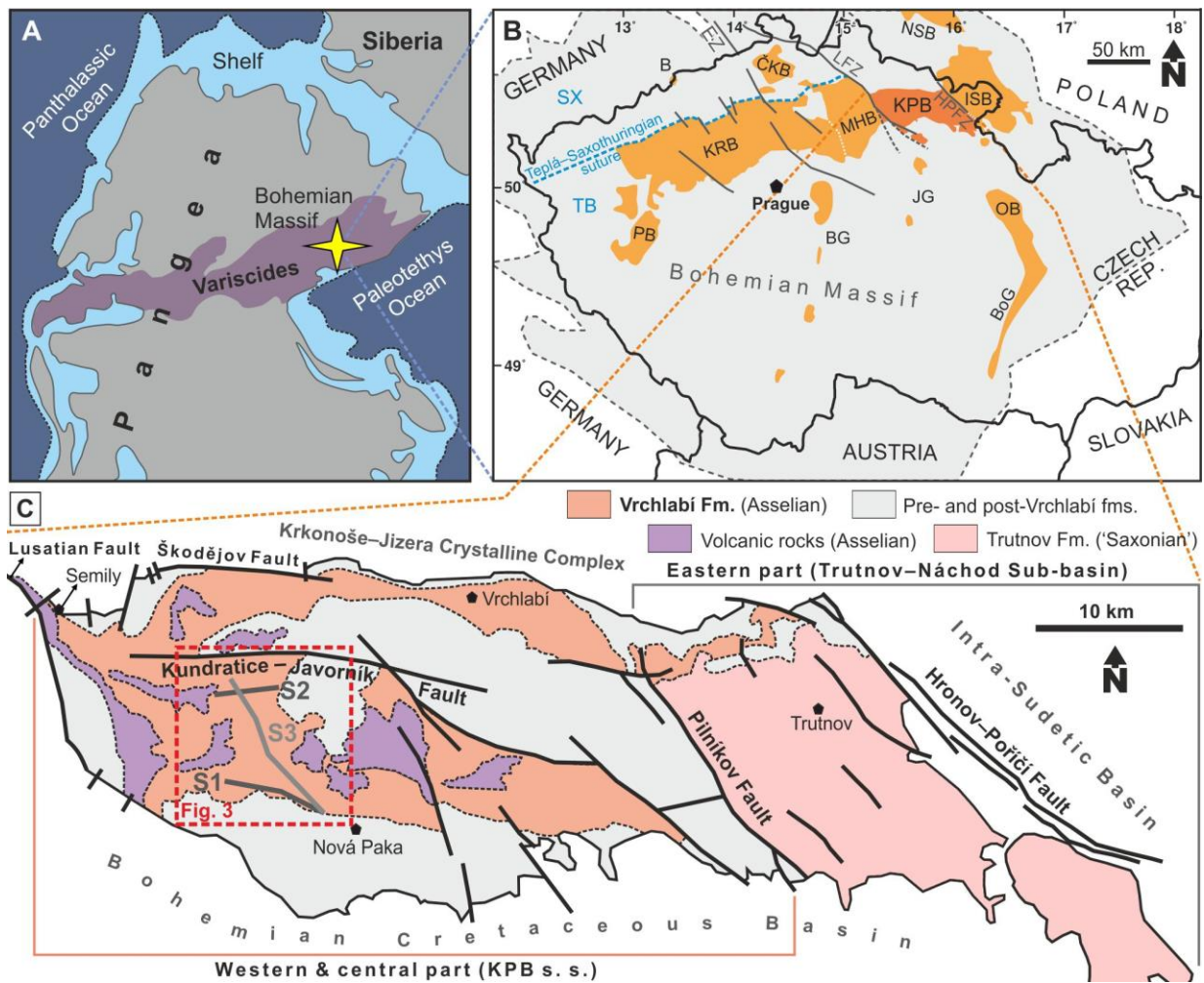
Figure 1. (a) Palaeogeographic reconstruction showing the approximate location of the Bohemian Massif within the Variscan Orogeny during early Permian times (c. 280 Ma). The simplified map is based on Blakey (2020). **(b)** Inset map of the Czech Republic shows location of the Krkonoše Piedmont Basin (KPB, dark orange) as a part of a large extensional Carboniferous-Permian basin system (light orange) that formed during post-Variscan times within the Bohemian Massif. **(c)** Detailed map of the KPB illustrating the basin structural configuration, the regional extent of the Vrchlabí Formation (including early Permian volcanic rocks) and the studied localities. Abbreviations: BG – Blanice Graben, BoG – Boskovice Graben, ČKB – Česká Kamenice Basin, HPFZ – Hronov–Poříčí Fault Zone, ISB – Intra-Sudetic Basin, JG – Jihlava Graben, KRB – Kladno–Rakovník Basin, LFZ – Lusatian Fault Zone, MHB – Mnichovo Hradiště Basin, NSB – Northern Sudetic Basin, OB – Orlice Basin, PB – Pilsen Basin, SX – Saxothuringian, TB – Teplá–Barrandian Unit.

Presumably during the Saale phase of the Variscan orogeny, i.e., between the 'Autunian' (Asselian–Sakmarian) and 'Saxonian' (Sakmarian–Kungurian; Opluštil et al. 2016), the KPB experienced inversion accompanied by pervasive brittle deformation and coeval formation of the Trutnov–Náchod Sub-basin (TNSB), a structure governed by dextral slip on NW-SE trending strike-slip faults (Uličný et al. 2002; Fig. 1c). Although, the easterly lying TNSB is associated with the KPB (e.g., Prouza and Tásler 2001), it represents a structurally distinct tectonic element that is superimposed on the older strata in the KPB. Based on correlation of marker horizons, the KPB possibly once formed an extensive depositional space with the neighbouring Mnichovo

Hradiště Basin (MHB) and Česká Kamenice Basin (ČKB) in the west and was likely connected with the Intra-Sudetic Basin (ISB) in the east (cf. Prouza et al. 1997 and Opluštil et al. 2016; Fig. 1b).

The infill of the KPB comprises in total 1800 m of Pennsylvanian (Moscovian/Kasimovian) to Lower Triassic non-marine deposits. Lithostratigraphic division of the KPB (Fig. 2; Tásler et al. 1981; Prouza and Tásler 2001) is based mainly on extensive geological mapping and records from several deep boreholes. In the KPB, abundant siliciclastic red-bed deposits are interbedded in several stratigraphic levels with coal seams, varicoloured mudstones to organic-rich shales or volcaniclastics. The upper part of the Vrchlabí Fm., together with the underlying Semily Fm., comprises the largest portions of volcanic rocks in the KPB. Predominantly in the western part of the KPB, effusive mafic volcanic rocks and subvolcanic bodies are locally interbedded with up to c. 40 m thick clastic deposits (Stárková et al. 2011; Fig. 3). Emplacement or deposition of volcanogenic rocks of the Vrchlabí Fm. coincided with the early Permian peak of volcanic activity associated with post-collisional extension-related magmatism (McCann et al. 2008).

The Vrchlabí Fm. (Asselian) is exposed mainly in the central and western parts of the KPB, less well preserved in the southwestern KPB and completely buried in the TNSB as well as in the MHB. The formation reaches a maximum thickness of 400–530 m (Tásler et al. 1981; Pešek 2004) in the northern KPB where it predominantly consists of lacustrine (black shales, grey to variegated mudstones) and red-brown alluvial facies (Martínek et al. 2006a). The most salient part of the lacustrine succession, termed the Rudník Mb., developed in the northern half of the KPB (e.g., in the vicinity of Košťálov; Fig. 3) and comprises c. 40–60 m thick grey mudstones interbedded with black shales, carbonates and subordinate sandstones and conglomerates (Tásler et al. 1981; Prouza and Tásler 2001). Martínek et al. (2006a) postulated that the Rudník Mb. was deposited in the deepest part of the depositional system.

In the southern KPB, the Vrchlabí Fm. reaches only up to c. 300 m in thickness (Tásler et al. 1981), comprises sandstone-dominated red to violet deposits and is divided into two stratigraphic members (Prouza and Tásler 2001). The older Stará Paka Sandstone predominantly consists of light brown, violet and red-brown weathered coarse-grained arkosic sandstones and conglomerates and is separated from the younger Čistá Sandstone by several metres thick variegated mudstones and siltstones with thin layers of limestone. The fine-grained interbed represents a stratigraphic equivalent of the Rudník Mb. as developed in the central and northern KPB. The Čistá Sandstone is characterized by red-brown and highly micaceous mudstones, which are gradually replaced in a vertical succession by red-brown fine- to coarse-grained fluvial-alluvial sandstones with subordinate amount of gravel (Tásler et al. 1981). However, some aspects
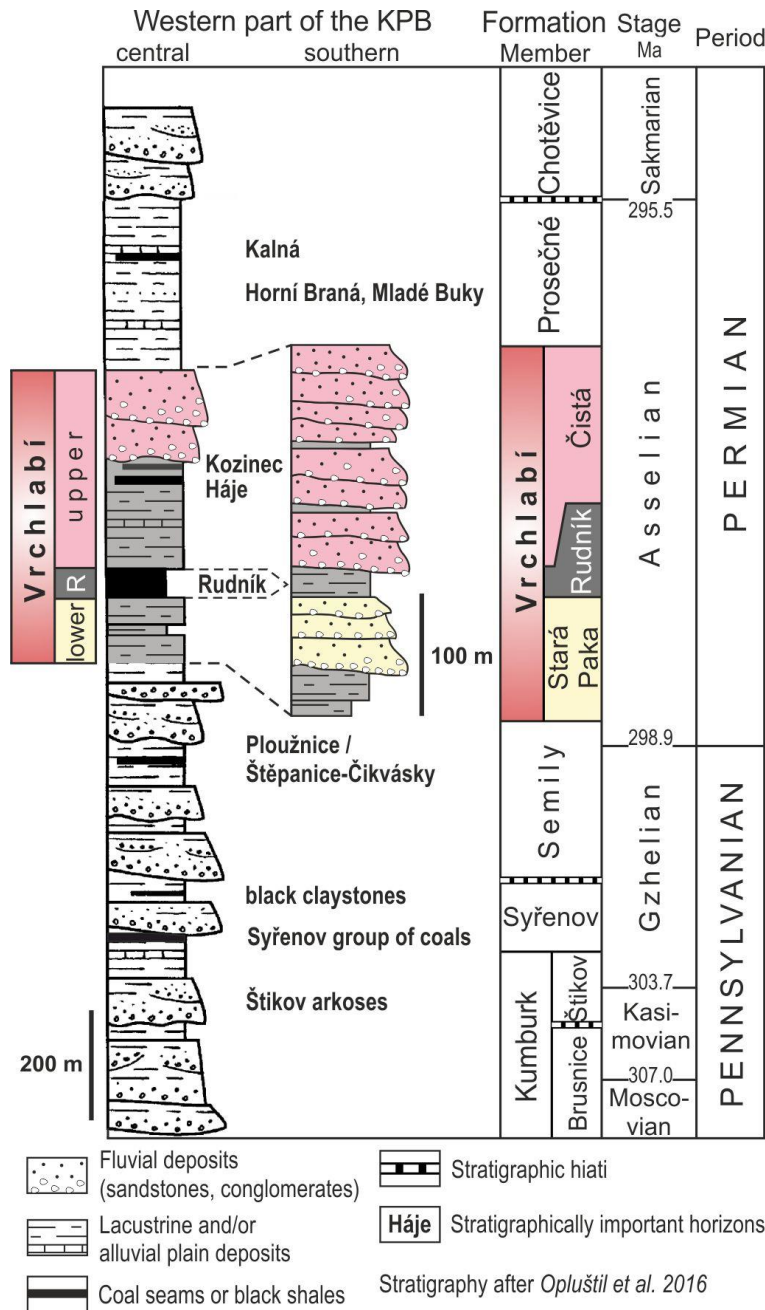
Figure 2. Two simplified stratigraphic columns showing the lithological evolution of the Vrchlabí Formation in the southern and central part of the western KPB. The most prominent horizon, termed Rudník Mb., comprises lacustrine deposits. In general, sandstone and conglomerate facies predominate in the south, while the central part is characterised by fine-grained facies with subordinate sandstone facies. Lithology and stratigraphy of the central part of the basin is based on the borehole HK-1 (after Martínek et al. 2006a). The numerical ages (Ma) are taken from the international chronostratigraphic chart v2019.

of the lower Permian deposits in the KPB, e.g., provenance of the clastic material, exact location of the source area as well as transport distance, are unanswered. Based on pebble composition analysis of conglomerates from the Stará Paka Sandstone, Prouza and Tásler (2001) proposed that some of the material was derived from local source and transported over short distance. On the other hand, the analysis of heavy minerals and exotic pebbles from the Stará Paka Sandstone pointed to a distant source area, such as high-grade metamorphic rocks of the Moldanubian Zone (Martínek and Štolfová 2009). The latter was corroborated by Sidorinová and Stárková (2017) who also interpreted a marked difference between heavy mineral spectra of the Vrchlabí Fm. and underlying Pennsylvanian formations as a result of source area shift coeval with reconfiguration of basin geometry towards asymmetric half-graben (cf. Martínek et al. 2006a).

The transition between fluvial-alluvial and lacustrine facies, i.e. interfingering of variegated mudstones, carbonates and sandstones, is only known from boreholes in the central KPB and has not been previously described from outcrops anywhere in the KPB.

Dataset and methods

Analysis of lithofacies and architectural elements

This study presents a field data from 24 measured sections from 39 localities in the southern and central KPB (Fig. 3). Sedimentological interpretations are based on investigating facies and architectures in outcrop, complemented by palaeocurrent measurements and detailed sandstone petrography performed on thin sections. Photomozaics were generated from field photographs using the Zone Photo Studio 17 software.

The description of lithofacies follows a widely applied scheme by Miall (1977), namely the classification considers lithology, grain size, texture, style of bedding, sedimentary structures, sorting and clast roundness (Table 1, Fig. 4). Additionally, the facies shape is implemented using the scheme by Ramos and Sopeña (1983). The architectural elements, i.e. geometric arrangement of facies assemblages, are defined by geometries and bounding surfaces, using the methodology of Bridge (1993).

Outcrop gamma-ray and well-logs

In addition to conventional sedimentological logs, spectral gamma-ray logs were obtained from 20 localities with proximity to deep boreholes with available geophysical well-logs (Table 2). The principal purpose of the field spectral gamma-ray logs was to constrain the stratigraphic position of key sections through their correlation to well-logs. This is a well-established approach applied frequently to complex sedimentary systems, such as fluvio-lacustrine or fluvio-deltaic/estuarine (e.g., Davies and Elliot 1996; Hampson et al. 2005; Hornung and Hinderer 2011), since it allows for correlation of key stratigraphic surfaces with much higher resolution. Field measurements were conducted using the GS-256 (Geofyzika Brno) device at variable increments ranging from 5 to 10 cm in mudstones and shales and up to c. 50 cm in coarse-grained channel fills. Although a complete spectrum (K, U, Th) was obtained, only total radioactivity curves were employed for cross-section correlation (Fig. 5).

The outcrop gamma-ray logs bridged few kilometres long distances between two neighbouring boreholes, which would not be possible using lithologic sections only. Subsurface lithological and well-log data were obtained from Czech Geological Survey – Geofond. In this study, gamma-ray (GR) logs were used as primary data for constructing stratigraphic cross-sections. Gamma-ray logs reflect summary concentrations of main radiogenic elements (K, Th,
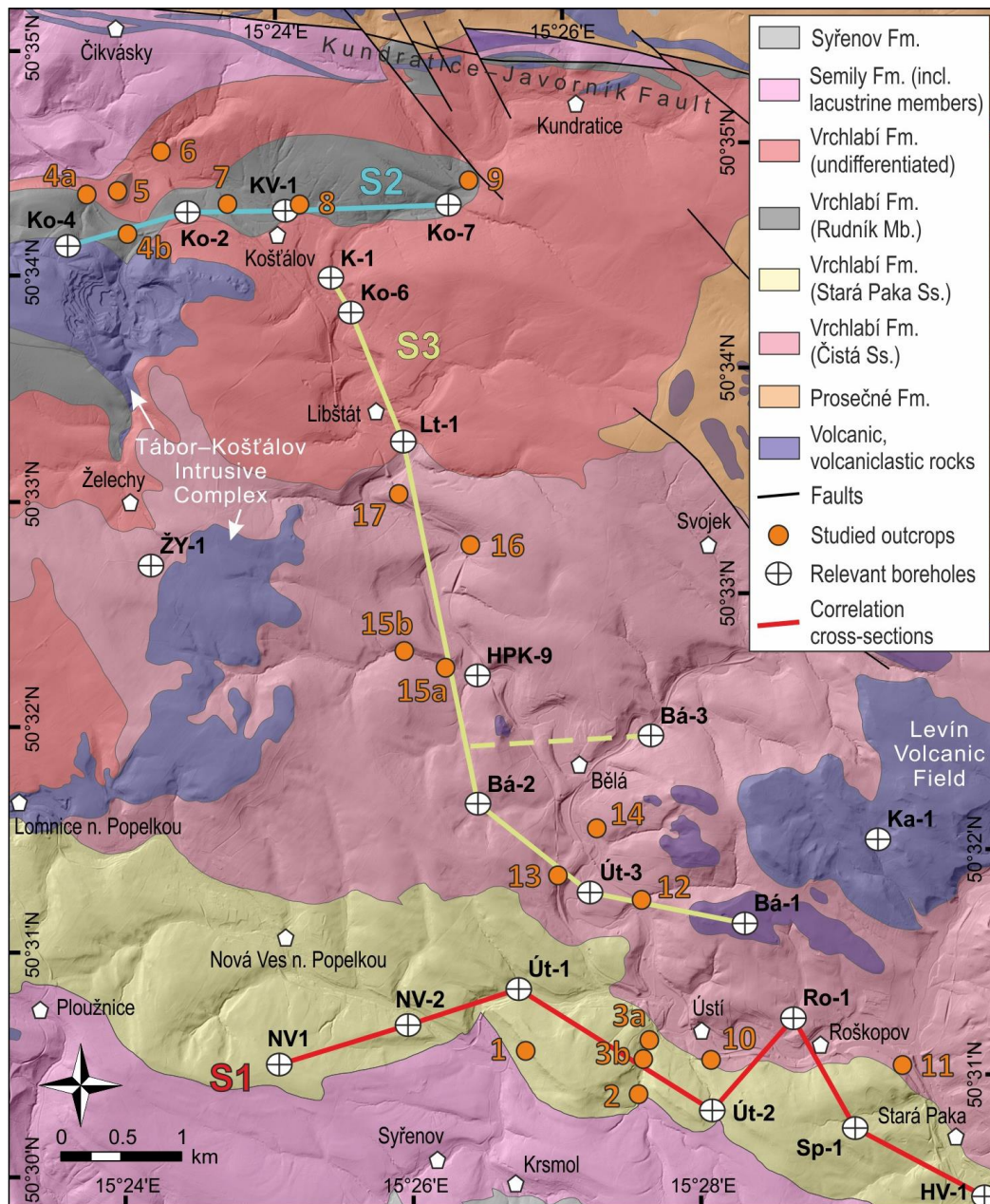
Figure 3. Geological map showing regional distribution of the Stará Paka Sandstone and the Čistá Sandstone (including the Rudník Mb.) together with locations of studied outcrops and three correlation panels S1 – S3 shown in Figure 15. Localities: 1 Brodky, 2 Ústí u Staré Paky – cemetery, 3a,b Ústí u Staré Paky – railway stop (cut banks), 4a Košťálov – railway cut (west), 4b Košťálov – railway cut (east), 5 Košťálov – castle, 6 Košťálov – gorge, 7 Košťálov – former mill, 8 Košťálov – former inn, 9 Kundratice, 10 Roškopov, 11 Stará Paka – railway station, 12 Bělá – V polsku, 13 Bělá – railway cut south, 14 Bělá - road cut, 15a Bělá – railway bridge (lower), 15b Bělá – railway bridge (upper), 16 Libštát – Vystrkov, 17 Libštát – raiway cut.

U) and are used as a proxy for clay mineral content – via potassium contained in illite (Rider 1996). Within sedimentary formations, an increase of clay mineral content reflects decreasing grain size (sand content) and vice versa. Together with sedimentological outcrop data the basin-scale correlations have provided information on large-scale sedimentary facies and architecture of the Stará Paka and the Čistá Sandstone and their relationship to lacustrine facies in the central KPB.

67

Accommodation/supply (A/S) ratio

Since sea-level changes played no role in the KPB, being a continental interior basin in topographically elevated position, we attempt to assess the changes in large-scale fluvial architectures in terms of changing accommodation vs. supply, employing A/S ratio sensu Martinsen et al. (1999). The construction of a sequence stratigraphic framework for the Vrchlabí Fm. is not sought in this paper, since the database is insufficient to track important stratigraphic surface across larger distances. However, the study aims to explore stratigraphic interactions of fluvial and lacustrine deposits in the southern and central KPB that could be later used to generate a basin-scale model that includes the northern part of the KPB.

Lithofacies

The lithofacies of the Vrchlabí Fm. include conglomerates, sandstones, siltstones and mudstones. In the southern KPB, the colour of the lithofacies varies from red, red-brown to purple/violet-red with common white or light yellow reduction spots whereas in the central part of the KPB, the colour is dark violet, grey to dark grey or even black. Significant colour change occurs also within one lithofacies, reflecting contrasting depositional environments. In order to avoid duplication of description, grey to black sediments are defined here as sub-facies. A short description of all lithofacies is provided in Table 1.

Conglomerates

Massive conglomerate (Gm)

Massive conglomerates form beds with thickness of 0.8 to 2 m, reach a maximum lateral extent of 9 to 12.5 m and have a concave-up erosional base (15–50 cm). Locally, conglomerates exhibit crude stratification and pass laterally to gravelly sandstones. Conglomerates are almost exclusively clast-supported (low proportion of coarse sandy matrix) with one encountered 212 exception of matrix-supported conglomerate (locally with imbricated clast floating in sandy matrix; Figs. 4a, f, g). They are moderately to poorly-sorted and contain polymict subangular to subrounded clasts with a size of 0.5–10 cm. The metamorphic (phylite, gneiss) and quartz clasts show better rounding, while altered volcanic clasts are typically subangular and less frequently rounded. Muddy rip-up clasts with a maximum size of 40 cm are preserved at the base of conglomeratic beds. The above described conglomerates are typically red to red-brown or violet, but several grey to pale grey beds comprising fine-grained massive conglomerates are exposed in the studied area and are defined here as sub-facies Gml.

Clast-supported conglomerates were deposited under high energy bedload deposition during flood flows (Ramos and Sopeña 1983). Small localized bodies of massive conglomerate

Table 1. Lithofacies identified in the southern and central KPB are divided according their colour into two groups – red and grey – representing different depositional settings.

Facies	Description	Interpretation
Gm/ Gml	Clast-supported conglomerates; fine- to coarse-grained; 0.8–2 m thick; massive or crudely stratified; pebble to cobble-sized clasts (0.5–10 cm); mud intraclasts (<40 cm); red, red-brown to violet but also grey colour (sub-facies Gml)	Clast-supported conglomerates – high energy bedload deposition during flood flows (Ramos and Sopeña 1983); matrix-supported conglomerates – cohesive debris/gravity flow/hyperconcentrated flow (Miall 1978, 1996)
Gt	Sandy matrix-supported conglomerates; 70 cm thick beds; erosional concave-up base; pebble-cobble-sized clasts (0.5–7 cm)	Gravel curve-crested dunes; transverse bars (Ramos and Sopeña, 1983, Miall, 1996)
Gp	Sandy matrix-supported conglomerates; 40 cm thick beds; red to red-brown, violet-red; sharp, step-like base; pebble-cobble-sized clasts (0.5–5 cm)	Gravel straight-crested dunes, transverse bars (Ramos and Sopeña 1983, Miall 1996)
Sp	Medium- to coarse-grained sandstones; moderately to poorly sorted; 0.15–3.5 m thick; tabular shape; flat non-erosive sharp base; mud intraclasts (<40 cm); abundant granule to cobble clasts (0.5–16 cm); mica-rich, calcite cement	Transverse or linguoid bars (Miall 1996); straight-crested dunes (Collinson et al. 2006)
Sl/ Sll	Medium- to coarse-grained sandstones; moderately to poorly sorted; 20–110 cm thick beds; tabular to sheet-like geometry; flat non-erosive sharp base; minor amount of granule and pebble clasts (0.5–8cm); calcite cement; local bioturbation	Flat bars with downstream accretion; straight-crested dunes (Collinson et al. 2006); sheet-like sandstones – crevasse splay deposits (Miall 1996) or channel avulsion (Bridge 2003, Nichols 1999)
St/ Stl	Medium- to coarse-grained sandstones; moderately sorted; 20–50 cm thick beds; through and lenticular bodies; flat top and concave-up base; minor amount of pebble clasts; highly micaceous; calcite cement; rarely bioturbated	Curve-crested and linguoidal dunes on channel floor/ top of bars (Collinson et al. 2006)
Sm/Sml	Medium- to coarse-grained sandstones; massive; tabular or lens geometry; flat non-erosive base; <1m thick; granule and pebble clasts mainly at the base; predominantly red to red-brown but also pale grey to grey (sub-facies Sml); calcite cement	Gravity-flow to high energy bedload-stream deposits (Miall 1977); grey-coloured (Sml) deposited at the lake margin, possibly represent fluvial channels on the subaquatic delta plain reworked by wave action or wave-induced currents
Sr/ Srl	Fine-coarse grained sandstones; well-sorted; 15–25 cm thick beds; tabular shape; no gravel-sized clasts; base is not sharply defined; calcite cement	Migration of ripples (lower regime flow); gravel at the base represent residual lag (Miall 1977)
Sh/Shl	Very-fine to fine sandstones; massive or horizontal lamination; 5–25 cm thick beds; bioturbation (animal burrows); interbedded with facies Fm	Suspension settling on floodplain/alluvial plain (Miall 1977, Foix et al. 2013) or in marginal lacustrine/prodelta setting
Scs	Fine-grained sandstones; erosive-based; fining upward from medium-grained with admixture of coarse-grained and granules; up to 25 cm thick beds; HCS-SCS bedding with well-developed swales; forming interbeds within facies Shl and Srl	Reworking of facies Shl and Srl by high-amplituded waves generated in lake during rare, exceptional storm events (cf. Eyles and Clark 1986)

Fm/Fml	Mudstones to siltstones; massive, red, red-brown, violet-red and grey (sub-facies Fml); abundant mica; intense bioturbation; up to 2 m thick	Poorly oxidized alluvial plain to lake margin, possibly mudflats occupying lake shore, occasionally eroded during fluvial channel avulsion on alluvial plain or subaquatic delta plain, or by mouth bar migration
Fl	Mudstones, siltstones, rarely argillaceous very fine- to fine- grained sandstones, predominantly grey; frequently bioturbated; "Shales" represented by laminated mudstones, claystones and bituminous shales (sometimes thinly bedded and fissile"paper shales") with intercalations of limestones (frequently rich in organic matter)	Open lacustrine, lake offshore; poorly oxidized; suspension settling from weak current or hypopycnic plumes (suspension plumes transported by river mouth close to the lake surface) or from hyperpycnic flows in distal prodeltaic setting; Shales deposited in open lacustrine, distal offshore setting, poorly oxidized to anoxic (cf. Martínek et al. 2006)

are interpreted as scour-fill or lag deposits. Rarely occurring matrix-supported massive conglomerate with high proportion of sandy matrix is interpreted as a result of cohesive debris/gravity flow or hyper-concentrated sheet flood.

Planar cross-bedded conglomerate (Gp)

This locally developed facies is preserved as laterally restricted beds (up to several metres wide) with irregular or lens geometry reaching 40 cm in thickness and sharp, locally step-like base. The predominantly quartzite conglomerate is matrix-supported, poorly-sorted and consists of moderately rounded pebbles and cobbles that are generally finer-grained than in the facies Gm (0.5 to 5 cm). They are predominantly red and red-brown in colour (Fig. 4b).

The planar cross-bedded conglomerates are either a result of gravel straight-crested dune migration or they reflect migration of a transverse channel bar (Ramos and Sopeña 1983; Miall 1996).

Trough cross-bedded conglomerate (Gt)

Red and red-brown conglomerates with a maximum lateral extent of 6 m and a thickness of up to 70 cm form a minor proportion of the studied outcrop sections. The matrix-supported conglomerates contain higher proportions of sandy matrix than facies Gp and typically exhibit erosional concave-up bases. Pebble to cobble-sized clasts (0.5–7 cm) are poorly sorted and subrounded to subangular (Fig. 4c).

Facies Gt is interpreted as a result of gravel curve-crested dune migration. Alternatively, trough cross-bedded conglomerates may have been formed by transverse bars, which migrated throughout the channel (Ramos and Sopeña 1983; Miall 1996).

Sandstones

The sandstone facies described here are listed below according to their prominence (i.e., by decreasing abundance in outcrop). In general, sandstones consist of quartz grains (46–63 % of the bulk rock), abundant metamorphic rock fragments (20–30%), such as para- and orthogneiss, quartzite and phylite, infrequent volcanic rock fragments, feldspars, micas and variable amounts of carbonate cement.

Planar cross-bedded sandstone (Sp)

Predominantly tabular planar cross-bedded sandstones are 0.15–3.5 m in thick, with foreset dips varying from 15° to 25° (Fig. 4d). In general, their bases are flat, non-erosive and sharp, but less frequently, scoured bases are exposed. At the beds' base, lenticular mud intraclasts (up to 40 cm long), that are longitudinally aligned with the base, are present. Medium- to coarse-grained gravely sandstones are moderately to poorly-sorted and contain clasts of various size ranging from 0.5 to 16 cm. Clasts are polymict with high proportion of subrounded quartz grains, followed by well-rounded metamorphic clasts and subangular volcanic clasts. The largest clasts are concentrated at the base of individual beds (pebble to cobble lags) and become rare or absent towards the top of the bed while the smaller clasts can form pebble layers within the bed. Mica is typically concentrated on the bed tops. The sandstones are cemented by calcite and locally dolomite. Rare bioturbation in the form of simple or branched crawl or resting animal traces, occur at or up to a few centimetres above the base. Thick successions of planar cross-bedded sandstones were formed by transverse or linguoid bars (Miall 1996), while the smaller sets of the facies could reflect deposits of straight-crested dunes that migrated on the channel floor or developed on the top of channel bar (Collinson 1996).

Low angle cross-bedded sandstone (Sl; subfacies Sll)

The sandstones form tabular beds with thickness ranging from 0.2 to 1.1 m and length of up to 30 m. The base is typically flat, non-erosive and sharp and foreset dips range from 5° to 15°. The medium- to coarse-grained sandstones are moderately or poorly sorted and contain minor or no amounts of gravel, which may be present either at the base of the beds or very locally throughout the entire vertical succession (Fig. 4e). The size of the subrounded to subangular clasts ranges from 0.5 to 8 cm. The sandstones are cemented by calcite cement and are commonly bioturbated. Subfacies Sll comprises fine- to medium-grained beige to grey sandstones (Fig. 4r).

The sandstone beds are deposits of flat bars that reflect downstream accretion and flat straight-crested dunes, that were both deposited under lower flow regime (Collinson 1996). In

contrast, sheet-like sandstones that extend laterally for more than 20 km and occur within fluvial channels are interpreted as a result of deposition under upper flow regime. The bioturbated sheet-like sandstones enclosed in floodplain deposits are interpreted as crevasse splay deposit (Miall 1996) or resulting from channel avulsion (e.g., Bridge 2003; Nichols 1999). Grey bioturbated counterparts (subfacies Sll) are interpreted as marginal lacustrine deposits.

Trough cross-bedded sandstone (St; subfacies Stl)

The sandstones of facies St are less frequently exposed, display trough and lenticular geometries with flat tops and concave-up erosive bases and have a maximum lateral extent of c. 2 m. The bed thickness ranges from 20 to 50 cm. These moderately sorted, medium- to coarse-grained sandstones infrequently contain pebbles, are highly micaceous, are cemented by calcite and are rarely bioturbated (Figs. 4h, k). Grey sandstones of subfacies Stl are fine- to medium-grained and form up to 30 cm thick sets with lateral extent of a few metres (Fig. 4r).

Facies St is the result of migration of curve-crested and linguoidal dunes on a channel floor or on the top of bars (lower flow regime; Collinson et al. 2006), while grey counterparts are interpreted to be marginal lacustrine deposits.

Massive sandstone (Sm; subfacies Sml)

Massive medium- to coarse-grained sandstones display tabular or trough/lens geometry. Sandstones have flat non-erosive or erosional base, thickness varying between c. 20 cm and up to 1 m and contain variable amounts of gravel that is concentrated mainly at the base of the successions. The facies exhibits two contrasting colour groups, a predominant red to red-brown (Figs. 4f, h, l) and a subordinate grey to pale grey group, the latter being defined as subfacies Sml (Fig. 4q). The massive sandstones of facies Sm were deposited by high energy bedload stream or represent hyperconcentrated flow (Miall 1977, 1996). Locally, they vertically pass into planar or trough cross-bedded sandstones indicating decreased flow energy. In case of erosive-based sandstones, gravel at the base of the channel represents a residual lag (Miall 1977). The grey to pale-grey coloured subfacies Sml is interpreted to reflect marginal lacustrine setting.

Ripple cross-laminated sandstone (Sr; subfacies Srl)

Fine- to coarse-grained, well-sorted and typically red to red-308 brown sandstones generally occur as tabular beds, reach thicknesses of 15–25 cm and lack gravel-size clasts (Figs. 4h, j, m). The base of this facies is not sharply defined, but gradual from underlying trough cross-bedded sandstone facies (St). Grey and pale grey coloured, fine- to medium-grained sandstones found at several localities are defined as sub-facies Srl (Fig. 4s). The sandstones of the subfacies

Figure 4. Representative lithofacies of the Vrchlabí Formation. Comments to individual facies in Table 1 and text.
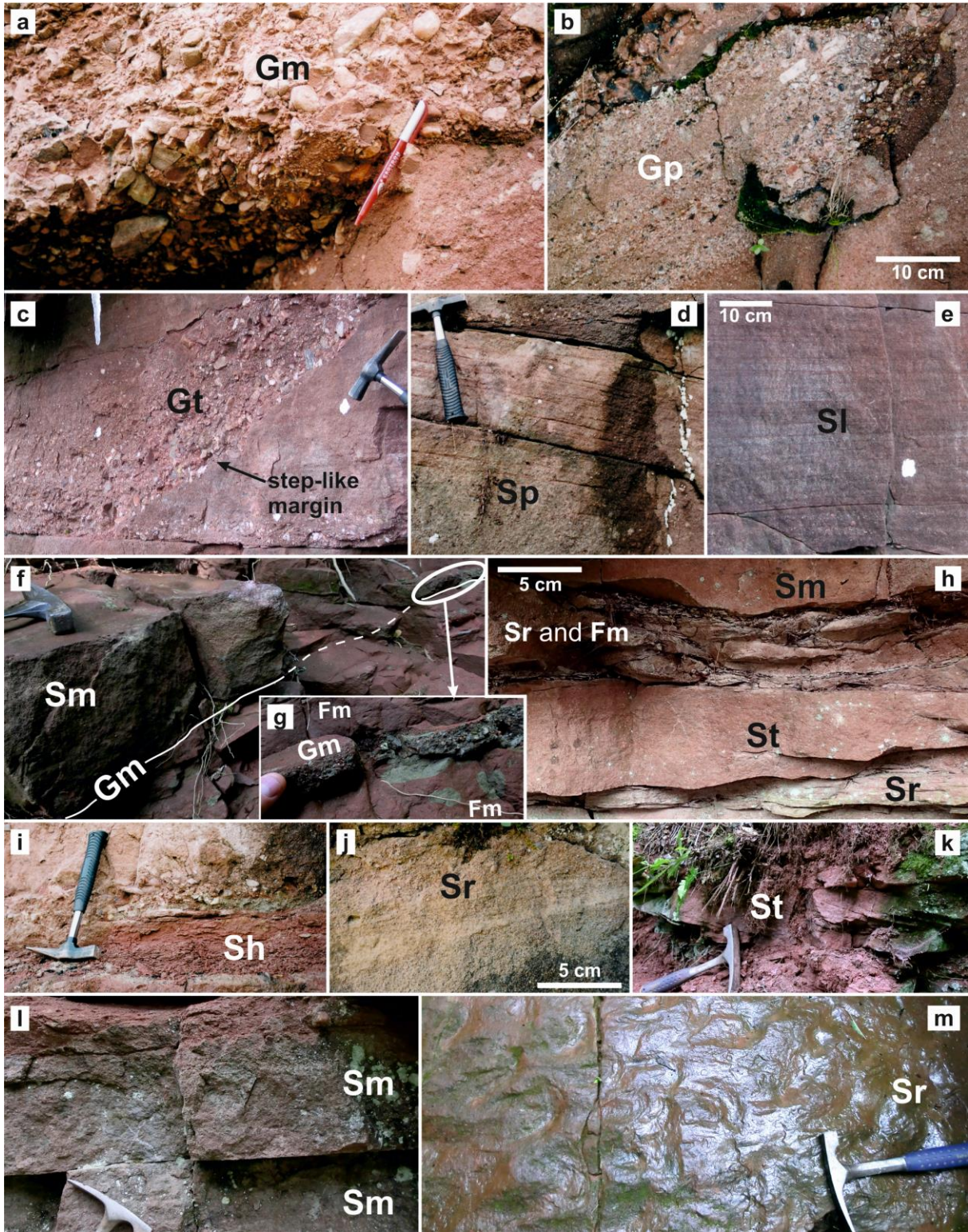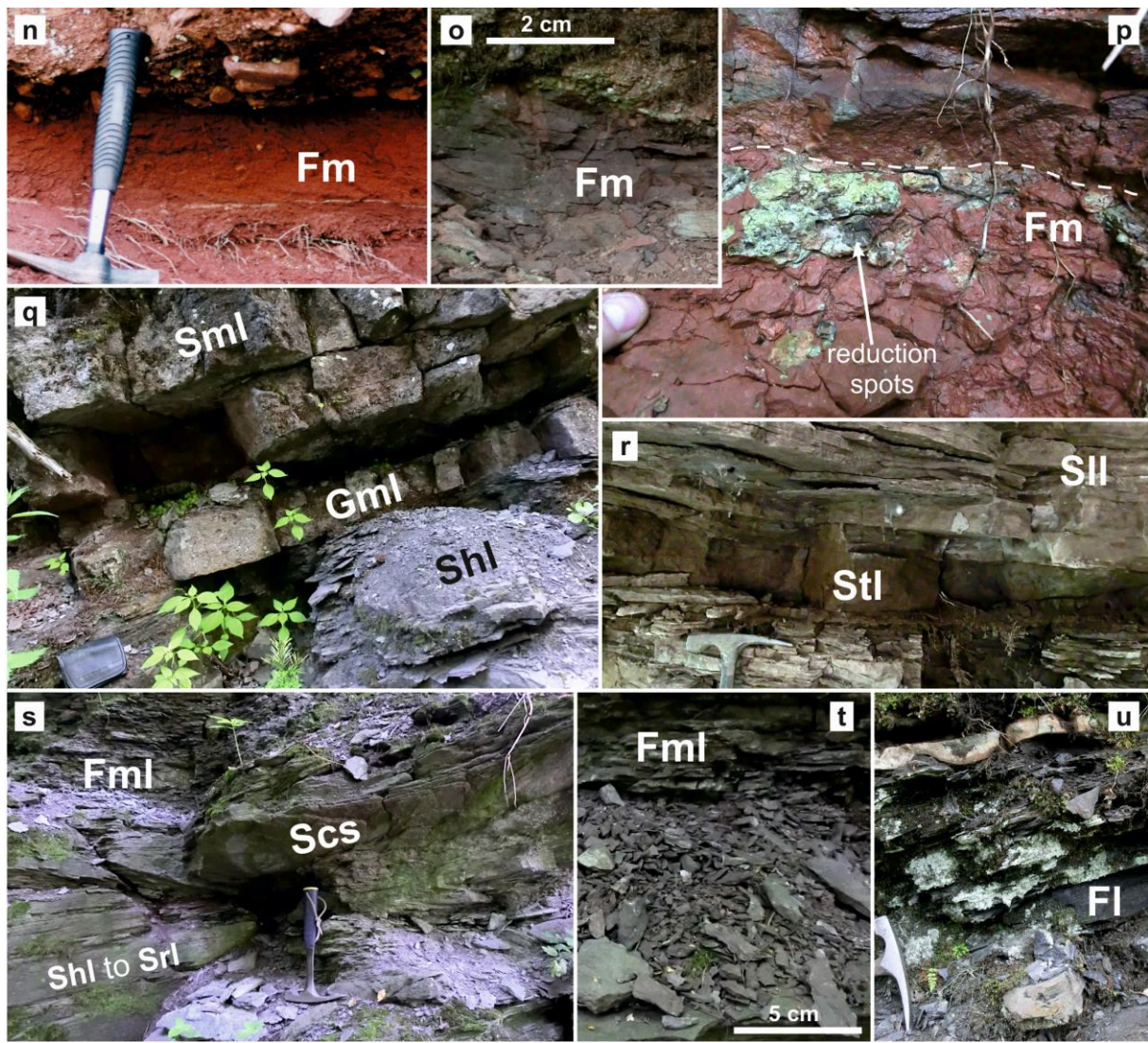
Srl form laterally extensive lenses or tabular beds up to c. 20 cm thick and are often interbedded with thin mudstone layers (up to few cm). The sandstones can be stacked to form up to c. 1 m thick bedsets. Within the stacked set, subfacies Srl displays transition into subfacies Sll.

Sediments of facies Sr are a result of ripple migration (lower flow regime) in a channel or on a floodplain (Miall 1977, 1996). Grey sandstones of subfacies Srl are interpreted as deposits of ripple migration in a marginal, relatively shallow-water lacustrine setting, driven by unidirectional current.

Very fine- to fine-grained sandstone (Sh; subfacies Shl)

The facies occurs infrequently and predominantly in the Čistá Sandstones as massive lenses or flat thin beds with horizontal lamination (Fig. 4i). The sandstones reach 5 to 25 cm in thickness with lateral extent of c. 2 m, are typically interbedded with mudstone/siltstone and are bioturbated (only animal burrows are present, root traces are absent). Grey coloured sandstones of subfacies Shl are strongly weathered (Figs. 4q, s).

This facies reflects deposition from suspension on proximal parts of the floodplain (Bridge 2003). Flows could have either emanated from channels or resulted from heavy rainfall (Collinson 1996). The grey coloured sediments indicate poorly-drained floodplain conditions (Allen et al 2013).

Basic well-log facies:
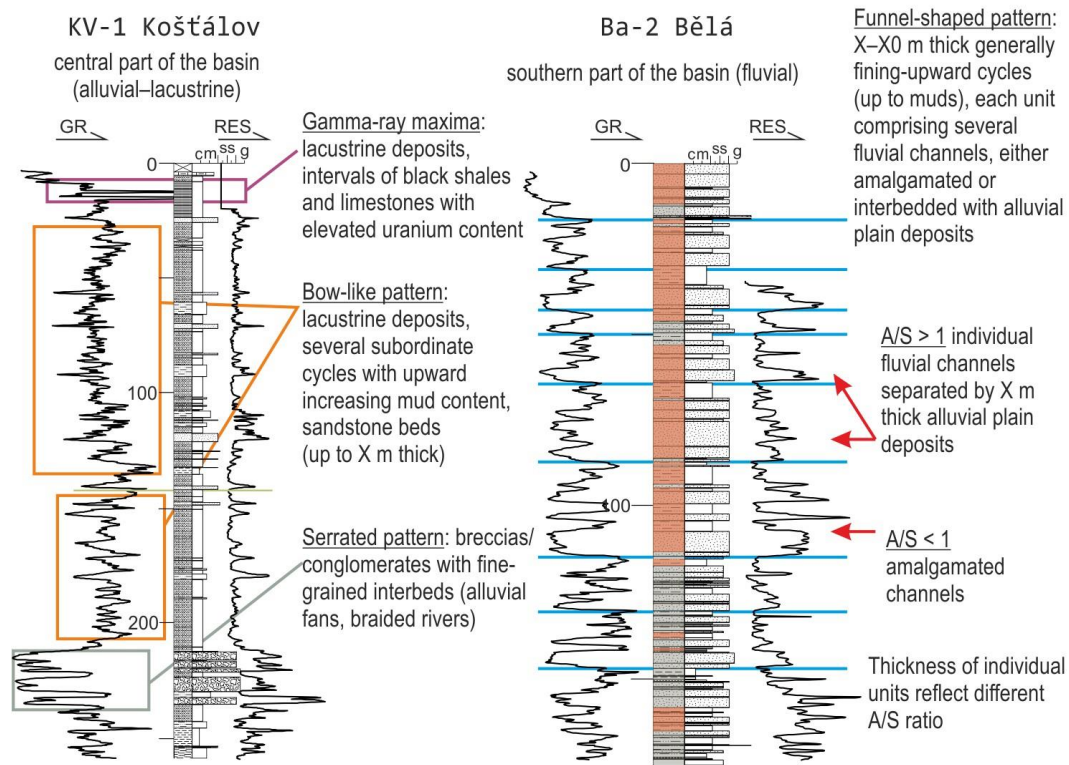
Figure 5. Diagram showing basic well-log pattern as exemplified by 1137 boreholes KV-1 (Košťálov; axial part of the basin, open lake) and Ba-2 (Bělá; basin margin, fluvial feeder system). Both gamma-ray (GR) and resistivity (RES) logs are shown here to demonstrate their value when interpreting lithology, and, in turn, a depositional environment. However, only the GR log is employed for correlating cross sections, as this method is lithology-dependent in siliciclastic rocks and better suited for stratigraphic correlations.

Very fine- to fine-grained sandstone; swaley-cross stratified (Scs)

This facies is very rare, but this may be due to the scarcity of exposure 331 with the corresponding lacustrine facies association. It comprises predominantly fine-grained sandstones arranged into striking concave sets and forms rare sets isolated within ambient sandstone (facies Shl or Srl; Fig. 4s). Internally, the individual laminae are parallel and do not form cross-cutting sets. The concave sets are up to 25 cm thick, display normal-grading (from medium-grained sandstones with admixture of coarse-grained and granules to fine-grained sandstone) and are top-truncated.

Concave sets are interpreted as 'swales' that develop as part of the HCS-SCS bedding (Dott and Bourgeois 1982). The convex 'hummocky' parts are not preserved due to truncation of the topmost part of the HCS-SCS set. The facies Scs forms interbeds within ambient Shl and Srl,

and is interpreted to have formed by reworking of the facies Shl and Srl by high-amplitude waves generated in the lake during rare, exceptional storm events (cf. Eyles and Clark 1986).

Fine-grained facies

Fine-grained facies consist predominantly of siltstone, mudstone and subordinately of limestone. The sediments are preserved as irregular bodies related to associated facies, are up to 150 cm thick, contain large amounts of mica and are intensively bioturbated. The sediment colour varies from red, red-brown, violet/grey-red in the southern KPB to grey and black in the central-northern KPB.

Mudstone and siltstone (Fm/Fml)

This facies represents the most abundant fine-grained facies, is up to 2 m thick and has up to 10 m of lateral extent. Mudstones and siltstones of the Čistá Sandstone are red and red-brown whereas of the Stará Paka Sandstone are predominantly violet-red to dark violet. The mudstones and siltstones contain large amount of mica and are highly disintegrated (forming flakes; Fig. 4n, o, p). In contrast to sandstone facies, they are bioturbated (predominantly *Planolites cf. montanus*). In the central KPB the facies is predominantly pale to dark grey and is regarded as sub-facies Fml (Figs. 4s, t). The grey sub-facies exhibits little or no bioturbation. Sub-facies Fml displays a gradual coarsening upwards, a trend evidenced by increasing number of ripple cross-laminated sandstone layers, and rarely contains volcaniclastic admixture and in one special instance a tuff bed (Figs. 3 – loc. 4a). Dark grey mudstones are soft and fissile and in places can show faint millimetre-scale lamination.

The red-coloured facies is interpreted as a deposit from suspension on a well-oxygenated floodplain (Bridge 2003, Collinson 1996), whereas grey sub-facies Fml reflects suspension settling from weak currents or standing water under poorly-oxidized conditions at a distal alluvial plain (Miall 1977; Foix et al. 2013). It may also reflect marginal lacustrine environment above the fair-weather wave base, being influenced by the relative proximity to fluvial mouths, as marked by an abundance of sandstone interbeds and a generally coarsening-upward trend.

Shales and bituminous shales, limestones (Fl)

Volumetrically, most of this facies is formed by frequently calcareous shales, with locally increased silt to fine sand and/or mica admixture (Fig. 4u). Sandy and silty mm thick laminae may be erosive-based and exhibit normal upward grading into ambient shales or carbonates (cf. Martínek et al. 2006a). In a vertical succession, a subordinate portion of shales is formed by fossiliferous, laminated, bituminous shales generally labelled as 'black shales' or 'paper shales'

when showing fissile millimetre-scale lamination. Bituminous shales alternate with limestones and dolomitic limestones, that are either dm-thick massive beds or up to c. 10 cm thick laterally continuous nodular interbeds. Bituminous shales, and in some cases limestones as well, contain high amounts of uranium, as reflected by gamma-ray logs, making them conspicuous horizons for well-log-based correlations.

This facies represents an offshore lacustrine environment and includes suboxic to anoxic facies of Martínek et al. (2006a). Deposition took place in the deepest and distal part of the lacustrine basin where reduced oxygenation or anoxia prevailed. The offshore areas 379 closer to the lake margin were periodically affected by gravity currents (underflow) generated at river mouths. Thinly bedded pairs of shale/black shale or carbonate and siltstone were termed 'laminites' by Martínek et al. (2006).

Facies associations

The Vrchlabí Fm. comprises five genetic facies associations: multi-storey and single-storey fluvial channel bodies, floodplain, deltaic and lacustrine (Fig. 6). The individual architectural elements are defined by their external geometries, bounding surfaces and the organisation of their internal structures (based on Allen 1983; Miall 1988 and Bridge 1993). In addition, a recently developed scheme based on the annual discharge variability (Fielding et al. 2018) is used in this study to examine the applicability of this relatively new scheme on an ancient Late Palaeozoic fluvial system. Fluvial and deltaic facies associations of the Vrchlabí Fm. are poorly studied hitherto, therefore this paper deals with them in a greater detail. Additionally, the previously described lacustrine facies (e.g., Martínek et al. 2006a; Blecha et al. 1997) are complemented by new results derived from this study to provide a better overview of the early Permian fluvial system. The character of individual associations and related architectural elements is provided by a series of outcrop-based photomosaics and line drawings (Fig. 7–12).

Multi-storey fluvial channel facies association (CHms)

This facies association consists of up to 8 m thick sandstone and conglomerate bodies with maximum lateral extent of 17 m (Figs. 7, 8 and 11). Conglomerate bodies are massive or cross-stratified (facies Gm, Gp) and cover the basal part of or are interbedded with the sandstone bodies (Fig. 11e). The sandstone bodies are composed of medium- to coarse-grained sandstones with predominant planar (facies Sp) and low-angle (facies Sl) cross-bedding and subordinate trough cross-bedding (facies St) and massive sandstones (Sm; Figs. 7, 8, 11). Individual bodies are 403 bounded by either an erosional concave-up or a sharp non-erosional base. Frequently, they exhibit a fining-upward trend with granules to pebble lags that are typically preserved at the base

of the individual bodies (Fig. 8). Up to 40 cm long rip-up clasts are preserved at the basal erosional surfaces (Figs. 8 and 11d). In outcrops, the tabular or sheet-like sandstone bodies are either stacked vertically or, less frequently, display lateral migration (Figs. 8, 10 and 11). The bodies are amalgamated and typically only their lowermost part with a residual lag is preserved (Figs. 8, 9 – Unit B). In places, the sandstones bodies are incised into fine-grained floodplain deposits with an erosional base up to 1.5 m (Fig. 11).

The sandstone bodies exhibit two architectural elements. Firstly, they are composed of single large-scale planar cross-strata (facies Sp and Sl) with thickness of 0.5–1.5 m and lateral extent up to 25 m (Fig. 9d). Planar foresets exhibit dips of 8–25° (local maximum is 35°). Secondly, the sandstone bodies consist of down-stream accretion strata with smaller sets of planar, trough and low-angle cross-bedding. The sets have thicknesses of 15–25 cm and are bounded by sharp sub-horizontal non-erosional surfaces (Fig. 9 – unit B). Directional data derived from cross-bedding, tool marks, lineation and imbricated clasts, indicate predominant palaeoflow towards north and northeast, but also less frequently to the northwest (Figs. 7–11).

Unit 1 of Mosaic 3 (Fig. 9) exhibits two areas of trough cross-bedding, separated by wider zones of planar cross-strata. The channel deposits lack evidence for desiccation and subaerial exposure.

Amalgamated sandstone and conglomerate bodies that are bounded by basal erosional surfaces with erosional relief of up to 150 cm are interpreted to reflect deposition in fluvial channels. The single large-scale planar cross-strata are interpreted as a result of downstream migration of gravel and sand bars within a fluvial channel, e.g., transverse or mid-channel bars. Small-scale cross-bedding represents dunes that migrated on the channel floor or developed on the top of a channel bar. Muddy intraclasts preserved at the basal erosional surfaces are interpreted as remnants of overbank sediments that were eroded during channel avulsion or flood event. Narrower zones of trough cross-bedding possibly indicate more persistent channel flow, whereas wider zones of planar cross-bedding could represent inter-channel bars or sandflat.

Single-storey fluvial channel facies association

Conglomeratic channel fill (CHc)

This facies association comprises conglomerate bodies with massive or stratified infill (facies Gm, Gt and rarely Gp; Figs. 8 and 9). The less than 1 m thick bodies span laterally for as much as 4 m, exhibit concave-up symmetrical bases with erosional relief of up to 40 cm and are commonly incised into floodplain deposits (facies Fm; Figs. 8, 10b). Conglomerates are generally confined to channel forms. Conglomerate channel bodies, consisting entirely of facies Gm, probably represent deposits of a single flood event. Smaller occurrences of massive

Figure 6 (on the opposite page). Facies associations with main architectonic elements. See text for further explanation.

conglomerates belong to scour-fill deposits or infill the deepest part of the channel representing a channel lag (Collinson 1996). The occurrences of stratified conglomerates that pass laterally or vertically into sandstones with gravel admixture reflect decreased flow energy.
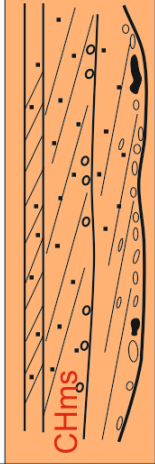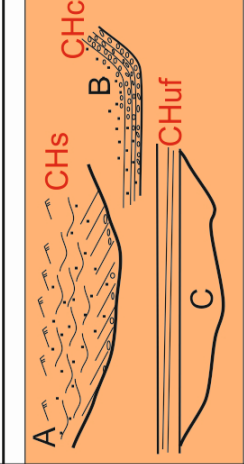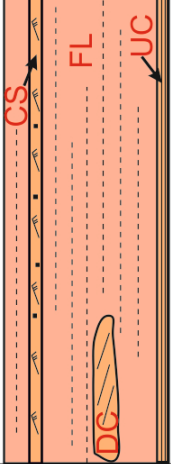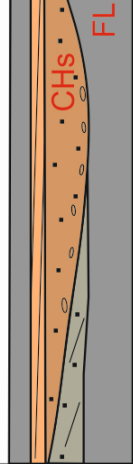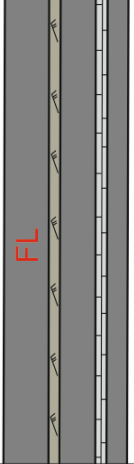
Sandstone channel fill (CHs)

This facies association includes up to 1 m thick sandstone bodies with variable concave-up base geometries, varying amount of gravel and lateral extent (1–20 m). The bodies are composed of medium- to coarse-grained sandstone with predominant planar or low-angle cross-bedding (facies Sp, Sl) and subordinate trough and ripple (facies St, Sr) cross-bedding (Figs. 7 and 8). The sandstone bodies display a fining-upward trend, but only few of them record the complete vertical succession that includes planar, trough and ripple cross-bedded sandstone, since their upper parts are commonly eroded (Fig. 9). Their basal erosional relief ranges from 30 to 80 cm. The bodies contain residual gravel lag, which is locally clast-supported (Fig. 8a), and pebbles, whose abundance and size decreases upwards (e.g., Fig. 10). Frequently, the basal parts of the sandstones contain muddy rip-up clasts (facies Fm) that reach a maximum size of 15 cm. Sandstone bodies are commonly incised into fine-grained floodplain deposits (Fig. 10a).

Two special cases of sandstone channel fill were identified: (i) low-angle bedded sandstone bodies with tabular or sheet-like appearance, that are laterally very pervasive and interlayered with other single-storey fluvial channels (Figs. 6, 9 and 10a – element CHuf); (ii) channel bodies with step-like margins and a flat sharp base geometry that is controlled by the shape of the underlying layer (Figs. 7, 9b, c). They can contain large amounts of gravel at their base, can be laterally restricted (1–5 m) and show reduced thicknesses (up to 0.5 m; Fig. 9).

The sandstone bodies of this facies association are interpreted as fluvial channel deposits from an active channel belt. Planar or low-angle bedded sandstones that overly residual lag at the channel base were formed by transverse or linguoid bars (Miall 1996; Fig. 9d). Smaller sets of cross-bedding resulted from migration of straight-crested dunes on channel floor or on the top of bars (Collinson et al. 2006). Both, rip-up clasts that occur at the basal erosional surfaces of sandstone bodies and fine-grained deposits that are erosionally preserved in-between sandstone bodies suggest that single-storey channel sandstones are closely associated with floodplain deposits.

Sheet-like laterally pervasive sandstones with low-angle bedding that occur within the active channel belt are interpreted to have formed under upper flow regime during flooding (Fielding 2006; Langford and Bracken 1987). This also might be the case with the pervasive

Facies association		Facies architecture and geometry	Description	Facies	Interpretation
Multistorey, amalgamated fluvial channel	CHms		Medium- to coarse sandstone and conglomerate, basal erosional surface with up to 1.5 m of relief; 1.5-8 m thick; intraformational clast (up to 40 cm); residual lag at the base	Gm, Gp, Gt Sp, St, Sl, Sm	Low-sinuosity, braided fluvial channel belt; bedload deposition; bars and dune migration
Single-storey, fluvial channel	CHs/ CHc		A - most common channel geometry; B - step-like margin, laterally restricted (CHs-sandstone, CHc-conglomerate); C - sheet-like/tabular, laterally extensive sandstone body associated with channel (CHuf); medium- to coarse sandstone and conglomerate; up to 1 m thick; erosional relief up to 40 cm	Gm, Gp, Gt Sp, St, Sl, Sr / Sl	Low-sinuosity, braided fluvial channel belt; Channel type B - shape influenced by early post-depositional cementation; Channel type C (CHuf) - upper flow regime
Floodplain	FL		CS-laterally extensive medium- to coarse-grained sandstone beds, commonly bioturbated DC-small lenses, crudely stratified UC-laterally extensive,sharp-based, medium-gr. FL- red silstone/mudstone preserved as irregularly shaped large bodies, lenses or thin laterally restricted layers, bioturbated	Sl, Sr / Sp, St, Sm / Sp, Sl, Sm / Fm	CS - crevasse deposits DC - distributary channel UC - unconfined channel FL - well drained fine-grained floodplain deposits
Deltaic	DA		Coarsening upward cycles; tabular to rarely channelized bodies (latter up to 20 cm thick); medium- to coarse-grained sandstone and fine-grained conglomerate; interbedded with FL that records transition from red to grey colour	Gml, Sml, Stl, Sll / Fml	Fluvial channels deposited on subaquatic part of delta plain; shallow water delta deposits; FL - poorly drained floodplain deposits
Lacustrine	LA		Very fine- to medium-grained sandstones (dm-m) enclosed within laminated mudstone, siltstone; intercalated with limestone and calcareous shales; enriched in organic matter FL - grey to dark grey colour	Sml, Shl, Sll, Srl, Scs / Fml, Fl	Lake - proximal and distal lacustrine offshore; generally poorly oxidized; suspension settling from weak currents, hypopycnic plumes or gravity currents

sheet-like sandstone bed that resides above the oldest channel in Mosaic 4 (Fig. 10a).

Channels with step-like margin are interpreted to reflect a different depositional condition, e.g., a warmer and drier climate with higher precipitation rate or decreased water discharge. It is speculated here that the shape of channel bases was influenced by early post-depositional cementation of underlying sandstone beds that inhibited an incision of younger channel. Although this assumption is supported by a handful of case studies (cf. Nash and Smith 2003; Nash and McLaren, 2004), confirmation of this process is beyond the scope of this paper and would require a detailed investigation of calcite cement microstructures.

Floodplain facies associations

Floodplain facies associations include (i) fine-grained deposits (mudstones, siltstones) representing the main volume and (ii) medium- to coarse-grained sandstone bodies that vary in size, geometry, lateral extent and position relative to fine-grained deposits.

Fine-grained sediments (FL)

Red to red-brown fine-grained deposits, belonging to facies Fm (Fig. 4), are preserved as irregularly shaped large bodies, lenses or thin laterally restricted layers (Figs. 8, 10 and 11). Their shapes resulted from incision of fluvial channels that eroded or redeposited fine-grained sediments elsewhere. They can be traced laterally for a maximum of 15 metres, vertically up to 2 metres and are strongly weathered or disintegrated into flakes (Figs. 10 and 11b). The deposits are intensively bioturbated by exclusively animal, simple, passively filled unbranched burrows (ichnofabric index = 4–5 sensu Droser and Bottjer 1986). The most abundant fossil is Planolites cf. montanus (Fig. 11c). Layers or pieces of drifted vegetation, fossilised roots or rootlets and desiccation cracks were not found.

The fine-grained sediments were transported in suspension and deposited on a floodplain during flood events. The abundance of ichnofossils together with sediment colour point to a well-oxygenated depositional environment while the absence of desiccation cracks might point to humid climate and a high groundwater table.

Crevasse splay (CS)

This group comprises medium to coarse-grained sandstones with low-angle cross-bedding (facies Sl) and ripple cross-lamination (Sr) that span laterally for tens of metres (Fig. 4m). Tabular or sheet-like sandstone beds have a sharp base and occur enclosed in or are interbedded with siltstone/mudstone of facies association FL. They are bioturbated by simple unbranching burrows of *Planolites cf. montanus* and show vertical variation, with low-angle bedding passing to
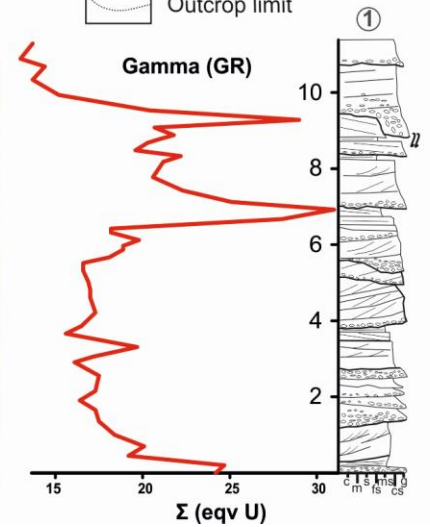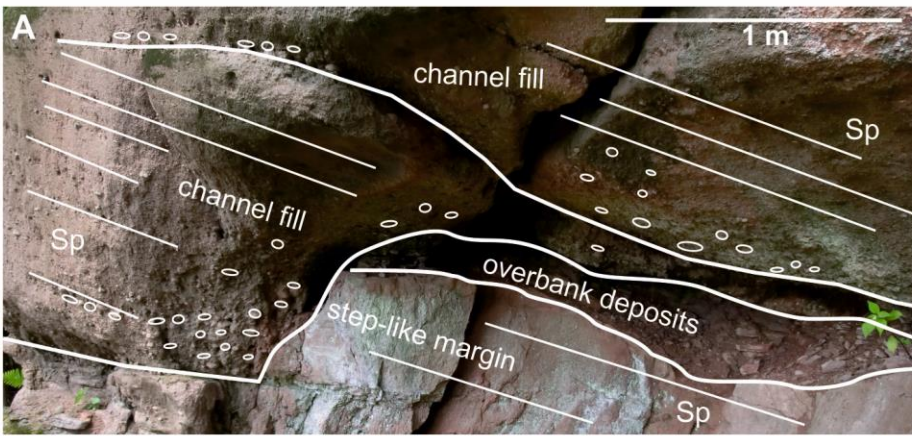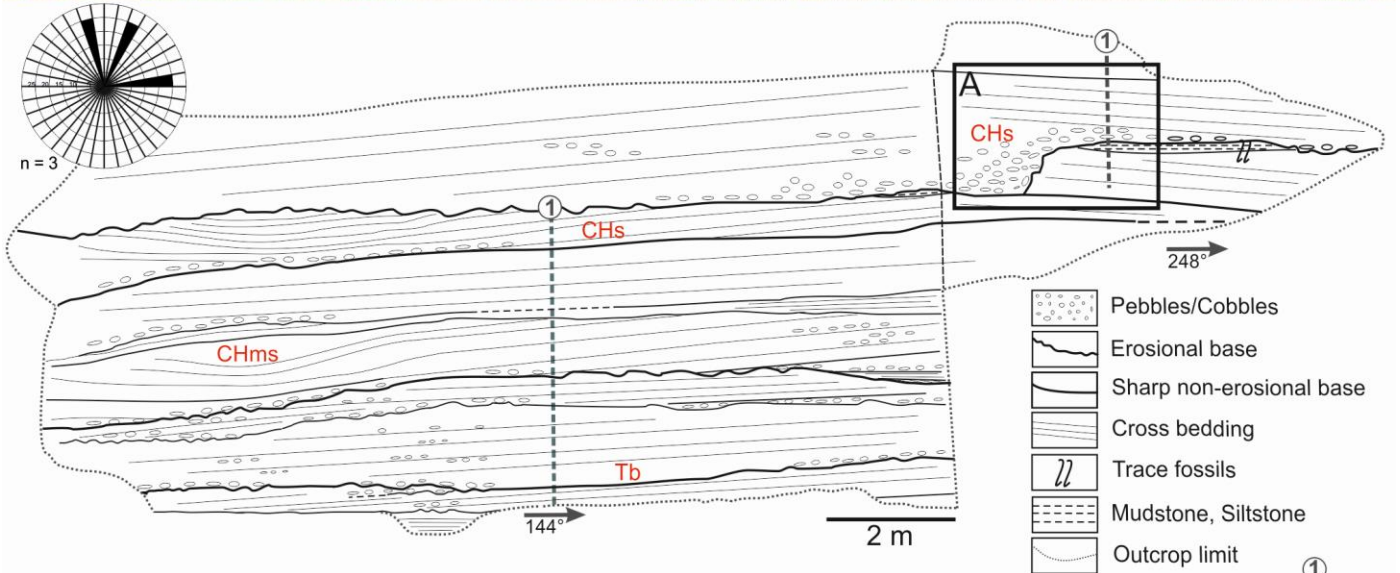
Figure 7. Photomosaic and line-drawing (Mosaic 1) showing amalgamated sandstone channel bodies with predominant planar cross-bedding of the Stará Paka Sandstone, the oldest stratigraphic succession M1, reflecting low A/S ratio. The overbank facies are only locally preserved as erosional thin remnants. Note the step-like base geometry of the fluvial channel shown in inset A. Locality Brodky. Abbreviations used in this figure and figures 8-12: CHms – multi-storey channel fill, CHs/Chc – single-storey channel fill (sst./congl.), CHuf – upper flow regime sheet deposits, DC – distributary channel, UC – unconfined channel, Tb- bar deposits, FL – floodplain deposits.

Figure 8. Photomosaic and line-drawing (Mosaic 2) showing amalgamated sandstone and conglomerate channel bodies with rip-up clasts at their base (inset A). Inset B illustrates multi-storey channel fill. The deposits belong stratigraphically to the Čistá Sandstone and form part of vertical succession M2, which exhibits higher A/S ratio than succession M1, but yet some bypass and erosion is evident. The overbank facies are well preserved. The measured palaeocurrents indicate sediment transport towards NW-N-NE, as determined from fluvial channel bodies. Locality Stará Paka – railway station (east).

Figure 9. Photomosaic and line-drawing (Mosaic 3) illustrating multi-storey channel association (succession M2) and overlying succession M3 that is characterized by a predominance of single-storey channel bodies and an absence of overbank deposits. Inset A illustrates trough-cross bedding. The sandstone bodies at the lower part of sucession M3 show reduced thickness, have step-like margins and flat sharp bases that do not erode underlying strata (insets B, C – shown by white arrows). The laterally pervasive, sheet-like sandstone body in the centre of unit C (CHuf) is interpreted as an upper flow regime sheet (inset C). The uppermost part of succession M3 consists of single-storey channel bodies with vertically preserved Sp, St and Sr facies. Inset D illustrates bar deposits belonging to succession M2. Locality Stará Paka – railway station (east).

Figure 10. Photomosaic and line-drawing (Mosaic 4) showing a succession of channel fills and overbank deposits (locality Bělá – railway cut south), representing succession M4. Roman numerals indicate stratigraphic succession of bedsets (I – oldest; IX – youngest). **(A)** Individual stratigraphic sections are labelled 1 to 8 in upsection direction (from left to right). The basal channel belt II is interpreted as multi-lateral, with an avulsion of individual channel fills towards the right (inset A). The channel belt is topped by a c. 5 cm thick siltstone layer that is overlain by a thin (c. 40 cm) but extensive sandstone bed covering the entire channel belt II (CHuf). The overlying bedset III comprises shallow, up to c. 20–50 cm thick, unconfined channels (UC, inset B). The above lying single-storey channel fill IVa contains up to c. 10 cm sized pebbles at its base, commonly of volcanic origin (inset C). This channel fill is erosively incised into overbank deposits to the right, but does not significantly erode underlying unconfined channels. The contact of bedsets III and IVa is planar, possibly due to early post-depositional carbonate cementation of the bedset III. The overlying channel belt V continuing farther north across the outcrop is interpreted as multi-storey. **(B)** Channel belt IVb (insets D, E) is interpreted as single-storey, while channels V-VIII represent multi-storey channel fill (inset F) and exhibit lateral migration. The convex-upward bedform (shown as A in inset F) is interpreted to form in antidune phase flow. The youngest bedset IX comprises unconfined channel bodies (inset G). Locality Bělá.

Figure 11. Photomosaic and line-drawing (Mosaic 5) illustrating the transition from succession M4 (represented by the oldest Unit 1) to succession M5 characterized by the incision of a several metres thick multi-storey channel fill which consisting of conglomeratic and sandstone channel bodies (Unit 2). Unit 1 comprises siltstone and mudstones that are intensively bioturbated and contain sandstone bodies completely enclosed in fine-grained sediments. The uppermost Unit 3 is formed by tabular, planar cross-bedded sandstone, with minor amount of gravel, and laterally extends beyond the margins of the main channel. Inset A: Detail of channel incision into floodplain. Note colour reduction along the channel base. Inset B: Detail of two sandbodies pinching out into floodplain sediments, representing deposition prior to incision of a large conglomeratic channel. Inset C: Intensively bioturbated mica rich siltstone with burrows identified as Planolites cf. montanus. Inset D: Elongate muddy intraclast preserved above the erosional channel base. Inset E: Detail of cross-bedded conglomerate within the main channel. Locality Stará Paka – railway station (far west).

Fig. 8

M2

B

1a

2

CHms

Tb

CHs

CHms

FL

2 m

5 m

3

CHs

Tb

FL

320°

4

CHc

CHms

FL

5

CHms

?   ?

1b

CHms

FL

Sp
Sp
Sp, St
Gm

Not exposed

Sl
Sp
Sp
Sp
Sl
Sl

Sp

4

2

0m   M   F CF C
        Sst Cong

Sp
St

Not exposed

Sp
Sp
Sp
Sp
Sp

Sl

8

6

4

2

0m   M   F CF C
        Sst Cong

	Pebbles/Cobbles
	Erosional base
	Sharp non-erosional base
	Cross bedding
	Limestone pebbles
	Rip-up clast
	Trace fossils
	Mudstone, Siltstone
	Outcrop limit

4

2

0m   M   F CF C
        Sst Cong

Sp
Sp

4

2

0m   M   F CF C
        Sst Cong

4

2

0m   M   F CF C
        Sst Cong

Sp
Sp
(1a)
Ms
Sl
Sp
(1b)
Sp

1m   M2

B

CHms

n = 60

A

CHs

Tb

Fig. 9

M3

A B C D

285°

1 2 3

CHs
CHuf
CHs
CHms
CHms
CHms
CHc
Tb

C
B

1m
2m

Column 1:
2
Sp
St
Sp
Sp
0m
M F C F C
Sst Cong

Column 2:
4
Sp
Sp
Sp
Gp
2
Not exposed
Sp
0m
Sp
M F C F C
Sst Cong

Column 3:
Sr
St
2
Gp
Sp, Sl
Gp
St
Sl
0m
M F C F C
Sst Cong

A
CHms

B
CHc

C
CHs CHc CHuf
CHc

D
Tb

Legend:
Pebbles/Cobbles
Erosional base
Sharp non-erosional base
Cross bedding
Limestone pebbles
Rip-up clast
Trace fossils
Outcrop limit

Fig. 10

A

B
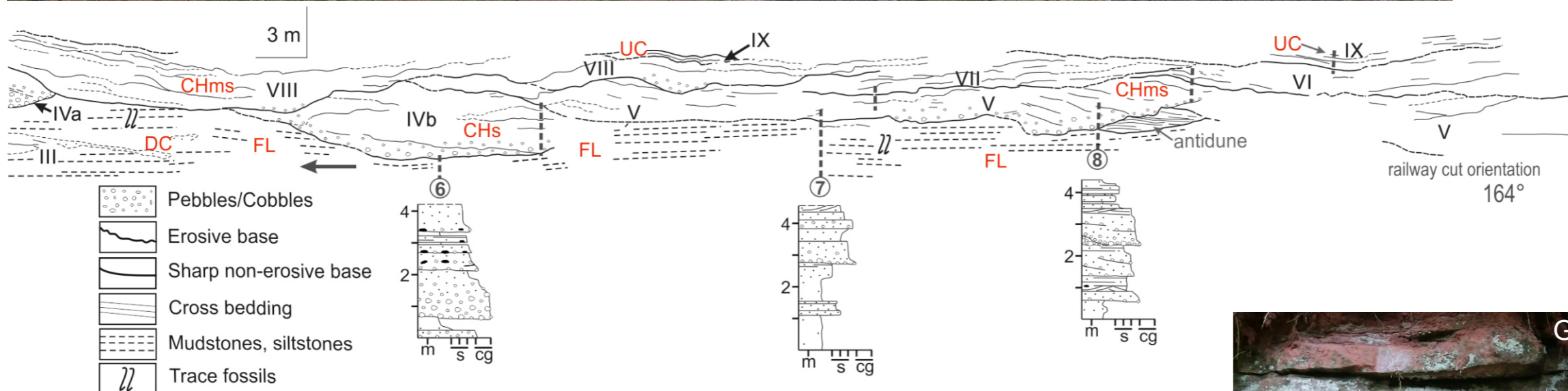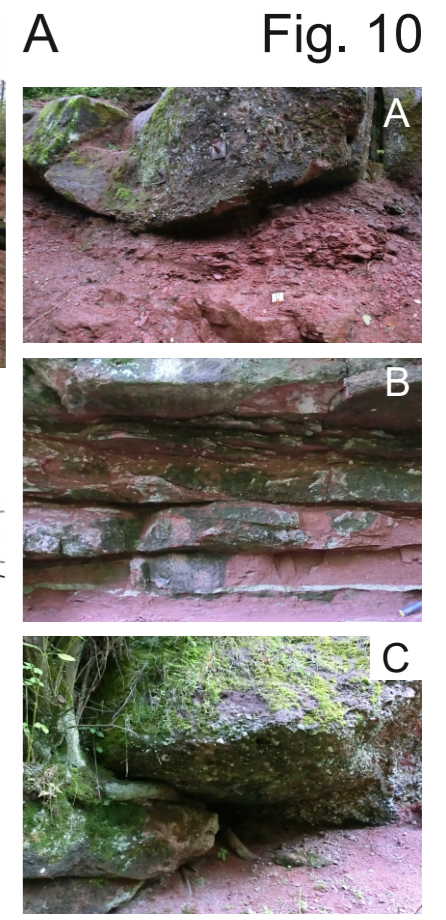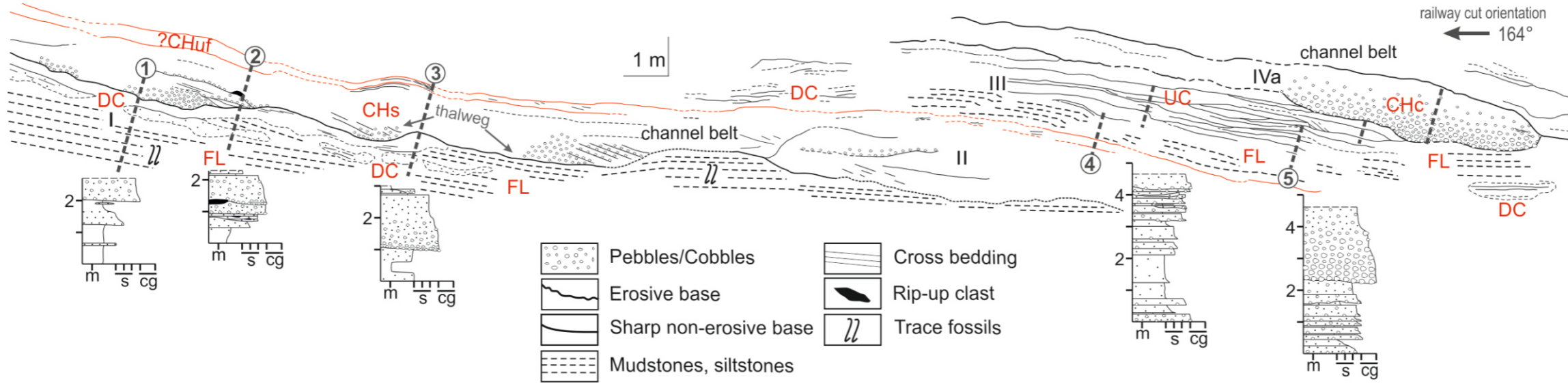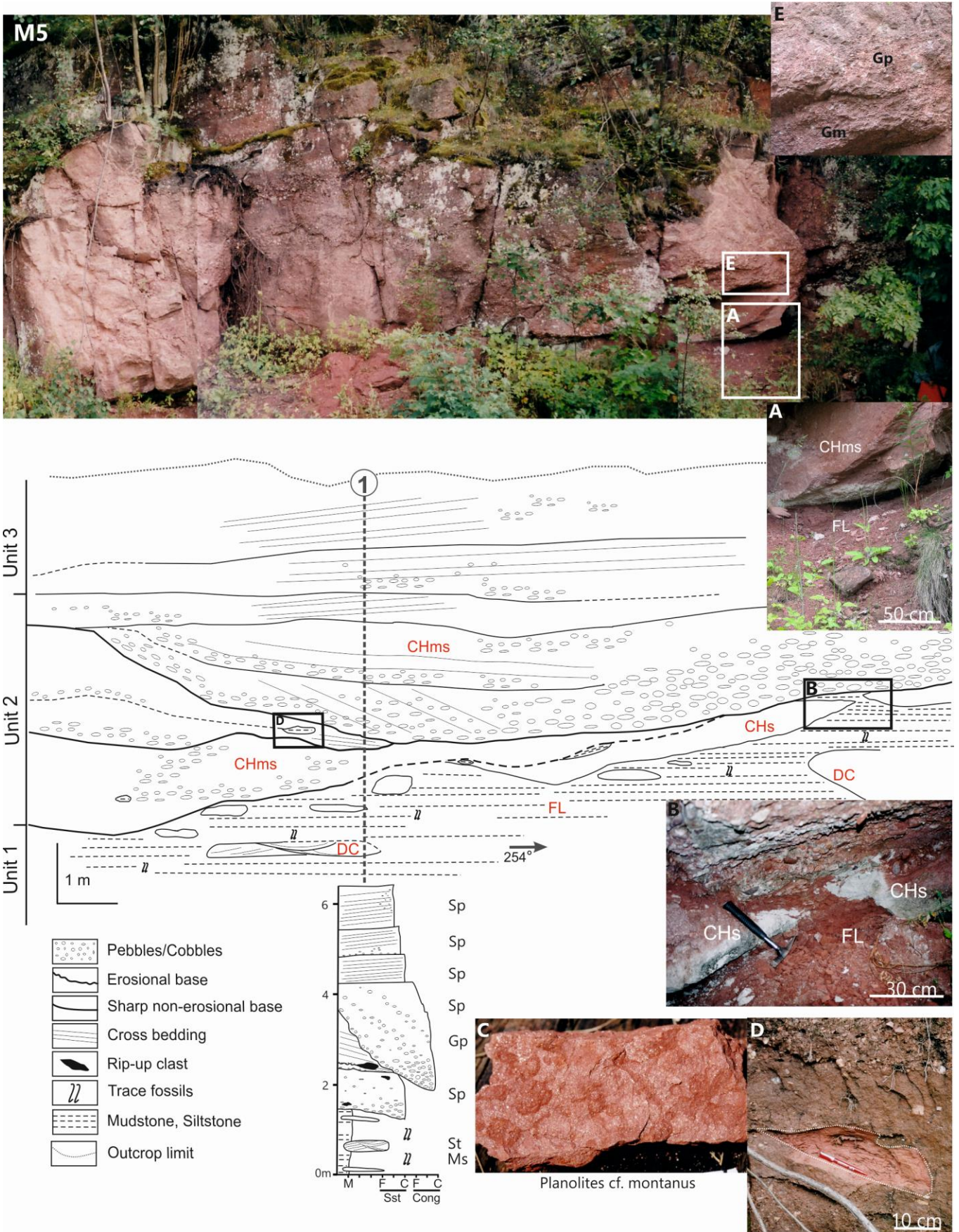
Fig. 11

ripple cross-lamination. The sandstone bodies are interpreted to have formed during flood, i.e. channel overspill and deposition outside the main fluvial channel (Miall 1996) or channel avulsion (e.g., Bridge 2003; Nichols 1999). The higher degree of bioturbation, when compared to channel-fill sandstones, indicates stabilized conditions after the flood-generated deposition enabling the animal colonization of the beds prior to the next flooding episode. The vertical change of low-angle stratification to ripple lamination indicates a progressive decrease in flow velocity.

Distributary channel (DC)

Small isolated well-defined sandstone lenses are fully encased in floodplain deposits (Figs. 4f, g and 10, 11 – unit 1), and typically occur below the base of the main fluvial channel. They are predominantly structureless, but locally exhibit crude stratification, planar or trough cross-bedding. Sandstone bodies with irregular or channelized form are interpreted to represent small distributary channels, which formed on the floodplain and were active during flood event or episodic rainfall. Massive structureless sandstones indicate hyperconcentrated flows (Miall 1996).

Unconfined channel (UC)

This facies association includes unconfined single-storey and less than 0.5 m thick channelized or tabular sandstone bodies (Fig. 10). They are laterally pervasive (up to 8 m), consist of medium-grained sandstone with faint cross-bedding (Sp, Sl) or lack internal stratification (Sm) and have generally sharp, but non-erosive base. They occur within overbank sediments and reside just below the main channel, which is partly truncating the uppermost unconfined channel section (Fig. 10a). Alternatively, thin sheet-like sandstone beds occur directly above the main channel fill (Fig. 10b). These sandstone bodies are interpreted to represent an ephemeral fluvial event on a floodplain, outside of the main channel belt, deposited by flow expansion. Massive sandstones represent hyperconcentrated flows (Miall 1996). Sandstones with their stratigraphic position just below the main channel may reflect a transitional channel avulsion (Jones and Hajek 2007).

Deltaic facies association (DA)

Deposits in transition between fluvial facies and open lacustrine facies (the latter previously defined by Martínek et al. 2006a in the northern KPB) are represented by several lithofacies. These are similar to the fluvial facies in terms of grain-size and sedimentary structure, but exhibit markedly different colouring, i.e. various shades of grey, as well as slightly different petrography and also vertically alternate with shale beds (Fig. 12). These ʻtransitional' deposits are exemplified by section Košťálov – railway cut west (Fig. 12a; locality 4a in Fig. 3). The

outcrop section exhibits several coarsening-upward cycles topped by relatively well-sorted sandstones or even fine-grained conglomerates that form several dm to c. 3 m thick tabular bodies (Fig. 12a). The thicker laterally consistent beds are sharp or are even erosive-based, exhibit frequently flute casts and comprise conglomerates or conglomeratic sandstones (facies Gml) that pass upwards into massive only several metres extending sandstones with faint cross-bedding (Sml). Facies Sll or Stl are subordinate and both alternate with facies Sml in the topmost part of the section shown in Fig. 12a. Rare channelized massive sandstone bodies are also exposed at other localities (locality 5 in Fig. 3), but are substantially thinner, only up to c. 20 cm thick, and are formed by facies Sml with dispersed granules, pebbles and rip-up clasts at the base. The described sandstone bodies represent fluvial channel fills deposited in the subaquatic part of a delta plain. The transition from poorly-drained grey floodplain deposits to sharp-based sandstones that display coarsening upwards is interpreted as shallow water delta deposits. The massive, and structureless facies Gml and Sml represent rapidly deposited possibly dewatered scour fills (cf. Hornung and Hinderer 2011). Decreasing grain-size and thickness of individual channel fills points to progressive filling of accommodation space that may have preceded a formation of a new delta lobe.

Lacustrine facies association (LA)

The lacustrine facies association (LA) represents facies deposited beyond the maximum progradation of the fluvial-deltaic system. On the basis of their relative proximity to the lake shore, two main LA subfacies are distinguished.

Proximal lacustrine

Below the thickest sandstone channel body (CH1) in Fig. 12a, fine- to medium-grained sandstones comprised of dm-thick beds that vertically become thinner (a few cm) form a succession with a total thickness of c. 2 m. Though some of the sandstone beds are massive (Sml; Fig. 4q) or horizontally-bedded (Shl; Fig. 4q), most of them exhibit planar cross- (Sll; Fig. 4r) and even more frequently ripple-cross bedding (Srl; Fig. 4s). Ripple-cross sets are predominantly asymmetric. Facies Sll and Sml dominate within section Košťálov – castle (loc. 5; Fig. 3) where only several thin (up to c. 20 cm) channel fills are present. In rare cases, facies Scs is present within ambient facies Shl, Sll or Srl (sandstones with SCS-bedding marked in Fig. 4s). The oldest strata are dark grey siltstone/mudstone that lie below fine-grained thinly bedded sandstones (Fig. 12a).

The proximal lacustrine facies association was deposited closer to the lake shore. However, grey colour and the absence of desiccation cracks or palaeosols indicate that its

Figure 12. Locality Košťálov. (A) Outcrop-based line drawing illustrating a deltaic-lacustrine depositional setting in the central KPB. Sandstones represent subaquatic deltaic deposits, whereas fine-grained grey deposits reflect a proximal lacustrine environment. (B) Predominant dark grey to black siltstone and mudstone reflect distal lacustrine environment. Locality Košťálov. The black palaeocurrent data represent cross-sets and flute casts in the shallow water deltaic channels indicating S–SW palaeoflow direction, while the grey data are from out-of-channel (e.g., wave action).

deposition was not affected by subaerial exposure attributed to periodic lake reduction (cf. Martínek et al. 2006a). Instead, the deposition took place in an environment with relatively well to reduced oxygenation (oxic to suboxic cf. Martínek et al. 2006a) at a water depth of a few metres. The water depth may be estimated from the sparse presence symmetric ripples that indicate an oscillatory regime generated by surface waves. More frequent asymmetric ripples, however, point to the action of longshore currents that distributed coarser clastic material (sand, silt) further away from its initial depositional loci at the river mouth. Rare facies Scs, embedded within ambient ripple-bedded or horizontally bedded sandstones, record reworking of 'fair-weather' deposits by waves generated during exceptional storm events. The dark grey siltstone/mudstone layers were likely deposited during periods of high lake-level, i.e., when the fluvial system retrieved towards the south, and hence could represent deeper lacustrine facies.

Distal lacustrine

The distal lacustrine deposits are represented by facies Fl (Fig. 4u), that crops out at localities in the vicinity of Košťálov (loc. 4–9 in Fig. 3). They comprise a wide variety of lithologies ranging from siltstones (as well as sparse argillaceous very fine- to fine-grained sandstones), mudstones to claystone and 'shales' (Fig. 12b). The latter are represented by thinly laminated mudstones and claystones, often fissile ('paper shales'). Shales are calcareous and intercalated with limestone (Figure 4u). Facies Fl is generally rich in organic matter, in fact some of the rocks can be labelled as 'bituminous' (Martínek et al. 2006a). Facies Fl interfingers mainly with facies Fml (Fig. 4t) and less frequently with other facies grouped as 'proximal lacustrine'. Both facies appear in a vertical 592 succession (mainly at the localities in the vicinity of Košťálov) and exhibit a shallowing-upward trend (e.g., Fig. 12). The open lake, lacustrine offshore facies association is generally, very poorly oxidized to oxygen-depleted and comparable to the suboxic to anoxic offshore facies of Martínek et al. (2006a). The depositional processes involved suspension settling from weak current or hypopycnic plumes (suspension plumes transported by a river mouth close to the lake surface) or from gravity currents. The latter may have been related to alternation of hydrologically open to closed basin regimes (Martínek et al. 2006), governed by precipitation/evaporation equilibrium. Presumably, during phases of a hydrologically open

Fig. 12 M6

A

coarsening upward
lake margin proximity

CH1

2 ← HCS–SCS

0.5 m

m s cg

CH1

①

CH1

②

②

fining upward channel succession

railway cut orientation
← 320°

③

2

m s cg

channel sandstone

subaquatic delta plain to delta front

tabular and lenticular sandstones
prodelta

HCS–SCS →

CH1

mudstones
offshore

n = 7
n = 24

B M6

SST

SST

SLT/MST

SST

SST
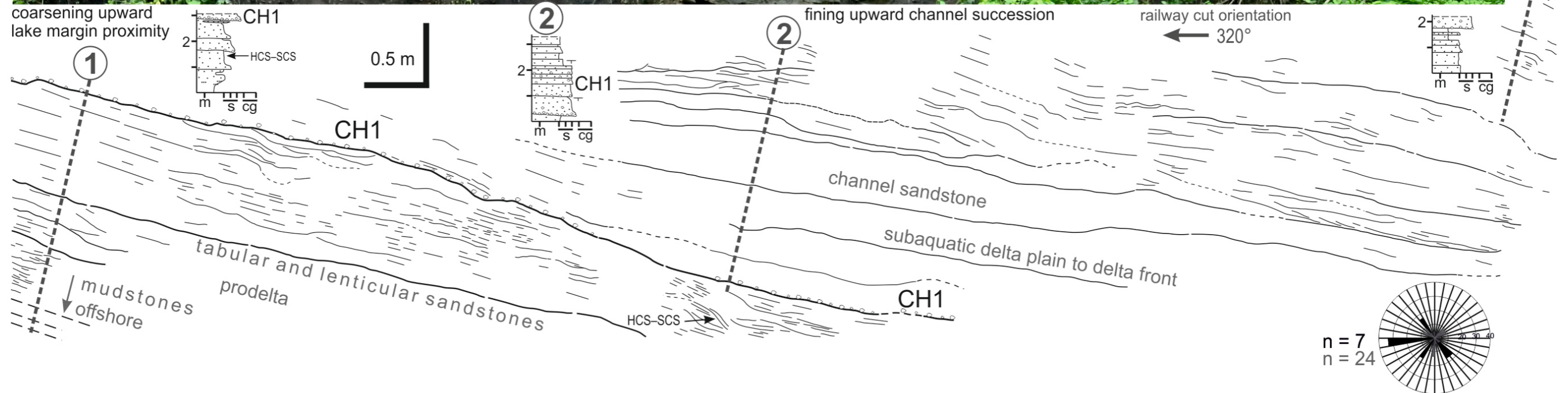
regime with sufficient water discharge, coarser siliciclastic material (sand) was delivered from fluvial mouths by likely hyperpycnal, sublacustrine gravity currents (cf. Zavala et al. 2006).

Discussion

Depositional model of fluvial system

The detailed analysis of lithofacies and architectural elements showed that amalgamated channel-fill elements with predominant downstream accretion of sandy to conglomeratic bedforms are characteristic for the Vrchlabí Formation in the southern and central KPB. From the above account, the predominance of cross-bedding suggests relatively stable discharge regime in a fluvial system with high-energy and bedload deposition (cf. Allen et al. 2013), so that a large proportion of sediment was carried by rolling and saltation along the channel floor.

Palaeocurrent measurements from the fluvial Stará Paka and Čistá sandstones located in the southern KPB indicate a moderate to low sinuosity braided fluvial system with a general N to NW palaeoflow direction (Fig. 13). The direction is consistent with the main source area that was located south of the KPB during the deposition of the fluvial strata of the Vrchlabí Formation (Martínek and Štolfová 2009). On the other hand, several measurements from sandstones that are interbedded with lacustrine sediments in the central part of the KPB indicate palaeoflow direction towards the S and SW. Oppositely directed palaeocurrents suggest the existence of a (segmented) intrabasinal high in the central KPB (Fig. 13) that was eroded during early Permian times. This hypothesis is supported by the proximity of the mentioned deposits to the present-day Kundratice–Javorník Fault (Figs. 1c, 13). According to Prouza et al. (2013), the fault is originally of Late Palaeozoic age. The Škodějov Fault, that partly forms the northern basin margin, is parallel to the Kundratice–Javorník Fault. The facies distribution and evolution of the early Permian fluvial system indicate that both faults were bounding the two principal grabens during the initial depositional stage of the Vrchlabí Fm.

The upper part of the Vrchlabí Formation contains locally weathered volcanic clasts which indicate fluvial erosion of volcanic edifices, likely products of coeval volcanic activity (cf. Stárková et al. 2011). Similarly, poorly sorted structureless sandstones have been described in channel bodies from a number of volcanic basins where abundant volcaniclastic debris, hyperconcentrated flows and short transport distances prevented textural sorting (e.g., Collinson 1991; Haughton 1993). Early Permian post-collisional, extension related magmatism that occurred in the Sudetic basins (McCann et al. 2008) has also been identified in the KPB, with one of the major peaks coinciding with the deposition of the uppermost part of the Čistá Sandstone. (Stárková et al. 2011).
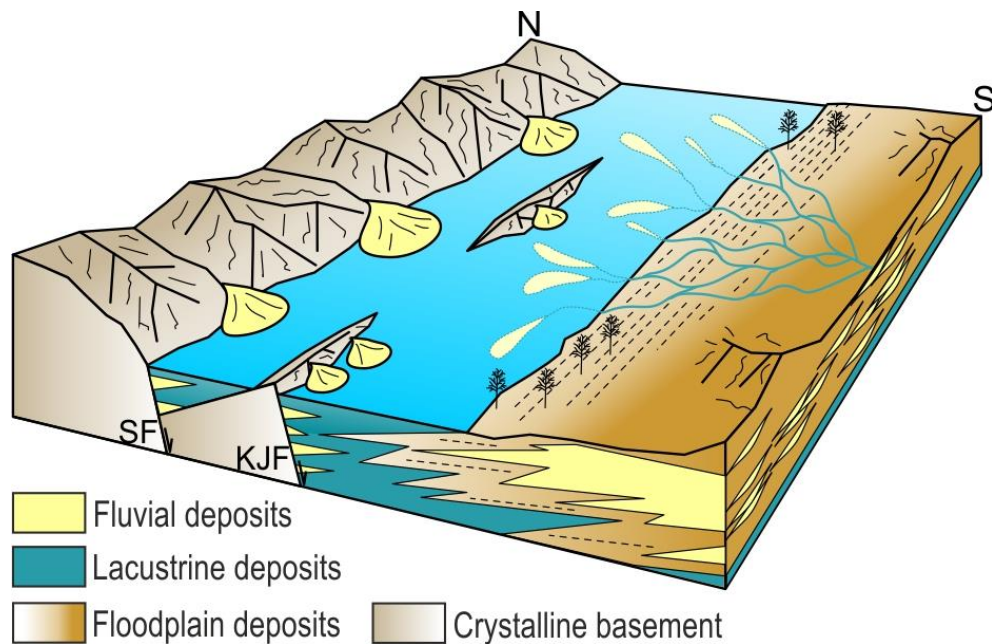
Figure 13. Sedimentary model for the fluvial system in the KPB during Asselian times (not to scale) showing that major sediment supply came from the south and south-west and highlighting the likely existence of an intra-basinal high in the central KPB, trending parallel to the northern basin margin fault. Both faults record syn-sedimentary activity. The vegetation was very sparse within the fluvial system, pointing to a significant topography along the southern basin margin. Abbreviations: SF – Škodějov Fault, KJF – Kundratice–Javorník Fault. Cardinal directions indicated.

Evidence for desiccation and subaerial exposure in the channel fills and on the floodplain was not found in the studied area. Martínek et al. (2006) has described features resembling desiccation cracks as well as suspected pedogennic features within lacustrine deposits of the Rudník Mb. (Vrchlabí section, northern part of the KPB; beyond limits of the study area). Their origin is, however, uncertain as they could alternatively represent syneresis cracks, found sporadically in boreholes in the central KPB. In the study area, syneresis cracks might also be locally present at the outcrops near Košťálov. This study additionally revealed a complete absence of well-developed palaeosols in the studied parts of the Vrchlabí Formation. The lack of sedimentary features developed by short-term subaerial exposure and weathering (e.g., desiccation cracks, protosols) as well as long-term exposure (well-developed palaeosols) indicate that groundwater table was relatively high to local surface topography (cf. Rosen 1994, Allen et al. 2013). Such a high groundwater level could have impeded vegetation, growth of pedogennic nodules and at the same time controlled the vertical limit of cementation. Fine-grained red to red-brown floodplain deposits are commonly eroded and incised by channel(s), are preserved as thin erosional layers between two channels or as intraclasts along the channel floor suggesting migration of channels on the alluvial plain and erosion of fine-grained sediments. Lateral shifting of channels within a channel belt points to a mobile river system (Collinson 1996).

The laterally extensive (tens of meters) tabular to sheet-like fine to medium-grained sandstones with sharp base and flat top are interpreted (i) as either being crevasse splay deposits (Collinson 1996) when embedded in floodplain sediments or (ii) as resulting from critical to supercritical flow occurring during exceptional hydrological flooding (e.g., Fielding et al. 2018; Trümper et al. 2020). The latter process could have produced the laterally pervasive flat-topped sheet-like sandstones embedded in-between two sandstone channel bodies (Fig. 9).

The mobility of the channel belt with unstable river banks is further supported by the absence of vegetation that would have helped stabilized the channel banks. The absence of plant roots and debris in the areas adjacent to the fluvial system contrasts to well-vegetated areas that were described along the lake margin in the central and northern KPB (Opluštil et al. 2013; Zajíc et al. 1997). Furthermore, a significant palaeotopographic gradient along the southern margin of the KPB is supported by a sediment colour change, i.e., red-brown deposits pass laterally into grey-coloured sediments that dominate along the lake margin.

According to long-established fluvial facies models, the studied fluvial system exhibits elements that are characteristic for a low-sinuosity perennial fluvial system that was closely connected with the floodplain (e.g., Miall 1978, 1996; Ramos and Sopeña 1983; Bridge 2003; Collinson et al 2006). The red to red-brown colour of fine-grained deposits and the presence of trace fossils, such as predominant *Planolites cf. montanus* or rare *Scoyenia*, point to a well-oxygenated floodplain environment (Bromley 1996; Pemberton and Frey 1982). The studied fluvial system reached a standing water body (in this case a lake) indicating that climate was not too arid so that evaporation did not exceed water supply (cf. Rosen 1994). Upon entering the Rudník lake, the fluvial system passed into a shallow-water delta, which is evident in N–S cross-section across the southern and central KPB (Fig. 14b).

According to the recently postulates scheme of Fielding et al. (2009, 2018), the fossil record of the early Permian fluvial system reflects large seasonal discharge variability, but relatively small inter-annual variability (peak flows of relatively consistent magnitude). The predominance of cross-bedding at various scales, abundant internal erosional surfaces, bar evolution and the absence of in-situ tree fossils in the channel bodies point to low discharge variance (Fielding et al. 2009). For instance, comparable depositional architectures that suggest low discharge variance are typical for middle–late Pennsylvanian fluvial system in the basins west of the KPB (Lojka et al. 2016; Opluštil et al. 2005, Fig. 14c).

However, sporadic occurrences of low-angle cross-bedded tabular or sheet-like sandstones with lateral extent (element CHuf in Figs. 9 and 10a) and isolated bedform with convex upward stratification, likely antidune (inset F in Fig. 10b), suggest episodes of near critical to supercritical flow, typically documented in rivers with intermediate discharge variance (Fielding

et al. 2009). Therefore, the final depositional model of the fluvial system spans mainly low but also partly intermediate discharge variance (Fig. 14b). The unconfined channels described in Fig. 10b (inset g) collated above the main channel could also represent upper flow regime sheets (cf. Fielding 2006; Leleu et al. 2009). However, the architectural elements mentioned above are sparse and possibly record exceptional flooding events in the KPB. In contrast, fluvial geometries resulting from an upper flow regime (Fig. 14a) were documented as predominant elements in the neighbouring Intra-Sudetic Basin (Kurowski 2004).

Figure 14. Based on the annual discharge variability, simplified models 'a' (high; modified from Fielding et al. 2009) and 'c' (low) show end members of this scheme. The final depositional model of the studied fluvial system is interpreted to span mainly low, but also partly intermediate discharge variance ('b'). The architectural elements indicating intermediate discharge variability are, however, sparse.

Vertical distribution of fluvial styles

The following section summarizes the outcrop-scale vertical changes in studied early Permian fluvial successions and integrate those with vertical and lateral changes derived from basin-scale subsurface data (Figs. 15 and 16). In general, the vertical succession is composed of individual outcrops exhibiting different preservation potential of fine-grained floodplain deposits, contrasting external geometry and internal architecture of channel bodies. Further, the vertical succession indicates that changes in fluvial style over time are not random, but that their distribution exhibit a certain pattern. The oldest stratigraphic succession M1, illustrated in Fig. 7, belongs to the Stará Paka Sandstone. It is characterized by multi-storey vertically amalgamated, planar cross-bedded 1–1.5 m thick sandstones that are only very locally interbedded with thin layers of fine-grained overbank deposits. Further up, the fluvial style of succession M1 is replaced by fluvial geometries of succession M2, that are best represented by the fluvial strata shown in Fig. 8. Typically, bed thicknesses are less than 1 m, sandstone bodies are amalgamated, exhibit lateral migration and form a multi- and single-storey channel facies association (Chms, Chs). Fine-grained overbank deposits are more abundant than in M1, and are commonly found also as rip-up clasts. Succession M2, as all following successions, belongs to the Čistá Sandstone.

The overlying succession M3, typified by the central part of Mosaic M3 (Fig. 9 – Unit 2), consists largely of small-scale, laterally restricted channels (CHss) with reduced thicknesses (less than 0.5 m) and completely lacks overbank deposits. In this case, successive fluvial cycles repeatedly reworked the upper parts of earlier fluvial deposits so that often only the basal channel lags and the lowermost parts of the channels are preserved. Succession M3 comprises a special type of channel that has step-like margin (Fig. 9 – Unit 2). The stratigraphically higher occurring succession M4 comprises large fluvial channels incising overbank sediments and channels that are commonly fully encased in floodplain sediments. The preservation potential of fine-grained sediments is larger than in any of the previously described successions. Sandstone bodies are generally up to 1 m thick and form single-storeys. Channels migrated across the floodplain as schematically shown by Arabic numerals in Fig. 10a, b. A similar fluvial style is present in the lower part of the overlying succession M5 (Fig. 11 – Unit 1). Floodplain deposits are richly preserved and bioturbated and contain small-scale isolated sandstone bodies. An overlying large-scale multi-storey fluvial channel with predominant Gp and Sp facies is incised into floodplain sediments and contains large rip-up clasts at its base (Fig. 11 – Unit 2). The youngest succession M5 that resides above a large channel comprises predominantly tabular or sheet-like, laterally extensive sandstones bodies (facies Sp, Sl) with thicknesses less than 1 m and minor amount of pebbles (Fig. 11 – Unit 3).

It appears that the above described discrete stratigraphic intervals (M1–M5) illustrate different fluvial style and preservation of floodplain deposits. Despite of the relatively small outcrop sizes that inhibit an extensive regional correlation, it is apparent that the stratigraphic record reflects variable depositional conditions. The fluvial styles may have been influenced by seasonality or by climate fluctuations that are inferred from the lacustrine sedimentary record, as exemplified by localities further north in the KPB (Martínek et al. 2006a).

Rapid vertical changes in the fluvial style, as observed in the Vrchlabí Fm., were documented in other Permian basins elsewhere (e.g., Arche and López-Gómez 2005; Fielding et al. 2009; Allen et al. 2013). The vertical changes in fluvial architecture can be rationalized by using the A/S ratio (Martinsen et al. 1999).

Thick amalgamated sandstones of the lower- and uppermost successions M1 and M5 are interpreted to reflect sufficient water discharge and significant channel depth. The ratio between channel and overbank deposits reflects low A/S ratio (Fig. 16). The reduced thickness (usually less than 1m) of succession M2 could be indicative of climatically driven decreased water 735 discharge. At the same time, widespread preservation of fine-grained overbank deposits corresponds to higher A/S ratio. The overlying succession M3 is interpreted to represent the lowest A/S ratio in the entire vertical succession (Fig. 16). The reduced stratal thickness could,

Figure 15. Correlation of subsurface data integrated with the newly measured outcrop gamma-ray curves. Black curves represent older borehole gamma log; red curves were newly obtained by field gammaspectrometry and represent total gamma log. A: Panel S1 illustrates vertical and lateral evolution of the Stará Paka Sandstone along an E–W cross-section across the southern KPB. B; Panel S2 shows an E–W cross-section through the lacustrine deposits in the central KPB. C: An N–S oriented cross-section S3 illustrates lateral and vertical interaction between fluvial and lacustrine deposits of the Čistá Sandstone in the southern and central KPB.

once again, reflect climate-driven reduced water discharge and/or little basin accommodation. Step-like channel margins may indicate that calcite cementation took place shortly after deposition. The cementation could have taken place in the uppermost part of the channel due to a drop of groundwater level or, alternatively, in partially abandoned channel due to lateral channel migration. As the channels in succession M3 are usually eroded almost down to their base, it is conceivable that the incipient palaeosols and desiccation cracks, if ever present, were probably eroded and are not preserved in the present-day depositional record. Contrasting fluvial geometries and extensive preservation of thick overbank deposits in succession M4 indicate the highest A/S ratio and an expansion of lake Rudník towards the southern basin margin. Abundant overbank deposits and fully encased fluvial channels are vertically replaced by incisions of a large-scale channel that pass upwards into tabular sandstones of succession M5 that contain almost no overbank deposits.

At the basin-scale, the three correlation panels (Fig. 3) illustrate the predominance of fluvial deposits along the southern margin (S1, Fig. 15a) and lacustrine deposits in the central part of the KPB (S2, Figure 15b). Vertically, the correlation panel S1 (Fig. 15a) shows basal amalgamated sandstone and conglomerate bodies of the Stará Paka Sandstone Mb. that span the entire length of the profile and are located above lacustrine sediments. The amalgamated bodies are vertically passing into fluvial sandbodies that are intercalated with overbank deposits, which pass, again, into more amalgamated sandstones and conglomerates. The vertical succession in panel S1 is capped by lacustrine deposits that correlate with the Rudník Mb. in the north and were likely deposited in a single lacustrine basin (cf. Martínek et al. 2006a). The fact that this succession is intercalated with two lacustrine intervals (representing maximum flooding surface) suggests that different preservation of overbank fine-grained sediments and changing A/S ratio was controlled by lake level (base level of the fluvial system) fluctuations.

The correlation panel S2 illustrates intercalation of lacustrine facies of lake Rudník with sandstone-dominated deposits of subaquatic deltas in the central KPB (Fig. 15b). The lateral transition from proximal to distal facies in the lacustrine environment shows a cyclic pattern reflecting lacustrine transgression-regression cycles (Fig. 15b). Individual fluvial channels within the deltaic system in the vicinity of Košťálov exhibit to some degree lateral avulsion, though the position of the system itself is relatively stable, within c. 1.5 km (Fig. 15b; between boreholes Ko-
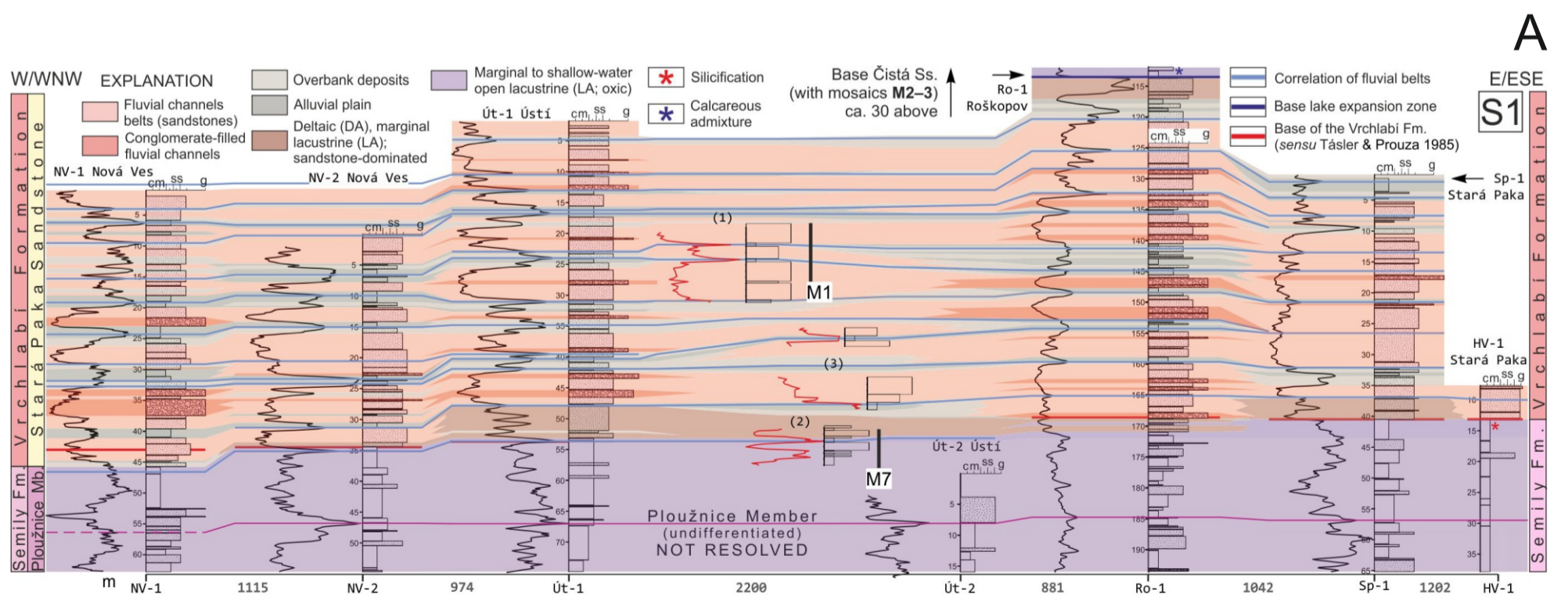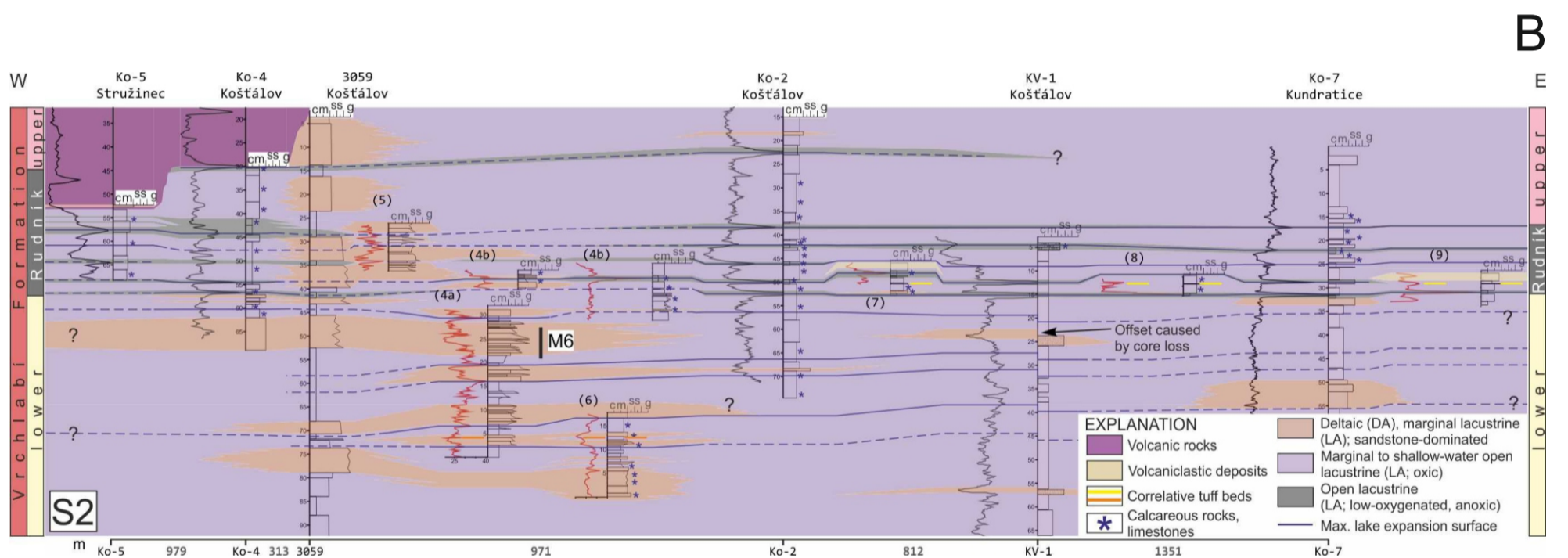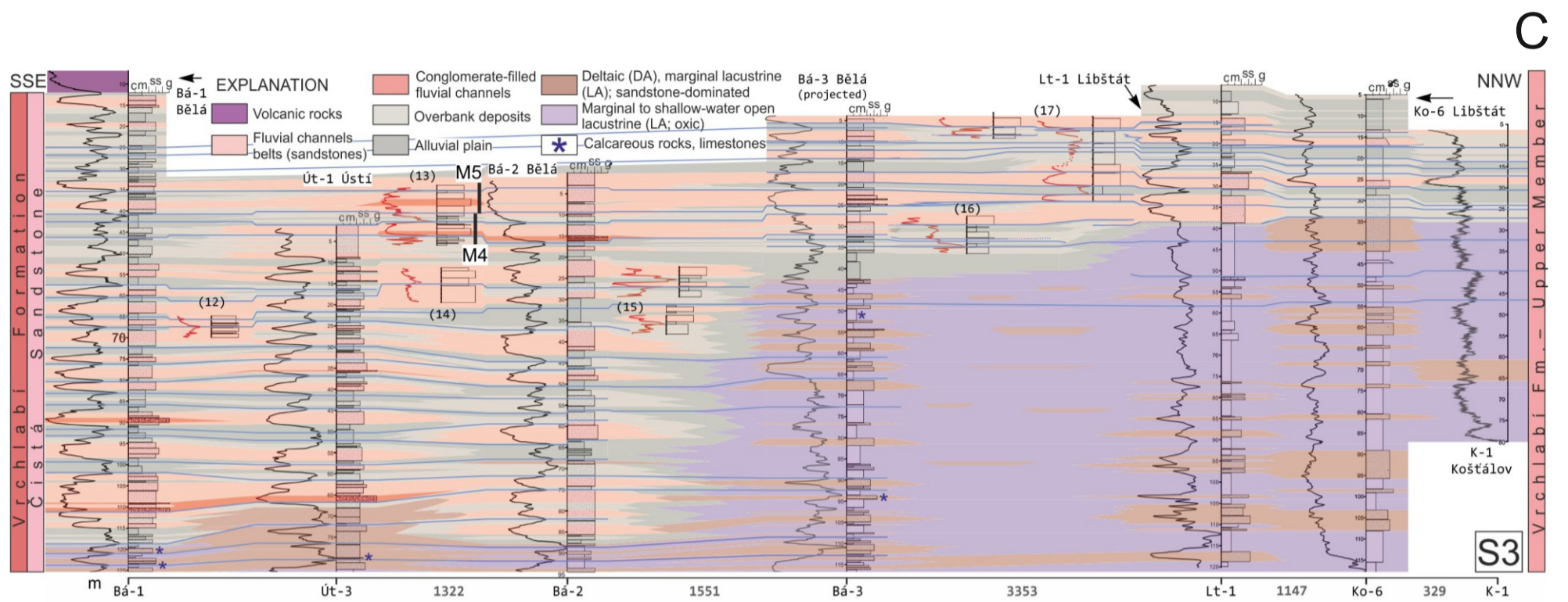
Fig. 15

4 and Ko-2). A few palaeocurrent measurements from the deltaic sandstones, however, document opposite flow direction (to the S–SW), that further support the existence of intra-basinal high in the central KPB and its erosion during early Permian times (Fig. 13). On the other hand, N-directed palaeocurrent measurements taking from sandstone bodies in the eastern part of panel S2 suggest that the fluvial system entered the lake at several locations.

The N-S oriented correlation panel S3 that crosses the southern and central part of the KPB illustrates a vertical evolution of the fluvial-lacustrine system during deposition of the Čistá Sandstone (the upper Vrchlabí Fm.; Fig. 15c). The subsurface correlation of well-logs, complemented with the field gamma-ray curves, indicates that lacustrine facies are interfingering with fluvial facies throughout the section with gradual but consistent back-stepping of the lacustrine facies towards the north. In the uppermost part, the fluvial facies infill the entire documented basin width indicating that the lake retreated and was completely replaced by a fluvial system during deposition of the youngest Čistá Sandstone in the central KPB. The only exception is the Háje Mb., a relatively thin coal-bearing horizon in the northern part of the basin, which records a short-lived environment with a high water table, likely a swamp or a shallow lake (cf. Šimůnek and Drábková 2010).

Controls on deposition – forcing factors

To discriminate the relative influence of controlling factors on fluvial architecture a simplified approach by Ethridge et al. (1998) was adopted. In case of the Vrchlabí Fm., controlling factors include climate and tectonics, which both influence base-level fluctuations (and the base level of the lake Rudník in the northern KPB) and sediment supply. Early post-Variscan near equatorial basins, traditionally labelled as 'intramontane', are envisaged as fault-controlled extensional or transtensional basins, with graben and half-graben geometry (e.g., McCann et al. 2008; Opluštil and Cleal 2007; Vai 2003). This is also the case for the middle Pennsylvanian to early Permian KPB, but the original controlling faults are poorly-defined due to the Late Cretaceous tectonic overprint (Martínek et al. 2006a, b; Uličný et al. 2009). Many features of the early Permian deposition as well as the tectonostratigraphic evolution of the KPB are very similar to other early Permian basins in Europe, e.g., the Autun (Châteauneuf et al. 1992), Lodève (Schneider et al. 2006), Constance-Frick Trough (Madritsch et al. 2018), Saar-Nahe (Schäfer 2011; Henk 1993), Thuringian Forest (Andreas 1988), Saale (Lützner et al. 1992), Intra-Sudetic (Mastalerz et al. 1995) and North Sudetic (Mastalerz and Raczyński 1993) basins, as well as in the North America, e.g, the Cumberland Basin (Allen et al. 2013). In all these basins, the fill comprises intercalated fluvial and lacustrine deposits with associated fossiliferous black shales and tuff layers and records a transition from grey lacustrine to red floodplain facies.
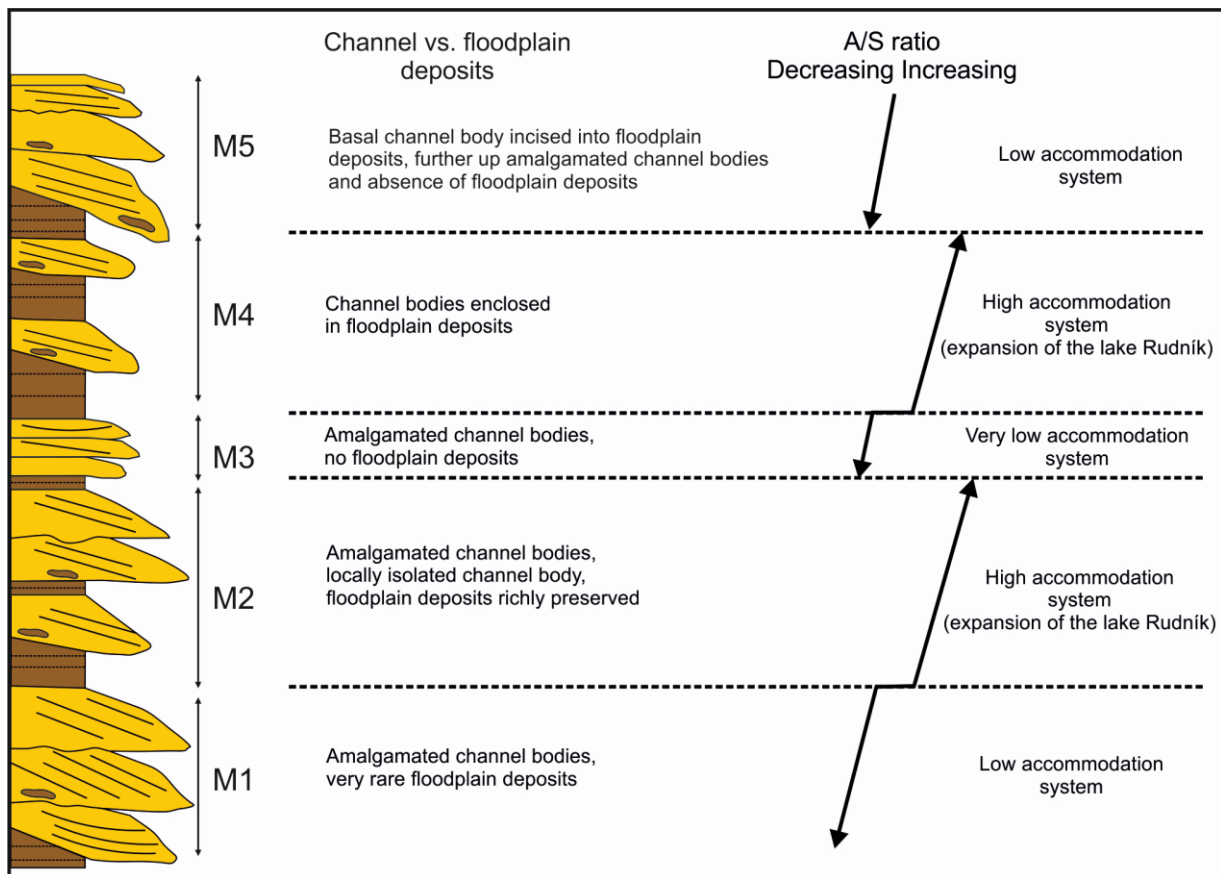
Figure 16. Schematic sketch showing five discrete stratigraphic intervals (M1-5) characterized by one predominant fluvial style and corresponding A/S ratio. The styles are interpreted to reflect climate variations (seasonal discharge variability and expansion of lake Rudník) during the deposition of the Vrchlabí Formation.

The long-term stratigraphic pattern characterized by initial progradation of the fluvial system, followed by lake expansion and later by renewed propagation of the fluvial system across the basin could have been fully or partly fault-controlled. Tectonic control is evident in the earlier phases of deposition of the Vrchlabí Fm.; both the formation of an extensive lake as well as the deposition of lacustrine black shales are regarded as a response to fault-driven subsidence in the northern half of the basin (Martínek et al. 2006a; Blecha et al. 1997). On the other hand, geometrical changes of fluvial bodies, preservation of overbank facies together with lake level fluctuations (Martínek et al. 2006a) indicate that climate had an important role during the deposition of the Vrchlabí Fm. Several studies have shown that red-beds are not necessarily an indicator for arid climate (e.g., Sheldon 2005; Roscher and Schneider 2006) and that the climate changes recorded in Permian basins elsewhere cannot be explained by increasing aridity (Schneider et al. 2006). Existence of perennial lakes, that experienced significant size changes over time – like the early Permian lake Rudník in the KPB – can be explained by annual changes of wet and dry seasons (Schneider et al. 2006; Luthardt et al. 2016). Alternatively, the formation of major lake systems in continental settings, where enhanced fluvial nutrient supply with increased productivity and preservation could have led to major carbon sequestration, could have

been a response to climate warming. The addition of greenhouse gases to the atmosphere, mostly by intraplate volcanic activity in case of early Permian, was associated with increase in hydrological cycling (cf. Xu et al. 2017).

Various characteristics of the fluvial system of the Vrchlabí Fm. indicate that the formation was deposited in a warm humid climate, either in the seasonal tropics or subtropics (cf. Fielding et al. 2009). The absence of evaporites as well as geometries formed by evaporitic dissolution in outcrop are both indicators for a rather humid climate during early Permian times. In fact, anhydrite was found within lacustrine sediments in one borehole, located in the central KPB, only (Martínek et al. 2006a). The changes in A/S ratio reflect sub-cycle variation in fluvial deposits and lake expansion towards the south. The fluctuation of the lake's water table was controlled by climate (Martínek et al. 2006a) and, in turn, influenced the base level fluctuation of the fluvial system. Long-term stratigraphic patterns (evolution of lacustrine vs. fluvial system) as well as short-term stratigraphic patterns recorded within the fluvial system indicate that the large-scale geometry of the KPB resulted from fault-controlled subsidence, but the sub-cycle variations within the studied fluvial system are significantly influenced by climate-driven base level and lake level fluctuations.

Conclusions

1. The fluvial successions of the Vrchlabí Formation represent deposits of a low-sinuosity, laterally mobile fluvial system with variable degree of preservation of floodplain deposits throughout the vertical profile. The internal architecture of channel bodies, and the different ratios between channel and overbank deposits enabled to distinguish the following fluvial styles: (1) amalgamated vertically stacked channels (more than 1m thick) with rare overbank facies; (2) amalgamated, laterally mobile channels (up to 1 m thick) with abundant overbank facies preserved also as rip-up clasts at the channel base; (3) laterally restricted channels (up to 0.5 m thick) with step-like margin and no overbank deposits; (4) laterally extensive channels, often encased in floodplain deposits that are also preserved as rip-up clasts at the channel base; (5) vertically stacked channels (more than 1 m thick), incised into floodplain deposits that become absent towards the top of the succession.

2. The deposition of the Vrchlabí Formation occurred during humid warm conditions and was influenced by well-developed seasonality. Sedimentary features (e.g., desiccation cracks, evaporites) pointing to dry climate, traditionally inferred by predominant red coloured sediments, were not found. However, the general fining-upward trend together with the gradual northward retreat of the lake Rudník, suggest waning tectonic activity contemporaneous with aridization during the deposition of the uppermost Čistá Sandstone.

3. Subsidence generated by faulting along the northern basin margin (the Škodějov Fault) controlled the deposition of the basal part of the formation. Fluvio-deltaic deposits in the central part of the KPB with palaeocurrents towards the south indicate proximity of a intrabasinal high (represented by the present-day Kundratice–Javorník Fault) and its erosion during the deposition of the Vrchlabí Formation. The facies distribution and evolution of the early Permian fluvial system indicate that both faults were active, forming two main half-grabens during the deposition of the Vrchlabí Fm.

4. Significant topography during early Permian times along the southern margin of the KPB is inferred from lateral colour change in fluvial (red/red-brown) and lacustrine (grey to dark grey) sediments and from the absence of plant remnants in the fluvial deposits, which are however abundant along the lake margin.

5. The studied early Permian strata that were deposited in a tectonically subsiding basins also exhibit stratigraphic patterns that clearly reflect climatic variations. This fluvial system also represents a good ancient example of a system with low to intermediate annual discharge variability and well-developed seasonality.

Acknowledgements

References

Allen, J.R.L. (1983): Studies in fluviatile sedimentation: bars, bar-complexes and sandstone sheets (low-sinuosity braided streams) in the Brownstones (L. Devonian), Welsh borders. Sedimentary Geology, 33, 533–555.

Allen, J.P., Fielding, C.R., Gibling, M.R., Rygel, M.C. (2011): Fluvial response to paleo-equatorial climate fluctuations during the late Paleozoic ice age. Geological Society of America Bulletin, 123, 1524–1538.

Allen, J.P., Fielding, C.R., Gibling, M.R., Rygel, M.C. (2013): Deconvolving signals of tectonic and climatic controls from continental basins: an example from the late Paleozoic Cumberland Basin, Atlantic Canada. Journal of Sedimentary Research, 83, 847–872.

Allen, J.P., Fielding, C.R., Gibling, M.R., Rygel, M.C. (2014): Recognizing products of palaeoclimate fluctuation in the fluvial stratigraphic record: An example from the Pennsylvanian to Lower Permian of Cape Breton Island, Nova Scotia. Sedimentology, 61, 1332–1381.

Andreas, D. (1988): The structural dual character of the Rotliegendes in the Thuringian Forest and its surroundings. Zeitschrift für Geologische Wissenschaften, 16, 979–992.

Arche, A., López-Gómez, J. (1999): Tectonic and geomorphic controls on the fluvial styles of the Eslida Formation, Middle Triassic, Eastern Spain. Tectonophysics, 315, 187–207.

Arche, A., López-Gómez, J. (2005): Sudden changes in fluvial style across the Permian−Triassic boundary in the eastern Iberian Ranges, Spain: Analysis of possible causes. Palaeogeography, Palaeoclimatology, Palaeoecology, 229, 104–126.

Blakey, R. (2020): Global Paleogeography and Tectonics in Deep Time Series. https://deeptimemaps.com/map-room/

Blecha, M., Martínek, K., Drábková, J., Šimůnek, Z., Zajíc, J. (1997): Environmental changes at the Carboniferous/Permian boundary and their impact on the floral and faunal assemblages of the fossiliferous lacustrine horizons of the Krkonoše Piedmont Basin. The Czech Science Foundation project 205/94/0692, 177 p. (in Czech)

Blum, M.D., Törnqvist, T.E. (2000): Fluvial responses to climate and sea‐level change: a review and look forward. Sedimentology, 47, 2–48.

Bourquin, S., Guillocheau, F., Péron, S. (2009): Braided rivers within an arid alluvial plain (example from the Lower Triassic, western German Basin): recognition criteria and expression of stratigraphic cycles. Sedimentology, 56, 2235–2264.

Bromley, R.G. (1996): Trace fossils – Biology and Taphonomy: Chapman & Hall, London, 361 p.

Bridge, J.S. (2003): Rivers and floodplains. Blackwell, Oxford, 491 p.

Catuneanu, O., Elango, H.N. (2001): Tectonic control on fluvial styles: the Balfour Formation of the Karoo Basin, South Africa. Sedimentary Geology, 140, 291–313.

Châteauneuf, J.J., Farjanel, G., Pacaud, G., Broutin, J. (1992): The Autun Permian Basin, the Autunian stratotype. Cahiers de Micropaléontologie, 2, 107–121.

Collinson, J.D. (1996): Alluvial sediments. In: Reading, H.G. (ed.): Sedimentary Environments: Processes, Facies and Stratigraphy. Blackwell Science, London, p. 37–82.

Collinson, J.D., Mountney, N., Thompson, D.B. (2006): Sedimentary Structures. 3rd edition. Dunedin Academic Press, Edinburgh.

Davies, S.J., Elliot, T. (1996): Spectral gamma ray characterization of high-resolution sequence stratigraphy: examples from Upper Carboniferous fluvio-deltaic systems, County Clare, Ireland. In: Howell, J.A., Aitken, J.F. (eds.): High Resolution Sequence Stratigraphy: Innovations and Applications. Geological Society, Special Publication 104, p. 25–35.

Dott, R.J., Bourgeois, J. (1982): Hummocky stratification: Significance of its variable bedding sequences. Geological Society of America Bulletin, 93, 663–680.

Droser, M.L. Bottjer, D.J. (1986): A semiquantitive field classification of ichnofabrics. Journal of Sedimentary Petrology, v. 56, p. 558–559.

Ethridge, F.G., Wood, L.J., Schumm, S.A. (1998): Cyclic variables controlling fluvial sequence development: problems and perspectives. In: Shanley, K.J., McCabe, P.J. (eds.): Relative Role of Eustasy, Climate and Tectonism on Continental Rocks. SEPM Special Publication 59, p. 17–29.

Eyles, N., Clark, B.M. (1986): Significance of hummocky and swaley cross-stratification in late Pleistocene lacustrine sediments of the Ontario basin, Canada. Geology, 14, 679–682.

Fielding, C.R. (2006): Upper flow regime sheets, lenses and scour fills: Extending the range of architectural elements for fluvial sediment bodies. Sedimentary Geology, 190, 227–240.

Fielding, C.R. (2009): Facies model for fluvial systems in the seasonal tropics and subtropics. Geology, 37, 623–626.

Fielding, C.R. (2018): The role of discharge variability in the formation and preservation of alluvial sediment bodies. Sedimentary Geology, 365, 1–20.

Foix, N., Paredes, J.M., Giacosa, R.E. (2013): Fluvial architecture variations linked to changes in accommodation space: Río Chico Formation (Late Palaeocene), Golfo San Jorge basin, Argentina. Sedimentary Geology, 294, 342–355.

Hampson, G.J., Davies, W., Davies, S.J., Howell, J.A., Adamson, K.R. (2005): Use of spectral gamma-ray data to refine subsurface fluvial stratigraphy: late Cretaceous strata in the Book Cliffs, Utah, USA. Journal of the Geological Society, 162, 603–621.

Haughton, P.D.W. (1993): Simultaneous Dispersal of Volcaniclastic and Non‐Volcanic Sediment in Fluvial Basins: Examples from the Lower Old Red Sandstone, East‐Central Scotland. In: Marzo, M., Puigdefábregas, C. (eds.): Alluvial Sedimentation (1993). IAS Special Publication 17, p. 451–471.

Henk, A. (1993): Late erogenic basin evolution in the Variscan Internides: the Saar-Nahe Basin, southwest Germany. Tectonophysics, 223, 273–290.

Holbrook, J., Schumm, S.A. (1999): Geomorphic and sedimentary response of rivers to tectonic deformation: A brief review and critique of a tool for recognizing subtle epeirogenic deformation in modern and ancient settings. Tectonophysics, 305, 287–306.

Hornung, J., Hinderer, M. (2011): Depositional Dynamics and Preservation Potential in a Progradational Lacustrine Fluvio-Deltaic Setting: Implications for High-Resolution Sequence Stratigraphy (Upper Triassic, Northwestern China). In: Davidson, S.K., Leleu, S., North, C.P. (eds.): From River To Rock Record: The Preservation Of Fluvial Sediments And Their Subsequent Interpretation. SEPM Special Publication 97, p. 281–310.

Jones, H.L., Hajek, E.A. (2007): Characterizing avulsion stratigraphy in ancient alluvial deposits. Sedimentary Geology, 202, 124–137.

Kurowski, L. (2004): Fluvial sedimentation of sandy deposits of the Słupiec Formation (Middle Rotliegendes) near Nowa Ruda (Intra-Sudetic Basin, SW Poland): Geologia Sudetica, 36, 21–38.

Langford, R., Bracken, B. (1987): Medano Creek, Colorado, a model for upper-flow-regime fluvial deposition. Journal of Sedimentary Petrology, 57, 863–870.

Leleu, S., Hartley, A.J., Williams, B.P.J. (2009): Large-scale alluvial architecture and correlation in a Triassic pebbly braided river system, lower Wolfwille Formation (Fundy Basin, Nova Scotia, Canada). Journal of Sedimentary Research, 79, 265–286.

Li, S., Yu, X., Chen, B., Li, S. (2015): Quantitative characterization of architecture elements and their response to base-level change in a sandy braided fluvial system at a mountain front. Journal of Sedimentary Research, 85, 1258–1274.

Lojka, R., Rosenau, N.A., Sidorinová, T., Strnad, L. (2016): Architecture, paleosols and cyclicity of the Middle–Late Pennsylvanian proximal fluvial system (Nýřany Member, Pilsen Basin, Czech Republic). Bulletin of Geosciences, 91, 111–140.

Lucas, S.G., Schneider, J.W., Cassinis, G. (2006): Non-marine Permian biostratigraphy and biochronology: an introduction. In: Lucas, S.G., Cassinis, G., Schneider, J.W. (eds.): Non-marine Permian Biostratigraphy and Biochronology. Geological Society, Special Publication 265, p. 1–14.

Luthardt, L., Rößler, R., Schneider, J.W. (2016): Palaeoclimatic and site-specific conditions in the early Permian fossil forest of Chemnitz—Sedimentological, geochemical and palaeobotanical evidence. Palaeogeography, Palaeoclimatology, Palaeoecology, 441, 627–652.

Lützner, H., Ellenberg, J., Falk, F. (1992): Continental Permocarboniferous Formations of the Saale Trough. In: Falk, F. (ed.): Excursion Guidebook. 13th IAS Regional Meeting of Sedimentology, Jena 1992, p. 7–44.

Mastalerz, K., Raczyński, P. (1993): Litostratygrafia i ewolucja basenu północnosudeckiego w karbonie i permie. In: II Krajowe Sympozjum Sedymentologów. Przewodnik. Instytut Nauk Geologicznych Uniwersytetu Wrocławskiego, p. 90–108.

Mastalerz, K., Prouza, V., Kurowski, L., Bossowski, A., Ihnatowicz, A., Nowak, G. (1995): Sedimentary record of the Variscian orogeny and climate — Intra-Sudetic Basin, Poland and Czech Republic. In: Guide to Excursion B1, XIII International Congress on Carboniferous–Permian, August 28–September 2, 1995. Państwowy Instytut Geologiczny, Kraków, p. 5–38.

Martínek, K., Uličný, D. (2001): Depositional Processes in a Low-Sinuosity Fluvial System: Facies and Depositional Geometries of the Permian Havlovice Member, Krkonoše Piedmont Basin. Geolines, 13, 89–90.

Martínek, K., Blecha, M., Daněk, V., Francŭ, J., Hladíková, J., Johnová, R., Uličný, D. (2006a): Record of palaeoenvironmental changes in a Lower Permian organic-rich lacustrine succession: Integrated sedimen-tological and geochemical study of the Rudník member, Krkonoše Piedmont Basin, Czech Republic. Palaeogeography, Palaeoclimatology, Palaeoecology, 230, 85–128.

Martínek, K., Svojtka, M., Filip, J. (2006b): Reconstructing Post-Carboniferous History of the Krkonoše Piedmont Basin Using Detrital Apatite Fission-Track Data. Geolines, 20, 91–92.

Martínek, K., Štolfová, K. (2009): Provenance study of Permian non-marine sandstones and conglomerates of the Krkonoše Piedmont Basin (Czech Republic): exotic marine limestone pebbles, heavy minerals and garnet composition. Bulletin of Geosciences, 84, 555–568.

Martinsen, O.J., Ryseth, A.L.F., Helland–Hansen, W., Flesche, H., Torkildsen, G., Idil, S. (1999): Stratigraphic base level and fluvial architecture: Ericson sandstone (Campanian), rock springs uplift, SW Wyoming, USA. Sedimentology, 46, 235–263.

McCann, T., Kiersnowski, H., Krainer, K. Vozárová, A., Peryt, T.M., Opluštil, S., Stollhofen, H., Schneider, J., Wetzel, A., Boulvain, F., Dusar, M., Török, Á., Haas, J., Tait, J., Körner. F. (2008): Permian. In: McCann T. (ed.): The Geology of Central Europe, p. 531–595.

Medici, G., Boulesteix, K., Mountney, N.P., West, L.J., Odling, N.E. (2015): Palaeoenvironment of braided fluvial systems in different tectonic realms of the Triassic Sherwood Sandstone Group, UK. Sedimentary Geology, 329, 188–210.

Miall, A.D. (1977): Lithofacies Types and Vertical Profile Models in Braided River Deposits: A Summary. In: Miall, A.D. (ed.): Fluvial Sedimentology – Memoir 5, p. 597–604.

Miall, A.D. (1988): Facies Architecture in Clastic Sedimentary Basins. In: Kleinspehn, K.L., Paola, C. (eds.): New Perspectives in Basin Analysis. Frontiers in Sedimentary Geology. Springer, New York, p. 67–81.

Miall, A.D. (1996): The Geology of Fluvial Deposits: Sedimentary Facies, Basin Analysis and Petroleum Geology. Springer-Verlag, Berlin, Heidelberg, 582 p.

Nash, D.J., Smith, R.F. (2003): Properties and development of channel calcretes in a mountain catchment, Tabernas Basin, southeast Spain. Geomorphology, 50, 227–250.

Nash, D.J., McLaren, S.J. (2004): Kalahari valley calcretes: their nature, origins, and environmental significance. Quaternary International, 111, 3–22.

Nichols, G. (1999): Rivers: The Fluvial Environment. Sedimentology & Stratigraphy, p. 111–127.

Opluštil, S. (2005): Evolution of the Middle Westphalian river valley drainage system in central Bohemia (Czech Republic) and its palaeogeographic implication. Palaeogeography, Palaeoclimatology, Palaeoecology, 222, 223–258.

Opluštil, S., Martínek, K., Tasáryová, Z. (2005): Facies and architectural analysis of fluvial deposits of the Nýřany Member and the Týnec Formation (Westphalian D – Barruelian) in the Kladno-Rakovník and Pilsen basins. Bulletin of Geosciences, 80, 45–66.

Opluštil, S., Cleal, C. (2007): A comparative analysis of some Late Carboniferous basins of Variscan Europe, Geological Magazine, 144, 417–448.

Opluštil, S., Šimŭnek, Z., Zajíc, J., Mencl, V. (2013): Climatic and biotic changes around the Carboniferous/Permian boundary recorded in the continental basins of the Czech Republic. International Journal of Coal Geology, 119, 114–151.

Opluštil, S., Lojka, R., Rosenau, N.A., Strnad, L., Sýkorová, I. (2015): Middle Moscovian climate of eastern equatorial Pangea recorded in paleosols and fluvial architecture: Palaeogeography, Palaeoclimatology, Palaeoecology, v. 440, p. 328–352.

Opluštil, S., Schmitz, M., Kachlík, V., Štamberg, S. (2016): Re-assesment of lithostratigraphy, biostratigraphy and volcanic activity of the Late Paleozoic Intra-Sudetic, Krkonoše-Piedmont and Mnichovo Hradiště basins (Czech Republic) based on new U-Pb CA-ID-TIMS ages. Bulletin of Geosciences, 91, 399–432.

Pemberton, S.G., Frey, R.W. (1982): Trace fossil nomenclature and the Planolites-Palaeophycus dilemma. Journal of Palaeontology, 56, 843–881.

Pešek, J. (2004): Late Palaeozoic limnic basins and coal deposits of the Czech Republic. Folia Musei Rerum Naturalium Bohemiae Occidentalis, Geologica, 1, 1–188.

Prouza, V., Skoček, V., Tásler, R. (1977): Evaporites in the Lower Permian of the Krkonoše – Piedmont Basin. Věstník Ústředního ústavu geologického, 52, 367–370.

Prouza, V., Šimůnek, Z., Zajíc, J. (1997): Nová lokalita rudnického obzoru (autun) v mnichovohradišťské pánvi u Proseče pod Ještědem. Zprávy o geologických výzkumech, 30, 1996, 37–38.

Prouza, V., Tásler, R. (2001): Podkrkonošská pánev. In: Pešek, J. (ed.): Geologie a ložiska svrchnopaleozoických limnických pánví České Republiky. Český geologický ústav, Praha, p. 128–166.

Prouza, V., Coubal, M., Adamovič, J. (2013): Problematika jihovýchodního pokračování lužického zlomu v západním Podkrkonoší. Zprávy o geologických výzkumech, 46, 59–63.

Ramos, A., Sopeña, A. (1983): Gravel bars in low-sinuosity streams (Permian and Triassic, central Spain). In: Collinson, J. D., Lewin, J. (eds.): Modern and Ancient Fluvial Systems. IAS Special Publication 6, 301–312.

Rider, M.H. (1996): The Geological Interpretation of Well Logs, 2nd ed. Whittles Publishing, Caithness, 280 p.

Roscher, M., Schneider, J.W. (2006): Permo-Carboniferous climate: Early Pennsylvanian to Late Permian climate development of central Europe in a regional and global context. In: Lucas, S.G., Cassinis, G., Schneider, J.W. (eds.): Non-Marine Permian Biostratigraphy and Biochronology. Geological Society, Special Publication 265, p. 95–136.

Rosen, M.R. (1994): The importance of groundwater in playas: A review of playa classifications and the sedimentology and hydrology of playas. In: Rosen, M.R. (ed.): Palaeoclimate and Basin Evolution of Playa systems. Geological Society of America Special Paper 289, p. 1–18.

Schäfer, A. (2011): Tectonics and sedimentation in the continental strike-slip Saar-Nahe Basin (Carboniferous-Permian, West Germany): Zeitschrift der Deutschen Gesellschaft für Geowissenschaften, 162, 127–155.

Scherer, C.M.S., Lavina, E.L.C., Dias Filho, D.C., Oliveira, F.M., Bongiolo, D.E., Aguiar, E.S. (2007): Stratigraphy and facies architecture of the fluvial–aeolian–lacustrine Sergi Formation (Upper Jurassic), Recôncavo Basin, Brazil: Sedimentary Geology, 194, 169–193.

Scherer, C.M.S., Goldberg, K., Bardola, T. (2015): Facies architecture and sequence stratigraphy of an early post-rift fluvial succession, Aptian Barbalha Formation, Araripe Basin, northeastern Brazil. Sedimentary Geology, 322, 43–62.

Schneider, J.W., Körner, F., Roscher, M., Kroner, U. (2006): Permian climate development in the northern peri-Tethys area — The Lodève basin, French Massif Central, compared in a European and global context. Palaeogeography, Palaeoclimatology, Palaeoecology, 240, 161–183.

Sidorinová, T., Stárková, M. (2017): Těžké minerály v sedimentech jižní části podkrkonošské pánve v kontextu změn sedimentace jednotlivých souvrství (permokarbon). Zprávy o geologických výzkumech, 50, 215–220.

Šimůnek, Z., Drábková, J. (2010): Paleobotanické a palynologické studie mezi Hájemi a Dolní Sytovou v podkrkonošské pánvi. Acta Musei Turnoviensis, 5, 119–137.

Stárková, M., Rapprich, V., Breitkreuz, C. (2011): Variable eruptive styles in an ancient monogenetic volcanic field: examples from the Permian Levín Volcanic Field (Krkonoše Piedmont Basin, Bohemian Massif). Journal of Geosciences, 56, 163–180.

Štolfová, K. (2004): Architectural element analysis of fluvial sandstones, Vrchlabí formation, Krkonoše Piedmont Basin, NE Czech Republic: Tectonic and climate controls. Unpublished MSc. Thesis, Charles University, Prague.

Tásler, R., Havlena, V., Prouza, V. (1981): Litostratigrafické členění centrální a západní části podkrkonošské pánve. Věstník Ústředního ústavu geologického, 56, 129–143.

Trümper, S., Gaitzsch, B., Schneider, J.W., Ehling, B.-C., Kleeberg, R., Rößler, R. (2020): Late Palaeozoic red beds elucidate fluvial architectures preserving large woody debris in the seasonal tropics of central Pangaea. Sedimentology, 67, 1973–2012.

Uličný, D., Martínek, K., Grygar, R. (2002): Syndepositional Geometry and Post-Depositional Deformation of the Krkonoše Piedmont Basin: A Preliminary Model. Geolines, 14, 101–102.

Vai, G.B. (2003): Development of the palaeogeography of Pangaea from Late Carboniferous to Early Permian. Palaeogeography, Palaeoclimatology, Palaeoecology, 196, 125–155.

Vandenberghe, J. (2003): Climate forcing of fluvial system development: an evolution of ideas: Quaternary Science Reviews, 22, 2053–2060.

Ventra, D., Nichols, G.J. (2014): Autogenic dynamics of alluvial fans in endorheic basins: Outcrop examples and stratigraphic significance: Sedimentology, 61, 767–791.

Xu, W., Ruhl, M., Jenkyns, H.C., Hesselbo, S.P., Riding, J.B., Selby, D., Naafs, B.D.A, Weijers, J.W.H., Pancost, R.D., Tegelaar E.W., Idiz, E.F. (2017): Carbon sequestration in an expanded lake system during the Toarcian oceanic anoxic event. Nature Geoscience, 10, 129–134.

Zajíc, J., Šimůnek, Z., Drábková, J. (1997): The fossil fauna, mega- and microflora of the Krkonoše Piedmont Basin. Proceedings of the XIII International congress on the Carboniferous and Permian (Prace panstwowego instytutu geologicznego cl VII), p. 197–204.

Zavala, C., Ponce, J., Drittanti, D., Arcuri, M., Freije, H., Asensio, M. (2006): Ancient lacustrine hyperpycnites: a depositional model from a case study in the Rayoso Formation (Cretaceous) of west-central Argentina. Journal of Sedimentary Research, 76, 41–59.

Chapter 2

Integrated stratigraphy of an offshore succession influenced by intense siliciclastic supply: Implications for Coniacian tectonosedimentary evolution of the West Sudetic area (NW Bohemian Cretaceous Basin, Czech Republic)

by Roland Nádaskay, Yulia V. Kochergina,

Stanislav Čech, Lilian Švábenická, Jaroslav

Valečka, Vojtěch Erban, Patricie Halodová

and Bohuslava Čejková

"Alles Gescheite ist schon gedacht worden.
Man muss nur versuchen, es noch einmal zu denken."

"All intelligent thoughts have already been thought;
what is necessary is only to try to *think them again*."

Johann Wolfgang Goethe:
Wilhelm Meister's Wanderjahre

Key words

Abstract

We present the interpretation of tectonosedimentary evolution of the West Sudetic area (central Europe) during the latest Turonian–middle Coniacian as recorded by deposits of the NW part of the Bohemian Cretaceous Basin. This paper provides the first strontium isotope curve from the Upper Cretaceous of the Bohemian Massif. The exact stratigraphic framework was provided by combining of macrofossils (inoceramids) and calcareous nannofossils. Six inoceramid zones were distinguished, from *Cremnoceramus deformis erectus* Zone to *Volviceramus koeneni* Zone. Biostratigraphic data were combined with XRF curves and geophysical logs which allowed for correlation of several key sections within the study area. Using the genetic stratigraphy, contrasting parts of the depositional system interpreted as nearshore to deltaic were successfully correlated. Six elementary sequences were defined within the studied succession. These are TUR 7 (latest Turonian), backstepping, aggradation-dominated, with a short-term progradational episode and CON 1 to 5 (earlyemiddle Coniacian), deposited during a period of increasing depth through time. The progradational pattern is most typical for the CON 4 sequence. Intensified sediment supply resulting in pronounced progradation is also evidenced by increased siliciclastic influx to the offshore zone and resulting changes in calcareous nannofossil assemblages.

Three major transgressive events are interpreted at the base of sequences: (1) CON 1 (close to the Turonian–Coniacian boundary); (2) CON 2 (near FO of *Cremnoceramus crassus crassus*); (3) CON 5. The transgressions were predominantly driven by basin-floor subsidence, although the transgression at the Turonian–Coniacian boundary and at the base of sequence CON 2 likely carried a component of eustatic sea-level rise. The accelerated basin-floor tectonic subsidence and source uplift in the NW part of BCB falls within the early Ilsede phase of the Late Cretaceous ('Subhercynian') deformation of the Alpine foreland.

Introduction

Depositional history of siliciclastic-dominated basins has been efficiently interpreted when combining conventional stratigraphic methods with the chemostratigraphic approach (e.g., Uličný et al. 2014; Olde et al. 2015; Plint et al. 2017). When sediment supply and/or tectonic subsidence obscures the eustatic component of sea-level changes, basin's transgressive-regressive history is interpreted from the stacking patterns of depositional bodies within the individual stratigraphic sequences (e.g., Gawthorpe et al. 1994; Martinsen and Helland-Hansen 1995; Gawthorpe and Leeder 2000; Varban and Plint 2008; Vakarelov and Bhattacharya 2009; Leren et al. 2010) representing a record of relative sea-level changes. Understanding the rate of eustatic control on deposition in local (single basin, sub-basin) scale vs. other extra- and intrabasinal controls (e.g., tectonics) aids to assess processes governing basin formation, filling and subsequent inversion.

During Late Cretaceous several basins formed in the Western and Central Europe by reactivation of major Variscan fault zones (e.g., Schröder 1987; Brandmayr et al. 1995; Scheck et al. 2002; Mazur and Scheck-Wenderoth 2005). In the Bohemian Cretaceous Basin (BCB), the acceleration of subsidence together with an increase in sediment supply that took place during the late Turonian–Coniacian, is evidenced by changes in large-scale stratigraphic architecture of nearshore siliciclastic deposits (e.g., Uličný et al. 2009a,b). However, little attention has been paid to the transition of nearshore/deltaic sandstones to offshore mudrocks. The latter area could provide evidence for propagation of siliciclastic influx from proximal setting (e.g., Uličný et al. 2014; Olde et al. 2015), and are suitable for tracing temporal and spatial variations of siliciclastic supply because trends of geochemical proxies can be directly linked to physical sedimentary record (e.g., Wilson and Schieber 2014; Schieber 2016). Because the stable isotope-based stratigraphy does not perform well in the mudrocks of the BCB (e.g., Uličný et al. 1993), we attempt to employ radiogenic strontium isotope stratigraphy.

The chemostratigraphy utilizing radiogenic strontium composition of marine carbonates is a well-established approach (e.g., McArthur et al. 1994; Veizer et al. 1999; Allègre et al. 2010).

However, there are no data available for the BCB. Particularly, relatively marginal parts of the basin dominated by siliciclastic deposits has been considered unsuitable for performing strontium analyses due to scarcity of the calcareous shell fragments. Here, we present the carbonate fraction $^{87}Sr/^{86}Sr$ ratio in comparison to the silicate fraction (insoluble residue from calcareous shells) composition to evaluate the applicability of strontium stratigraphy and silicate fraction analysis for provenance constraints. Moreover, the information on Sr isotope signature of the Upper Cretaceous deposits provides badly needed sedimentary endmember composition constraints for discussions on possible crustal contaminationof Cenozoic alkaline magmas crosscutting the BCB (Rapprich et al. 2017).

Based on the integrated stratigraphy, this work aims at the interpretation of tectonosedimentary evolution of the NW part of BCB during the Coniacian, a critical interval of the basin's evolution. Unlike previous isotope-stratigraphic studies focused exclusively on stable isotopes (e.g., Uličný et al. 1993, 1997, 2014; Jarvis et al. 2015), this paper focuses on radiogenic strontium isotope analysis to provide the first stratigraphically calibrated strontium isotope curve from the BCB. We aim to discuss the limitations of this method and its possible future use within the framework of the BCB.

Geological framework

Geological setting of the Bohemian Cretaceous Basin with emphasis on the Coniacian

The Bohemian Cretaceous Basin (BCB) was established by the mid-Cretaceous tectonic reactivation of the Variscan basement and by the late Cenomanian it formed a narrow marine basin connecting the Tethys and Boreal Sea (e.g., Voigt et al. 2008; Čech 2011, Klein et al. 1979; Uličný et al. 2009b; Fig. 1A, B). It consists of several individual sub-basins that formed as a result of syndepositional tectonic partitioning during three contrasting tectonosedimentary episodes (Fig. 1C; Voigt et al. 2008). The best evidence of syndepositional tectonic activity provides the late Cenomanian–Coniacian record of the Lužice–Jizera sub-basin (NW part of the BCB), neighbored at that time by the Central European Island on the west/southwest and on the east by West Sudetic Island (Ziegler 1990). The latter served as its principal source area (e.g., Scupin 1936; Valečka 1979a,b; Skoček and Valečka 1983). Initially, the Lužice–Jizera sub-basin subsided rapidly due to its proximity to the marginal Lusatian (Lužice, Lausitz) Fault and was filled with material derived from the uplifted source area (e.g., Skoček and Valečka 1983). Since the latest Turonian, the tectonic acceleration initiated the incipient deformation of the earlier basin infill (Uličný et al. 2009a). The present-day structure of the BCB results from postdepositional deformation after ca. 85–86 Ma (Santonian; Voigt et al. 2008), related to continental-scale changes in the paleostress field in Europe (Coubal et al. 2015).

In the Lužice–Jizera sub-basin, the Coniacian succession is formed by the upper part of Teplice Formation and overlying Březno Formation. Defined by combination of the litho- and biostratigraphic criteria (Čech et al. 1980), these units are partly diachronous (Laurin and Uličný 2004; Uličný et al. 2014), and in various parts of the BCB comprise hiatuses of several hundred kyr timespan (Vodrážka et al. 2009; Uličný et al. 2009a). The Teplice Formation in the study area is represented by two contrasting lithofacies. The lower part is formed by dominantly fine-grained sandstones with an extent limited to the area close to the marginal Lusatian Fault (e.g., Nádaskay and Uličný 2014). Basinward, they pinch out into a sequence of the lower–middle Coniacian mudstones and marlstones. In the axial part of the basin, this interval comprises the Rohatce Member, an alternation of silicified limestones and marlstones. If present, their top marks the top of the Teplice Fm. (Čech et al. 1980) and is used as a datum in basin-scale stratigraphic correlations (e.g., Uličný et al. 2009a). Although typical Rohatce Mb. is not developed in the study area, the time-equivalent strata have been determined by index fossil finds (e.g., Čech et al. 1987).

Most of the Coniacian of the BCB corresponds to the overlying Březno Formation, defined as a succession of mudstones in the Březno type section in the axial part of the basin (Čech et al. 1980; Čech and Švábenická 1992). In the study area, the Březno Formation consist of three facies groups deposited within a single depositional system (e.g., Valečka, 1979a,b; Nádaskay and Uličný 2014): i) sandstone facies arranged as coarsening-upward cycles; ii) mudstone-dominated facies, and iii) heterolithic facies ('flyschoid' sensu Valečka and Rejchrt 1973).

Biostratigraphy

The earliest biostratigraphic subdivision of the Turonian–Coniacian ('Emscherian') sequence of the NW part of BCB ('Kreibitz–Zittau' region) was introduced by Andert (1911, 1934) and was based mainly on inoceramids. According to him, *Inoceramus waltersdorfensis* Andert, 1911, *I. incostans* Woods, 1911, *I. schloenbachi* Böhm, 1911 and *I. crassus* Petrascheck, 1903 belong to the Upper Turonian ('Oberturon'), while *I. kleini* Müller, 1888 is the index fossil of the so-called 'Emscherian', the youngest part of the Upper Cretaceous in the study area. Andert's collection of inoceramids from the topmost Turonian and lowerelowermost middle Coniacian from this region was revised, re-described and newly illustrated by Walaszczyk (1996). Macák and Müller (1963) and Macák (1967) recognized the younger middle–upper Coniacian inoceramid succession spanning the zones *Volviceramus koeneni* (Müller) to *Magadiceramus subquadratus* (Schlüter 1887) in the NW BCB. The *Didymotis* events and problems concerning the Turonian–Coniacian stage boundary in the BCB were discussed by Čech (1989). Identification of Turonian–Coniacian
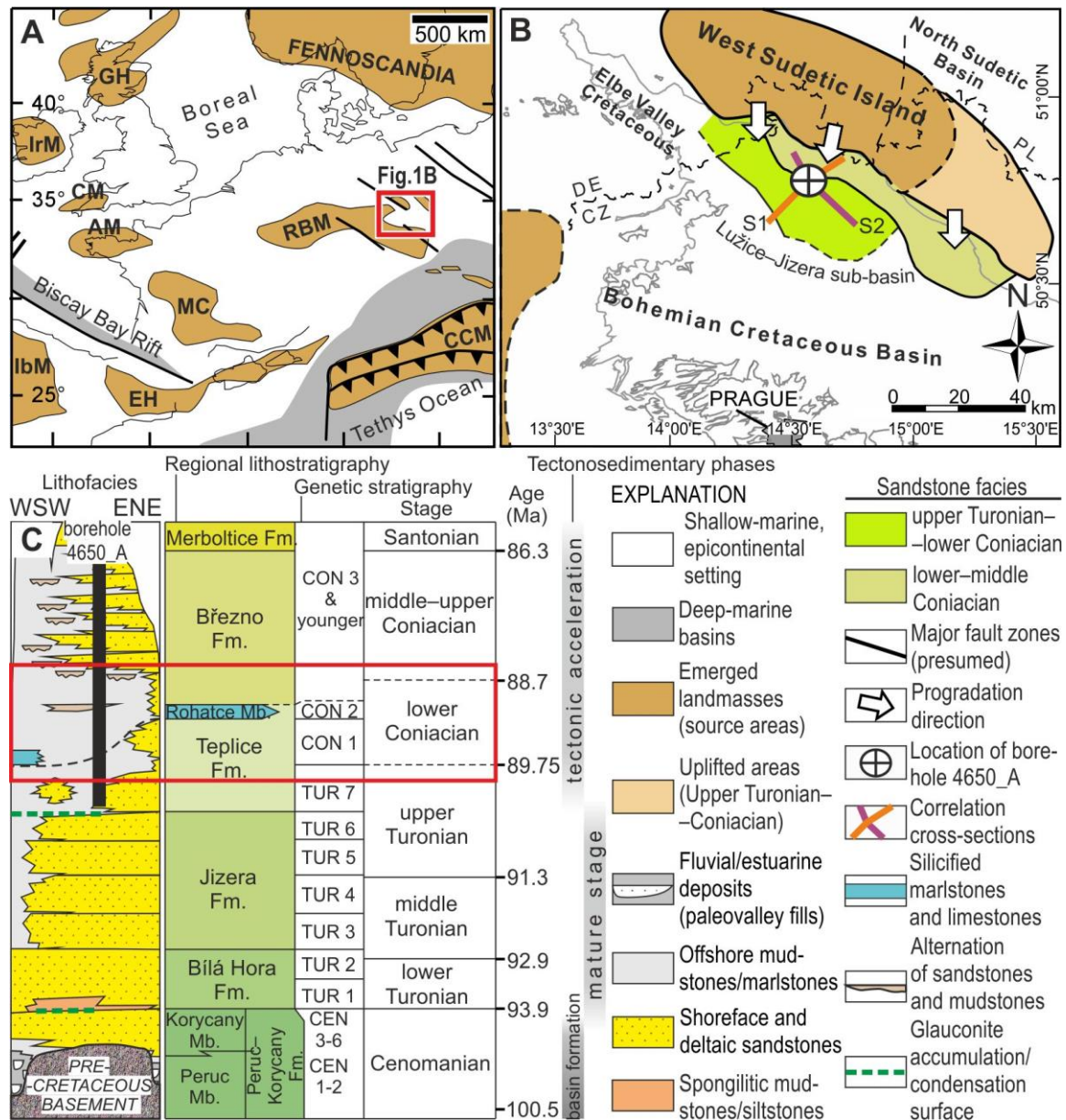
Figure 1. **(A)** Late Cretaceous paleogeography of the western and central Europe (modified after Ziegler, 1990). Emerged landmasses: AM – Armorican Massif, CM – Cornubian Massif, CCM – Central Carpathian Massif, EH – Ebro High, GH – Grampian High, IbM – Iberian Massif, IrM – Irish Massif, MC – Massif Central, RBM e Rheno-Bohemian Massif. **(B)** Paleogeographic map of the northwestern part of the BCB (Lužice–Jizera sub-basin). The contour of the maximum extent of sandy facies progradation during deposition of sequence CON 1 is shown; uppermost Turonian TUR 7 sequence is added for comparison. Modified after Uličný et al. (2009) and Uličný et al. (2014). **(C)** Simplified stratigraphic chart of the Lužice–Jizera sub-basin, showing lithofacies development, regional lithostratigraphic units (Čech et al., 1980) and genetic sequences (sensu Uličný et al., 2009). Time interval of the present study is highlighted.

boundary within mudstone-dominated offshore successions by integration of macro- and micropaleontological finds was resolved by Čech and Švábenická (1992). Nannofossils of the Coniacian strata have been already studied in several locations across the BCB, both in the western (Čech et al. 1987; Čech and Švábenická 1992; Svobodová et al. 2014; Švábenická et al.

106

Figure 2. Correlation cross-sections S1 (A) and S2 (B); parallel and perpendicular to the general direction of the clastic supply, respectively. Individual boreholes are plotted equidistantly; true distances in kilometres listed below the section. Wireline logs, namely gamma-ray log (GR), resistivity- (RES) and neutron (NL) log are depicted without a quantitative log-scale in order to keep clarity of figures. Graphic explanations to both correlation cross-sections are in Fig. 2A. Abbreviations of biostratigraphic markers: Ccc – *Cremnoceramus crassus crassus (Petrascheck)*, Cd – *C. deformis* (Meek), Cde – *C. deformis erecrus* (Meek), Cwh – *C. waltersdorfensis hannovrensis* (Heinz), Cww – *C. waltersdorfensis waltersdorfensis*, Ifr – *Inoceramus frechi Flegel*, Pm – *Platyceramus mantelli* (Mercey), Vko – *Volviceramus koeneni* (Müller).

2016) and in the central part (Uličný et al. 2014; Švábenická and Havlíček 2017). Particular attention has been paid to the horizon with common Marthasterites furcatus spanning from around the Turonian–Coniacian boundary to the lower Coniacian (Švábenická 2010, 2012; Švábenická and Valečka 2011). In recent years, the macro- and nannofossil correlations have been carried out in other parts of the European Platform as well (e.g., Lees 2008; Kędzierski 2008).

Dataset and methods

Sedimentology and sequence stratigraphy

Drill core provided primary data for a stratigraphic division of the mudstone-dominated Coniacian section and chemostratigraphic analyses. The section was correlated within the Coniacian depositional system using new data that enabled its modification. To visualise spatial and temporal transitions of facies within the depositional system, a stratigraphic correlation of geophysical well-logs was employed. The typical well-log signatures of lithofacies are summarized in Fig. 4. Well-logs were correlated using the genetic sequence-stratigraphic methodology as adapted for the BCB by Uličný and Laurin (2001), Laurin and Uličný (2004) and Uličný et al. (2009a). This methodology follows the genetic sequence concept of Galloway (1989), based on tracing maximum flooding surfaces (MFS), i.e., maximum transgressive surfaces (MTS, this paper) sensu Helland-Hansen and Martinsen (1996), separating the genetic sequences and the maximum regressive facies within composite sequences. Maximum transgressive surfaces can be traced into the offshore as correlative conformities merely by fossil markers, or by geochemical proxies that are, however, not widely applicable because of the missing core from most of the historical boreholes. Genetic sequences are subdivided into lower order sequences, formed by individual progradational sandstone bodies, meters to tens of meters thick, bounded by transgressive surfaces usually covering conglomeratic transgressive lags (e.g., Uličný 2001; Nádaskay and Uličný 2014), termed 'elementary sequences' by Laurin and Uličný (2004).
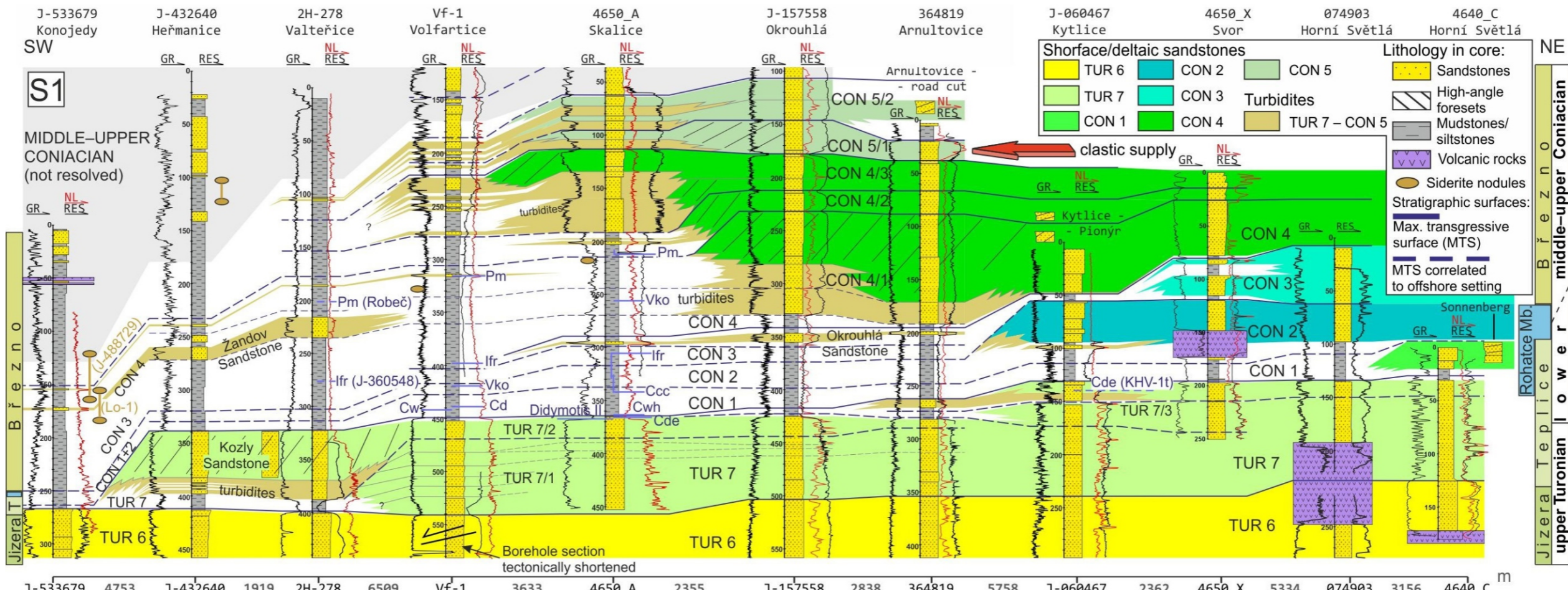
Fig. 2
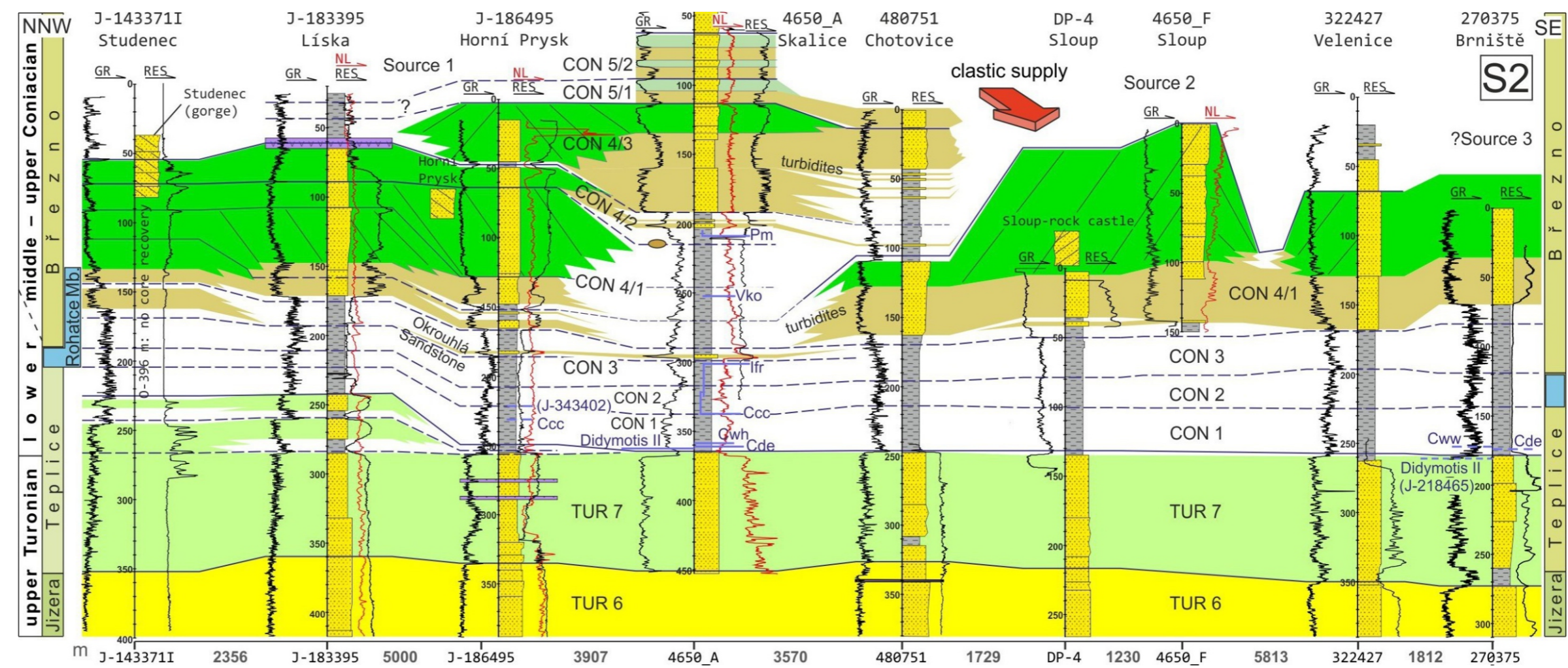
Microfossils and macrofossils

Nearly 30 specimens of inoceramids were collected from the core, 7 cm in diameter, from the mudstones and siltstones of the Teplice and Březno formations at depth interval 205.15–362.57 m. For nannofossil study, 53 samples were taken at approximately 5 m intervals between 134.15 and 366.05 m. Sampling focused on coquina-like layers and horizons with shell debris accumulations. Nannofossils were investigated in the 1–30 mm fraction (Švábenická 2012). Smear-slides were inspected at 1000x magnification using an oil-immersion objective on a Nikon Microphot-FXA light microscope. Photographs were taken by Nikon DXM1200F digital camera and SW ACT-1. Biostratigraphic data were interpreted with respect to Burnett (1998) and Lees (2008). In the text, the abbreviations FO and LO are used to denote first occurrence and last occurrence of a taxon, respectively. Smear-slides and inoceramid specimens are stored in the Department of Collections of the Czech Geological Survey (CGS), Prague. The SEI images were obtained using scanning electron microscope FEG-SEM Tescan Mira 3GMU. Samples were coated by 10 nm thick layer of Au to avoid charging and to enhance the contrast (relief). Following analytical conditions were applied: 20 kV accelerating voltage, 15 mm working distance, probe current approximately 200 pA. The eucentric stage was used during imaging to easily tilt/rotate the sample into the required position.

Geochemical proxies

Element concentrations were measured in-situ (on drill core) by Niton XL3tGoldD+ handheld XRF analyzer. In total, 625 analyses were performed between depths of 192 and 370 m with 3 min acquisition time each. The measurements were taken at interval 0.25 m in homogeneous parts of the core while at 0.1 m interval around conspicuous lithological transitions. In a handful of cases when disintegrated drill core did not allow taking a sample, measurements were rendered at interval 1 m.

Bulk rock analyses of 10 representative samples were conducted by Central Laboratories of the Czech Geological Survey, Prague. Major elements were analyzed by wet quantitative methods and expressed as weight % of oxides (SiO_2, TiO_2, Al_2O_3, Fe_2O_3, FeO, MgO, MnO, CaO; Table 1). Details to analytical procedures, relative standard deviations and standard errors for individual oxides are provided by Dempírová et al. (2010). Selected trace-element abundances (Cr, Ni, Cu, Zn, As, Rb, Sr, Y, Zr, Nb, Mo, Sn, Pb, U; Table 2) were analyzed by laboratory XRF analyzer ARL 9400 Advant XP and presented as weight ppm values. The whole-rock Ca concentrations acquired by portable XRF were re-calculated to $CaCO_3$ since calcite is deemed to be the only significant Ca-bearing mineral phase that appears both as the main constituent of bioclasts and a rock-matrix micrite (other Ca-minerals are negligible in volume compared

Figure 3 (on the opposite page). Stratigraphic and lithological section of the lower and middle Coniacian in the borehole 4650_A. Fossil finds are listed in detail in chapter 4.2 and discussion to biostratigraphic constraints is provided by chapter 5.1. Concise description and interpretation of facies groups are provided by Fig. 4.

Table 1. Bulk-rock major element composition of selected representative samples.

Sample/ depth (m)	Lithology	SiO$_2$	Al$_2$O$_3$	TiO$_2$	Fe$_2$O$_3$	FeO	MgO	MnO	CaO
		wt. %	wt. %	wt. %	wt. %	wt. %	wt. %	wt. %	wt. %
204.28	mudstone	55.46	13.74	0.76	3.23	1.99	1.96	0.032	5.40
221.31	mudstone	54.66	13.51	0.72	3.89	1.50	2.04	0.017	5.61
240.46	mudstone	57.13	11.43	0.59	3.82	0.84	1.93	0.007	5.59
256.20	mudstone	50.25	14.47	0.74	4.39	1.51	1.71	0.022	7.00
270.36	mudstone	54.74	13.69	0.72	3.07	0.98	1.82	0.026	6.86
292.12	mudstone	58.93	11.85	0.52	3.40	0.89	1.79	0.016	5.30
341.18	mudstone	51.68	10.60	0.49	2.71	0.75	1.79	0.005	10.96
356.56	mudstone	52.75	10.99	0.56	2.96	0.61	1.87	0.012	10.38
366.85	claystone	62.10	14.78	0.80	4.75	0.62	1.35	0.002	0.65

Table 2. Bulk-rock trace element composition of selected representative samples.

Sample / depth (m)	Lithology	Cr	Ni	Cu	Zn	As	Rb	Sr	Y	Zr	Nb	Mo	Sn	Pb	U	Rb/Sr
		ppm	ppm	ppm	ppm	ppm	ppm	ppm	ppm	ppm	ppm	ppm	ppm	ppm	ppm	
204.28	mudstone	89	42	19	81	< 1	133	226	22	215	13	< 1	< 2	31	4	0.6
221.31	mudstone	89	39	16	68	< 1	129	251	18	169	11	< 1	< 2	30	2	0.5
240.46	mudstone	73	31	15	56	< 1	114	247	17	156	11	< 1	3	23	< 2	0.5
256.20	mudstone	92	48	15	64	< 1	133	254	19	163	14	< 1	< 2	29	< 2	0.5
270.36	mudstone	87	29	16	67	< 1	126	259	20	169	13	< 1	2	30	4	0.5
292.12	mudstone	71	27	14	53	< 1	110	242	17	123	11	< 1	< 2	26	< 2	0.5
341.18	mudstone	64	26	12	51	< 1	104	332	15	86	8	< 1	< 2	15	< 2	0.3
356.56	mudstone	68	28	14	56	< 1	110	298	16	108	8	< 1	< 2	19	< 2	0.4
366.85	claystone	110	41	13	64	18	149	89	20	261	14	< 1	< 2	33	3	1.7

to calcite). Calcite sparite is uncommon, but it might fill voids in foraminifers in rare cases. Several ratios of major and minor elements bound to silicate minerals (i.e., Si/Al, Ti/Al and Zr/Al) were applied as proxies of the siliciclastic influx (e.g., Jarvis et al. 2001), suitable in this setting due to prevalence of silicate rocks in the source area (Skoček and Valečka 1983). Excessive values of Si/Al (>8) and Zr/Al (>0.01) ratio indicating sandstone intercalations were excluded from graphic representation to emphasize otherwise minor contrasts in relevant fine-grained facies.
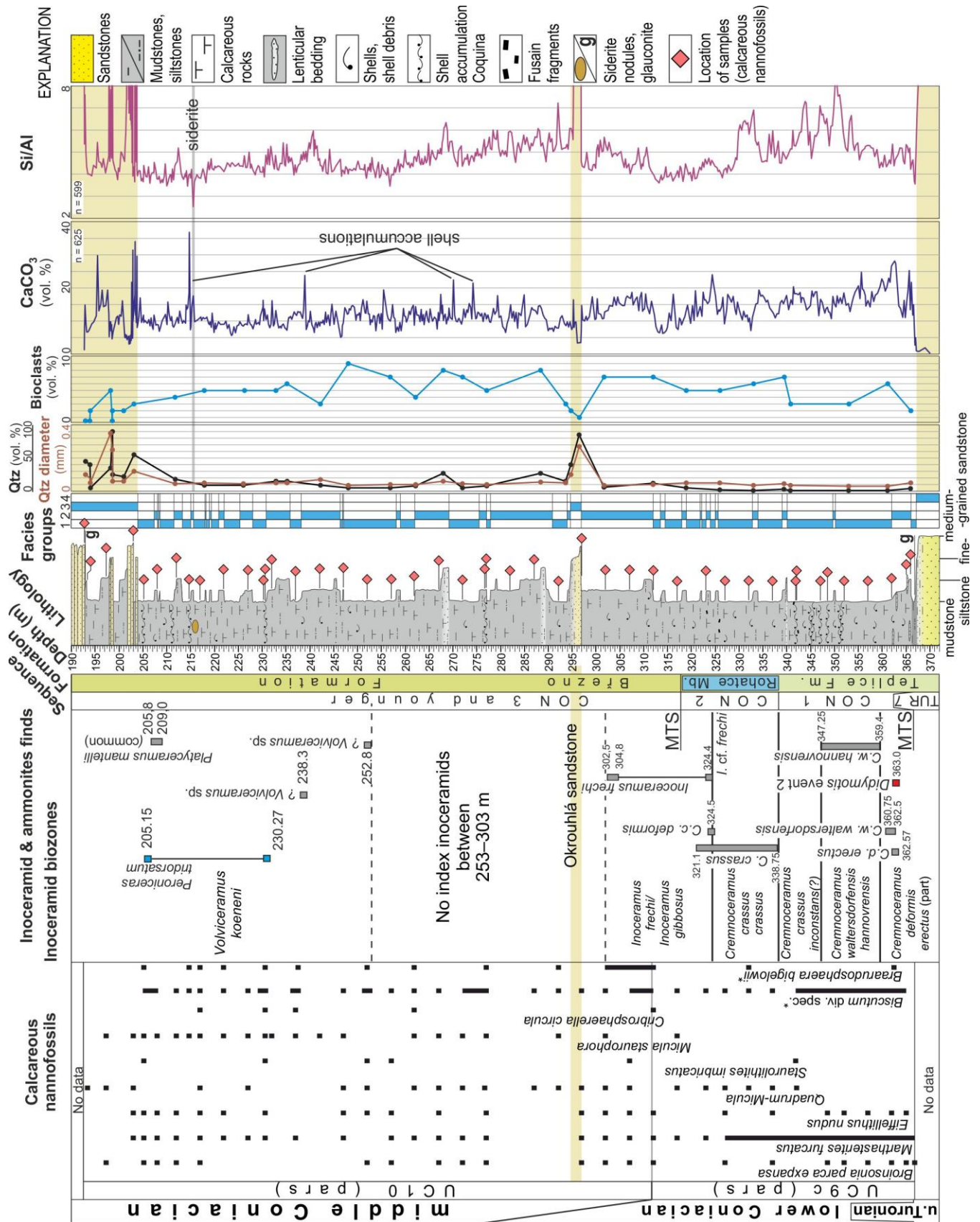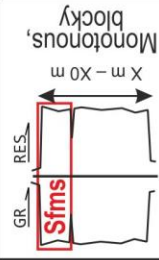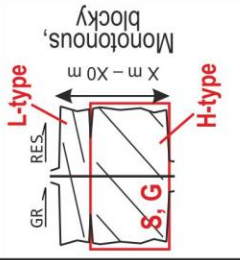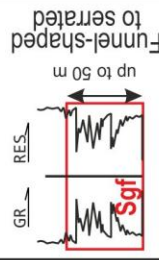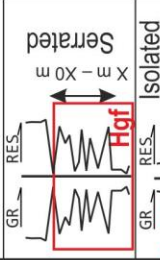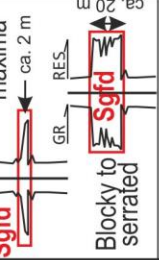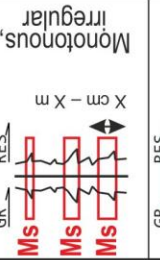
Figure 4 (on the opposite page). Summary table of the lithofacies described in chapter 4.1. Modified after Nádaskay and Uličný (2014) and Uličný et al. (2009a). Numbers in circles refer to facies groups as presented in Fig. 2.

Selected well-logs were used as lithological proxies compared to element concentrations. Well-logging was conducted after drilling at 5 cm increment, providing the dataset even denser than the one acquired by XRF. Gamma-ray log reflects summary concentrations of main radiogenic elements (K, Th, U) and is used as a proxy of clay mineral content (Rider 1996). In the BCB, an increase of clay mineral content reflects decreasing grain size (sand content) and vice versa (e.g. Uličný and Laurin 2001). Gamma-ray log values are displayed in micro-Röntgen per hour (mR/h); according to (Harrison 1995), 1 mR/h equals to ca. 10–15 API depending on the detector type. Neutron log represents variations in hydrogen content that significantly increases with the higher rate of connectedmacroporosity, accounting for effective hosting of moveable water (e.g., Rider 1996). Neutron log values are displayed in counts per minute (cpm).

Strontium, carbon and oxygen isotope analyses

Isotope analyses were performed on macroscopic fragments of calcium carbonate shells, predominantly calcite-shelled bivalves, subordinately aragonite-shelled gastropods or ammonites (Fig. 5, list in Table 3). These samples were obtained by selective leaching with weak acid from the silicate (non-carbonate) fraction. The residual fractions of five selected samples (195.25, 230.8, 246.37, 276.75 and 290.35 m) were also analysed for $^{87}Sr/^{86}Sr$ to evaluate the difference between marine and terrigenous sediments and possible contamination of carbonate. Analyses were also performed on carbonate fraction of a bulk rock sample (361.5 m) formed predominantly by micrite containing microscopic tests of foraminifers and calcareous nannofossils. The intention was to assess possible 'vital effects' on the isotopic composition of C and O, as well as quantify the $^{87}Sr/^{86}Sr$ composition of the micrite.

For $^{87}Sr/^{86}Sr$ isotope analysis, samples were cleaned by mechanical abrasion, rinsed in milli-Q water and leached in 4 ml of warm 0.1 N acetic acid for 10 min in an ultrasonic bath in order to dissolve the carbonate phase. The residual silicate phases were removed by centrifugation. Selected residual samples were dissolved in the mixture of concentrated HF and HNO_3. Strontium was in all cases separated using Sr-spec resin after Pin et al. (2014). The Sr isotope composition was analyzed using Thermo Fisher Triton Plus thermal ionization mass spectrometer. The external precision was established by repeated measurement of the international reference standards (NBS987: $^{87}Sr/^{86}Sr$ = 0.710253 ± 22 (2σ, n = 50). Carbonate reference material EN-1 (USGS) yields $^{87}Sr/^{86}Sr$ value 0.709171 ± 29 (2σ, n = 6).

Facies	Texture	Sedimentary structures and ichnofabrics	Geometries & spatial relationships	Interpretation	Typical well-log pattern
Sfms	Sandstone, fine- to medium-grained, well sorted	Structureless or cross-bedded, ii=1–2, *Planolites*, *Ophiomorpha*	Tabular or lenticular external geometry, subhorizontal internal stratification, overlying coarsening-upward sandstone beds, sharp contact with overlying mudstones	Upper shoreface, lateral transitions into shallow-water deltas (cf. Uličný 2001), intensely reworked by tidal-current action	Monotonous, blocky; Sfms
S, G ④	Sandstone, usually medium to coarse-grained, locally conglomerates, poorly sorted, mud-free (in cross-sections only)	Trough cross-bedding (indicating S/SE palaeocurrents), presence of upper flow regime structures, sparsely burrowed, ii ca. 1–2, *Ophiomorpha*, *Thalassinoides*	Tabular or lenticular external geometry. Two types: i) slightly inclined bedsets (2°, max. up to 10°) and up to 20 m thick bodies; ii) steeply-inclined bedsets (up to 30°), up to ca. 90 m thick bodies. Pass basinward into **Hgf** or **Sgf** or pinch out (into **Ms**, **Mm**)	Delta-front facies, low- (L-type) or high-type (H-type) foresets; shallow- vs. deep-water deltas (cf. Uličný 2001). L-type: intense tidal-current reworking, gravity-flow deposits negligible; H-type: Episodes of down-slope transport by gravity currents followed by tidal-current reworking of foresets	Monotonous, blocky; L-type, H-type; S, G
Sgf	Gravity-flow (sandstone-dominated) deposits, predominantly sandstones with mud-rich intercalations	Sharp-based beds or lithological transitions, massive to parallel-bedded, rarely rippled or normal-graded, mud-rich inter-calations strongly burrowed, ii ca. 4–5, *Planolites*, *Thalassinoides*	Tabular to lenticular external geometry, individual sandstone bed few cm up to ca. 2 m thick, complex internal stratification of thicker beds, passes landward into facies **S**, **G**, basinward transition into facies **Hgf** or **Mm/Ms**	Gravity flow-dominated bottom-sets passing from high-angle foresets, most proximal prodelta deposits of deep-water deltas (cf. Uličný 2001)	Funnel-shaped to serrated, up to 50 m; Sgf
Hgf	Gravity-flow (heterolithic) deposits, predominantly mudstones with sand-stone intercalations	Sharp-based, massive to parallel-bedded, fining-upwards, frequently calcite-cemented, ii ca. 4–5, *Planolites*, *Thalassinoides*	Tabular to lenticular external geometry, cm thick sandstones (up to 20 cm) interbeds in facies **Ms** or **Mm**, passing landwards into facies **S**	Gravity flow-dominated bottomsets passing from high-angle foresets, prodelta deposits of deep-water deltas (cf. Uličný 2001)	Serrated; Hgf
Sgfd ③	Sandstone, single interbed (in core), amagalmated sand-stones with possible mud-rich interbeds (in cross-sections only)	Erosive-based, fining-upwards into facies **Ms**, massive at the base, relics of parallel bedding in the top	External geometry tabular (deposited over facies **Ms/Mm**) or lenticular (incised-channel fill), single bed or amalgamated beds, passing basinward into facies **Ms/Mm**, nearshore equivalent unclear	Gravity-flow deposits detached from delta bodies, possibly forming a part of submarine turbidite lobe, amalgamated beds=channel fill deposits(?), single-bed sandstone=unconfined deposits(?)	Isolated maxima, ca. 2 m; Sgfd. Blocky to serrated, ca. 20 m; Sgfd
Ms ②	Siltstones, clay or subtle fine sand admixture	Diffuse boundaries with facies **Mm**, relics of primary horizontal bedding recognizable locally, strongly burrowed, ii ca. 5–6, *Cruziana* ichnofacies	Basinward transition and interfingering with facies **Mm**, passes landward into facies **Hgf** or **S**, possible lateral transition into facies **Sgf**	Offshore setting, distal deposits of prodelta, deposition of mud/silt (+/- sand) from lofting suspension plumes of waning hyperpycnal currents	Monotonous, irregular; Ms Ms Ms
Mm ①	Mudstone, moderate silt admixture	Diffuse boundaries with facies **Ms**, almost completely burrowed, ii=5–6, *Cruziana* ichnofacies	Interfingering with facies **Ms**, basinward transition into hemipelagic marlstones to limestones (cf. Laurin & Uličný 2004)	Low-energy, offshore setting, not disturbed by hyperpycnal currents	Mono-tonous; Mm
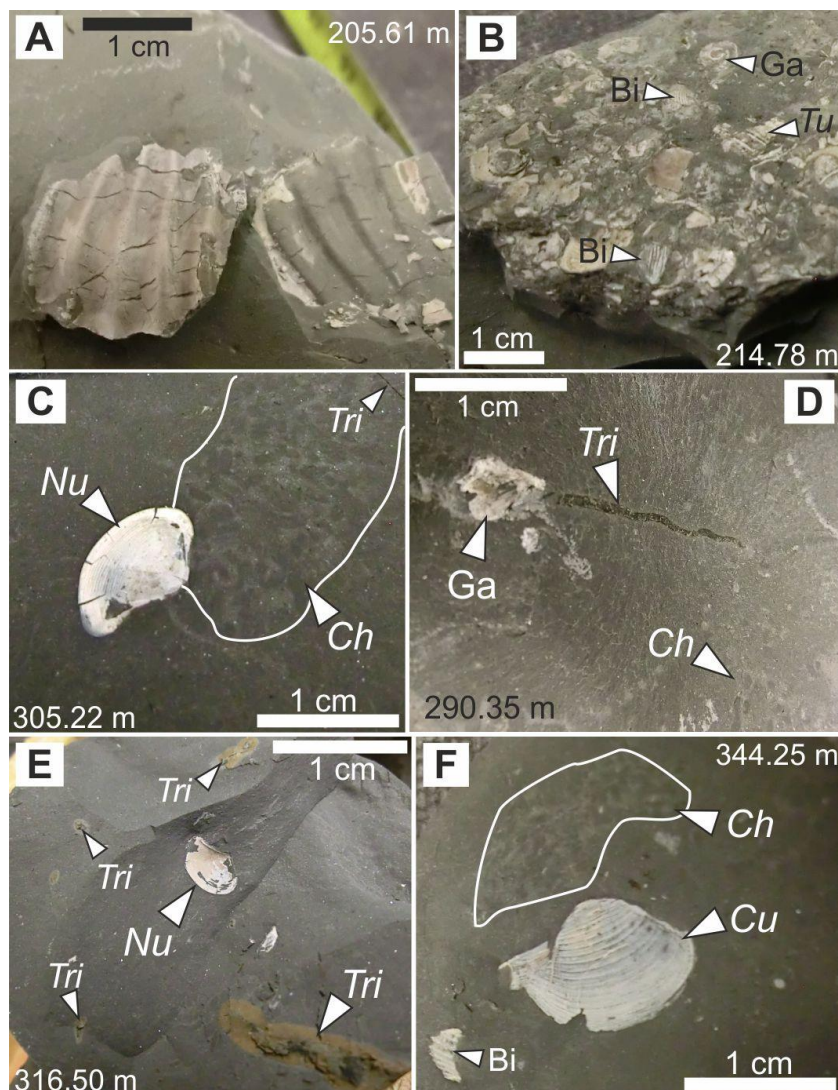
Figure 5. Photographs of macrofauna sampled for isotope analyses. **(A)** Shell fragment of an undetermined inoceramid. Depth 205.61 m, middle Coniacian, Březno Fm. **(B)** Fragments of bivalves and gastropods, forming ca. 5 mm thick coquina layer within lithofacies Ms. Bi – undetermined bivalve; Ga – undetermined gastropod; Tu – gastropod *Turritella*. Depth 214.78 m, middle Coniacian, Březno Fm. **(C)** Shell of bivalve *Nuculana semilunaris* associated with *Chondrites* isp. burrows. Depth 305.22 m, lower Coniacian, Březno Fm. Nu – *Nuculana*; Ch – *Chondrites* isp.; Tri – *Trichichnus* isp. **(D)** Shell fragment of undetermined gastropod, associated with *Trichichnus* isp., 1 mm in diameter. Depth 290.35 m, lower Coniacian, Březno Fm. Ga – undetermined gastropod; Ch – *Chondrites* isp.; Tri – *Trichichnus* isp. **(E)** Shell of *Nuculana* within interval intensely penetrated by filaments (cf., Kędzierski et al., 2015) of *Trichichnus* isp., up to ca. 5 mm in diameter. Depth 316.50 m, lower Coniacian, Březno Fm. Nu – *Nuculana*; Tri – *Trichichnus* isp. **(F)** Shell of bivalve *Cuspidaria* sp. and *Chondrites* isp. burrows. Depth 344.25 m, lower Coniacian, Teplice Fm. Bi – undetermined bivalve; Cu – *Cuspidaria* sp.; Ch – *Chondrites* isp.

Selective leaching of samples was applied to acquire $\delta^{13}C$ and $\delta^{18}O$ values for the carbonate fraction following the methodology of McCrea (1950). In brief, H_3PO_4 with $K_2Cr_2O_7$ was administered to the sample powder and reacted at room temperature under vacuum for 24 h. The measurements were performed using a dual inlet Delta V Advantage mass spectrometer (Thermo Fisher). The results for C and O are presented relative to V-PDB and V-SMOW reference materials, respectively, with the total analytical error of <0.1‰ (2δ). Because of

different acid fractionation factors for calcite and dolomite, the $\delta^{18}O$ value for dolomite was corrected by –0.84‰ (Becker and Clayton 1976; Kim et al. 2015).

Results

Lithology and facies

Four principal lithofacies have been distinguished within the studied core section and additional two in cross-sections only. Together, they are grouped with respect to depositional processes and energy of the environment, and hence ordered by decreasing influence of high-energy processes with increasing distance from the presumed shoreline.

Lithofacies **Sfms** (Sandstone fine- to medium-grained, well-sorted) underlies the studied interval of Coniacian claystones, mudstones and siltstones. It is formed by pale gray medium- to coarse-grained quartzose sandstones, structureless and well sorted, except for the uppermost, argillaceous part. Vertical transition to mudstones/siltstones is quick with no remarkable evidence of erosive or omission surface. Top of the sandstones is bioturbated, with some burrows (*Planolites*) penetrating ca. 10–20 cm into the sandstone from overlying mudstones.

Interpretation: Lithofacies Sfms was deposited in a shallowwater environment with the intense action of sorting processes, presumably driven by tidal-induced currents (Valečka 1979a,b; Uličný 2001; Mitchell et al. 2010). It may form as current-modified shoreface sand bodies (Valečka 1994) or by progradation of shallow-water deltas (Uličný et al. 2009a; Vacková and Uličný 2011).

Lithofacies **S and/or G** refer to medium- to coarse-grained sandstones (S), locally up to conglomerates, mostly fine-grained (G). Both facies are present in borehole 4650_A above the studied section but are present in the correlation cross-sections (Fig. 2A, B). Uličný (2001) distinguished two sub-types of the facies by typical sedimentary structures they exhibit: i) trough cross-bedded sandstones of variable grain size; and ii) mostly medium- to coarse-grained sandstones (Fig. 6A), locally conglomerates, containing a spectrum of sedimentary structures developed under upper flow regime, such as parallel bedding (Fig. 6B) or backset lamination (Fig. 6A), the latter often developed within erosive-based chute channels (e.g., Massari, 1996, 2017; Fig. 6A). Trough cross-bedded sandstones are subordinate in these facies. In outcrop, both facies show alternation in vertical sections, with variable volume proportion of each of them.

Interpretation: Lithofacies S and/or G are interpreted as being deposited within the delta-front setting (cf. Nádaskay and Uličný 2014), forming foreset strata. Based on typical outcrop-scale depositional features and well-log patterns, two types of foresets are distinguished: low- (L-type) and high-angle (H-type). Trough cross-bedded sandstones are interpreted as deposited by migration of small-scale 3D dunes in a shallow-marine environment with more efficient action of

tidal (Valečka 1979a; Uličný 2001) currents. In case of H-type foresets, sorting processes by tidal currents were not as pronounced and rapid downslope transport of coarse clastic material prevailed. Gravity currents were responsible for downslope transport of large portions of coarse clastics entering the basin during hydrological floods (cf. Mulder et al. 2003).

Lithofacies **Sgf** (gravity-flow, sandstone-dominated) overlies the studied section and reaches ca. 47 m thickness. Most of this interval is only present in correlation cross-sections (Fig. 2) and only the basal part is depicted in stratigraphic section in Fig. 3. The base of the interval in depth 192.8 m is sharp, most likely erosive. Facies Sgf is formed dominantly by sandstone beds (Fig. 6C) few cms up to ca. 2 m thick, commonly separated up to few cm thick layers of argillaceous sandstones to sandy mudstones (Fig. 7A), rarely pure mudstones. Individual sandstone beds are amalgamated, forming continuous sequence resembling 'amalgamated flyschoid facies' sensu Valečka and Rejchrt (1973). In most cases, sandstone beds are sharp- or erosive-based, massive or parallel-bedded, scarcely ripple-bedded. Normal grading from medium sand at the base to fine sand at the top may be present. Frequently, spaced planar lamination (sensu Talling et al. 2012) was observed at the base of beds. Thicker beds (tens of cm) exhibit complex internal arrangement, usually represented by the alternation of massive and laminated parts with indistinct transitions. Coal and mudstone rip-up clasts up to ca. 8 cm large are abundant especially in thicker beds and are frequently concentrated into distinct layers. Sandstone beds show a relatively low rate of biogenic reworking, except for their uppermost parts passing into intensely burrowed mud-rich interbeds.

Interpretation: In accord with Nádaskay and Uličný (2014), lithofacies Sgf is interpreted as bottomsets deposited by gravity flows, fed by material bypassed through and/or redeposited from high-angle foreset slopes. It represents proximal prodelta deposits attached to deep-water deltas, possibly filing scoured basin floor. Large portions of sand were delivered into the prodelta by the action of sustained high-density turbidity currents, hyperpycnal (cf. Mulder and Syvitski 1995) in nature. This assumption is supported by an abundance of terrestrial plant debris (Zavala et al. 2012), abundant diffuse rip-up clast-rich interlayers as well as complex internal structure of some of the sandstone beds, reflecting fluctuating flow behavior within individual hyperpycnal events (cf. Mulder et al. 2003).

Lithofacies **Hgf** (gravity-flow, heterolithic) reaches 11 m thickness (interval 192.8–203.8 m) and is formed by the alternation of gray mudstones/siltstones and pale gray, fine-grained sandstones. Slightly calcareous mudstones to siltstones are identical to those described either as facies Ms or Mm and contain the same variety of bioclasts. Sandstones are mostly fine-grained (Fig. 7B), argillaceous and slightly calcareous, less commonly fine- to medium-grained quartzose

Figure 6. Selected features of deltaic succession in outcrop: the Coniacian Březno Fm. in the northwestern BCB. Photographs by J. Valečka (A) and R. Nádaskay (B, C, D). **(A)** The succession of delta-front deposits formed by the alternation of parallel-bedded foresets and foresets with trough cross-bedding with chute-channels and backset lamination. The visible part of the section is 55 m thick. Such successions in the Sloup and close vicinity are interpreted as deposits of deep-water deltas (Nádaskay and Uličný, 2014). Locality: Svojkov-Dědovy kameny near Nový Bor. **(B)** Detail to parallel-bedded medium- to coarse-grained sandstones. Locality: Prysk-Pustý zámek near Česká Kamenice. **(C)** Foreset strata of an older deltaic body in contact with bottomset strata of the overlying, younger deltaic body. The topmost part foreset strata is formed by sandstone with *Ophiomorpha* burrows, secondary enriched in Fe-hydroxides (note veneers of Fe-hydroxides surrounding the joints), overlain by ca. 0.5 m thick bed of gray argillaceous sandstone with abundant fusain clasts. The bed is truncated at the top and was deposited as horizontal (the apparent dip results from post-depositional tectonic tilting). It is interpreted as a transgressive lag overlain by the MTS at the base of CON 5. **(D)** Detail of the conglomeratic sandstone comprising floating clasts up to 1 cm in diameter (highlighted in circle), interpreted as a transgressive lag covering a transgressive surface. Plane view. Locality: Radvanec-Havraní skály near Nový Bor.

with clay/silt admixture. Both lithological types contain a high amount of fusain fragments (Fig. 7C), often accumulated in laminae. Clastic mica is represented by muscovite, very rarely by biotite (Fig. 7C). Angular to subangular magmatic quartz grains are dominant, while subrounded to rounded, recycled grains are less common. In sandstone beds, bioclasts form up to 3 vol. % (Fig. 3). In the uppermost part of the interval, close to the base of the facies Sgf (depth 192.80 m),

116

Figure 7 (on the opposite page). Lithofacies in core (retrieved from borehole 4650_A). **(A)** Example of alternating quartzose and argillaceous sandstones of the lithofacies Sgf (depth 173.61–173.65 m). Note sharp, erosive or scoured bases of quartzose sandstones. Sandstone bed in the middle part exhibits vertical sequence from structureless fine- to medium-grained quartzose sandstone via parallel-bedded (Pb) sandstone to argillaceous sandstone, representing uppermost part of the section, affected by intense burrowing. Parallel bedding is often highlighted by coalified plant debris or small fusain fragments (Cp). Note the *Thalassinoides* (Th) burrows. **(B)** Example of the sandstone interbeds within the lithofacies Hgf. The interbed is approximately 4 cm thick, formed by fine-grained sandstone with parallel bedding marked by accumulations of fine plat debris. Secondary calcite (Ca) cementation and pyrite (Py) impregnations are well visible. Top of the bed is obscured as a result of intense burrowing. Th – *Thalassinoides* burrows. **(C)** Photomicrograph of the upper part of the sandstone interbed within the lithofacies Hgf (depth 203.15 m). The interbed is formed by fine-grained sandstone with an admixture of clay and silt. Note the accumulation of coalified plant debris (Cp) and mud marking discontinuous laminae. Biotite (Bt) identified in this particular thin section is otherwise relatively rare accessory. No secondary calcification is present. Note the accessory pyrite (Py). **(D)** Photomicrograph of porous, quartzose sandstone forming the main mass of the lithofacies Sgfd (depth 296.5 m). Framework quartz grains are mainly monocrystalline subangular, less commonly angular or rounded. Feldspar grains are found here only as an accessory. Distribution of framework grains is chaotic, without any preferential orientation. Crossed polars. **(E)** Photomicrograph of fine-grained sandstone in the topmost part (depth 294.85 m) of the sandstone interbed labelled as lithofacies Sgfd. In comparison to underlying quartzose sandstone (Fig. 7D) is has an apparently higher admixture of clay, silt, and coalified plant debris (Cp), the latter marking vague laminae of parallel bedding. **(F)** Photomicrograph of siltstone of the lithofacies Ms (depth 288.40 m). The framework of the rock is formed by quartz silt with an admixture of fine sand grains. Matrix principally composes of clay and carbonate micrite mixture with accessory pyrite (Py) and glauconite (G). Small (<0.2 mm) coalified plant debris (Cp) is scattered within the matrix but may be represented by outsize (>1 mm) fragments as well. A brown particle ca. 0.1 mm in diameter is interpreted (cf., Heřmanová and Kvaček 2012; Heřmanová et al. 2016; Břízová and Kvaček, pers. comm.) as a fruit fragment (Fr). **(G)** Photomicrograph of mudstone of the lithofacies Ms (depth 211.78 m). Rock framework composes of quartz silt grains, albeit in a smaller volume than in related siltstones (Fig. 5G) with which they form a continuum. Fine-sand quartz grains up to 0.1 mm in diameter are present as an accessory. Note intense bioturbation (ichnofabric index ~ 5 to 6) affecting the entire volume of the rock. In this particular case, burrows are filled with darker fine material, mostly clay, and are depleted in coarser (silt- and sand-grained) component that forms a surrounding matrix. Such structures were macroscopically identified as Chondrites isp. (Ch), even though they do not clearly show distinctive branching of individual burrows. **(H)** Photomicrograph of mudstone of the lithofacies Ms (depth 235.25 m). Calcareous mudstone with fine sand admixture. Note the fine-sand quartz grains (Qz), fine-grained coalified plant debris (Cp) and sparse glauconite (G) grains. **(I)** Photomicrograph of mudstone of the lithofacies Mm(depth 256.88 m). Quartz silt grains (Qz) up to 0.1 mm are typically monocrystalline, less rounded to angular, and form ca. 15% of the rock volume. The mudstone is heavily impregnated by pyrite (Py) that is present as fine-graines framboids scattered in the rock matrix or fill the voids in bioclasts. In general, foraminifers (Fm) form up to 80% of determinable bioclasts. Coalified plant debris is much less abundant than in the lithofacies Ms and forms up to ca. 3% (not present in the photograph). **(J)** Photomicrograph of claystone (with calcareous admixture) of the lithofacies Mm (353.00 m), the finest lithology present in the studied section. Note whitish terrigenous quartz silt grains (Qz), forming an accessory component. A darker shade of the rock results from elevated content of fine-grained organic carbon scattered in the matrix.
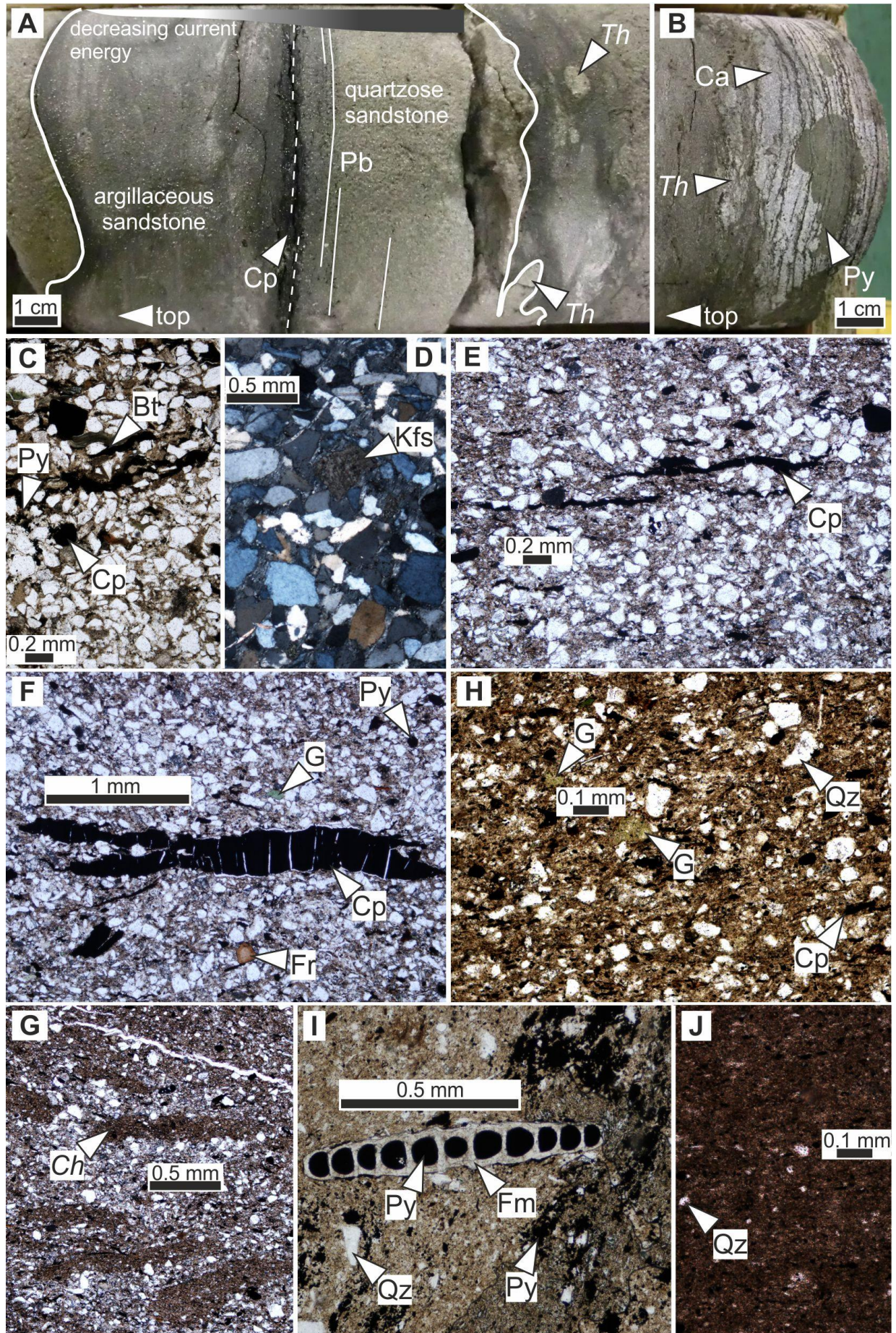
accessory green to brown glauconite grains are present. Sandstones form 2–25 cm thick beds, like those of facies Sgf, arranged into two amalgamated bedsets. In most cases, sandstones are sharp-based, massive or parallel-bedded or normalgraded. Most of the sandstone beds are pervasively burrowed exhibiting highest ichnofabric index (sensu Taylor and Goldring 1993) in their topmost parts, where may be completely bioturbated. Calcite cementation (Fig. 7B) that may preserve primary lamination, is present in some beds, rarely accompanied by finegrained pyrite impregnations.

Interpretation: Lithofacies Hgr is genetically related to facies Sgf, both forming a spatial continuum within the prodelta of gilbert-type ('deep-water') delta bodies. The depositional process involves an action of low-density turbidity currents that were initiated as hyperpycnal currents gradually penetrating into muddominated offshore. Volumetric dominance of mudstones over sandstones in the facies is interpreted as an effect of current deceleration over the distance from main loci of bottomset deposition represented by facies Sgf.

In core, lithofacies **Sgfd** (gravity-flow, sandstone-dominated, 'detached') is formed by a single, ca. 2 m thick (interval 294.7–296.9 m) fining-upward sandstone interbed with no internal boundaries. Its base is erosive, sharply overlying the sequence of calcareous siltstones. At the base, the bed is formed by massive, well-sorted fine- to medium-grained sandstone (Fig. 7D) passing upwards into fine-grained sandstone. Quartz grains form approximately 85 vol. % (Fig. 3). Bioclasts of the same type as in the facies Ms and Mm are present in accessory amount. Increasing content of clay, silt and fusain fragments (Fig. 7E), as well as presence of burrows (possibly *Planolites* or *Thalassinoides*), is evident in the top of the bed. In the topmost part, vague parallel bedding has been preserved. According to well-log pattern (Fig. 4) facies, Sgfd might be formed by amalgamated sandstone beds. Lithofacies Sgfd share similar features with both facies Sgf (higher thickness of individual beds, an amalgamation of sandstone beds) and Hgf (ambience of mudstones in vertical succession).

Interpretation: Lithofacies Sgfd represent a special feature of the depositional system not previously described in detail, although mentioned as possible 'turbidites' by Uličný et al. (2015). By internal arrangement as well as depositional process, it is related to both facies Sgf and Hgf. It is interpreted as deposited by gravity currents penetrating into otherwise low-energy, mudstone-dominated offshore. Following the tentative interpretation of Uličný et al. (2015), it is assumed that lithofacies Sgfd represents a submarine turbidite lobe.

Lithofacies **Ms** forms together with lithofacies Mm the vast majority of the studied core section. It comprises gray calcareous siltstones with locally elevated fine sand admixture, forming a noncyclic continuum with less silty/sandy facies Mm; the vertical transition between both is smooth and boundaries are indistinct. In a few cases, gradually increasing fine sand content

reflects the lateral transition of lithofacies Ms into facies Hgf. The most substantial difference to the facies Mm is an elevated content of terrigenous quartz grains (Fig. 7F, G), both silt- a fine sand-sized (average size 0.6 mm), forming 25–40 vol. %. $CaCO_3$ content varies between ca. 7 and 17 wt. % (Fig. 3) and is attributed to either carbonate mud, forming rock matrix together with siliclastic clay-size particles, or bioclasts (up to 8 vol. %). Macroscopic bioclasts are represented mostly by small shell debris while the microscopic fraction is represented by foraminifers and calcareous nannofossils. In one particular case, shell fragments are concentrated in ca. 5 mm thick sharp-based clast-supported layer resembling coquina. Plant debris (phytoclasts) and small fusain fragments up to 1 mm, rarely few mm (Fig. 7F) in size, are very abundant. Accessory feldspars, micas, and glauconite (Fig. 7F) are present. Primary horizontal bedding marked with fusain and plant debris is sparsely preserved. Most of the lithofacies Ms in the studied section is, however, intensely burrowed (Fig. 7G), reaching ichnofabric index 5–6. Ichnotaxa *Chondrites* and *Trichichnus* are the most common.

Interpretation: Lithofacies Ms was deposited in a low-energy offshore environment below the storm wave base. The elevated admixture of terrigenous material (framework silt/fine sand, plant debris) and abundant shell fragments indicate the action of hyperpycnal currents, primarily depositing facies Sgf and Hgf. It is assumed that lithofacies Ms was deposited from finest suspended load carried by hyperpycnal currents, representing their most distal expression.

Lithofacies **Mm** is the finest and volumetrically dominating lithofacies within the studied section (Fig. 3). It interfingers with facies Ms and its thickness increases basinward in correlated boreholes (Fig. 2). It is formed by gray claystones, predominantly calcareous, with non-calcareous occupying solely the lowermost part of the section above the top of the uppermost Turonian–lowermost Coniacian sandstones. Due to locally elevated $CaCO_3$ content (ca. 5–25 wt. %, Fig. 3), they appear massive, while in other parts of the section are fissile due to relatively low carbonate and presumably slightly elevated clay mineral content. Accessory glauconite is present; in places, grains up to 1 mm are scattered in the matrix and the only macroscopically obvious accumulation marks the base of the Coniacian sequence. Feldspars and micas (predominantly muscovite) are accessories; however, the amount of micas may exceed 1 vol. % as plenty of small fibrous fragments are of submicroscopic size. The facies is abundant in small carbonate shell debris (diverse bivalves, inoceramid prismatic layers, rarely ammonites) either scattered in the matrix or quasi-concentrated into indistinct accumulations. Shell fragments larger than 1–2 cm are scarce. Among bivalves, deposit feeders of *Nucula-Nuculana* assemblage dominate. Plant debris as well as small fusain fragments up to 1 mm large form 1–3 vol. %. Primary bedding is virtually missing because of intense biogenic reworking. Ichnotaxa *Chondrites* and *Trichichnus* are the most common;

Figure 8 (on the opposite page). Selected specimens of stratigraphically important inoceramid species. "CGS SC" refers to the signature of the Collections Department of the Czech Geological Survey, Prague. Scale bar equals 10 mm. (**A, B, E, F**) *Inoceramus frechi* Flegel, uppermost lower to middle Coniacian, I. frechi/I. gibbosus Zone. A e right valve, CGS SC20, borehole 4650_A Skalice, depth 302.5 m. B e left valve, CGS SC21, borehole 4650_A Skalice, depth 303.2 m. E   left valve, CGC SC40, borehole Vf-1 Volfartice, depth 393.5 m. F e left valve, CGS SC58, borehole J-360548 Žandov, depth 444.6 m. (**C, D**) *Cremnoceramus waltersdorfensis hannovrensis* (Heinz), lower Coniacian, *C. w. hannovrensis* Zone. C – left valve, CGS SC22, borehole 4650_A Skalice, depth 350.4 m. D – right valve, CGS SC23, borehole 4650_A Skalice, depth 347.25 m. (**G, O**) *Platyceramus mantelli* (Mercey), middle Coniacian, *V. koeneni* Zone. G – apical part of the right valve, CGS SC24, borehole 4650_A Skalice, depth 205.8 m. O – left valve. CGS SC35, loc. Robeč near Česká Lípa. (**H**) *Cremnoceramus deformis erectus* (Meek), right valve, CGS SC 73, borehole KHV-1t Kytlice, depth 167.3 m, lower Coniacian, *C. d. erectus* Zone. (**I**) *Didymotis costatus* (Frič), left valve, CGS SC43, borehole J-218465 Brniště, depth 176.8 m, uppermost Turonian, *Mytiloides scupini* Zone (acme with *M. herbichi* Atabekjan). (**J**) *Didymotis* sp., right valve, CGS SC25, borehole 4650_A Skalice, depth 363.0 m, lower Coniacian, *C. d. erectus* Zone. (**K, L**) *Cremnoceramus waltersdorfensis waltersdorfensis* (Andert), lower Coniacian, *C. d. erectus* Zone. K – left valve, CGS SC 44, borehole J-218465 Brniště, depth 167.5 m. L – right valve, CGS SC26, borehole 4650_A Skalice, depth 360.75 m. (**M, N**) *Cremnoceramus crassus crassus* (Petrascheck), lower Coniacian, *C. c. crassus* Zone. M – right valve, CGS SC38, borehole J-343402 Markvartice, depth 253.85 m. N – right valve, CGS SC 27, borehole 4650_A Skalice, depth 328.6 m.

the latter is less abundant than in the facies Ms. At the base, Planolites burrows filled with sand from underlying Turonian strata were identified.

Interpretation: Lithofacies Mm occupied a part of offshore realm relatively the most distal to contemporary shoreline and was deposited under low-energy conditions below the storm wave base. A depositional mechanism was the same as in lithofacies Ms, although, in addition, substantial contribution of overflow suspension plumes is expected. Lithofacies Mm corresponds to facies Mc ("calcareous mudstone") sensu Laurin and Uličný (2004), i.e., low-carbonate (<30 wt. % CaCO3), low-silt/sand (1–5 vol. %), kaolinite-dominated facies natural to the hemipelagic setting.

Paleontology

Macrofauna

In the borehole 4650_A (Fig. 3) the molluscan macrofauna (especially inoceramids and ammonites) were found only in mudstone-dominated lithofacies (Mm, Ms) of the Teplice and Březno formations. An incomplete internal mold of *Cremnoceramus deformis erectus* (Meek 1877) was found in the siltstones of the Teplice Formation (sequence CON 1) at depth 362.57 m and near (depth 363.0 m) also a fragment of the bivalve *Didymotis* sp. (Fig. 8J). Few specimens of *C. waltersdorfensis waltersdorfensis* (Andert 1911) were collected at the depth 360.75 (Fig. 8L) and 362.5 m. Common occurrences of inoceramid *C. waltersdorfensis hannovrensis* (Heinz 1932) were observed in claystones and mudstones of the Teplice Formation in depth interval 347.25–359.4 m
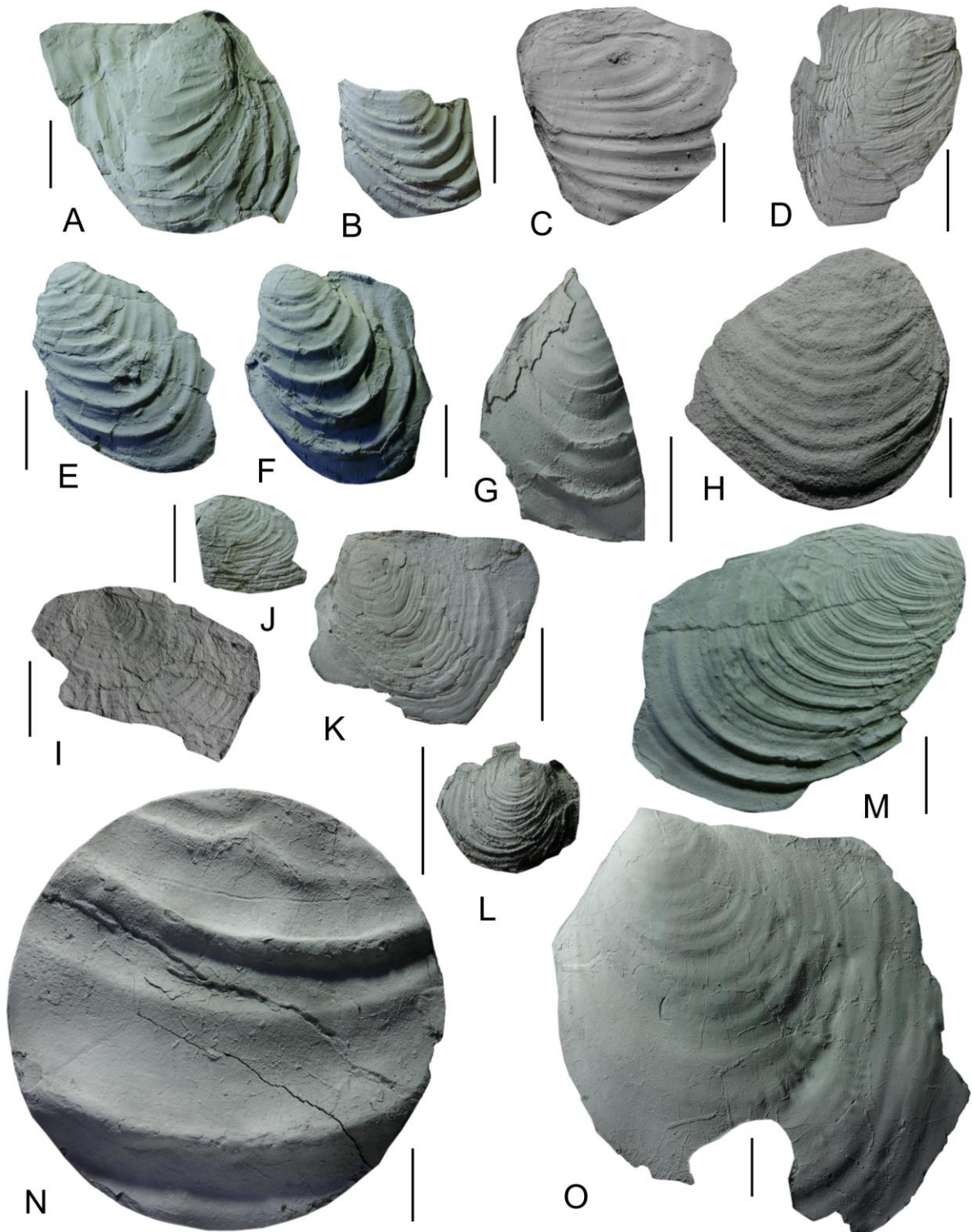
(Fig. 8C, D). Mudstones and siltstones with common *Chondrites* burrows (corresponding to Rohatce Mb.) yielded large specimens of *C. crassus crassus* (Petrascheck 1903) within depth interval 321.1–338.75 m (Fig. 8N). One specimen of *C. c. deformis* (Meek 1871) was identified at the depth 324.5 m. *Inoceramus frechi* (Flegel 1904) is abundant in mudstones of Březno Formation within depth interval 302.5–324.4 m (Fig. 8A, B), just above occurrences of C. c. crassus. Overlying mudstones of Březno Formation up to 253 m were barren of inoceramids. Findings of fragments

of volviceramids were recognized at depths 238.3–252.8 m. First specimens of *Platyceramus mantelli* (Mercey 1872) were found in the upper part of the Březno Formation mudstones at depth 205.8 m and 209 m (Fig. 8G). In the neighbouring boreholes and outcrops volviceramids and platyceramids (Fig. 8O) are usually associated with horizons of pelosiderite nodules in the Březno Formation (Fig. 2A). In the upper part of Březno Formation, ammonites *Peroniceras tridorsatum* (Schlüter 1877) were recognized at depth 205.15 and 230.27 m.

Calcareous nannofossils

Smear slides provided mostly poor spectrum of nannofossils (1–9 specimens per 10 fields of view of the microscope). Non-nannofossil sediment was the major component forming >90% volume of samples. Nannofossil preservation was influenced by strong carbonate dissolution especially in the upper part of the section. Central fields of placoliths are etched and outer rims are present mostly in fragments. This phenomenon makes species identification difficult. Less damaged are those nannofossils that are more resistant to dissolution, such as Polycyclolithaceae and genera *Watznaueria*, *Zygrhablitus*, and *Gartnerago* (Fig. 9I, P). Marker species *Micula staurophora*, and also *M. adumbrata*, transitional forms *Quadrum-Micula* and *Uniplanarius gothicus* (Fig. 9K–N) occur irregularly and in low numbers. Representatives of genus *Lucianorhabdus* were present only in a handful of samples. Apical parts of these holococcolits, which are species diagnostic, were not preserved (Fig. 9Q). A total monotonous poor fossil record is interrupted several times by horizons where nannofossils or their fragments form 70–90% of components (217.00 m, 307.02 m, 312.02 m, 342.05 m, and the interval of 352.0–362.05 m). The quantitative enrichment of the otherwise dissolution sensitive taxa is here significant. They are *Sollasites horticus*, *Biscutum* div. sp., *Repagalum* sp. and Stephanolithiaceae, delicate coccoliths with bars in the central area (Fig. 9A, B, CA–B, DA–B). These nannofossil enrichments well reflect the change in lithology as a result of variations of siliciclastic supply. A slight quantitative increase in *Marthasterites furcatus* (Fig. 9TA–B) was observed from the base of the section up to 327.0 m. *Braarudosphaera bigelowii* and calcispheres *Thoracosphaera* sp. appear irregularly. Samples ranging from 134.15 to 192.81 m and from the depth of 242.15 m were barren of calcareous nannofossils. At depths of 252.00 m, 261.98 a 267.00 m, nannofossils redeposited from the older Turonian strata were rarely found (e.g. *Eprolithus octopetalus*, *E. moratus*, and *Helenea chiastia*) – see Fig. 9U, V.

Major and trace element geochemistry

Trace element analyses of 9 representative bulk rock samples are summarized in Table 1. All samples (except sample 366.85) are homogeneous in trace element composition. Sample 366.85 (siltstone with sand admixture) is characterized by elevated Cr (110 ppm) and Zr
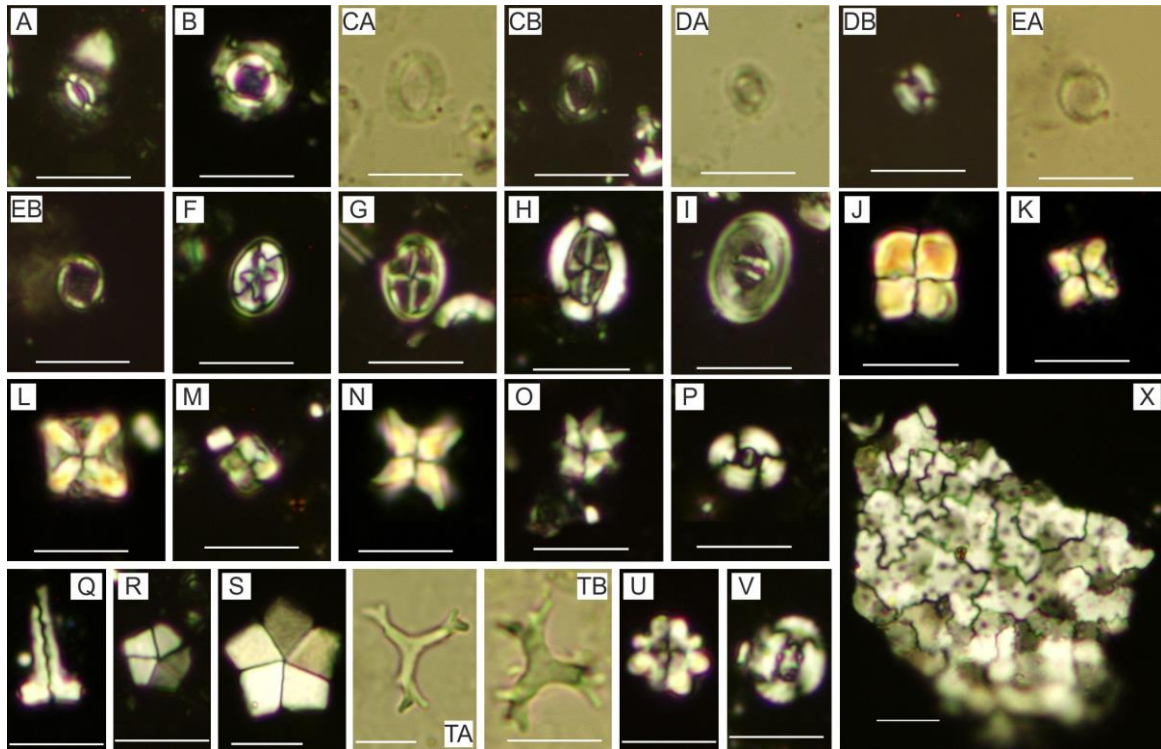
Figure 9. Photomicrographs of calcareous nannofossils mentioned in the text. A detailed description of individual species and their stratigraphic and ecological significance is in chapter 4.2.2. Cross-polarized light (except figs. 3, 5, 7, 23 and 24). All the samples retrieved from the borehole 4650_A Skalice. Scale bars = 5 mm. **(A)** *Biscutum ellipticum*, 237.05 m. **(B)** Stephanolithiaceae, *Cylindralithus biarcus*, 312.02 m. **(CA, CB)** *Sollasites horticus*, 252.00 m. **(DA, DB)** *Repagalum parvidentatum*, 317.00 m. (**EA, EB)** *Cribrosphaerella circula*, 217.00 m. **(F)** *Eiffellithus nudus*, 327.09 m. **(G)** *Staurolithites imbricatus*, 230.63 m. **(H)** *Broinsonia parca expansa*, 332.00 m. **(I)** Zeugrhabdotus biperforatus, 307.02 m. **(J)** *Quadrum gartneri*, 342.05 m. **(K)** *Quadrum-Micula*, 332.00 m. **(L)** *Micula staurophora*, 312.02 m. **(M)** *Micula adumbrata*, 307.02 m. **(N)** *Uniplanarius gothicus*, 327,00 m; **(O)** *Lithastrinus septenarius*, 208.00 m. **(P)** *Watznaueria britannica*, 342.00 m. **(Q)** *Lucianorhabdus* cf. *quadrifidus*, 342.00 m. **(R)** *Braarudosphaera bigelowii parvula*, 307.02 m. **(S)** *Braarudosphaera bigelowii bigelowii*, 277.00 m. **(TA, TB)** *Marthasterites furcatus*, 312.02 m and 317.00 m. **(U)** *Eprolithus octopetalus*, 297.00 m, reworked specimen from the older Turonian strata. **(V)** *Helenea chiastia*, 252.00 m, reworked specimen from the older Turonian strata. **(X)** *Thoracosphaera operculata*, 208.00 m.

(261 ppm) and low Sr (89 ppm) composition. Most of the samples have Rb/Sr ratios between ~0.3 and 0.6. Sample 366.85 has Rb/Sr ~1.7.

In the siliciclastic samples, Si, Ti, and Zr are usually slightly covariant with Ca as an effect of carbonate dilution (constant sum effect, cf. Jarvis et al. 2001). If normalized to Al, the ratios provide valuable information on mineralogical variations in the siliciclastic fraction. Zircon tends to be concentrated in coarse grained fraction; the Zr/Al ratio is thus a grain-size proxy and can be used for approximation of distance to siliciclastic source area (e.g., Kumpan et al. 2015). Accordingly, it may also reflect increased siliciclastic input to the distal parts of the basin (Rachold and Brumsack 2001; Sageman and Lyons 2005). Increased Ti/Al ratio in fine-grained deep-sea deposits correlates with increased current energy and detrital supply, especially when no

input of mafic volcanogenic material is involved (Schmitz 1987; Zabel et al. 1999). In mudrocks, element concentrations may be governed by different factors, including sediment source, provenance, solubility, weathering, grain size and hydrodynamic sorting, oxygen availability, biogenic reworking and diagenesis (Spencer et al. 1967; Wintsch and Kvale 1994; Young and Nesbitt 1998).

Based on the different proportion of diagnostic elements and characteristic trends of element-ratio curves, three lithologic types have been distinguished within the studied section: i) sandstones or quartzose sandstones; ii) mudstones (with elevated silt/fine sand content) to siltstones; iii) silicified mudstones. Sandstones to quartzose sandstones belong to the nearshore lithofacies Sfms (bed 1a in Fig. 10) or distal lithofacies Sgf (1f), Hgf (1c–e) and Sgfd (1b). Generally, these sandstones are characterized by elevated (>7) Si/Al ratio and low gamma-ray values, reflecting low clay content and good sorting. Extremely low Zr/Al and Ti/Al ratio in the facies Sfms compared to Hgf and Sgfd indicate that Zr-bearing (heavy) minerals (chiefly zircons) are concentrated in relatively finer, less sorted and rapidly deposited sandstone beds. On the contrary, lower Ti/Al ratio of all the sandstone facies, in comparison to ambient mudstones, point to possible winnowing of very fine-grained Ti-bearing phases. Mudstones with elevated silt and fine sand content to siltstones (beds 2a–i) are distinguishable by a typical serrated pattern of Zr/Al and Ti/Al curves (between ca. 205–290 m) where maxima represent individual laminae with coarser siliciclastic admixture. Elevated values of both Zr and Ti are interpreted as evidence of coarser siliciclastic admixture in shales, whereas silt fractions are commonly enriched in Zr and Ti (e.g., Fralick and Kronberg 1997). The 'type 2' beds also display relatively high gamma-ray values, reflecting low clay content, and usually exhibit local maxima in the neutron log that points to their relatively higher porosity compared to surrounding calcareous mudstones/claystones ('type 4'). The latter is typical for very low Ti/Al (~0.5e0.8) and Zr/Al (~0.03–0.04) ratios as well as relatively monotonous curves of both ratios. However, both ratios show slightly increased trends in comparison to offshore shales analyzed by e.g., Hild and Brumsack (1998) and Rachold and Brumsack (2001) as well as to the average shale (Wedepohl 1971). They also exhibit maxima of gamma-ray log and respective minima of neutron-log, indicating low porosity induced by more efficient compaction of clay-sized particles. The Si/Al maxima (up to ~6–7 within 'type 2' beds) reflect mainly a primary terrestrial input. Olde et al. (2015) attributed the increase of Si (silt/fine sand) with decrease of Al (clay) contents in the hemipelagic sediments of the BCB to periods of regression, and higher Al values with transgression, as a result of proximity-controlled grain-size effects. This is also evidenced by analogous patterns of other proxies for siliciclastic input, i.e., Ti/Al and Zr/Al (cf. Uličný et al. 2014), with an exception of 'type 3' beds. These are formed by calcareous mudstones that are partially affected by scattered, submicroscopic silicification
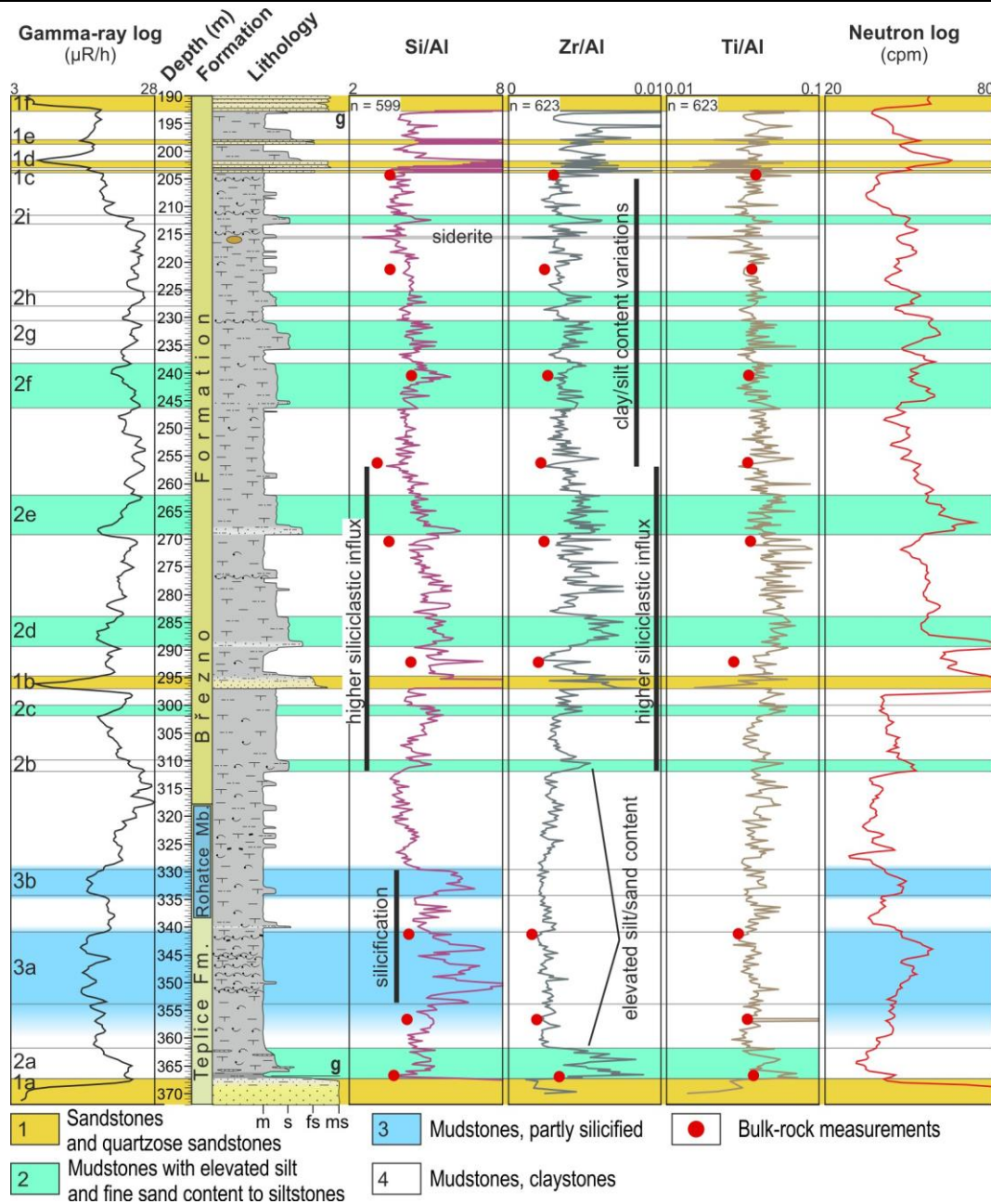
Figure 10. Chart showing an interpretation of individual conspicuous maxima and minima of selected element-ratio curves and their correlation to gamma-ray and neutron (porosity) log.

(e.g. Fig. 11E) that is relatively subtle, but well definable by serrated pattern and conspicuousmaxima of Si/Al curve between ca. 320 and 355 m. Similar Si/Al peak in borehole Bch-1 (Uličný et al. 2014) at the base of CON 2 sequence reflects more intense or complete diagenetic silicification at the level where Rohatce Mb. occur.

Isotope geochemistry

For stable carbon and oxygen isotopes, fifteen samples were analysed; out of them, fourteen were represented by calcareous shell fragments and one by homogenized bulk-rock carbonate. Because of low sampling density, i.e., one sample per 12.5 m of drill core, $\delta^{13}C_{carb}$ and

$\delta^{18}O$ curves (Fig. 12A) are not suitable for interpreting stratigraphic trends. Following three samples within lower Coniacian revealed reliable positive values of $\delta^{13}C_{carb}$: at 205.61 (3.32‰), 230.8 (2.9‰) and 328.6 m (3.04‰). Other samples fall within the range of –2.62–1.38‰. A decrease of primary $\delta^{13}C$ record of marine carbonate rocks (i.e., below 1 and towards negative values) and $\delta^{13}C_{carb}$ values of several samples (Fig. 12A) is considered as indicator of their postdepositional/diagenetic modification (see discussion in 5.2).

The $^{87}Sr/^{86}Sr$ isotopic data obtained for 24 carbonate samples vary in a wide range between 0.7073 and 0.7082. For most samples the Rb/Sr ratio is at or below 0.01, making the radiogenic ^{87}Sr contribution comparable to analytical uncertainty or even negligible. This is also true for all samples with Rb content below the detection limit. Samples 205.61 and 344.25 have elevated Rb contents and the correction for radiogenic ingrowth of ^{87}Sr is an order or two higher than the $^{87}Sr/^{86}Sr$ measurement error. The range of Sr isotopic ratio corrected to the presumed age of 88 Ma shifts thus to 0.7069–0.7082.

Available trace elements compositions for carbonate leachates vary in wide range, as illustrated by Table 1. Compared to larger fossils preserved under favorable conditions (McArthur et al. 2000; Frijia et al. 2015; Boix et al. 2011), the overall content of Fe is much higher in most cases, as well as Rb and Sr in some cases. Remarkable is sample 205.61 with anomalously elevated content of Fe, Mg, Na, and Rb. With this sample omitted, there is a hint of correlation of Fe with Mn, Mg with Rb and Sr with Na. On the other hand, Na weakly negatively correlates with the Fe, Mn and Rb while Mg tends to negatively correlate with Sr. If individual samples are clustered according to trace elements, a group with low Mg/Sr, Rb/Sr, Fe/Na, Mn/Na and Fe/Mn can be identified (246.37, 301.88, 319.95, 328.6, 338.58).

Five randomly selected samples of silicate residuum remaining after sample acid leaching were analyzed for $^{87}Sr/^{86}Sr$ as well. Unlike in the carbonate, the range 0.7190–0.7212 is surprisingly narrow. The trace element data for the silicate residuum samples are not available, thus it is not possible to calculate the initial $^{87}Sr/^{86}Sr$ ratio. However, chemistry of the clastic admixture represents averaged composition of a wide source area and thus the Rb/Sr ratio can be roughly estimated. Taylor and McLennan (1995) present for global upper crust average the Rb/Sr value 0.32. This would lead to the $^{87}Sr/^{86}Sr$ ratio ingrowth of ~0.0010 over 88 Ma. The initial $^{87}Sr/^{86}Sr$ composition of the silicate fraction would thus be 0.7180–0.7202. A pessimistic guess of Rb/Sr = 1.5, which can be considered as an upper limit for most siliciclastic rocks, would lead to the initial ratio in the range 0.7140–0.7162 (0.0050 ingrowth). Such value can be considered as lower limit to the initial $^{87}Sr/^{86}Sr$ ratio of the sediment siliciclastic admixture.

Genetic sequence	Sample No.	Sample type	^{87}Sr/^{86}Sr	2SM	δ^{13}C$_{carb}$ ‰ PDB	δ^{18}O ‰ PDB	Fe ppm	Mg ppm	Mn ppm	Na ppm	Rb ppm	Sr ppm	Mg/Sr	Fe/Mn
Březno Formation														
CON 4	195.25	bivalve *Venus* sp.	0.708271	10	-0.58	-7.61								
	195.25	silicate residuum	0.718996	13	–	–								
CON 4	205.61	ammonite	0.707793	15	3.32	-1.56	123442	16409	590	3967	131	2951	5.6	209
CON 4	208.5	inoceramid (prismatic layer)	0.707476	10	–	–								
CON 4	214.78	coquina (fragmented bivalves/ gastropods)	0.707691	9	-2.62	-9.7	30509	2774	803	94	11.1	967	2.9	38
CON 4	230.8	bivalve	0.707776	9	2.9	-3.75	26228	2950	423	355	3.4	2393	1.2	62
		silicate residuum	0.719919	11	–	–								
CON 4	246.37	bivalve 1	0.707391	9	1.38	-2.02	16627	529	67	791	4.8	15852	0.03	31
		bivalve 2	0.707697	10	–	–								
CON 4	255.32	bivalve	0.707512	9	0.29	-4.75								
CON 4	261.51	gastropod	0.707974	7	–	–								
CON 4	261.51	inoceramid (prismatic layer)	0.707505	9	–	–	10401	1765	422	195	-	1590	1.1	25
CON 4	276.75	bivalve	0.708202	9	-0.65	-5.56								
CON 4	276.75	silicate residuum	0.720007	9	–	–								
CON 3	290.35	gastropod?	0.708235	10	0.58	-7.48	31651	4243	321	963	11.5	1770	2.4	99
CON 3	290.35	silicate residuum	0.719365	7	–	–								
CON 3	296.24	non-leached bulk rock (qtz. sandstone)	0.721195	15	–	–								
CON 3	301.88	inoceramid	0.707384	10	–	–	1025	3258	54	2305	-	1820	1.8	19
CON 3	305.22	bivalve *Nuculana semilunaris*	0.707849	9	0.87	-4.41	38049	5723	268	450	9.6	1803	3.2	142
CON 3	316.5	bivalve *?Nuculana*	0.707811	9	-1.12	-7.84								
CON 3	319.95	bivalve	0.707407	11	–	–	2108	373	20	1397	-	6131	0.1	104
Rohatce Member														
CON 2	323.08	gastropod *Aporrhais megaloptera* or *stenoptera*	0.707406	7	–	–								
CON 2	328.6	inoceramid	0.707353	10	3.04	-2.79	1407	2488	57	1323	0.91	9213	0.3	25
CON 2	330	*Amphisbaena* tube	0.707397	10	–	–	61002	3904	261	732	-	4016	1.0	233
CON 2	338.58	gastropod *Turbo*	0.707611	9	–	–	8767	659	142	965	-	3902	0.2	62
Teplice Formation														
CON 1	344.25	bivalve *Cuspidaria* sp.	0.707833	10	1.38	-4.73	15801	4583	160	320	96.2	393	12	99
CON 1	353.2	bivalve	0.708052	8	1.18	-3.42	21726	3105	108	216	-	1131	2.7	201
CON 1	361.2	inoceramid (prismatic layer)	0.707926	10	1.11	-3.86	16716	4162	151	242	34	5082	0.8	111
CON 1	361.5	leached bulk rock (siltstone)	0.70811	9	1.39	-4.54								

Discussion

Biostratigraphic constraints

Six inoceramid zones sensu Walaszczyk and Wood (1998, 2018) were distinguished in the mudrock-dominated facies (Ms, Mm) of the Teplice and Březno formations (Fig. 3; sorted ascending by stratigraphic position):

1)   *Cremnoceramus deformis erectus* Interval Zone: although the occurrence of the *C. d. erectus* together with *C. w. waltersdorfensis* and with bivalve of the genus *Didymotis* indicate presence of this zone, the FO of *Cremnoceramus d. erectus* (a marker species for the base of the Coniacian), as well as underlying *Cremnoceramus waltersdorfensis waltersdorfensis* Interval Zone, is probably hidden in the glauconitic layer (interpreted as MTS) of the mudstone sequence in the borehole 4650_A Skalice. Similar situation can be observed in the neighboring boreholes, e.g., Vf-1 Volfartice (Čech et al. 1987), 480751 Chotovice, J-218465 Brniště and KHV-1t Kytlice (Čech, unpublished data; Fig. 2, Fig. 8H, I, K). Presence of nannofossil species *Broinsonia parca expansa* and *Lithastrinus septenarius* (Fig. 9H, O) in the lowermost part of the section indicates the UC9c zone that spans the Turonian–Coniacian boundary interval and lower Coniacian (Lees 2008). At the depth of 365.0 m and in the overlying strata were recorded scarce specimens of *Eiffellithus nudus* (Fig. 9F), the FO of which mentioned Shamrock and Watkins (2009) in the Coniacian.

2)   *Cremnoceramus waltersdorfensis hannovrensis* Interval Zone: base of the zone is defined by the FO of index taxa at depth 359.4 m and top of the zone is placed probably at the depth 347.25 m.

3)   *Cremnoceramus crassus inconstans* Interval Zone: no specimen of *C.c. inconstans* was found in the core material of the 4650_A borehole. Therefore, the zone is here interpreted by the LO of the *C. w. hannovrensis* and by the FO of *C.c. crassus*. In this interval, specimens of transitional forms *Quadrum-Micula* are observed at the depth of 342.05 m. The presence of the *C.c. inconstans* Zone is documented below the *C.c.crassus* Zone in the borehole KP-1 Křížový Buk (Čech, unpublished data) and elsewhere in the BCB (e.g., Čech and Švábenická 1992).

4)   *Cremnoceramus crassus crassus* Interval Zone: This zone is characterized by the appearance of large specimens of the index taxa from depth 338.75–321.1 m (Fig. 8N). Inoceramids of this zone are abundant also in the neighboring boreholes (Fig. 8M). In physical terms, the range of the *C. c. crassus* coincides with the extent of the Rohatce Member – a regionally important lithostratigraphic marker unit. At the depth of 327.0 m, the top of the interval with common *Marthasterites furcatus* was determined.

5)   *Inoceramus frechi/Inoceramus gibbosus* Interval Zone: The zone was defined by Walaszczyk and Wood (in Niebuhr et al. 1999) and Walaszczyk and Wood (2018) by the FO of *Inoceramus gibbosus* Schlüter 1877. This species is in the BCB very rare but co-occurs with more frequent species of *gibbosus* Interval Zone which is defined by the first occurrence of any of index taxa
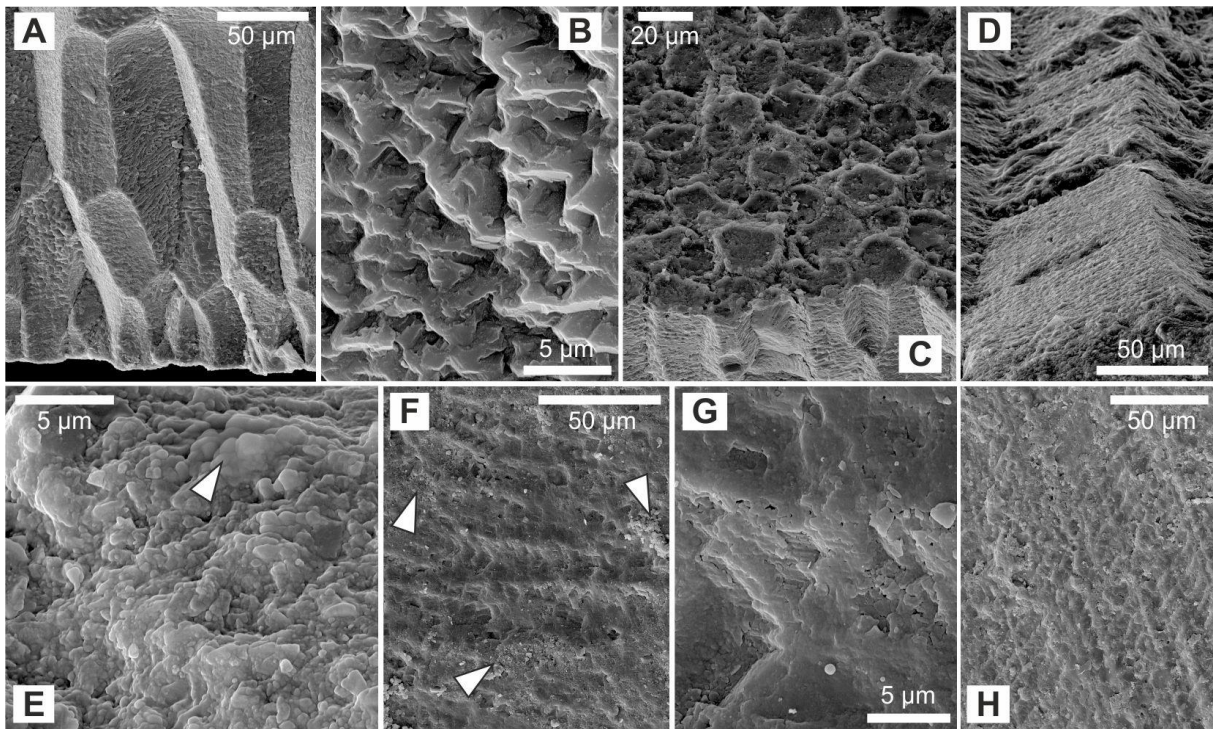
Figure 11. Selected SEM photomicrographs of analyzed shell fragments: **(A)** The prismatic layer of an undetermined inoceramid (depth 328.6 m). **(B)** Close-up view of the inoceramid prismatic layer from the Fig. 9A. Note the slightly corroded surface of the prismatic calcite crystal. **(C)** External surface of the prismatic layer from the previous sample. **(D)** Another fragment of inoceramid from the sample 328.6 m. Minor indurations on the prismatic calcite crystal are possibly relics of undissolved ambient rock (mudstone). **(E)** Close-up view of the calcite prism depicted in Fig. 9D. Arrow points to a very small (ca 5 mm) SiO_2 aggregate possibly formed by secondary silicification. **(F)** Sample 208.5 m, view to an outer surface of an undetermined bivalve shell affected by corrosion of the topmost layer of calcite crystals. All three arrows indicate particles interpreted as various insoluble minerals (e.g., clay minerals, pyrite); G. The latter sample, close-up view showing corroded and partially fused and micritized surface (cf. Frijia et al. 2015). **(H)** Sample 214.78 m (coquina), view to outer surface of an undetermined bivalve shell unaffected by corrosion.

and the first occurrence of *Volviceramus* sp. and/or *Platyceramus mantelli*. In the borehole 4650_A Skalice *I. frechi* appears at the depth 324.4 m and overlaps the upper limit of the range of the *C. c. crassus*. This species is traced up-section to the depth 302.5 m (Fig. 8A). The FO of *Micula staurophora*, marking the base of the UC10 zone was found in 312.2 m. Burnett (1998) correlates this event with the base of the middle Coniacian. *M. staurophora* does not occur continuously in poorly preserved and secondary depleted assemblages up to 237.0 m. Above the latter depth, it occurs regularly. Together with the FO of *M. staurophora* scarce specimens of *Cribrosphaerella circula* were recorded as well.

Formerly, *Inoceramus frechi* was described from the BCB as *Inoceramus kleini* Müller 1888 from surface outcrops (Andert 1911, 1934; Čech and Švábenická 1992). Specimens found in borehole 4650_A as well as in outcrops by Čech and Švábenická (2017) correspond to the neotype of *Inoceramus frechi* Flegel 1904 figured by Walaszczyk and Tröger (1996) from Czaple (Hockenau; late lower to early middle Coniacian). In comparison, *I. kleini* is more inflated with small auricle.

6)   *Volviceramus koeneni* Interval Zone: the zone was recognized in the borehole 4650_A in depth between 252.8 m and 205.8 m where the assemblage of *Volviceramids* and *Platyceramids* together with ammonites of *Peroniceras tridorsatum* was found. Due to lack of inoceramids between depth 253–302.5 m, the base of the *Volviceramus koeneni* Interval Zone cannot be defined. Second International Symposium on Cretaceous Stage Boundaries held in Brussels in 1995 (Kauffman et al. 1996) approved the first occurrence of the inoceramid genus *Volviceramus* (*V. koeneni*) as the criterion for defining the lower/middle Coniacian Substage Boundary. In the borehole 4650_A the FO of *V. koeneni* falls to the barren interval. Recently, Čech and Švábenická (2017) proposed the FO *Inoceramus frechi*/*I. gibbosus* and the FO *Micula staurophora* as markers for the base of the middle Coniacian.

The occurrence of Broinsonia parca expansa and *Lithastrinus septenarius* (Fig. 9H, O) in the lowermost part of the section indicates the UC9c zone that spans the Turonian–Coniacian boundary interval and lower Coniacian (Lees 2008). It is accompanied by Eiffellithus nudus (Fig. 9F), the FO of which is mentioned from the Coniacian (Shamrock and Watkins 2009). The overlying strata provide scarce specimens of *Quadrum-Micula* and *Micula adumbrata*. The top of the horizon with relatively common *M. furcatus* was recorded in 327.0m. The FO of *Micula staurophora*, marking the base of the UC10 zone was found at 312.2 m. It can be correlated with the uppermost part of the lower Coniacian (Kędzierski 2008; Čech and Švábenická 2017). He drew attention to the possible occurrence of this species already in the highest part of the lower Coniacian. In the BCB, the FO of *M. staurophora* in the *Inoceramus frechi* zone (previously *I. kleini*) was pointed out by Čech and Švábenická (2017).

The Vf-1 core (Čech et al. 1987) contained poor nannofossils, whose abundance and preservation are comparable to other ones of the same age in the borehole 4650_A. Švábenická et al. (2016) confirmed decreasing number of nannofossils and their worse preservation upsection. In the lower part of the section (402.5–447.0 m), *Marthasterites furcatus* and *Broinsonia* ex gr. *furtiva-lacunosa*, now known as *Broinsonia parca expansa* were found and correlated with nannoplankton zone CC13 (Sissingh 1977). In this interval, transitional forms of *Quadrum-Micula* and *Micula* cf. *decussata* (syn. *M. staurophora*) were mentioned. A similar phenomenon was observed in the borehole 4650_A within 317.0–342.05 m. The FO of *M. decussata* (syn. *M. staurophora*) in the borehole Vf-1 was recorded in 397.6 m and the interval 136.0–397.6 m correlated with the base of CC14 zone. The base of zone CC14 (Sissingh 1977) corresponds to the base of the zone UC10 (e.g., Burnett 1998). It should be emphasized that (Sissingh 1977) correlated the FO of *M. furcatus* with the base of Coniacian. Later, the FO of *M. furcatus* is mentioned during late middle Turonian. Moreover, the onset of this species was found to be diachronous (Burnett 1998; Švábenická and Bubík 2014). In the upper part of the section after the FO of *M. staurophora*, rare

Cribrosphaerella circula and Staurolithites cf. imbricatus (Fig. 9EA–B, G) were recorded. Although both last named nannofossils are usually regarded as of Santonian age, in the BCB, they have already been found in the Coniacian (Švábenická et al. 2016; Švábenická and Havlíček 2017).

The interpretive potential of radiogenic strontium and stable carbon and oxygen isotopes

Stable isotopes are useful tools for interpreting environmental conditions under which sedimentary rocks were formed. These methods are based on the isotopic fractionation between H_2O and mineral and/or organic phases. During the precipitation of calcite/aragonite, isotopic fractionation occurs between $^{13}C/^{12}C$ in the mineral and the bicarbonate and carbonate ion solution, and $^{18}O/^{16}O$ in the mineral and water, respectively. For the stratigraphic purpose, $\delta^{13}C$ curves from the studied section and reference section are correlated by matching the patterns (trends, excursions) under an assumption that both represent the original record of the global ocean isotopic signal and are well chronostratigraphically calibrated. There are, however, several processes which could disrupt the equilibrium of carbon isotope system with the surrounding water: recrystallization, reaction with meteoritic waters, the presence of different of calcite and/or aragonite organisms ('vital effect' sensu Ziveri et al. 2003) and others.

As noted by Hudson (1977), most diagenetic processes, except methanogenesis (e.g., Whiticar 1999), result in decrease of primary $\delta^{13}C$ record of marine carbonate rocks; thus, low $\delta^{13}C_{carb}$ values, i.e., below 1 and negative, indicate postdepositional/diagenetic modification primary isotope record of analyzed samples (e.g., Oehlert and Swart 2014). Strong positive covariance of $\delta^{13}C$ and $\delta^{18}O$ commonly points to diagenetic alteration of primary isotope signature of marine carbonate under the influence of meteoric water (e.g., Allan and Matthews 1982), or within a freshwater phreatic zone (Swart 2015). Fluctuating, low $\delta^{13}C_{carb}$ values invariant to $\delta^{18}O$ values are interpreted as a result of subsurface meteoric diagenesis (Allan and Matthews 1982; Lohmann 1988). Low to negative $\delta^{13}C_{carb}$ values as well as strong covariance of $\delta^{13}C_{carb}$ and $\delta^{18}O$ values from the majority of samples (Fig. 12B) imply a postdepositional alteration of $\delta^{13}C_{carb}$ record of the studied section, possibly by the interaction of primary carbonate and pore water. Relatively low carbonate contentdup to ca. 25% (Fig. 12C) including both bioclasts and micrite causes $\delta^{13}C_{carb}$ to be governed by water exchange rather than preserving a primary record of seawater–shell isotope interaction (cf. Uličný et al. 1993). Thus, carbon isotope analyses concerning $\delta^{13}C_{carb}$ are only applicable to high-carbonate rocks due to their low porosity and permeability preventing isotope exchange through pore waters. Similar fineg-rained siliciclastic rocks from borehole Bch-1 farther SE from the study area were analyzed by Uličný et al. (2014) using $\delta^{13}C_{org}$ high-resolution isotope stratigraphy. As proved by Jarvis et al. (2015), $\delta^{13}C_{org}$ and $\delta^{13}C_{carb}$ curves from Bch-1 display good geometric fit except for upper Turonian–lower Coniacian

interval, covering the upper part of the Teplice and base of the Březno formations. For comparison, data of Jarvis et al. (2015) from Coniacian ($\delta^{13}C_{carb}$, $\delta^{18}O$ and $CaCO_3$ content) were plotted (Fig. 12B, C). This interval is characterized by minima of CaCO3 content with coincident gammaray maxima and exhibit negative excursions in $\delta^{13}C_{carb}$ and $\delta^{18}O_{carb}$. The low absolute values of $\delta^{13}C_{carb}$, $\delta^{18}O_{carb}$ and coincident depletion in both isotopes are explained by a significant local diagenetic overprint of carbonate at this level. Nevertheless, data of Jarvis et al. (2015) revealed that regardless to varying carbonate content (between ca. 8–38 wt. %), they cluster in a narrow range of $\delta^{18}O$ values (Fig. 12C), suggesting that stable isotope signatures result from pore water-governed exchange with no involvement of meteoric waters.

The Sr isotopic composition of seawater reflects steady-state equilibrium between various Sr sources (rock weathering, volcanic activity, seafloor alteration) and sinks (mainly marine carbonates). Generally, low or decreasing $^{87}Sr/^{86}Sr$ reflect periods characterised by high seafloor activity (mantle $^{87}Sr/^{86}Sr$ lower than 0.703), whereas increasing $^{87}Sr/^{86}Sr$ reflects periods of elevated weathering rates of continental felsic rocks with high time-integrated $^{87}Sr/^{86}Sr$ (Kump 1989). A composite Phanerozoic seawater $^{87}Sr/^{86}Sr$ curve (Veizer et al. 1999; McArthur et al. 2001; McArthur et al. 2012) is widely applied as a chemostratigraphic tool (e.g., McArthur et al. 1994, 1998, 2000; Steuber 2001; Frijia et al. 2015) or can be, in turn, used to identify the influence of continental sources (e.g., Richter et al. 1992; Goddéris et al. 2017).

The $^{87}Sr/^{86}Sr$ curve of the studied section (Fig. 12D) is generally characterized by a shift towards values more radiogenic than the coeval marine carbonate (cf., Steuber 2001; Frijia et al. 2015). The $^{87}Sr/^{86}Sr$ obtained for carbonate fraction of studied samples from the NW part of BCB is between 0.7073 and 0.7082. The Fig. 13 also shows evidence of $^{87}Sr/^{86}Sr$ data periodicity in time (Fig. 12D). This may indicate short time oscillations of marine carbonate Sr composition or variable input of dissolved terrestrial Sr.

Thanks to long strontium residence time in the oceans (~3.5My, Lécuyer 2016) relative to its fast global-mixing rate (about 1 kyr) the oceanic $^{87}Sr/^{86}Sr$ signal is globally constant within analytical uncertainty margins in a given time. The long Sr ocean residence time together with planetary character of Sr sources and sinks (e.g., various tectonic processes) effectively buffers all short-time $^{87}Sr/^{86}Sr$ anomalies. Several high-precision field studies presenting the Upper Cretaceous data (McArthur et al. 1994; Veizer et al. 1999; Steuber et al. 2005; Frijia et al. 2015) show that the global oceanic $^{87}Sr/^{86}Sr$ evolved gradually only from 0.70730 to 0.70738 during early to the middle Coniacian (ca. 89.5–87 Ma). Even marginal seas with significant input of riverine water (tens of %) show none or minimum deviance from the global $^{87}Sr/^{86}Sr$ signal (Löfvendahl et al. 1990; Kuznetsov et al. 2012). This is an effect of large concentration contrast between Sr in the seawater (~8.6 ppm, Millero et al. 2008) and the riverine water (10–500 ppb
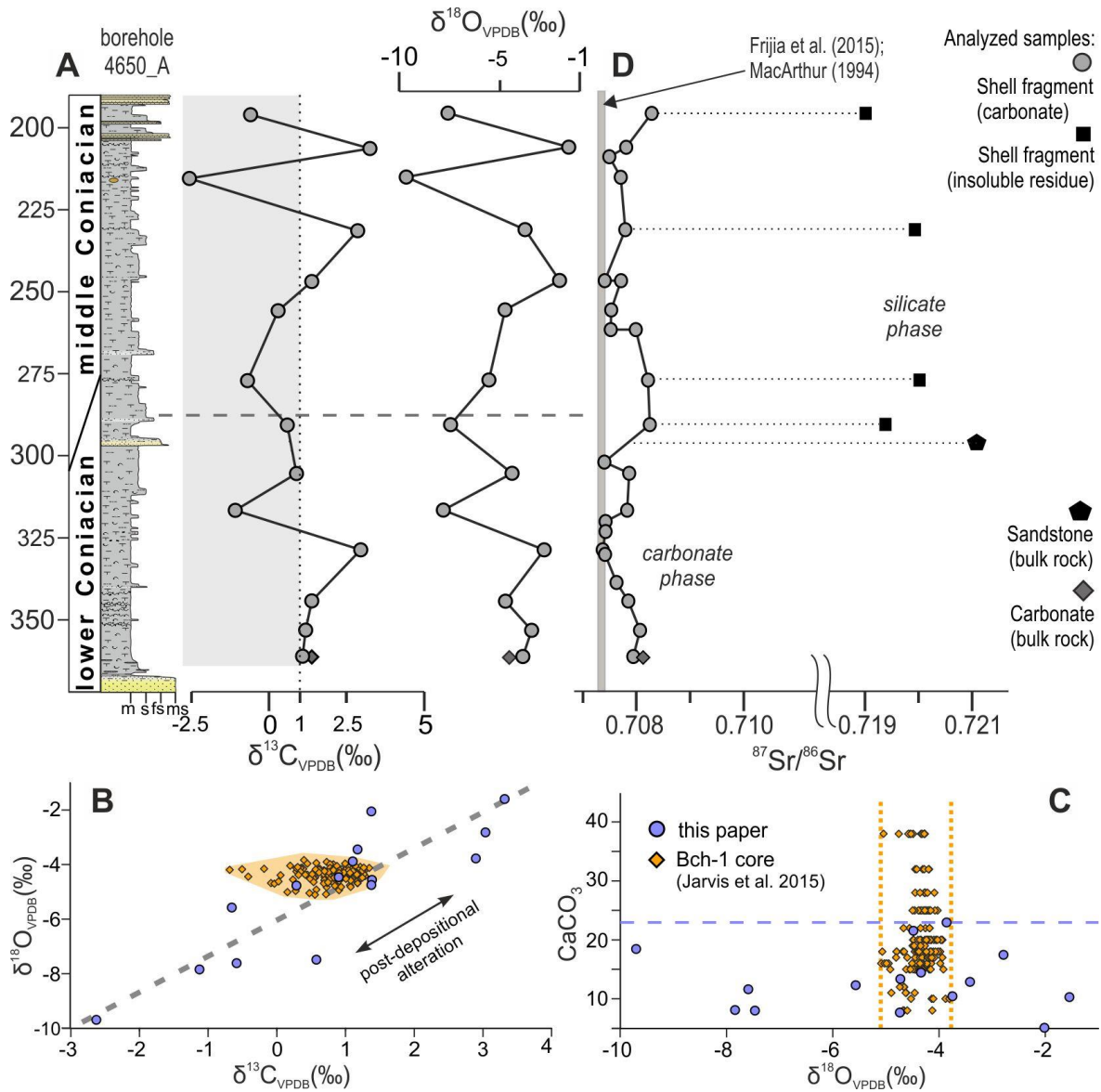
Figure 12. Summary chart of the stable carbon and oxygen and radiogenic Sr isotope analyses. **(A)** Stratigraphic section of the borehole 4650_A with corresponding curves of δ¹³C$_{carb}$, δ¹⁸O and ⁸⁷Sr/⁸⁶Sr. Coniacian Sr-isotope data range of Frijia et al. (2015) and McArthur et al. (1994) is added for comparison. Dashed line indicates the interpreted boundary between lower and middle Coniacian. **(B)** Graph showing the relationship between stable carbon and oxygen isotopes. Data of Jarvis et al. (2015) for Coniacian (in total 153 measurements) from the borehole Bch-1 Běchary, the central part of the BCB, were added for comparison. Dashed line indicates linear correlation trend. **(C)** Graph showing a relationship between δ¹⁸O and CaCO₃ content. CaCO₃ content for borehole 4650_A calculated from whole-rock Ca concentrations acquired by handheld XRF analyzer. Data of Jarvis et al. (2015) for Coniacian from the borehole Bch-1 Běchary were added for comparison. Dashed lines indicate value extent of individual datasets. **(D)** ⁸⁷Sr/⁸⁶Sr curve from the studied section of earlyemiddle Coniacian age (borehole 4650_A). Note the comparison of ⁸⁷Sr/⁸⁶Sr ratio obtained for carbonate and silicate fractions of analyzed samples, respectively.

with a global average ~60 ppb (Gaillardet et al. 2013). A simple mixing calculation indicates that even ~65% proportion of theoretical riverine water with assumed ⁸⁷Sr/⁸⁶Sr 0.715 (value based on Tichomirowa et al. 2010; Pawellek et al. 2002) increases the mixture ratio of only 0.0001, a fraction of observed range. Almost 90% mixing with riverine fresh water is needed to explain the

whole range. Higher $^{87}Sr/^{86}Sr$ in rivers was observed in intensely folded regions (e.g., Himalayas; Richter et al. 1992). During the Late Cretaceous, the Alpine Orogeny did not directly involve the Bohemian Massif, despite indirect evidence (e.g., Danišík et al. 2010; Hofmann et al. 2018) for tectonic reactivation and uplift of the northern Bohemian Massif. It should be also noted that the seawater side of the mixing model is relatively robust to river input composition uncertainty thanks to the exponential character of the equation.

The above conclusions indicate that the observed $^{87}Sr/^{86}Sr$ range is simply too large and cannot represent the original carbonate composition. The scatter should thus be an effect of diagenetic processes. The high-resolution studies (e.g., McArthur et al. 2012 and references therein) were performed under favourable conditions, e.g., analysing pure carbonates and large fossil remnants. On the other hand, samples available in the studied section comprise ambient sediment with a variable proportion of silicate material (5–80 wt. %) and the available shell fragments are only of millimeter size.

Several chemical proxies were proposed to indicate the open system diagenetic process capable to disturb the Sr isotopic system of the carbonate. Increased Fe and Mn concentrations are considered the most reliable indicator of disturbed environment (e.g., Brand and Veizer 1980; Al-Aasm and Veizer 1986; Brand et al. 2012), although low Fe and Mn concentrations in diagenetic calcite are possible suggesting that diagenetic fluids are not necessarily enriched in Fe and Mn (e.g., Steuber et al. 2005; Boix et al. 2011). Strontium content is another indicator of marine system preservation; the samples with Sr concentration below 750 ppm are normally rejected (McArthur et al. 2001). A mean value of Sr concentration in modern brachiopods and bivalves is about 1000 ppm or higher (Al-Aasm and Veizer 1986; Kuznetsov et al. 2012). As the distribution coefficient D_{Sr} between calcite and fluid is lower than unity (Gabitov and Watson 2006), the strontium partitions into the circulating pore-water. Low Sr content thus indicates possible fluid involvement including Sr re-precipitation from locally oversaturated fluids. As noted by Frijia et al. (2015), samples with Sr concentration higher than 750 ppm can be used in case they do not show significant apparent recrystallization. It is also important to use low-Mg carbonate samples only, as these are more stable than Mg-rich carbonates or aragonites.

Although the leached carbonate samples presented here show only weak correlations of mentioned element concentrations, a group characterized by low Mn (20–260 ppm), Mg (373–3258 ppm), Fe (1025 ppm–1.6%) and high Sr (>1800 ppm) contents can be distinguished (further referred as low-Mn group; samples 208.5, 246.37, 301.88, 319.95, 328.6, 330). If compared to concentrations presented by McArthur et al. (2000) in the samples of Late Cretaceous age from Antarctica, the Mn and Mg contents of the low-Mn group are comparable to data presented here, while the Fe concentrations are several orders higher.

Figure 13. Detailed comparison of low-Mn samples (208.5, 246.37, 301.88, 319.95, 328.6, 338.58) with the literature data (McArthur et al. 1994; Frijia et al. 2015). The mixing model shows a theoretical influence of radiogenic riverine water on the seawater isotopic signature
(sea: c_{Sr} = 8600 ppb, $^{87}Sr/^{86}Sr$ = 0.7073; river: c_{Sr} = 60 ppb, $^{87}Sr/^{86}Sr$ = 0.715).
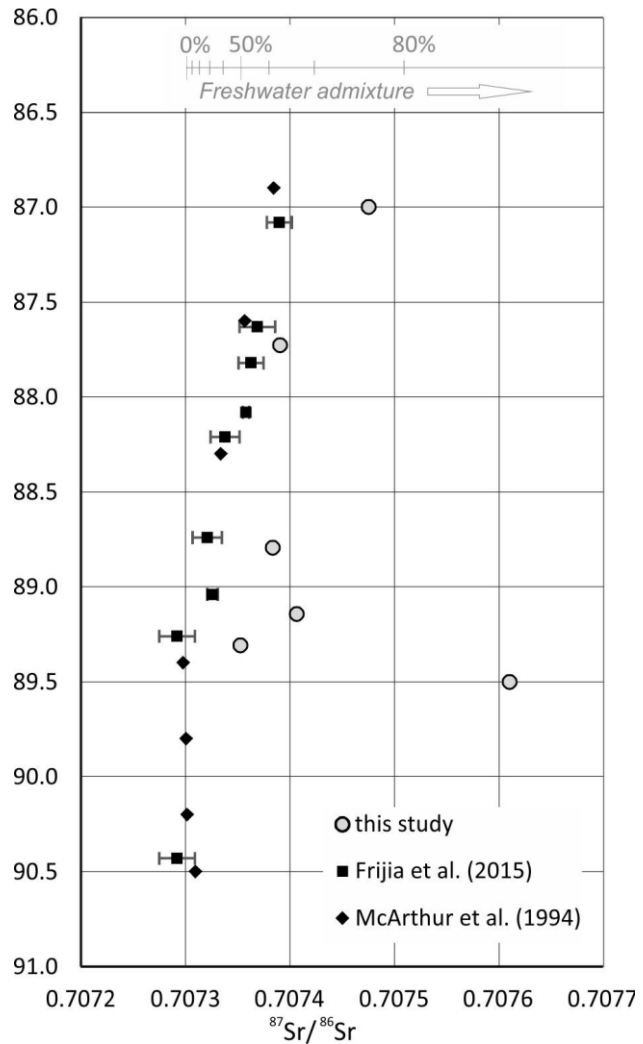
Nevertheless, other samples have even higher Fe and Mn contents, up to 12% and 803 ppm, respectively. We suggest that Fe (and to a lower extent, the Mn) are constituent part of the surface coating of Fe/Mn oxyhydroxides on crystallites. Such oxyhydroxides were observed on SEM photomicrographs of shell fragments of an inoceramid (sample 328.6, Fig. 11D). It is assumed that these samples might be altered, and structural alteration could disrupt the Sr-isotopic system.

The $^{87}Sr/^{86}Sr$ of the low-Mn group is within much narrower range between 0.70735 and 0.70761. The data represent the lower margin of the whole dataset. This suggests that the postdepositional alteration lead to an increase in the $^{87}Sr/^{86}Sr$ values. Such observation is in accordance with the continental character of the area, where almost all contamination sources have more radiogenic Sr. Several analyses of the silicate fraction (0.714–0.720) provide direct evidence for such assumption. In fact, the alteration leading to $^{87}Sr/^{86}Sr$ increase is almost universal rule as pointed out by Shields and Veizer (2002). Also, the lack of correlation between Sr isotopes from corresponding carbonate and silicate fractions indicates that carbonate Sr isotopic composition is not driven by direct contamination from non-carbonate phases (e.g., silicates, apatite; Fig. 12A).

A detailed view of the low-Mg samples provides Fig. 13. As already mentioned, the marine strontium composition increased from 0.70730 to 0.70738 between 89.5 and 87 Ma (McArthur et al. 1994). Our low-Mn samples, if plotted to the same age interval according to depth in the profile, are in all cases shifted towards higher $^{87}Sr/^{86}Sr$ values. The offset is only slightly higher than the calibration curve uncertainty (McArthur et al. 2001), however, it indicates that even the best-preserved samples from the BCB, presented in this study, are affected by the post-depositional processes, and as such are not suitable for the high-resolution Sr stratigraphy (cf. Steuber et al. 2005; Frijia et al. 2015; Boix et al. 2011).

Evolution of depositional system in time and space

Depositional model

The current depositional model (Fig. 14) is, in its salient features, concurrent with the one presented by Nádaskay and Uličný (2014). Individual facies represent here parts of the depositional system adjacent to tectonically driven basin margin. Proximal part of the depositional system with prevailing high-energy depositional processes is characterized by clastic coast amalgamation as well as progradation of clastic wedges, interpreted as coarse-grained deltas (e.g., Uličný 2001; Nádaskay and Uličný 2014). Based on thickness and dip angle, which are parameters directly related to available accommodation space and rate of clastic supply, individual foreset packages may be regarded as a lateral continuum between socalled H-type (high-angle), and the L-type (low-angle) foresets. Uličný (2001) associated H-type typically with 'deep-water' Gilbert-type deltas while L-type are attributed to shallow-water deltas (for position of both geometric types of foresets within the deltaic system see Fig. 2A, B). A single foreset package can reach up ca. 80 m (borehole 364819, cross-section S1, Fig. 2A), suggesting progradation of delta bodies into the basin at least 80 m deep at an original topset/foreset break (Nádaskay and Uličný 2014). Delta-front foresets are interpreted to be deposited principally by periodic downslope transport of clastic material by gravity flows. Deposits of gravity flows were subsequently reworked by tidal (Valečka 1979a) currents, as evidenced by varied trough crossbedding in sandstones, formed by migration of small-scale 3D dunes.

Gravity flows may have been triggered by slope failures ('ignitive' turbidity currents), but we assume that more frequently by the excessive influx of sediment-laden riverine water into a marine basin, typically during hydrological floods (cf. Milliman and Syvitski 1992; Mulder and Syvitski 1995) in an adjacent catchment area. Thus, these gravity flows can be termed as hyperpycnal currents sensu Mulder et al. (2003). The action of hyperpycnal currents is interpreted here as the main mechanism by which large portions of clastic material, originating from hinterland as well as subaerial delta plain, were transported from the shoreline into more
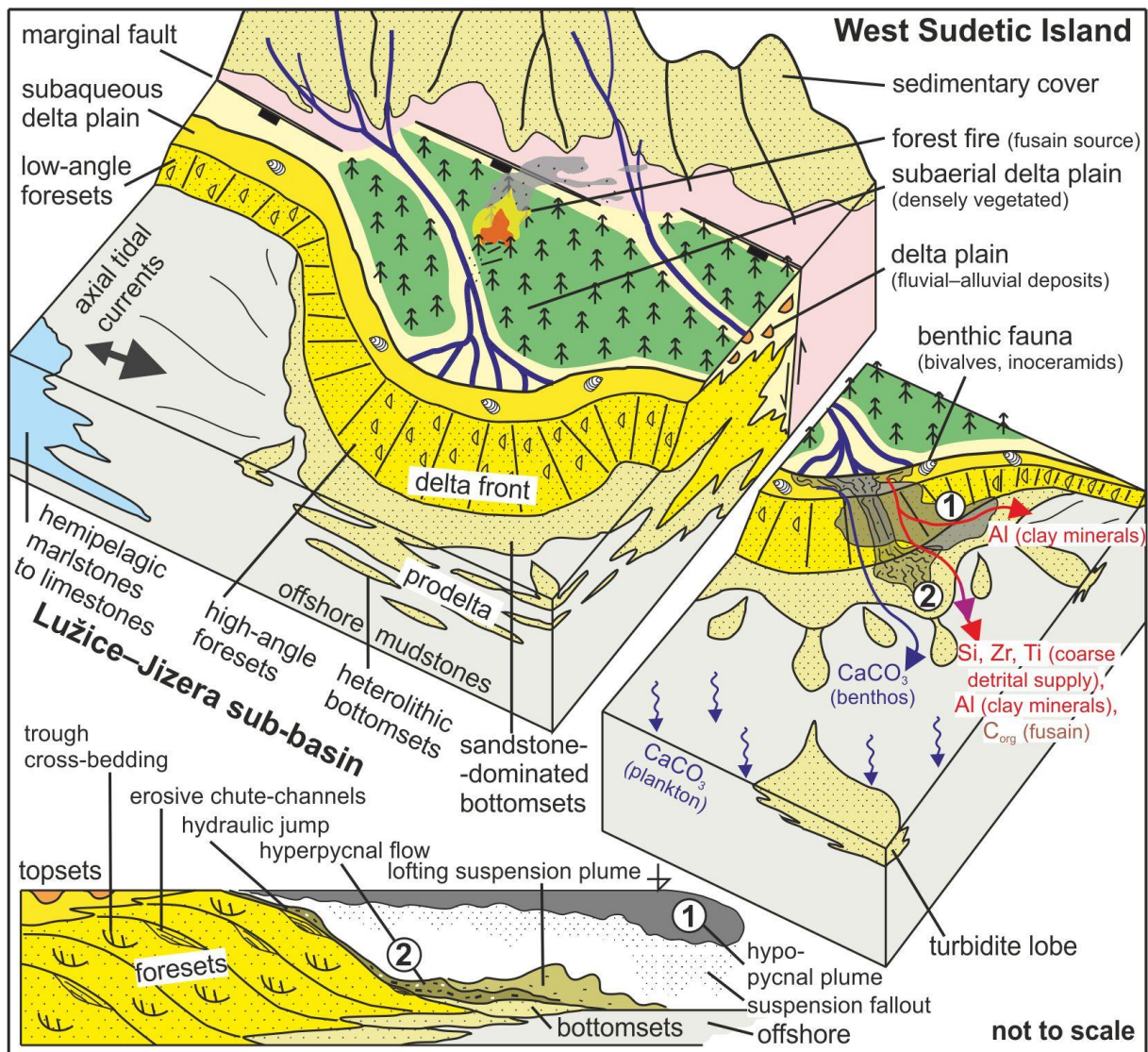
Figure 14. Schematic depositional model of the Coniacian deltas in the Lužice–Jizera sub-basin of the BCB with presumed dominant depositional processes (gravity flows, tidal currents). Presumed pathways of the main proxy elements are indicated.

profound parts of the basin. Zavala et al. (2011) coined the term E-type currents ('extrabasinal', i.e., originating in the terrestrial part of the fluvio-deltaic system) for gravity flows of sustained nature carrying a large amount of suspended terrigenous material. Hyperpycnal nature of the currents operating on delta slopes is supported also by highly abundant plant material as well as fusain/coal fragments (cf., Zavala et al., 2012) within delta front and prodelta lithofacies.

Sedimentary structures generated in the upper flow regime (parallel bedding or backset lamination) that developed within foresets of upper Turonian–Coniacian deltas from various parts of the BCB (e.g., Uličný 2001; Uličný et al. 2003; Nádaskay and Uličný 2014), are genetically attributed to hyperpycnal currents. Downslope-directed transition from upper plane-bedded foresets to erosive-based, massive to backset-stratified chute channels (as observed in outcrop by Nádaskay and Uličný 2014) possibly result from formation of hydraulic jumps (Nemec 1990; Cartigny et al. 2011) and subsequent transformation of supercritical flow to subcritical when

passing the crest of cyclic step 'bedform' (Postma et al. 2014; Postma and Cartigny 2014). Upon its final deceleration at the delta front/prodelta brake, most of the material transported by waning hyperpycnal or turbidity current is deposited as bottomsets. Although the depositional mechanism has been principally explored in this particular case, the comprehension of the exact physical behavior of gravity flows since their initiation until cessation requires thorough research.

Prodelta bottomsets may appear either as more or less amalgamated sandstone beds or heterolithic strata (Fig. 5A and B, respectively); juxtaposition of both facies cannot be observed in outcrop, but is interpreted in wider context, e.g. between boreholes J-157558, 4650_A and Vf-1 (cross-section S1, Fig. 2A), or J-186495, 4650_A and 480751 (cross-section S2, Fig. 2B). Amalgamated sandstone bottomsets represent the most proximal part of the prodelta close to its transition from the deepest part of the delta front. Further basinward, with increasing distance from delta front and decreasing sediment concentration, isolated sandstone beds capped by mudrocks form heterolithic bottomsets. A number of sandstone beds in the bottomset strata are virtually reworked (Fig. 7A, B), revealing that action of gravity currents in this setting was intermittent, punctuated by periods of non-deposition (as evidenced by the presence of accessory glauconite and bioturbation; cf. Valečka and Rejchrt, 1973).

Gravity-flow deposits, penetrating farther into the mudrock-dominated offshore sequence, are referred to as 'detached' to emphasize their depositional setting in the foreground of the delta progradation area outside the prodelta itself. In the study area, two sandstone bodies of this kind has been correlated over the offshore setting in different stratigraphic levels: i) within genetic sequence CON 3, e.g., in borehole J-157558 (Okrouhlá Sandstone sensu Nádaskay et al. 2017; Fig. 2A, B), and ii) within genetic sequence CON 4 (Fig. 2A) between boreholes 2H-278 and J-432640, informally labelled 'Žandov Sandstone' by Uličný et al. (2015; Fig. 2A). Unnamed sandstone body located between boreholes Vf-1 and J-533679; Fig. 2A) is displayed to show a possible presence of more sandstone bodies of the same kind, although this particular correlation remains dubious. By internal arrangement, two types of the 'detached' sandstone bodies, forming a lateral continuum, are distinguished: i) single sandstone intercalation, recorded by borehole 4650_A (Fig. 2A, B, close-up view in Fig. 3, depth 295 m); ii) amalgamated sandstone beds, interpreted from well-log pattern (e.g., boreholes 2H-278 or J-157558, Fig. 2A). They are interpreted here as deposits of submarine turbidite lobes (cf. Uličný et al. 2015) presumably formed during episodes of forced regression by intensified erosion of emerged delta topsets/foresets and redeposition of the clastic material into remote part of the basin. They resemble Type III turbidite bodies sensu Mutti (1985) or 'shingled' turbidites sensu Vail et al. (1991). Amalgamated sandstone beds may be attributed to multi-generation, possibly channelized

fills of the turbidite distributary system, while single, upward fining beds may represent unconfined overbank or levee deposits (cf. Shanmugam and Moiola 1988; Grundvåg et al. 2014).

Delta foresets and bottomsets pass basinward (possible lateraltransition scenarios are summarized in Fig. 4) into mudstones, representing the offshore realm. Whilst most of the sand and other coarse debris delivered into the basin was deposited within delta front and prodelta, only fine-grained component of the hyperpycnal currents proceeds further towards the axial part of the basin. It is assumed that mudstones containing relatively higher proportion of terrigenous material (quartz silt, clay minerals ± fusain) as well as shallow-marine shell debris, represent the most distal expression of plunging hyperpycnal currents (cf. Zavala et al. 2011; Wilson and Schieber 2014), most probably deposited by lofting suspension plumes (e.g., Sparks et al. 1993; Rimoldi et al. 1996). Dense ichnofabric of these mudstones (Fig. 7G) indicates that although the delivery of terrigenous clastic material still played a significant role, deposition took part by occasional incursions of plunging hyperpycnal currents punctuated by relatively "quiet" periods. These are dominated by deposition from suspension delivered into the basin by buoyant plumes, or hypopycnal plumes (sensu Mulder and Alexander, 2001; Bates, 1953). Formation of hypopycnal plumes may be concurrent with the onset of hyperpycnal gravity flows, where the former represents an overflow and the latter an underflow (Mulder and Alexander, 2001; Mulder et al. 2003). Separation of both currents transporting contrasting grain sizes results from the density contrast between the seawater and the suspension-laden riverine freshwater (Uličný 2001). Lower density of freshwater causes the buoyancy of suspended load carried away from the delta front as hypopycnal plumes near the sea surface by the same basinal currents that caused the dune migration along delta slopes (cf. Nemec 1995). The efficient separation of bedload and suspended load finally lead to an obvious contrast—in terms of prevailing grain size—between delta front (typical for relatively 'clean' sandstones, colored in correlation cross-sections, Fig. 2A, B) and heterolithic prodelta/offshore facies (cf. Uličcný 2001; Uličný et al. 2003). As suggested by Uličný et al. (2003), clay/fine silt was transported within near sea-surface hypopycnal plumes into the axial part of the basin far beyond the sites of bedload deltaic deposition. Deposition from the hypopycnal plumes may occur early in their evolution, although the suspension fallout could have been transported further by the mid-depth currents (cf. Morehead and Syvitski 1999).

The mentioned depositional processes govern the physical and mineralogical sorting of sedimentary material (different grain-size fractions, clay minerals vs. SiO_2 in clay fraction, siliciclastic particles vs. organic matter and bioclasts) influence the eventual element signature of the deltaic and adjacent offshore deposits. Delta foresets deposited primarily by hyperpycnal, sand-laden gravity currents, are rich in silica from detrital quartz and relatively enriched in Zr and Ti bound by heavy minerals. Underflow was the primary mechanism by which larger fusain and

coal fragments, as well as calcareous shell debris, were delivered into the delta foreground. The proportion of clay minerals, that are virtually missing in the foresets, is relatively favorable within bottomsets, where higher quantities of fine-grained sediments were deposited either from lofting suspension associated with decelerating hyperpycnal currents or fromhypopycnal suspension fallout.

In addition to the physical sedimentary evidence, the proximity of source mainland may also be confirmed by the presence of nannofossil species *Braarudosphaera bigelowii* in certain levels of the studied section (Fig. 3). Cunha and Shimabukuro (1997) explained enrichment in braarudosphaereids in coastal environments by lowering of salinity coupled with eutrophication, owing to either an influx of nutrient-rich continental waters from rivers or estuaries or coastal upwelling. Švábenická (1999) pointed out that the *Braarudosphaera*-rich deposits in the BCB are linked to the input of terrigenous material during deceleration of sea-level rise, or sea-level stillstand. The horizon with common *Marthasterites furcatus* (Fig. 3) is not as obvious as in other locations in the basin (cf. Švábenická 2012), which is also explained by the proximity of the mainland and related depositional processes.

Stratigraphic history

Detailed biostratigraphic division of the studied section (Fig. 3) and its correlation to neighbouring boreholes (Fig. 2A, B) allowed for revision of the genetic sequences previously defined in the study area by Uličný et al. (2009a) and Nádaskay and Uličný (2014). The latest Turonian sequence TUR 7 and part of the underlying sequence TUR 6 were incorporated into the correlation panels (Fig. 2) as well as into a summary of the depositional history (Fig. 14) to provide the context for interpretation of the Coniacian transgressive-regressive history, subsidence and supply regime.

Overall, TUR 7 sequence was interpreted by Uličný et al. (2009a) as an aggradation-dominated composite sequence formed by few meters thick vertically stacked bundles of elementary sequences; its deposition began shortly after the FO of *Prionocyclus germari*. In detail, the TUR 7 sequence was studied by Uličný et al. (2009a) and Vacková and Uličný (2011) and divided into three stacked small-scale sequences. Older of them, TUR 7/1 and 7/2, together form a major regressive wedge reaching ca. 40 km basinward from the tectonic margin, the Lusatian Fault. The lower part of the TUR 7 sequence is dominated by stack of upward-fining cycles that are, when correlated basinward to the SW (Fig. 2A), abruptly terminated between boreholes Vf-1 and 2H-278 and at the same level replaced by up to ca. 60 m thick sandstone package, named Kozly Sandstone (sensu Klein and Růžička 1990) extending approx. 20 km farther basinward. Depositional architectures of this sandstone package in its outcrop area

around Kozly hill as well as its lithofacies development in the area south of correlation cross-section S1 are in sharp contrast to those present within the TUR 7 sequence in borehole Vf-1 (Čech et al., 1987) and northward. This lead to a tentative interpretation of Kozly Sandstone as deposits of gilbert-type delta whose progradation into previously distal region implies a notable regressive phase (Uličný et al. 2015). The marker fossils place Kozly Sandstone within the uppermost Turonian and suggest that condensed section in the top of Kozly Sandstone, interpreted as a sequence boundary (TUR 7–CON 1), conceal part of the lowermost Coniacian (Nádaskay et al., 2018). The top Turonian sequence TUR 7/3 forms a retrogradational succession backstepping towards the Lusatian Fault, where reaching maximum thickness due to the highest subsidence rate. Uppermost part of the TUR 7/3 sequence is marked by the FO of *C. waltersdorfensis* in boreholes 4650_A and 270375 (this study) and Vf-1 (Čech et al. 1987), correlated from the *C. waltersdorfensis* type locality at Sonnenberg (Andert 1911; Walaszczyk 1996) at the NE margin of the study area (Fig. 2A).

The base of the Coniacian, marked by the FO C. deformis erectus (e.g., Walaszczyk et al. 2010) directly post-dating the FO *C. waltersdorfensis*, is possibly located below the base CON 1 sequence in the distal setting, given the condensation of part of the Coniacian at the top of TUR 7 (Nádaskay et al. 2018); in the proximal setting, the base of Coniacian is placed at or closely above the top of the TUR 7 sequence (Nádaskay and Uličný 2014). In the study area, the FO C. deformis erectus is located ca. 5 m above the base of the CON 1 sequence (Uličný et al. 2009a) and, thus, it post-dates the Turonian–Coniacian boundary. Because of missing correlation to the most proximal part of the depositional system, Nádaskay and Uličný (2014) only recognized one sequence (CON 1) in the lower part of the Coniacian. In this study, the lower part of the Coniacian that is divided into three sequences (CON 1–3).

The CON 1 sequencewas deposited during a sea-level highstand and represents the peak of landward backstepping of sandstone wedges starting with sequence TUR 7/3. In the proximal setting, the sequence is formed by shallow-water sandbodies ranging ca. 5 km from the presumed basin margin. Offshore part of the sequence is marked by the presence of subtle silicification (Fig. 10) of mudstones ushering later deposition of Rohatce Mb. (sequence CON 2, silicified hemipelagic marlstones/limestones), developed typically in the axial part of the basin (Čech et al. 1980). Overlying CON 2 sequence is defined at the base by the FO of *C. crassus crassus* and is roughly overlapping the temporal extent of Rohatce Mb. Although the top of the sequence is generally associated with the top of the C. crassus crassus interval zone as well as the top of interval with common *Marthasterites furcatus*, it is placed in this study at the local maximum of gamma-ray log in the borehole 4650_A correlated to neighbouring boreholes (Fig. 2). It is interpreted as a maximum transgressive surface (MTS) at the base of overlying sequence CON 3.

Base of the CON 3 sequence is placed within the zone of *Inoceramus frechi/I.gibbosus* that coincides with FO of nannofossil *M. staurophora*. Both latter mark the lower‑middle Coniacian boundary within the BCB (Čech and Švábenická 2017). Compared to the older CON 1, sequences CON 2 and 3 are typical for renewal of basinward progradation of sandstone wedges that reach Kytlice area (borehole J-060467). Both sequences CON 2 and 3 comprise shallow‑water, nearshore sandstone bodies in the proximal part, as recorded, e.g., by borehole 4650_X. In addition, well logs suggest that their counterparts are present in the neighbouring borehole 074903 as well.

In the upper part of the CON 3 sequence, a relatively thin sandbody was distinguished within the sequence of mudstones. The sandbody termed Okrouhlá Sandstone by Nádaskay et al. (2017; Fig. 2A, B) is interpreted here as a turbidite fan detached from the main loci of nearshore/deltaic deposition into the offshore setting. Formation of such turbidite fans in a passive margin setting is commonly associated with sea-level fall (Mutti 1985; Posamentier and Vail 1988; Shanmugam and Moiola 1988) facilitating erosion and redeposition of nearshore deposits. Despite lacking data for correlation over a wider area, we infer that the Okrouhlá Sandstone might have been deposited during short-term sea-level fall within CON 3 sequence, accompanied by partial or complete redeposition in the nearshore setting. The well-log correlation revealed that the other such sandstone body found in the study area, the Žandov Sandstone, is slightly younger in age, being part of the CON 4/1. We assume that no erosion and redeposition associated with sea-level fall involved formation of the Žandov Sandstone. It instead formed as gravity flows penetrated farther into the basin and deposited a lobe or system of lobes within the offshore. Because of scarcity of boreholes available for correlation, it is not possible to infer whether this lobe (or lobes) was somehow attached to prodelta, or completely detached (as suggested by Fig. 2A). Given that formation of submarine turbidite lobes do not necessarily require a lowstand incision (e.g., Burgess and Hovius 1998; Covault and Graham 2010), we assume that the Žandov Sandstone formed as a result of the increased delivery of siliciclastic material into the distal part of the basin within supply dominated, progradational deltaic system (cf., Carvajal and Steel 2006; Grundvåg et al. 2014). The CON 4 sequence is defined at the base by correlative conformity to MTS covering the CON 3 sequences, as evidenced by correlation to the nearshore setting; this MTS was recognized by Nádaskay and Uličný (2014) as well, though sequences it bounds were labelled differently. In terms of biostratigraphy, the boundary between sequences CON 3 and 4 is placed in the zone of *Inoceramus frechi/I. gibbosus* and concurrent FO of *Volviceramus koeneni*. The sequence is subdivided into four stacked elementary sequences. The entire sequence CON 4 is in sharp contrast with underlying sequences by conspicuous
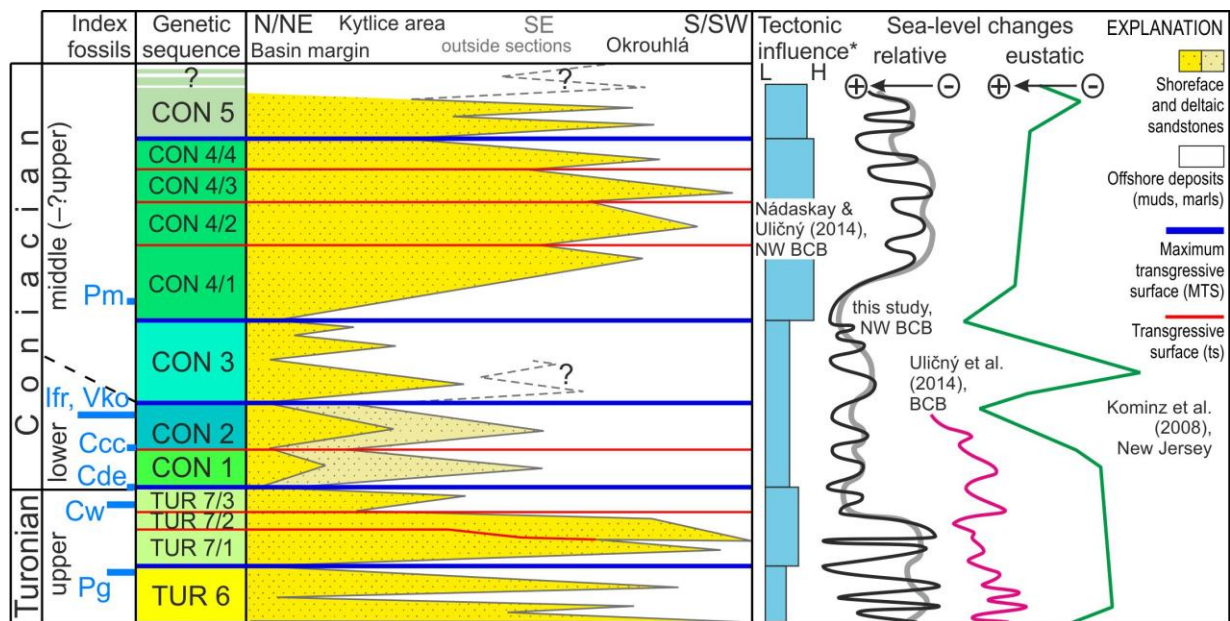
Figure 15. Overview of depositional history of the late Turonian–middle Coniacian in the NW part of the BCB. 'Tectonic influence' refers to an inferred relative role of tectonic basin-floor subsidence on the accommodation rate within individual genetic sequences (after Nádaskay and Uličný 2014). Relative (Uličný et al. 2014, central BCB) and global eustatic (Kominz et al. 2008, New Jersey Atlantic margin) sea-level curves are added for comparison.

progradational pattern, resulting from heavily increased sediment supply, compensating for basin-floor subsidence that had increased since the latest Turonian.

The base of the uppermost recognizable sequence, CON 5 (labelled as CON 3 by Nádaskay and Uličný 2014), is defined by MTS covering the top of sandstone of CON 4 sequence. Sandstone bodies forming the CON 5 sequence are interpreted to be either shallowwater or transitional (cf. Uličný 2001). The sequence forms uppermost ca. 100 m in the borehole 4650_A and can be traced to the north of Nový Bor (borehole 364819); farther to the north the sequence is missing because of erosion of the youngest Coniacian deposits. Southward, the progradation of deltaic bodies of the CON 5 sequence does not exceed the point of maximum progradation of those in the underlying CON 4 sequence. Overall, the CON 5 sequence exhibit rather aggradational stacking pattern.

In accordance with Nádaskay and Uličný (2014) three major transgressive events are interpreted within the latest Turonian–middle Coniacian interval (Fig. 15): i) at the base of the CON 1 sequence, i.e., approximately at, or close to the Turonian–Coniacian boundary; ii) at the base of CON 2 sequence (near FO *C. crassus crassus*), which corresponds with the onset of deposition of Rohatce Mb. in the axial part of the basin; iii) and at the base of CON 5 sequence.

The relative role of eustatic component of sea-level change during the major transgressive events in the study area is uneasy to be assessed, since the presumed global (e.g., Hardenbol et al. 1998; Haq 2014) or regional T–R cycle charts from different parts of the world (e.g., Miller et al.

144

2003; Kominz et al. 2008; Xi et al. 2016) do not offer adequate resolution in the critical interval of the Turonian–Coniacian boundary and the early–middle Coniacian. Nevertheless, the global importance of particular stratigraphic surfaces in the BCB has been recently discussed by Uličný et al. (2014) and Jarvis et al. (2015). In the BCB, the transgression at the Turonian–Coniacian boundary (base of CON 1 sequence), carrying a global significance (e.g., Walaszczyk et al. 2010, 2014; Plint et al. 2017), is found in a generally regressive succession in the Český Ráj depocenter (Uličný et al. 2014), located ca. 50 km to the southeast of the study area. A substantial part of the progradational succession in the mentioned area belongs to the TUR 7 sequence and correlate with predominantly aggradation-dominated succession in the study area. However, as noted by Nádaskay and Uličný (2014), the juxtaposition of both depocenters is complicated by remarkable differences in their stacking patterns (cf., Uličný et al. 2014). An abrupt appearance of progradational body (Kozly Sandstone) within aggradation-dominated sequence suggest a minor short-term sea-level fall during TUR 7 sequence (Uličný et al. 2009a) recorded at least in the NW part of the BCB (Lužice–Jizera sub-basin). Richardt and Wilmsen (2012) support this assumption by recognition of an unconformity within the upper Turonian *M. scupini* Zone in the Münsterland Basin (NW Germany, ca. 400 km out of the study area).

The transgression at the base of CON 2 sequence, near the FO of *C. crassus crassus* (base of the Rohatce Mb., cf., Uličný et al. 2009a) has its counterpart in the Western Canada foreland basin (Walaszczyk et al. 2014; Plint et al. 2017), which supports an eustatic origin of this particular sea-level fluctuation (Uličný et al. 2014).

Tectonosedimentary evolution

The juxtaposition of individual depositional sequences, latest Turonian–middle Coniacian in age, namely TUR 7 to CON 5, as well as investigation of the physical depositional record revealed that volume of siliciclastic supply and rate of creation of accommodation space differed over the studied stratigraphic interval, but also in comparison to older Turonian sequences.

The latest Turonian (sequence TUR 7) is dominated by aggradational stratal packages, interpreted as deposits of shallow-water (L-type) deltas (Uličný et al. 2009a; Vacková and Uličný 2011). The aggradation of depositional sequences implies compensation of increasing accommodation space by increasing sediment supply. In comparison, TUR 6 and older Turonian sequences, formed by shallow-water (L-type) deltas as well, exhibit progradational pattern (Uličný et al. 2009a). This results from overfilling during the "mature stage" of the basin evolution, characterized by relatively low subsidence and supply, although enough to fill the accommodation and cause basinward shift of the shoreline. The presence of the Kozly Sandstonedcharacterized by the development of H-type foresetsdwithin the TUR 7 sequence

implies the sea-level fall and consequent forced-regression, followed by the sea-level rise and consequent landward backstepping of shallow-water delta bodies.

In turn, early to middle Coniacian sequences CON 1 to 5 were deposited during a period of increasing depth through time. Besides a series of transgressions driven by eustatic sea-level rise (the most conspicuous ones at the base of sequence CON 1 and CON 2), the increased basin-floor subsidence is interpreted as amajor factor governing the creation of accommodation space in the study area as well as other parts of the BCB (e.g., Uličný et al. 2003, 2009a). Regardless to transgressiveeregressive shift of shoreline, the stacking patterns were locally governed by seafloor topography (e.g., Nádaskay and Uličný 2014), for instance by accommodation left after the deposition of underlying foreset packages. Increasing sediment supply throughout the sequences CON 2 and 3 caused the renewal of progradation punctuated by the sea-level rise at the Turonian–Coniacian boundary. Prograding sandstone wedges interpreted as deltas (with H-type foresets) have been attributed to sequences CON 1–3 in the Cvikov area, slightly SE of the section S1 (Fig. 2A).

During the deposition of CON 4 sequence, the sediment supply substantially increased compared to previous sequences. The thickest deltaic body was deposited within the sequence CON 4/1 – the maximum depth of progradation, as assumed from preserved sections (e.g., boreholes 364819 in Fig. 2A or 4650_F in Fig. 2B), was up to 100 m and while prograding basinward, generally to the S/SE, the delta bodies reached less than ca. 25 km from the basin margin. The range of delta progradation was, thus, as twice pronounced compared to sequences CON 1–3 in the SE of the study area (Fig. 15). However, the juxtaposition with CON 4 and younger sequences is not possible in this particular area because of postdepositional erosion of the younger part of Coniacian.

The lateral pinchout illustrated in Fig. 2B suggest either presence of at least three separate delta bodies within the sequence CON 4/1, each of them possibly attached to a different point source (fluvial mouth; as proposed in Fig. 14), or larger deltaic system composed of several lobes attached to the same fluvial source. The river systems served as a principal conduit of siliclastic material from catchments areas on the West Sudetic Island, an exclusive source area for the Lužice–Jizera sub-basin during the late Turonian–Coniacian (e.g., Skoček and Valečka 1983; Uličný et al. 2009a; Nádaskay and Uličný 2014).

Since the long-term climate conditions are considered stable throughout the Turonian–Coniacian (e.g., Friedrich et al. 2012), we interpret an abrupt change in large-scale depositional geometries to be driven more likely by increasing tectonic subsidence and sediment supply. The increased tectonic activity during the late Turonian–middle Coniacian (the phase of 'tectonic acceleration', Fig.1) has been reported in the BCB by Laurin and Uličný (2004) and Uličný et al.

(2009a). The latter estimated that in the Lužice–Jizera sub-basin, the sediment supply was twofold during the mentioned interval in comparison to preceding intervals of the Turonian. Accelerated uplift of adjacent source area, the West Sudetic Island, is supported by increased 'immaturity' of the latest Turonian–Coniacian deposits, documented by an increase in the content of unstable mineral grains, i.e., feldspars and micas (e.g., Valečka 1979a), as well as their elevated natural radioactivity (Vacková 2010). It has been assumed that the siliciclastic material deposited along the basin margin was derived predominantly from granites contributing by about twofold more material than their sedimentary cover (Skoček and Valečka 1983). The granites underwent deep weathering during the Jurassic–Late Cretaceous (e.g., Malkovský 1979), but as an effect of physical separation at mouths, tidal reworking, and transport by marine currents, most of the kaolinite clay and unstable mineral fragments were removed from the nearshore depositional environments (Skoček and Valečka 1983). The finest fraction of the sediment is interpreted to be transported from fluvial mouths as suspended in hypopycnal (overflow) plumes and deposited after reaching the distal parts of the basin. However, according to Štaffen (2002), distal fines are composed of a mixture of calcite, silt- to clay-sized quartz and clay minerals, predominantly kaolinite – that, however, does not exceed 25 vol. %. Relatively low content of feldspars and clay minerals, respectively, renders the assumption about long-term erosion of both weathered and fresh granites in the source area unlikely. The increasing complexity of clay minerals towards younger Upper Cretaceous deposits (Štaffen 2002) may indicate the contribution of several contrasting lithologies exposed in the source area, as a result of its more intense topographic differentiation and fluvial incision attributed to accelerated tectonic uplift since the latest Turonian. On the contrary to Skoček and Valečka (1983), Voigt (1994, 2009) assumed that the present-day Lusatian Massif formed a subsiding area during the late Middle–Late Jurassic presumably to the Early Cretaceous filled with carbonates as well as siliciclastic deposits. During the Late Cretaceous, the Jurassic rocks formed an exposed part of the West Sudetic Island and were gradually eroded and redeposited into the BCB. The presence of Jurassic in the source area and its Late Cretaceous recycling is supported by Hofmann et al. (2013, 2018) based on the presence of Baltica-sourced zircons within the upper Turonian–Coniacian as well as contribution of older zircon populations towards younger Upper Cretaceous formations, suggesting an 'unroofing' of a crystalline core of the West Sudetic Island. However, even during at least the early Coniacian, the substantial part of crystalline basement was most likely covered by the pre-Late Cretaceous deposits. Our original assumption was that more pronounced erosion and delivery of clastic material into the basin would cause the shift of the Sr-isotope composition towards more radiogenic values when mixing with low-Sr seawater. Even though several analyzed

samples proved to be post-depositionally altered, the mixing model shows that this is not possible in spatial and temporal scale of this study.

In accord with previous authors (Laurin and Uličný 2004; Uličný et al. 2009a; Nádaskay and Uličný 2014), we consider the acceleration of basin-floor tectonic subsidence and source uplift in the NW part of BCB to have been one of the precursor events of the Late Cretaceous inversion of the Alpine foreland (cf., Ziegler et al. 1995). The style and timing of the Late Cretaceous inversion of Mesozoic epicontinental basins have been studied by a number of authors in the Western and Central Europe (e.g., Voigt 1963; Kockel 1986; Mortimore and Pomerol 1997; Mortimore et al. 1998; Vejbæk and Andersen 2002; Voigt et al. 2006; von Eynatten et al. 2008; Mortimore 2018). In the BCB, Uličný et al. (2009a) interpreted the tectonic regime as transtensional during the Turonian with accelerating strain rates and consequent basin-floor subsidence towards the late Turonian. Although the present-day Lusatian Fault, separating the basin fill from the basement, is possibly a successor of the original marginal fault zone (e.g., Voigt et al. 2008; Uličný et al. 2003, 2009a; Nádaskay and Uličný 2014), the evidence lacks for its exact kinematic role during the pre-Campanian times (cf. Coubal et al. 2015).

The timing of the onset of inversion of the BCB corresponds to the early Ilsede phase (Mortimore 1998, 2018; termed after Stille 1924) of the Late Cretaceous ('Subhercynian') deformation of Alpine foreland. Outside the BCB, the Ilsede phase is marked by hiati in the Cretaceous basins of northern Germany, or by a presence of submarine slides, as well as presence of condensed sections with hardgrounds in the Anglo-Paris Basin (Mortimore 1998, 2018 and references therein). Contemporaneous in age, the interplay of intensified basin subsidence and uplift of adjoining source area in the NW BCB thus represent a part of a broader series of tectonic processes related to continental-scale changes in the paleostress field in Europe. These have so far been interpreted as due to the onset of Alpine collision (Ziegler 1990), or changes in motion between European, African, and Iberian plates (Kley and Voigt 2008).

Conclusions

1. Six inoceramid interval zones have been distinguished within the studied section: i) *Cremnoceramus deformis erectus*; ii) *Cremnoceramus waltersdorfensis hannovrensis*; iii) *Cremnoceramus crassus inconstans*; iv) *Cremnoceramus crassus crassus*; v) *Inoceramus frechi/Inoceramus gibbosus*; vi) *Volviceramus koeneni*. The combination of the FO of *Inoceramus frechi/I. gibbosus* and of the FO of *Micula staurophora* are applied as markers for the base of the middle Coniacian in the BCB, in contrast to the classic inoceramid subdivision as indicated in Kaufmann et al. (1996). The base of Rohatce Mb. was defined biostratigraphically as the base of *Cremnoceramus crassus crassus* interval zone because no silicified limestone defining the member was present in the

study area; moreover, as indicated by Si/Al ratio, slight silicification was present in the underlying strata belonging to the *Cremnoceramus deformis erectus* interval zone.

2. We present the first strontium isotope dataset for the BCB, obtained from macrofossil shell fragments and supplemented by C–O stable isotopes. Out of the 24 analyzed macrofossil samples, 6 were identified as comparable with the Sr-isotope signature of Coniacian seawater (cf., Frijia et al. 2015; McArthur et al. 1994; Fig. 13). The rest of the samples were affected by postdepositional alteration, leading to an increase in the $^{87}Sr/^{86}Sr$ ratio. The total $^{87}Sr/^{86}Sr$ range of the studied section of Coniacian of the BCB is between 0.7073 and 0.7082 (carbonates) and 0.7190 to 0.7212 (silicates, recent values). Most of the Sr budget is bound to the lower part of the range as the carbonates have significantly higher Sr content. The low-Mn samples are only slightly shifted from the global $^{87}Sr/^{86}Sr$ curve towards more radiogenic values. The assumption that the pronounced erosion and clastic supply could be identified by calculation of mixing of seawater and more radiogenic riverine water has not been proven. The model suggests that the observed shift of the Sr isotope ratio from the contemporary seawater is too large to be explained by terrigenous influx into the sea in spatial and temporal scale of this study. It is more probable that most of the analyzed carbonate samples underwent post-depositional alteration causing the modification of the original $^{87}Sr/^{86}Sr$ ratio.

3. The depositional setting of the Coniacian in the NW BCB is interpreted as nearshore to deltaic (Fig. 14). The transition from proximal to the distal part of the depositional environment is marked by a change in depositional geometries, i.e., by the transition from shallow-water (low-angle foresets) to deepwater (high-angle foresets) deltas. The latter are predominantly formed by an alternation of downslope transport by gravity flowsdmost commonly the hyperpycnal currents triggered by hydrological floodsdand subsequent reworking of deposited clastic material by tidal currents. Progradation of deltas is marked by progadation of prodelta of basically two types: sandstone-dominated, interpreted as proximal bottomset strata, and distal heterolithic. In offshore, the progradation is recorded by indistinct intervals with elevated Si/Al, Ti/Al and Zr/Al ratio (Fig. 10). Sandstone bodies detached from the main locations of deltaic deposition are interpreted as submarine turbidite lobes. The older Okrouhlá Sandstone (sequence CON 3) was possibly formed as a result of short-term sea-level fall and consequent erosion and redeposition of clastic material from nearshore setting, while the younger Žandov Sandstone (sequence CON 4) as an element of a highstand, supplydominated progradational deltaic system.

4. Three major transgressive events are interpreted within the latest Turonian–middle Coniacian interval (Fig. 15): i) at the base of the CON 1 sequence, i.e., approximately at, or close to the Turonian–Coniacian boundary; ii) at the base of CON 2 sequence (near FO *C. crassus crassus*);

iii) and at the base of CON 5 sequence. Although uneasy to assess the relative role of eustatic component of sea-level change during the mentioned transgressive events, we interpret transgressions at the TuronianeConiacian boundary and at the base of sequence CON 2 as carrying a component of eustatic sea-level rise.

The stacking patterns of individual depositional sequences in the studied interval of latest Turonian–Coniacian is interpreted as a result of increasing accommodation space through increasing basin-floor subsidence, possibly enhanced in particular stratigraphic levels (at the base of sequences CON 1 and CON 2) by eustatic sea-level rise, compensated by increasing sediment supply. The latter resulted from accelerated uplift of the source area, the West Sudetic Island that together with increased subsidence in adjacent Lužice–Jizera sub-basin commenced in the latest Turonian. The latest Turonian TUR 7 sequence is interpreted as aggradation-dominated with backstepping of sandstone bodies towards the basin margin in its later stage. However, the Kozly Sandstone, occupying the middle part of the sequence, may have been deposited as a result of short-term sea-level fall and consequent pronounced basinward progradation. The early–middle Coniacian sequences CON 1 to 5 are characterized by deposition during the period of increasing depth through time as well as by progradational pattern, most remarkably the CON 4 sequence. The latter is dominated by deep-water deltas depositing up to 100 m thick high-angle foreset packages at the maximum limit of their progradation, as well as thick prodelta bottomsets and even detached turbidite lobe (e.g., Žandov Sandstone). The acceleration of basin-floor tectonic subsidence and source uplift in the NW part of BCB, accompanied by increased sediment supply, falls within the early Ilsede phase of the Late Cretaceous ('Subhercynian') deformation of Alpine foreland coeval with inversion-related processes in the western and central European basins. It is assumed that the late Turonian–Coniacian 'tectonic acceleration' represented a precursor event to the later (Santonian or Campanian) inversion of the BCB.

Acknowledgements

References

Al-Aasm, I.S., Veizer, J., (1986): Diagenetic stabilization of aragonite and low-Mg calcite, I. Trace elements in rudists. Journal of Sedimentary Research, 56, 138–152.

Allan, J.R., Matthews, R.K. (1982): Isotope signatures associated with early meteoric diagenesis. Sedimentology, 29, 797–817.

Allègre, C.J., Louvat, P., Gaillardet, J., Meynadier, L., Rad, S., Capmas, F. (2010): The fundamental role of island arc weathering in the oceanic Sr isotope budget. Earth and Planetary Science Letters, 292, 51–56.

Andert, H. (1911): Die Inoceramen des Kreibitz-Zittauer Sandsteingebirges. Festschrift des Humboldtvereins zur Feier seines 50 jährigen Bestehens am 22. Oktober 1911, 33–64.

Andert, H. (1934): Die Kreideablagerungen zwischen Elbe und Jeschken. Teil III. Die Fauna der obersten Kreide in Sachsen, Böhmen und Schlesien. Abhandlungen der Königlich Preußischen Geologischen Landesanstalt, Neue Folge, 159, 1–477.

Bates, C.C. (1953): Rational theory of delta formation. Bulletin of the American Association of Petroleum Geologists, 37, 2119–2162.

Becker, R.H, Clayton, R.N. (1976): Oxygen isotope study of a Precambrian banded iron-formation, Hamersley Range, Western Australia. Geochimica et Cosmochimica Acta, 40, 1153–1165.

Boix, C., Frijia, G., Vicedo, V., Bernaus, J.M., Di Lucia, M., Parente, M., Caus, E. (2011): Larger foraminifera distribution and strontium isotope stratigraphy of the La Cova Limestones (Coniacian–Santonian, 'Serra Del Montsec', Pyrenees, NE Spain). Cretaceous Research, 32, 806–822.

Brand, U., Veizer, J. (1980): Chemical diagenesis of a multicomponent carbonate system – 1: Trace elements. Journal of Sedimentary Research, 50, 1219–1236.

Brand, U., Jiang, G., Azmy, K., Bishop, J., Montañez, I.P. (2012): Diagenetic evaluation of a Pennsylvanian carbonate succession (Bird Spring Formation, Arrow Canyon, Nevada, U.S.A.) – 1: Brachiopod and whole Rock comparison. Chemical Geology, 308–309, 26–39.

Brandmayr, M., Dallmeyer, R.D., Handler, R., Wallbrecher, E. (1995): Conjugate shear zones in the southern Bohemian Massif (Austria): Implications for Variscan and Alpine tectonothermal activity. Tectonophysics, 248, 97–116.

Burgess, P.M., Hovius, N. (1998): Rates of delta progradation during highstands: Consequences for timing of deposition in deep-marine systems. Journal of the Geological Society, 155, 217–222.

Burnett, J.A. (1998): Upper Cretaceous. In: Brown, P.R. (ed.): Calcareous Nannofossil Biostratigraphy, 1st edition. Kluwer, Dordrecht, p. 132–199.

Cartigny, M.J.B., Postma, G., van den Berg, J.H., Mastbergen, D.R. (2011): A comparative study of sediment waves and cyclic steps based on geometries, internal structures and numerical modeling. Marine Geology, 280, 40–56.

Carvajal, C.R., Steel, R.J. (2006): Thick turbidite successions from supply-dominated shelves during sea-level highstand. Geology, 34, 665–668.

Coubal, M., Málek, J., Adamovič, J., Štěpančíková, P. (2015): Late Cretaceous and Cenozoic dynamics of the Bohemian Massif inferred from the paleostress history of the Lusatian Fault Belt. Journal of Geodynamics, 87, 26–49.

Covault, J.A., Graham, S.A. (2010): Submarine fans at all sea-level stands: Tectono-morphologic and climatic controls on terrigenous sediment delivery to the deep sea. Geology, 38, 939–942.

Cunha, A.S., Shimabukuro S. (1997): Braarudosphaera blooms and anomalous enrichments of Nannoconus: Evidence from the Turonian South Atlantic, Santos Basin, Brazil. Journal of Nannoplankton Research, 19, 51–55.

Čech, S. (1989): Upper Cretaceous Didymotis events from Bohemia. In: Wiedmann, J. (ed.): Cretaceous of the Western Tethys. Proceedings of the 3rd International Cretaceous Symposium, Tübingen 1987. Schweizerbart, Stuttgart, p. 657–676.

Čech, S. (2011): Palaeogeography and stratigraphy of the Bohemian Cretaceous Basin (Czech Republic) – An overview. Geologické výzkumy na Moravě a ve Slezsku, 18, 18–21.

Čech, S., Klein, V., Kříž, J., Valečka, J. (1980): Revision of the Upper Cretaceous stratigraphy of the Bohemian Cretaceous Basin. Věstník Ústředního ústavu geologického, 55, 277–296.

Čech, S., Švábenická, L. (1992): Macrofossils and nannofossils of the type locality of the Březno Formation (Turonian–Coniacian, Bohemia). Věstník Ústředního ústavu geologického, 67, 311–326.

Čech, S., Švábenická, L. (2017): Inoceramids and calcareous nanoplankton at the Lower and Middle Coniacian substage boundary in the Bohemian Cretaceous Basin. In: Sames, B. (ed.): 10th International Symposium on the Cretaceous – Abstracts, 21–26 August 2017, Vienna. Berichte der Geologischen Bundesanstalt, 46.

Čech, S., Hercogová, J., Knobloch, E., Pacltová, B., Pokorný, V., Sajverová, E., Slavík, J., Švábenická, L., Valečka, J. (1987): Svrchní křída ve vrtu Volfartice Vf-1. Sborník Geologických věd, Geologie, 42, 113–159.

Danišík, M., Migoń, P., Kuhlemann, J., Evans, N.J., Dunkl, I., Frisch, W. (2010): Thermochronological constraints on the long-term erosional history of the Karkonosze Mts., Central Europe. Geomorphology, 117, 78–89.

Dempírová, L., Šikl, J., Kašičková, R., Zoulková, V., Kříbek, B. (2010): Zhodnocení přesnosti a relativní chyby stanovení hlavních složek silikátových analýz v Centrální laboratoři České geologické služby. Zprávy o geologických výzkumech, 27, 326–330.

Fralick, P.W., Kronberg, B.I. (1997): Geochemical discrimination of clastic sedimentary rock sources. Sedimentary Geology, 113, 111–124.

Friedrich, O., Norris, R.D., Erbacher, J. (2012): Evolution of Middle to Late Cretaceous oceans – A 55 M.y. record of Earth's temperature and carbon cycle. Geology, 40, 107–110.

Frijia, G., Parente, M., Di Lucia, M., Mutti, M. (2015): Carbon and strontium isotope stratigraphy of the Upper Cretaceous (Cenomanian–Campanian) shallow-water carbonates of Southern Italy: Chronostratigraphic calibration of larger foraminifera biostratigraphy. Cretaceous Research, 53, 110–139.

Gabitov, R.I., Watson, E.B. (2006): Partitioning of strontium between calcite and fluid. Geochemistry, Geophysics, Geosystems, 7.

Gaillardet, J., Viers, J., Dupré, B. (2013): Trace elements in river waters. In: Holland, H.D., Turekian, K.K. (eds.): Treatise on Geochemistry. 2nd Edition. Elsevier Science, p. 225–272.

Galloway, W.E. (1989): Genetic stratigraphic sequences in basin analysis I: Architecture and genesis of flooding-surface bounded depositional units. Bulletin of the American Association of Petroleum Geologists, 73, 125–142.

Gawthorpe, R.L., Leeder, M.R. (2000): Tectonosedimentary evolution of active extensional basins. Basin Research, 12, 195–218.

Gawthorpe, R.L., Fraser, A.J., Collier, R.E.L. (1994): Sequence stratigraphy in active extensional basins: Implications for the interpretation of ancient basin-fills. Marine and Petroleum Geology, 11, 642–658.

Goddéris, Y., Le Hir, G., Macouin, M., Donnadieu, Y., Hubert-Théou, L., Dera, G., Aretz, M., Fluteau, F., Li, Z.X., Halverson, G.P. (2017): Paleogeographic forcing of the strontium isotopic cycle in the Neoproterozoic. Gondwana Research, 42, 151–162.

Grundvåg, S.A., Johannessen, E.P., Helland-Hansen, W., Plink-Björklund, P. (2014): Depositional architecture and evolution of progradationally stacked lobe complexes in the Eocene Central Basin of Spitsbergen. Sedimentology, 61, 535–569.

Haq, B.U. (2014): Cretaceous eustasy revisited. Global and Planetary Change, 113, 44–58.

Hardenbol, J., Thierry, J., Farley, M.B., Jacquin, T., de Graciansky, P.-C., Vail, P.R. (1998): Mesozoic and Cenozoic sequence chronostratigraphic framework of European basins. In: de Graciansky, P.-C., Hardenbol, J., Jacquin, T., Vail, P.R. (eds.): Mesozoic and Cenozoic Sequence Stratigraphy of European Basins. SEPM Special Publication, 60, 3–13.

Harrison, B. (1995): Russian-Style Formation Evaluation. The London Petrophysical Society & The Geological Society London.

Helland-Hansen, W., Martinsen, O.J. (1996): Shoreline trajectories and sequences: Description of variable depositional-dip scenarios. Journal of Sedimentary Research, 66, 670–688.

Hild, E., Brumsack, H.-J. (1998): Major and minor element geochemistry of Lower Aptian sediments from the NW German Basin (core Hohenegglesen KB 40). Cretaceous Research, 19, 615–633.

Hofmann, M., Linnemann, U., Voigt, T. (2013): The Upper Cretaceous section at Schmilka in Saxony (Elbsandsteingebirge, Germany) – Syntectonic sedimentation and inverted zircon age populations revealed by LA-ICP-MS U/Pb Data. Geologica Saxonica, 59, 101–130.

Hofmann, M., Voigt, T., Bittner, L., Gärtner, A., Zieger, J., Linnemann, U. (2018): Reworked Middle Jurassic sandstones as a marker for Upper Cretaceous basin inversion in Central Europe – a case study for the U–Pb detrital zircon record of the Upper Cretaceous Schmilka section and their implication for the sedimentary cover of the Lausitz. International Journal of Earth Sciences, 107, 913–932.

Hudson, J.D. (1977): Stable isotopes and limestone lithification. Journal of the Geological Society, 133, 637–660.

Heřmanová, Z., Kvaček, J. (2012): A new record pf the genus Caryanthus from the Cretaceous of South Bohemia (Czech Republic). Acta Musei Nationalis Pragae, Series B – Historia Naturalis, 68, 47–50.

Heřmanová, Z., Kvaček, J., Dašková, J. (2016): Caryanthus diversity in the Late Cretaceous. Review of Palaeobotany and Palynology, 231, 33–47.

Jarvis, I., Trabucho-Alexandre, J.P., Gröcke, D.R., Uličný, D., Laurin, J. (2015): Intercontinental correlation of organic carbon and carbonate stable isotope records: Evidence of climate and sea-level change during the Turonian (Cretaceous). The Depositional Record, 1, 53–90.

Jarvis, I., Murphy, A.M., Gale, A.S. (2001): Geochemistry of pelagic and hemipelagic sediments: Criteria for identifying systems tracts and sea-level change. Journal of the Geological Society, 158, 685–696.

Kauffman, E.G, Kennedy, W.J., Wood, C.J. (1996): The Coniacian stage and substage boundaries. Bulletin de l'Institut royal des sciences naturelles de Belgique, Sciences de la Terre, 66, 81–94.

Kędzierski, M. (2008): Calcareous nannofossil and inoceramid biostratigraphies of a Middle Turonian to Middle Coniacian section from the Opole Trough of SW Poland. Cretaceous Research, 29, 451–467.

Kędzierski, M., Uchman, A., Sawlowicz, Z., Briguglio, A. (2015): Fossilized bioelectric wire – the trace fossil Trichichnus. Biogeosciences, 12, 2301–2309.

Kim, S.-T., Coplen, T.B., Horita, J. (2015): Normalization of stable isotope data for carbonate minerals: Implementation of IUPAC guidelines. Geochimica et Cosmochimica Acta, 158, 276–289.

Klein, V., Müller, V., Valečka, J. (1979): Lithofazielle und Paläogeographische Entwicklung des Böhmischen Kreidebeckens. In. Wiedmann, J. (ed.): Aspekte Des Kreide Europas. IUGS Series A, 6, p. 435–446.

Klein, V., Růžička, M. (1990): Geologické mapování na Českolipsku (02-42 Česká Lípa). Zprávy o geologických výzkumech v roce 1988, 49–52.

Kley, J., Voigt T. (2008): Late Cretaceous intraplate thrusting in Central Europe: Effect of Africa-Iberia-Europe convergence, not alpine collision. Geology, 36, 839–842.

Kockel, F. (1986): Upper Cretaceous biostratigraphy – the key to the understanding of inversion tectonics in NW-Germany. Annales de la Société géologique de Belgique, 109, 357–361.

Kominz, M.A., Browning, J.V., Miller, K.G., Sugarman, P.J., Mizintseva, S., Scotese, C.R. (2008): Late Cretaceous to Miocene sea-level estimates from the New Jersey and Delaware coastal plain coreholes: An error analysis. Basin Research, 20, 211–226.

Kump, L.R. (1989): Alternative modeling approaches to the geochemical cycles of carbon, sulfur, and strontium isotopes. American Journal of Science, 289, 390–410.

Kumpan, T., Bábek, O., Kalvoda, J., Grygar, T.M., Frýda, J., Becker, R.T., Hartenfels, S. (2015): Petrophysical and geochemical signature of the Hangenberg Events: An integrated stratigraphy of the Devonian–Carboniferous boundary interval in the Northern Rhenish Massif (Avalonia, Germany). Bulletin of Geosciences, 90, 667–674.

Kuznetsov, A.B., Semikhatov, M.A., Gorokhov, I.M. (2012): The Sr isotope composition of the world ocean, marginal and inland seas: Implications for the Sr isotope stratigraphy. Stratigraphy and Geological Correlation, 20, 501–515.

Laurin, J., Uličný, D. (2004): Controls on a shallow-water hemipelagic carbonate system adjacent to a siliciclastic margin: Example from late Turonian of Central Europe. Journal of Sedimentary Research, 74, 697–717.

Lécuyer, C. (2016): Seawater residence times of some elements of geochemical interest and the salinity of the oceans. Bulletin de la Société Géologique de France, 187, 245–260.

Lees, J.A. (2008): The Calcareous nannofossil record across the Late Cretaceous Turonian/Coniacian boundary, including new data from Germany, Poland, the Czech Republic and England. Cretaceous Research, 29, 40–64.

Leren, B.L.S., Howell, J., Enge, H., Martinius, A.W. (2010): Controls on stratigraphic architecture in contemporaneous delta systems from the Eocene Roda Sandstone, Tremp-Graus Basin, Northern Spain. Sedimentary Geology, 229, 9–40.

Löfvendahl, R., Aberg,G., Hamilton, P.J. (1990): Strontium in rivers of the Baltic Basin. Aquatic Sciences, 52, 315–329.

Lohmann, K.C. (1988): Geochemical patterns of meteoric diagenetic systems and their application to studies of paleokarst. In: James, N.P., Choquette, P.W. (eds.): Paleokarst. Springer, New York, p. 58–80.

Macák, F. (1967): Spodní a svrchní coniak v západní části Českého středohoří. Věstník Ústředního ústavu geologického, 62, 41–43.

Macák, F., Müller, V. (1963): Svrchní coniak až santon v křídě Českého středohoří. Věstník Ústředního ústavu geologického, 30, 193–195.

Malkovský, M. (1979): Tektogeneze platformního pokryvu Českého masívu. Ústřední ústav geologický/Academia, Praha.

Martinsen, O.J., Helland-Hansen, W. (1995): Strike variability of clastic depositional systems: Does it matter for sequence-stratigraphic analysis? Geology, 23, 439–442.

Massari, F. (1996): Upper-flow-regime stratification types on steep-face, coarse-grained, Gilbert-type progradational wedges (Pleistocene, Southern Italy). Journal of Sedimentary Research, 66, 364–375.

Massari, F. (2017): Supercritical-flow structures (Backset-bedded sets and sediment waves) on high-gradient clinoform systems influenced by shallow-marine hydrodynamics. Sedimentary Geology, 360, 73–95.

Mazur, S., Scheck-Wenderoth, M. (2005): Constraints on the tectonic evolution of the Central European Basin System revealed by seismic reflection profiles from Northern Germany. Netherlands Journal of Geosciences, 84, 389–401.

McArthur, J.M., Howarth, R.J., Shields, G.A. (2012): Strontium Isotope Stratigraphy. In: Gradstein, F.M., Ogg, J.G., Schmitz, M., Ogg, G. (eds.): The Geologic Time Scale 2012. Elsevier.

McArthur, J.M., Howarth, R.J., Bailey, T.R. (2001): Strontium isotope stratigraphy: LOWESS version 3: Best fit to the marine Sr-isotope curve for 0–509 Ma and accompanying look-up table for deriving numerical age. The Journal of Geology, 109, 155–170.

McArthur, J.M., Kennedy, W.J., Chen, M., Thirlwall, M.F., Gale, A.S. (1994): Strontium isotope stratigraphy for Late Cretaceous time: Direct numerical calibration of the Sr isotope curve based on the US Western Interior. Palaeogeography, Palaeoclimatology, Palaeoecology, 108, 95–119.

McArthur, J.M., Thirlwall, M.F., Engkilde, M., Zinsmeister, W.J., Howarth, R.J. (1998): Strontium isotope profiles across K/T boundary sequences in Denmark and Antarctica. Earth and Planetary Science Letters, 160, 179–192.

McArthur, J.M., Crame, J., Thirlwall, M.F. (2000): Definition of Late Cretaceous stage boundaries in Antarctica using Strontium isotope stratigraphy. The Journal of Geology, 108, 623–640.

McCrea, J.M. (1950): On the isotopic chemistry of carbonates and a paleotemperature scale. The Journal of Chemical Physics, 18, 849–857.

Miller, K.G., Sugarman,P.J., Browning, J.V., Kominz, M.A., Hernandez, J.C., Olsson, R.K., Wright J.D., Feigenson, M.D. (2003): Late Cretaceous chronology of large, rapid sea-level changes: Glacioeustasy during the greenhouse world. Geology, 31, 585–588.

Millero, F.J., Feistel, R., Wright, D.G., McDougall, T.J. (2008): The composition of standard seawater and the definition of the reference-composition salinity scale. Deep sea research part I. Oceanographic Research Papers, 55, 50–72.

Milliman, J.D., Syvitski, J.P.M. (1992): Geomorphic/tectonic control of sediment discharge to the ocean: The importance of small mountainous rivers. The Journal of Geology, 100, 525–544.

Mitchell, A.J., Uličný, D., Hampson, G.J., Allison, P.A., Gorman, G.J., Piggott, M.D., Wells, M.R., Pain, C.C. (2010): Modelling tidal current-induced bed shear stress and palaeocirculation in an epicontinental seaway: The Bohemian Cretaceous Basin, Central Europe. Sedimentology, 57, 359–388.

Morehead, M.D., Syvitski, J.P.M. (1999): River-plume sedimentation modeling for sequence stratigraphy: Application to the Eel Margin, northern California. Marine Geology, 154, 29–41.

Mortimore, R.N. (2018): Late Cretaceous tectonosedimentary events in NW Europe. Proceedings of the Geologists' Association, 129, 392–420.

Mortimore, R.N., Pomerol, B. (1997): Upper Cretaceous tectonic phases and end Cretaceous inversion in the Chalk of the Anglo-Paris Basin. Proceedings of the Geologists' Association, 108, 231–255.

Mortimore, R.N., Wood, C.J., Pomerol, B., Ernst, G. (1998): Dating the phases of the Subhercynian tectonic epoch: Late Cretaceous tectonics and eustatics in the Cretaceous Basins of Northern Germany compared with the Anglo-Paris Basin. Zentralblatt für Geologie und Paläontologie, Teil I, 1996, 1349–1401.

Mulder, T., Syvitski, J.P.M. (1995): Turbidity currents generated at river mouths during exceptional discharges to the world oceans. The Journal of Geology, 103, 285–299.

Mulder, T., Alexander, J. (2001): The physical character of subaqueous sedimentary density flow and their deposits. Sedimentology, 48, 269–299.

Mulder, T., Syvitski,J.P.M., Migeon, S., Faugères, J.-C., Savoye, B. (2003): Marine hyperpycnal flows: Initiation, behavior and related deposits. A review. Marine and Petroleum Geology, 20, 861–882.

Mutti, E. (1985): Turbidite systems and their relations to depositional sequences. In: Zuffa, G.G. (ed.): Provenance of Arenites. Reidel Publishing Company, Dordrecht, p. 65–93.

Nádaskay, R., Čech, S., Švábenická, L., Valečka, J. (2017): Stratigraphy of the Lower–Middle Coniacian section (NW-part of the Bohemian Cretaceous Basin): Deciphering T-R history and linking offshore to proximal deposits. In: Sames, B. (ed.): 10th International Symposium on the Cretaceous – Abstracts, 21–26 August 2017, Vienna. Berichte der Geologischen Bundesanstalt, 120, p. 192.

Nádaskay, R., Uličný, D. (2014): Genetic stratigraphy of Coniacian deltaic deposits of the northwestern part of the Bohemian Cretaceous Basin. Zeitschrift der Deutschen Gesellschaft für Geowissenschaften, 165, 547–575.

Nádaskay, R., Valečka, J., Čech, S. (2018): Stratigrafie, sedimentární prostředí a tektonická stavba tzv. kozelského pískovcového tělesa v severozápadní části české křídové pánve. Zprávy o geologických výzkumech, 51, 167–180.

Nemec, W. (1990): Aspects of sediment movement on steep delta slopes. In: Colella, A., Prior, D.B. (eds.): Coarse-Grained Deltas. Blackwell Publishing, Oxford, p. 29–73.

Nemec, W. (1995): The dynamics of deltaic suspension plumes. In: Oti, M.N., Postma, G. (eds.): Geology of Deltas. A.A. Balkema, Rotterdam, p. 31–93.

Niebuhr, B., Baldschuhn, R., Ernst, G., Walaszczyk, I., Weiss, W., Wood, C.J. (1999): The Upper Cretaceous succession (Cenomanian–Santonian) of the Staffhorst shaft, Lower Saxony, northern Germany: Integrated biostratigraphic, lithostratigraphic and downhole geophysical log data. Acta Geologica Polonica, 49, 175–213.

Oehlert, A.M., Swart P.K. (2014): Interpreting carbonate and organic carbon isotope covariance in the sedimentary record. Nature Communications, 5, 1–7.

Olde, K., Jarvis, I., Uličný, D., Pearce, M.A., Trabucho-Alexandre, J.P., Čech, S., Gröcke, D.R., Laurin, J., Švábenická, L., Tocher, B.A. (2015): Geochemical and palynological sea-level proxies in hemipelagic sediments: A critical assessment from the Upper Cretaceous of the Czech Republic. Palaeogeography, Palaeoclimatology, Palaeoecology, 435, 222–243.

Pawellek, F., Frauenstein, F., Veizer, J. (2002): Hydrochemistry and isotope geochemistry of the Upper Danube river. Geochimica et Cosmochimica Acta, 66, 3839–3853.

Pin, C., Gannoun, A., Dupont, A. (2014): Rapid, simultaneous separation of Sr, Pb, and Nd by extraction chromatography prior to isotope ratios determination by TIMS and MC-ICP-MS. Journal of Analytical Atomic Spectrometry, 29, 1858–1870.

Plint, A.G., Hooper, E.A., Grifi, M.D., Walaszczyk, I., Landman, N.H., Gröcke, D.R., Trabucho-Alexandre, J.P., Jarvis, I. (2017): Chapter 1: Integrated, high-Resolution allostratigraphic, biostratigraphic and carbon-isotope correlation of Coniacian strata (Upper Cretaceous), western Alberta and northern Montana. Bulletin of the American Museum of Natural History, 2017, 9–53.

Posamentier, H.W., Vail, P. R. (1988): Eustatic controls on clastic deposition II – Sequence and systems tract models. In: Wilgus, C.K., Hastings, B.S., Ross, C.A., Posamentier, H., Van Wagoner, J., Kendall, C.G.St.C. (eds.): Sea-Level Changes; an Integrated Approach: Society for Sedimentary Geology. SEPM Special Publication, 42, 125–154.

Postma, G., Cartigny, M.J.B. (2014): Supercritical and subcritical turbidity currents and their deposits – A synthesis. Geology, 42, 987–990.

Postma, G., Kleverlaan, K., Cartigny, M.J.B. (2014): Recognition of cyclic steps in sandy and gravelly turbidite sequences, and consequences for the Bouma facies model. Sedimentology, 61, 2268–2290.

Rachold, V., Brumsack, H.-J. (2001): Inorganic geochemistry of Albian sediments from the Lower Saxony Basin NW Germany: Palaeoenvironmental constraints and orbital cycles. Palaeogeography, Palaeoclimatology, Palaeoecology, 174, 121–143.

Rapprich, V., Kochergina, Y.V., Magna, T., Laufek, F., Halodová, P., Bůzek, F. (2017): Carbonate-rich dyke in Roztoky Intrusive Complex – An evidence for carbonatite magmatism in the Eger Rift? Journal of Geosciences, 62, 121–136.

Richardt, N., Wilmsen, M. (2012): Lower Upper Cretaceous standard section of the southern Münsterland (NW Germany): Carbon stable-isotopes and sequence stratigraphy. Newsletters on Stratigraphy, 45, 1–24.

Richter, F.M., Rowley, D.B., DePaolo, D.J. (1992): Sr isotope evolution of seawater: The role of tectonics. Earth and Planetary Science Letters, 109, 11–23.

Rider, M. H. (1996): The Geological Interpretation of Well Logs, 2nd edition. Whittles Publishing, Caithness.

Rimoldi, B., Alexander, J., Morris, S. (1996): Experimental turbidity currents entering density-stratified water: Analogues for turbidites in Mediterranean hypersaline basins. Sedimentology, 43, 527–540.

Sageman, B.B., Lyons, T.W. (2005): Geochemistry of fine-grained sediments and sedimentary rocks. In: MacKenzie, F.T. (ed.): Sediments, Diagenesis, and Sedimentary Rocks. Treatise on Geochemistry, 7. Amsterdam, Elsevier, p. 115–158.

Scupin, H. (1936): Zur Palaeographie des sudetischen Kreidemeeres. Zeitschrift der Deutschen Gesellschaft für Geowissenschaften, 88, 309–325.

Shamrock, J.L., Watkins, D.K. (2009): Evolution of the cretaceous calcareous nannofossil genus Eiffellithus and its biostratigraphic significance. Cretaceous Research, 30, 1083–1102.

Shanmugam, G., Moiola, R.J. (1988): Submarine fans : Characteristics, models, classification, and reservoir potential. Earth Science Reviews, 24, 383–428.

Shields, G., Veizer, J. (2002): Precambrian marine carbonate isotope database: Version 1.1. Geochemistry, Geophysics, Geosystems, 3, 1–12.

Scheck, M., Bayer, U., Otto, V., Lamarche, J., Banka, D., Pharaoh, T. (2002): The Elbe Fault System in north central Europe – a basement-controlled zone of crustal weakness. Tectonophysics, 360, 281–299.

Schieber, J. (2016): Mud re-distribution in epicontinental basins – exploring likely processes. Marine and Petroleum Geology, 71, 119–133.

Schmitz, B. (1987): The TiO_2/Al_2O_3 ratio in the Cenozoic Bengal Abyssal Fan sediments and its use as a paleostream energy indicator. Marine Geology, 76, 195–206.

Schröder, B. (1987): Inversion tectonics along the western margin of the Bohemian Massif. Tectonophysics, 137, 93–100.

Sissingh, W. (1977): Biostratigraphy of Cretaceous calcareous nannoplankton. Geologie en Mijnbouw, 56, 3–65.

Skoček, V., Valečka, J. (1983): Paleogeography of the Late Cretaceous Quadersandstein of Central Europe. Palaeogeography, Palaeoclimatology, Palaeoecology, 44, 71–92.

Sparks, R.S.J., Bonnecaze, R.T., Huppert, H.E., Lister, J.R., Hallworth, M.A., Mader, H., Phillips, J. (1993): Sediment-laden gravity gurrents with reversing buoyancy. Earth and Planetary Science Letters, 114, 243–257.

Spencer, D.W., Degens, E.T., Kulbicki, G. (1967): Factors affecting element distributions in sediments. In: Ahrens, L.H. (ed.): Origin and Distribution of the Elements. Pergamon Press, New York, p. 981–998.

Steuber, T. (2001): Strontium isotope stratigraphy of Turonian–Campanian Gosau-type Rudist formations in the Northern Calcareous and Central Alps (Austria and Germany). Cretaceous Research, 22, 429–441.

Steuber, T., Korbar, T., Jelaska, V., Gušić I. (2005): Strontium-isotope stratigraphy of Upper Cretaceous platform carbonates of the Island of Brač (Adriatic Sea, Croatia): Implications for global correlation of platform evolution and biostratigraphy. Cretaceous Research, 26, 741–756.

Stille, H. (1924): Grundfragen der vergleichenden Tektonik. Gebrüder Borntraeger, Berlin.

Svobodová, A., Košťák, M., Čech, S., Švábenická, L. (2014): New biostratigraphic evidence (Texanitid ammonites, inoceramids and calcareous nannofossils) for the Upper and the uppermost Coniacian in the Bohemian Cretaceous Basin. Zeitschrift der Deutschen Gesellschaft für Geowissenschaften, 165, 577–589.

Swart, P.K. (2015): The geochemistry of carbonate diagenesis: The past, present and future. Sedimentology, 62, 1233–1304.

Štaffen, Z. (2002): Chemostratigraphic determination of equivalent strata and formations in Bohemian Cretaceous Basin. Acta Montana, Ser. A, 21, 77–109.

Švábenická, L. (2010): Svrchní turon a hranice turon-coniac na základě studia vápnitých nanofosilií v jizerském vývoji české křídové pánve. Zprávy o geologických výzkumech, 43, 58–64.

Švábenická, L., Valečka, J. (2011): Pelitická facie v nadloží pískovcového tělesa Příhrazských skal, severovýchodní Čechy (litologie a biostratigrafie na základě studia vápnitých nanofosilií). Zprávy o geologických výzkumech, 44, 50–56.

Švábenická, L. (1999): Braarudosphaera-rich sediments in the Turonian of the Bohemian Cretaceous Basin, Czech Republic. Cretaceous Research, 20, 773–782.

Švábenická, L. (2012): Nannofossil record across the Cenomanian–Coniacian interval in the Bohemian Cretaceous Basin and Tethyan foreland basins (Outer Western Carpathians), Czech Republic. Geologica Carpathica, 63, 201–217.

Švábenická, L., Bubík, M. (2014): Biostratigraphical correlations of the calcareous nannofossil Marthasterites furcatus in the Bohemian Cretaceous Basin and Outer Flysch Carpathians, Czech Republic. Cretaceous Research, 51, 386–398.

Švábenická, L., Havlíček, P. (2017): Acme Marthasterites furcatus jako indikátor hranice turon-coniaku a spodního coniaku v jizerském vývoji české křídové pánve. Zprávy o geologických výzkumech, 50, 111–116.

Švábenická, L., Kycl, P., Rapprich, V. (2016): Stratigraficky nejmladší vápnité nanofosilie v sedimentech české křídové pánve. Zprávy o geologických výzkumech, 49, 19–25.

Talling, P.J., Masson, D.G., Sumner, E.J., Malgesini, G. (2012): Subaqueous sediment density flows: Depositional processes and deposit types. Sedimentology, 59, 1937–2003.

Taylor, A.M., Goldring, R. (1993): Description and analysis of bioturbation and ichnofabric. Journal of the Geological Society, 150, 141–148.

Taylor, S.R., McLennan, S.M. (1995): The geochemical evolution of the continental crust. Reviews in Geophysics, 33, 241–265.

Tichomirowa, M., Heidel, C., Junghans, M., Haubrich, F., Matschullat, J. (2010): Sulfate and strontium water source identification by O, S and Sr Isotopes and their temporal changes (1997–2008) in the region of Freiberg, central-eastern Germany. Chemical Geology, 276, 104–118.

Uličný, D. 2001. Depositional systems and sequence stratigraphy of coarse-grained deltas in a shallow-marine, strike-slip setting: The Bohemian Cretaceous Basin, Czech Republic. Sedimentology, 48, 599–628.

Uličný, D., Jarvis, I., Gröcke, D.R., Čech, S., Laurin, J., Olde, K., Trabucho-Alexandre, J.P., Švábenická, L., Pedentchouk, N. (2014): A high-resolution carbon-isotope record of the Turonian stage correlated to a siliciclastic basin fill: Implications for mid-Cretaceous sea-level change. Palaeogeography, Palaeoclimatology, Palaeoecology, 405, 42–58.

Uličný, D., Laurin, J. (2001): Well-log based correlation of Turonian through Lower Coniacian depositional systems in the western part of the Bohemian Cretaceous Basin: New basis for reconstructing the basin history. Geolines, 13, 121.

Uličný, D., Špičáková, L., Cajz, V., Hronec, L. (2015): Podklady pro prostorový model hydrogeologicky významných stratigrafických rozhraní ve vybraných Hydrogeologických Rajonech. Geofyzikální Ústav AV ČR. Závěrečná zpráva. Česká geologická služba, Praha.

Uličný, D., Čech, S., Grygar, R. (2003): Tectonics and depositional systems of a shallow-marine, intra-continental strike-slip casin : Exposures of the Český Ráj region, Bohemian Cretaceous Basin. Geolines, 16, 133–148.

Uličný, D., Hladíková, J., Hradecká, L. (1993): Record of sea-level changes, oxygen depletion and the $\delta^{13}C$ anomaly across the Cenomanian–Turonian boundary, Bohemian Cretaceous Basin. Cretaceous Research, 14, 211–234.

Uličný, D., Hladíková, J., Attrep M.J., Čech, S., Hradecká, L., Svobodová, M. (1997): Sea-level changes and geochemical anomalies across the Cenomanian–Turonian boundary: Pecínov quarry, Bohemia. Palaeogeography Palaeoclimatology Palaeoecology, 132, 265–285.

Uličný, D., Laurin, J., Čech, S. (2009a): Controls on clastic sequence geometries in a shallow-marine, transtensional basin: The Bohemian Cretaceous Basin, Czech Republic. Sedimentology, 56, 1077–1114.

Uličný, D., Špicáková, L., Grygar, R., Svobodová, M., Čech, S., Laurin, J. (2009b) Palaeodrainage systems at the basal unconformity of the Bohemian Cretaceous Basin: Roles of inherited fault systems and basement lithology during the onset of basin filling. Bulletin of Geosciences, 84, 577–610.

Vacková, L. (2010): Architektury, stratigrafie a sedimentární režim pískovcových těles svrchního turonu v severozápadní části české křídové pánve. Unpublished PhD. thesis. Charles University, Prague.

Vacková, L., Uličný, D., 2011. Sedimentary record of increased subsidence and supply rates during the late Turonian, Bohemian Cretaceous Basin (Czech Republic). In: Travaux Géophysiques XL. Abstracts of the 9th Central European Tectonic Groups Meeting, p. 90.

Vail, P.R., Audemard, F., Bowman, S.A, Eisner, P.N., Perez-Cruz, C. (1991): The stratigraphic signatures of tectonics, eustasy and sedimentology – an overview. In: Einsele, G., Ricken, W., Seilacher, A. (eds.): Cycles and Events in Stratigraphy, Springer–Verlag, Berlin, New York, p. 617–659.

Vakarelov, B.K., Bhattacharya, J.P. (2009): Local tectonic control on parasequence architecture: Second Frontier Sandstone, Powder River Basin, Wyoming. AAPG Bulletin, 93, 295–327.

Valečka, J. (1979a): Paleogeografie a litofaciální vývoj severozápadní části české křídové pánve. Sborník geologických věd, Geologie, 33, 47–81.

Valečka, J. (1979b): Barier island in the Bohemian Upper Cretaceous Basin. Časopis pro mineralogii a geologii, 24, 175–184.

Valečka, J. (1994): Litologické změny v nejvyšší části jizerského souvrství v ssv. okolí České Kamenice a jejich vztah k paleoproudovému režimu. Zprávy o geologických výzkumech, 1993, 96–97.

Valečka, J., Rejchrt, M. (1973): Litologie a geneze tzv. flyšoidní facie coniaku ve východní části Českého středohoří. Časopis pro mineralogii a geologii, 18, 379–391.

Varban, B.L., Plint, A.G. (2008): Sequence stacking patterns in the Western Canada Foredeep: influence of tectonics, sediment loading and eustasy on deposition of the Upper Cretaceous Kaskapau and Cardium formations. Sedimentology, 55, 395–421.

Veizer, J., Ala, D., Azmy, K., Bruckschen, P., Buhl, D., Bruhn, F., Carden, G.F., Diener, A., Ebneth, S., Godderis, Y., Jasper, T., Korte, C., Pawellek, F., Podlaha, O.G., Strauss, H. (1999): $^{87}Sr/^{86}Sr$, $\delta^{13}C$ and $\delta^{18}O$ Evolution of Phanerozoic Seawater. Chemical Geology, 161, 59–88.

Vejbæk, O.V., Andersen, C. (2002): Post mid-Cretaceous inversion tectonics in the Danish Central Graben – Regionally synchronous tectonic events? Bulletin of the Geological Society of Denmark, 49, 139–44.

Vodrážka, R., Sklenář, J., Čech, S., Laurin, J., Hradecká, L. (2009): Phosphatic intraclasts in shallow-water hemipelagic strata: A source of palaeoecological, taphonomic and biostratigraphic data (Upper Turonian, Bohemian Cretaceous Basin). Cretaceous Research, 30: 204–222.

Voigt, E. (1963): Über Randtröge vor Schollenrändern und ihre Bedeutung im Gebiet der mitteleuropäischen Senke und angrenzender Gebiete. Zeitschrift der Deutschen Gesellschaft für Geowissenschaften, 114, 378–418.

Voigt, S., Wagreich, M., Surlyk, F., Walaszczyk, I., Uličný, D., Čech, S., Voigt T., Wiese, F., Wilmsen, M., Niebuhr, B., Reich, M., Funk, H., Michalík, J., Jagt, J.W.M., Felder, P.J., Schulp, A.S. (2008): Cretaceous. In: McCann, T. (ed.): Geology of Central Europe, Volume 2: Mesozoic and Cenozoic. Geological Society, London, p. 923–997.

Voigt, T. (1994): Faziesentwicklung und Ablagerungssequenzen am Rand eines Epikontinentalmeeres – Die Sedimentationsgeschichte der Sächsischen Kreide. Unpublished PhD. thesis, TU Bergakademie Freiberg.

Voigt, T. (2009): Die Lausitzer-Riesengebirgs-Antiklinalzone als kreidezeitliche Inversionsstruktur: Geologische Hinweise aus den umgebenden Kreidebecken. Zeitschrift füt geologische Wissenschaften, 37: 15–39.

Voigt, T., Wiese, F., von Eynatten, H., Franzke, H.-J., Gaupp, R. (2006): Facies evolution of syntectonic Upper Cretaceous deposits in the Subhercynian Cretaceous Basin and adjoining areas (Germany). Zeitschrift der Deutschen Gesellschaft für Geowissenschaften, 157, 203–243.

von Eynatten, H., Voigt, T., Meier, A., Franzke, H.-J., Gaupp, R. (2008): Provenance of Cretaceous clastics in the Subhercynian Basin: Constraints to exhumation of the Harz Mountains and timing of inversion tectonics in Central Europe. International Journal of Earth Sciences, 97, 1315–1330.

Walaszczyk, I. (1996): Inoceramids from Kreibitz-Zittauer area (Saxony and Northern Bohemia): Revision of Andert's (1911) descriptions. Paläontologische Zeitschrift, 70, 367–392.

Walaszczyk, I., Shank, J.A., Plint, A.G., Cobban, W.A. (2014): Interregional correlation of disconformities in Upper Cretaceous strata, Western Interior Seaway: Biostratigraphic and sequence-stratigraphic evidence for eustatic change. Bulletin of the Geological Society of America, 126, 307–316.

Walaszczyk, I., Tröger, K.-A. (1996): The species Inoceramus frechi (Bivalvia, Cretaceous); Its characteristics, formal status, and stratigraphical position. Paläontologische Zeitschrift, 70, 393–404.

Walaszczyk, I., Wood, C.J. (1998): Inoceramids and biostratigraphy at the Turonian/Coniacian boundary; based on the Salzgitter-Salder Quarry, Lower Saxony, Gemany, and the Słupia Nadbrzeżna section, Central Poland. Acta Geologica Polonica, 48, 395–434.

Walaszczyk, I., Wood, C.J., Lees, J.A., Peryt, D., Voigt, S., Wiese, F. (2010): The Salzgitter-Salder quarry (Lower Saxony, Germany) and Słupia Nadbrzeżna river cliff section (central Poland): A proposed candidate composite global boundary stratotype section and point for the Coniacian stage (Upper Cretaceous). Acta Geologica Polonica, 60, 445–447.

Walaszczyk, I., Wood, C.J. (2018): Inoceramid bivalves from the Coniacian (Upper Cretaceous) of the Staffhorst shaft (Lower Saxony, Germany) – Stratigraphical significance of a unique succession. Cretaceous Research, 87, 226–240.

Wedepohl, K.H. (1971): Environmental influences on the chemical composition of shales and clays. Physics and Chemistry of the Earth, 8, 307–333.

Whiticar, M.J. (1999): Carbon and hydrogen isotope systematics of bacterial formation and oxidation of methane. Chemical Geology, 161, 291–314.

Wilson, R.D., Schieber, J. (2014): Muddy prodeltaic hyperpycnites in the Lower Genesee Group of central New York, USA: Implications for mud transport in epicontinental seas. Journal of Sedimentary Research, 84, 866–874.

Wintsch, R.P., Kvale, C.M. (1994): Differential mobility of elements in burial diagenesis of siliciclastic rocks. Journal of Sedimentary Research. 64, 349–361.

Xi, D., Cao, W., Cheng, Y., Jiang, T., Jia, J., Li, Y., Wan, X. (2016): Late Cretaceous biostratigraphy and sea-level change in the southwest Tarim Basin. Palaeogeography, Palaeoclimatology, Palaeoecology, 441, 516–527.

Young, G.M, Nesbitt, H.W. (1998): Processes controlling the distribution of Ti and Al in weathering profiles, siliciclastic sediments and sedimentary rocks. Journal of Sedimentary Research, 68, 448–455.

Zabel, M., Bickert, T., Dittert, L. (1999): Significance of the sedimentary Al:Ti ratio as an indicator for variations in the circulation patterns of the equatorial North Atlantic. Paleoceanography, 14, 789–799.

Zavala, C., Arcuri, M., Blanco Valiente, L. (2012): The importance of plant remains as diagnostic criteria for the recognition of ancient hyperpycnites. Revue de Paléobiologie, 31, 457–469.

Zavala, C., Arcuri, M., Di Meglio, M., Gamero Diaz, H., Contreras, C. (2011): A genetic facies tract for the analysis of sustained hyperpycnal flow deposits. AAPG Studies in Geology, 61, 31–52.

Ziegler, P.A. (1990): Geological Atlas of Western and Central Europe. 2nd edition. Shell International Petroleum Maatschappij B.V., The Hague.

Ziegler, P.A., Cloetingh, S., van Wees, J.-D. (1995): Dynamics of intra-plate compressional deformation: The Alpine Foreland and other examples. Tectonophysics, 252, 7–59.

Ziveri, P., Stoll, H., Probert, I., Klaas, C., Geisen, M., Ganssen, G., Young, J. (2003): Stable isotope 'vital effects' in coccolith calcite. Earth and Planetary Science Letters, 210, 137–149.

Chapter 3

Deciphering the Late Paleozoic to Mesozoic tectonosedimentary evolution of the northern Bohemian Massif from detrital zircon geochronology and heavy mineral provenance

by Roland Nádaskay, Jiří Žák, Jiří Sláma,

Tamara Sidorinová and Jaroslav Valečka

"Mein Sohn! Nichts in der Welt ist unbedeutend.
Das Erste aber und Hauptsächlichste
Bei allem ird'schen Ding ist ***Ort*** und ***Stunde***."

"My son, there's nothing insignificant,
Nothing! But yet in every earthly thing
First and most principal is ***place*** and ***time***."

Friedrich Schiller:
Die Piccolomini ('Wallenstein' trilogy)

Key words

Basin inversion; Bohemian Cretaceous Basin; Detrital zircon geochronology; Heavy mineral provenance; Intra-plate stress; U–Pb LA-ICP-MS

Abstract

From Permian to Late Cretaceous, the northern Bohemian Massif experienced a complex intra-plate tectonosedimentary evolution involving development of at least four generations of sedimentary basins in different settings. We examine this protracted evolution using stratigraphic changes in sediment provenance, analyzed through heavy mineral assemblages and U–Pb detrital zircon geochronology (by laser ablation ICP-MS) in Permian, Jurassic, and Late Cretaceous successions. The provenance data point to multiple, temporally evolving sources ranging from local (e.g., the 'West Sudetic Island') through more distant from elsewhere in the Bohemian Massif to exotic, likely derived from Baltica. The latter is interpreted as a trace of now completely eroded Late Jurassic to Early Cretaceous basin that once covered the Lusatian (Lausitz) Block and received the Baltica-derived detritus from northerly fluvial and deltaic depositional systems. We suggest that fill of this basin was recycled into the Bohemian Cretaceous Basin during progressive unroofing of the West Sudetic Island. A time-slice reconstruction of the paleogeographic and tectonosedimentary evolution of the northern Bohemian Massif is then developed to show that periods of basin development and deposition (early Permian, late early Permian to Early Triassic, Middle Jurassic–Early Cretaceous, Late Cretaceous) were interrupted by major depositional gaps (Middle Triassic–Early Jurassic, mid-Cretaceous, post-early Campanian). The Mesozoic depositional episodes resulted from reactivation of major NW–SE

strike-slip fault zones due to stress transfer from the North Atlantic Rift during Jurassic to Early Cretaceous, overridden by the far-field effect of convergence of Iberia, Africa, and Europe during Late Cretaceous.

Introduction

The northern foreland of the Alpine orogenic belt is underlain by the Variscan lithosphere, which contains extensively reworked Neoproterozoic (Cadomian) and Lower Paleozoic crustal components (Fig. 1a; e.g., Edel and Weber 1995; Franke 2000, 2006; Winchester et al. 2006; Schulmann et al. 2009; Nance et al. 2010; Kroner and Romer 2013). From the late Carboniferous to recent, the Variscan basement north of the Alps recorded multiple phases of intraplate tectonic deformation caused by diverse geodynamic processes and related far-field plate-boundary forces (e.g., Ziegler 1990a; Brink et al. 1992; Mattern 2001; Ventura and Lisker 2003; Nielsen et al. 2005, 2007; Kley and Voigt 2008; Reicherter et al. 2008; Scheck-Wenderoth et al. 2008; Coubal et al. 2015; Meier et al. 2016). In general, such forces are sufficient to produce intraplate compressional structures, reactivate inherited basement faults, and control basin development in orogenic forelands (e.g., Hayward and Graham 1989; Ziegler 1990b; Ziegler et al. 1995, 1998; Marshak and Paulsen 1996; van der Pluijm et al. 1997; Cloetingh et al. 2007).

In brief, the main intraplate tectonic events recorded in Western and Central Europe included: (1) a late Carboniferous to earliest Triassic phase driven by relative dextral motion of Gondwana and Laurussia (e.g., Arthaud and Matte 1977; Dallmeyer et al. 1995; Pastor-Galán 2015); (2) a Triassic phase related to subduction of the Paleotethys Ocean (e.g., Ziegler 1989; Golonka et al. 2000; Stampfli et al. 2002); and (3) a Jurassic to Cenozoic phase linked to the broadly coeval opening of the North- and Mid-Atlantic rift, thrusting in the Alpine orogenic belt, and changes in the relative motions between the European, African, and Iberian plates (e.g., Illies 1975; Ziegler 1987, 1990; Bergerat 1987; Le Pichon et al. 1988; Dewey et al. 1989; Giraud and Bosworth 1999; Scheck and Bayer 1999; Kley and Voigt 2008; Schmid et al. 2008).

One of the major consequences of the Mesozoic to Cenozoic intraplate tectonic phases were vertical crustal motions in the Alpine foreland. These motions involved exhumation and surface uplift generated by compression and subsidence and basin development, the latter often related to extensional graben formation or pull-apart structures along strike-slip faults (e.g., Lake and Karner 1987; Liboriussen et al. 1987; Norling and Bergström 1987; Tucker and Arter 1987; van Wijhe 1987; Voigt et al. 2006). Particularly during the Late Cretaceous (Fig. 1b), the development of sedimentary basins occurred in coincidence with global sea-level changes and
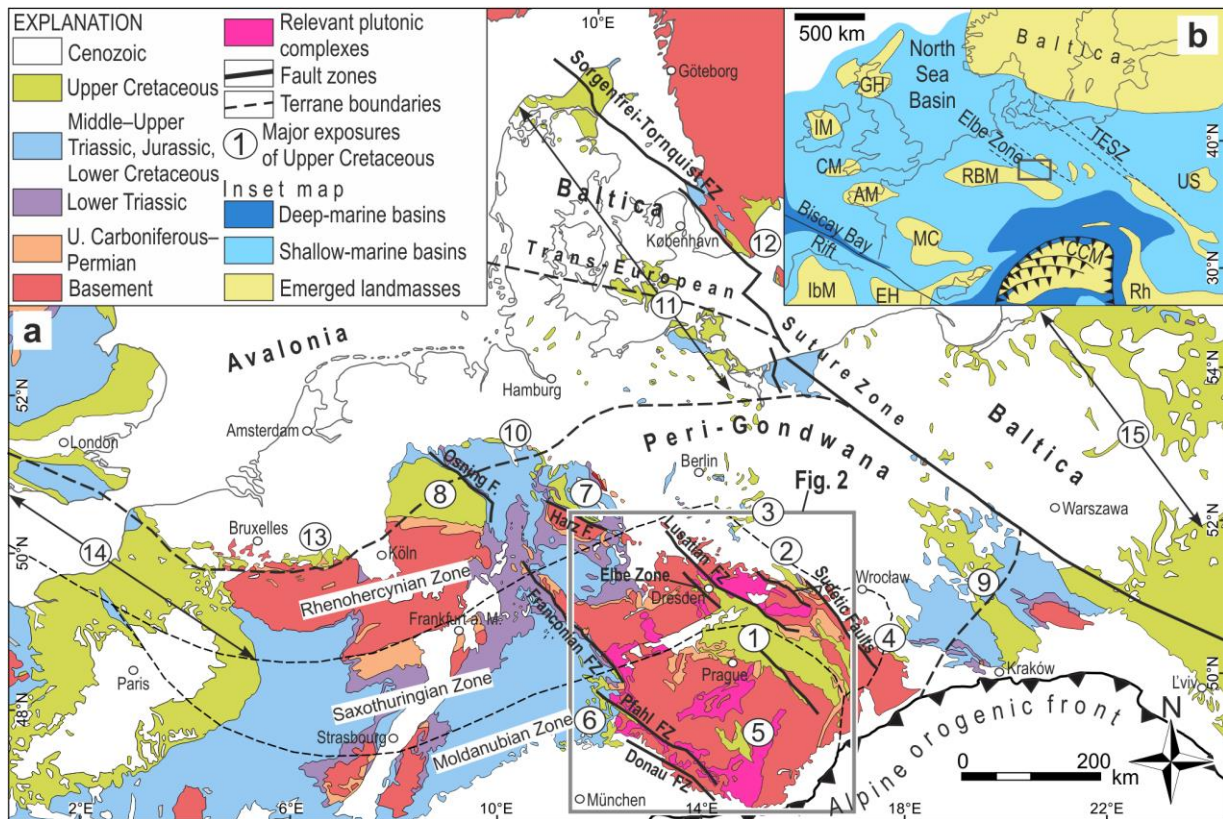
Figure 1. (a) Map of the central Europe (modified after Asch 2005) showing major exposures of Upper Cretaceous rocks: (1) Bohemian Cretaceous Basin, (2) North Sudetic Basin, (3) East Brandenburg Basin, (4) Opole Basin, (5) Southern Bohemian basins, (6) Braunau–Regensburg Basin, (7) Subhercynian Basin, (8) Münsterland Basin, (9) Mid-Polish Trough, (10), Hannover area and Damme Basin, (11) Danish Trough, (12) Scania region, (13) Liège–Limburg Basin, (14) Anglo–Paris Basin, (15) Pomerania–Warsaw–Lublin–Lviv Synclinorium. Geological units with pre-Upper Cretaceous rocks that may have served as source areas during Late Cretaceous include: (i) igneous, metamorphic, and (meta-)sedimentary basement of Proterozoic, Lower Paleozoic, and Lower Carboniferous age; (ii) Upper Carboniferous–Permian fill of early post-Variscan basins; (iii) Lower Triassic; (iv) Middle–Upper Triassic, Jurassic and Lower Cretaceous. The Bohemian Massif is highlighted; close-up view on the study area is in Fig. 3. **(b)** Inset map depicting the Late Cretaceous (Turonian) palaeogeography of the Western and Central Europe (modified after Janetschke and Wilmsen 2014). Position of the Bohemian Cretaceous Basin (BCB) highlighted. Emerged landmasses: AM – Armorican Massif, CM – Cornubian Massif, CCM – Central Carpathian Massif, EH – Ebro High, GH – Grampian High, IM – Irish Massif, IbM – Iberian Massif, MC – Massif Central, RBM – Rhenohercynian–Bohemian Massif, Rh – Rhodope, US –Ukrainian Shield.

marine transgressive–regressive cycles at different scales (e.g., Voigt et al. 2006; Uličný et al. 2009a,b, 2014; Wilmsen et al. 2010; Niebuhr et al. 2011; Janetschke and Wilmsen 2014). In addition, temporal changes in the intraplate stress fields themselves are able to cause short-term, relative sea-level variations (e.g., Cloethingh et al. 1985; Cloethingh 1986). Therefore, a number of recent studies pointed to a rather complex picture of the interaction between the eustatic sea-level changes and intra-plate crustal deformations during the Cretaceous Period (e.g., Voigt et al. 2004, 2006; Mortimore 2018).

Although well-known from the Mesozoic basins of Western Europe (e.g., Kockel 1986; Betz et al. 1987; Mortimore 1986, 2018; Mortimore and Pomerol 1997; Mortimore et al. 1998;

160

Vejbæk and Andersen 2002), the sedimentary response to post-Variscan intra-plate deformation still remains poorly understood in basins of the Bohemian Massif and vicinity. For instance, Hofmann et al. (2018) demonstrated that sedimentary basins formed diachronously in the northern Bohemian Massif during Late Jurassic to Early Cretaceous (Fig. 1), but were later completely destructed by subsequent tectonic processes and their fill was recycled into younger basins over a relatively short time span.

The purpose of this paper is to examine the post-Variscan, Late Paleozoic to Late Cretaceous tectonosedimentary evolution of the northern Bohemian Massif as a case example of complex intra-plate movements in the Alpine foreland. We present new heavy mineral analyses and detrital zircon ages from the Bohemian Cretaceous Basin as well as from the underlying successions (Figs. 3, 4) to interpret the source areas and their changes through time. Expanding on previous studies of Voigt (1994, 2009) and Hofmann et al. (2013, 2018), we then put our interpretations into a broader context and discuss the role of intra-plate tectonic movements in the basin development, inversion, and rapid recycling during the Mesozoic times.

Geological setting

The northern part of the Bohemian Massif represents a complex mosaic of uplifted basement blocks and intervening sedimentary basins of Late Paleozoic to Mesozoic age (Figs. 1, 2). The basement blocks are made up of a Upper Neoproterozoic (Ediacaran) metasedimentary succession (the Lausitz Group) intruded by ca. 540 Ma Ma granite plutons (Zieger et al. 2018 and references therein). The overlaying, post-Variscan sedimentary successions examined in this study are as follows (Fig. 3).

Carboniferous–Permian continental successions

The Carboniferous–Permian successions make up the Česká Kamenice Basin, largely concealed beneath younger deposits (Fig. 3; the subcrop area is about 300 km²; Pešek 2001) and strongly deformed slivers along the Lusatian Fault (labelled 'CP' in Fig. 3). The basin is filled with an up to 620 m thick succession of alternating mudstones, sandstones, and conglomerates with intercalations of basic to intermediate volcanic and volcaniclastic rocks, Gzhelian–Asselian in age. They were deposited in a high-energy, braided fan to fluvial environment, which evolved into alluvial and lacustrine (e.g., Štolfová 2004; Martínek et al. 2006). The deformed slivers, only several tens of meters long and with a reduced stratigraphic range ('Saxonian', i.e., Sakmarian–Artinskian), are composed of alternating sandstones and conglomerates with intercalations of volcanic and volcaniclastic rocks (e.g., Fediuk et al. 1958). It has been assumed that they once formed a single depositional space with the Česká Kamenice Basin (cf. Coubal et al. 2014).
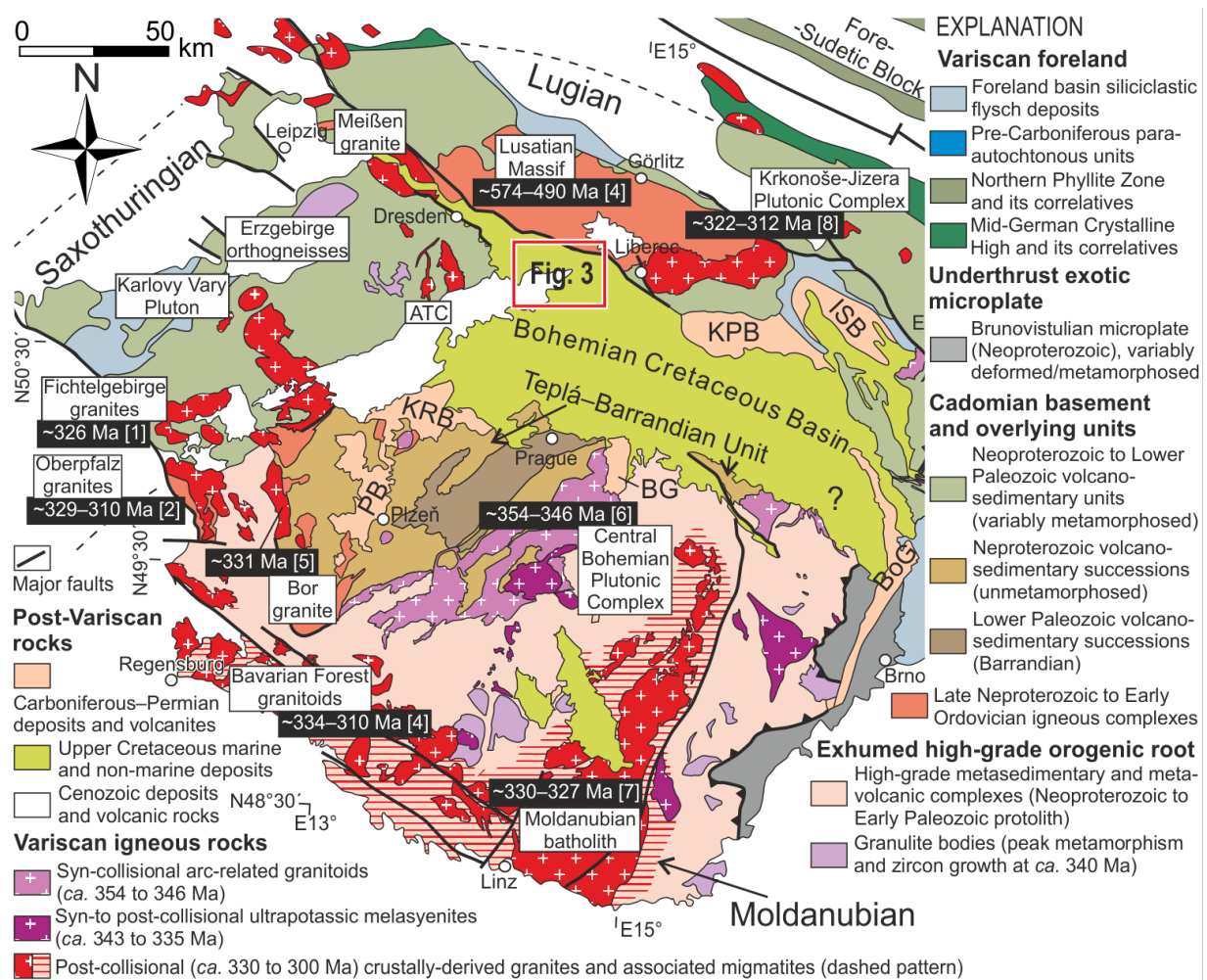
Figure 2. Simplified geological map showing the main zones and lithotectonic units of the Bohemian Massif. Large data base of geochronological data exists for the Bohemian Massif, thus only intervals directly relevant for this study are included in the map. Based on the Geological map of the Czech Republic 1:500,000 (Cháb et al. 2007). Geochronological data taken from: [1] Hecht et al. (1997), [2] Siebel et al. (1997), [3] Klein et al. (2008), [4] Linnemann et al. (2000), [5] Dörr and Zulauf (2010), [6] Janoušek et al. (2010), [7] Žák et al. (2011), and [8] Kryza et al. (2014). ATC – Altenberg–Teplice Complex, BG – Blanice Graben, BoG – Boskovice Graben, ISB – Intra-Sudetic Basin, KPB – Krkonoše Piedmont Basin, KRB – Kladno–Rakovník Basin, PB – Plzeň Basin.

However, recent borehole data revealed a different depositional pattern, suggesting that the Permian slivers along the Lusatian fault may represent remnants of a separate basin. In terms of tectonic setting, the Carboniferous–Permian successions are components of post-orogenic intra-continental extensional/transtensional basin system developed at ca. 320–280 Ma (Mattern 2001; Uličný et al. 2002; Opluštil et al. 2016).

Jurassic marine successions

The Carboniferous–Permian deposits are overlain disconformably by a Middle–Upper Jurassic succession, exposed in several deformed and tilted blocks (up to a few tens of meters in along-strike length) along the Lusatian Fault (labelled 'J' in Fig. 3). The Jurassic is composed of quartzose and dolomitic sandstones at the base (the Brtníky Formation; Fig. 4), interpreted as

162

representing near-shore deposits locally recycling material from the Carboniferous–Permian red beds (Eliáš 1981). This basal unit is overlain conformably by dolomitic limestones and dolomites (the Doubice Formation; Fig. 4), paleontologically dated at Oxfordian–Tithonian (Hrbek 2014; Holcová and Holcová 2016) and interpreted as deposited in the hemipelagic, offshore environment (Eliáš 1981). The original tectonic setting of the Jurassic deposits is a matter of discussion (Malkovský 1987; Voigt 2009).
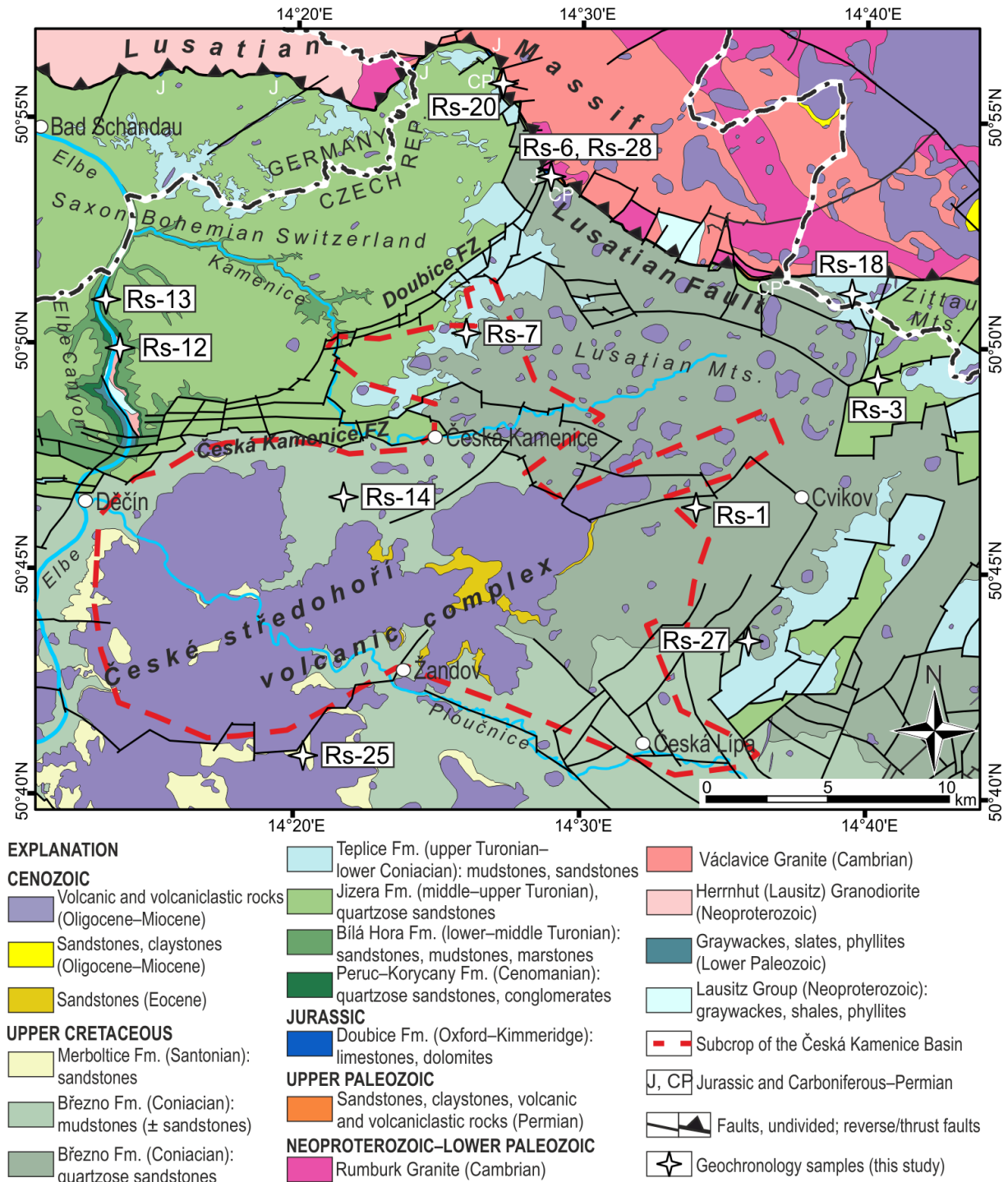

Figure 3. Detailed map of the northwestern part of the Bohemian Cretaceous Basin. Localities sampled for heavy mineral analysis and U–Pb detrital zircon geochronology are indicated. Modified after Mlčoch et al. (2018).

163

The Bohemian Cretaceous Basin

The northern and northeastern Bohemian Massif is extensively overlain by the ca. 14,600 km^2 Bohemian Cretaceous Basin (BCB; see, e.g., Voigt 1994; Uličný 2001; Herčík et al. 2003; Laurin and Uličný 2004; Voigt et al. 2008; Uličný et al. 2009a, b; and Čech 2011 for recent overviews and references). The BCB formed as a result of mid- to Late Cretaceous reactivation of the Variscan basement faults during early phases of the Alpine Orogeny (e.g., Voigt et al. 2008) and was filled during Cenomanian to Santonian by up to 1 km thick coarse marine siliciclastic successions, concentrated along the most intensely subsiding, tectonically driven basin margins bordered by uplifted basement blocks (e.g., Voigt et al. 2008; Uličný et al. 2009a). After deposition, the BCB was inverted and overprinted by multiple deformation events, the main phase of basin inversion occurred after 86–85 Ma (Voigt et al. 2008). The post-depositional deformation involved displacement along intrabasinal strike-slip faults and reverse/thrust faults at the basin margins (e.g., Coubal 1990; Coubal et al. 2014, 2015).

In the northwestern part of the BCB, the Lužice–Jizera sub-basin (sampled in this study) was one of the main depocenters that developed as sites of rapid subsidence, tectonically controlled by major strike-slip faults. The infill of the sub-basin is characterized by a thickness of up to 1 km and is subdivided into six formations ranging from Cenomanian to Santonian (Figs. 3, 4, 5). It was estimated that about 500 m of the basin fill was removed by inversion and erosion (Uličný et al. 2009a).

(1) The basal <u>Peruc–Korycany Formation</u> comprises two contrasting units. The lower to middle Cenomanian Peruc Member (Figs. 4, 5), not exposed in the study area, includes fluvial to estuarine sandstones and conglomerates with mudstone/claystone intercalations (Voigt 1998; Valečka 1975, 2015) that presumably filled paleovalleys in the pre-Late Cretaceous basement (Uličný et al. 2009b). In contrast, the upper Cenomanian Korycany Member covers virtually the entire northwestern part of the BCB, mostly in subcrop (Fig. 3). It comprises quartzose and argillaceous sandstones and conglomerates of an average thickness of 30–70 m; a notable increase in thickness up to between 80–130 m is observed along the Lusatian Fault. This member was interpreted as recording widespread shallow-marine environment after filling up of the fluvial–estuarine paleovalleys (Uličný et al. 2009b).

(2) The <u>Bílá Hora Formation</u> (lower–middle Turonian) in the northeastern part of the BCB is characterized by a relatively constant thickness (ca. 80–120 m) and monotonous facies development. Basal part of the formation is a ca. 15 m thick sequence of marlstones, passing upwards to partly silicified quartzose sandstones with intercalations of conglomerates.

(3) The <u>Jizera Formation</u> (middle–upper Turonian) is lithologically more varied and thicker (up to 420 m near the Lusatian Fault) than the Bílá Hora Formation. It is formed by
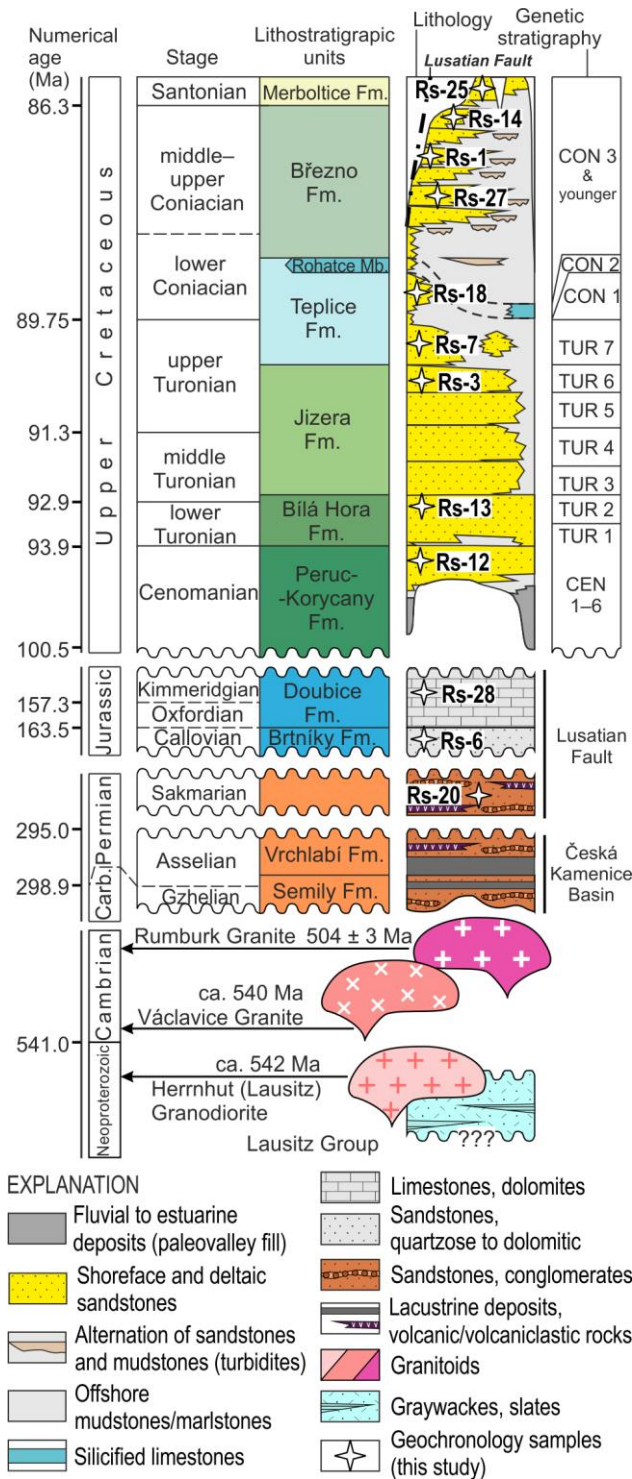
Figure 4. Simplified stratigraphic chart for the northwestern part of the Bohemian Cretaceous Basin showing Neoproterozoic to Lower Paleozoic basement units overlain by Upper Paleozoic (Česká Kamenice Basin), Jurassic (Lusatian Basin), and Upper Cretaceous (Lužice–Jizera sub-basin) successions. Lithostratigraphy after Kučera and Pešek (1982), Eliáš (1981), and Čech et al. (1980); genetic sequences of the Bohemian Cretaceous Basin after Uličný et al. (2009a).

quartzose sandstones and conglomerates arranged into several tens of meters thick coarsening-upward cycles (e.g., Valečka 1989).

The Bílá Hora and Jizera formations were deposited under similar conditions in terms of sedimentary processes and tectonic activity (e.g., Klein et al. 1979; Valečka 1979; Uličný et al. 2009a). Individual sequences within both formations were interpreted by Uličný et al. (2009a) as recording progradation-dominated nearshore to deltaic environment. Deposition of the Bílá Hora Formation marks the onset of Turonian transgression, one of the major transgressive events in Central Europe (e.g., Klein et al. 1979; Valečka and Skoček 1991; Voigt et al. 2008) that

165

flooded most of the pre-Cenomanian intrabasinal highs and significantly widened the epicontinental marine realm. The clastic material was delivered from two uplifted source areas located northeast and west of the basin, referred to as the 'West Sudetic Island' and 'Most–Teplice elevation', respectively (e.g., Scupin 1936; Klein 1966; Valečka 1979; Skoček and Valečka 1983; Uličný et al. 2009a). From the early middle Turonian onwards, the latter was drowned and the West Sudetic Island remained the dominant source area for this part of the basin (Uličný et al. 2009a).

(4) The Teplice Formation (upper Turonian–lower Coniacian) is formed by well-sorted fine-grained sandstones in its lower (Turonian) part, locally argillaceous and with a rare conglomeratic layer (Valečka et al. 2006), interpreted as relatively shallow-water, tide-modified prograding nearshore sandbodies (Valečka 1994). Basinward, they pinch out and are overlain by a sequence of lower–middle Coniacian offshore mudstones and marlstones.

(5) The Březno Formation (uppermost lower–upper Coniacian) covers substantial part of the study area (Fig. 3) where it fills the deepest part of the Lužice–Jizera sub-basin, reaching a thickness of about 450 m (Čech et al. 1987). The formation comprises three lithofacies (Valečka 1979): quartzose sandstones of variable grain-size arranged into coarsening-upward cycles, mudstone-dominated facies, and a heterolithic ('flyschoid' sensu Valečka and Rejchrt 1973) facies formed by alternation of fine- to medium-grained sandstones and mudstones. Nádaskay and Uličný (2014) connected these facies into a single progradational nearshore to deltaic depositional system. The coarsening-upward cycles of quartzose sandstones represent the delta front (foreset) facies with gravity flows operating on steep delta slopes. Farther basinward, the heterolithic facies represents gravity flow-dominated prodelta and the mudstone-dominated facies represent offshore deposits (Nádaskay et al. 2019).

Deposition of the Teplice and Březno formations took part during a period of gradual deepening of the basin, coinciding with a series or marine transgressions around the Turonian–Coniacian boundary and during the early Coniacian (Uličný et al. 2009a, 2014). The most salient feature of the Coniacian deposition is accelerated creation of the accommodation space by tectonic subsidence, compensated by gradually increasing amounts of siliciclastic material delivered into the basin from the uplifted West Sudetic Island.

(6) The Merboltice Formation (Santonian) is the least areally extensive formation of the BCB, preserved only as relics under Cenozoic volcanic complexes (Fig. 3). It is predominantly formed by fine-grained arkosic or quartzose sandstones with feldspar admixture (Valečka and Slavík 1985), interpreted as deposited in relatively shallow-water, probably deltaic environment (Voigt et al. 2008). It remains unclear whether the deposition terminated in Santonian or continued until Campanian (Klein et al. 1979).

Figure 5 (on the opposite page). Field photographs showing representative outcrops of the Upper Cretaceous formations. **(a)** Outcrop with the boundary between the Bílá hora and Jizera formations. Basal part of the Jizera Fm. contains abundant burrows penetrating into underlying sandstones of the Bílá Hora Fm. Locality: Belveder near Děčín [WGS84 coordinates: N 50.8495258°, E 14.2215303°]. **(b)** Jizera Fm. (middle–upper Turonian): part of a spectacular outcrop with almost complete stratigraphic sections of the formation. Locality: the vicinity of Pravčická brána (Prebischtor) near Hřensko [WGS84 coordinates: N 50.8837122°, E 14.2810267°]. Note up to 20 m-thick coarsening-upward cycles, typical for the Jizera Formation. **(c)** Březno Fm. (lower–middle Coniacian): coarse-grained to conglomeratic sandstones with admixture of quartz grains up to 1 cm in diameter, abundant altered feldspar grains as well as rip-up clasts (very fine- to fine-grained argillaceous sandstones) at the base. This sandstone is interpreted as a chute-channel fill generated by erosion around hydraulic jump and subsequent filling of erosive topography on a delta slope (Nádaskay and Uličný 2014). Locality: Sloup near Nový Bor [WGS84 coordinates: N 50.7349800°, E 14.5806511°]. **(d)** About 30 m-thick succession of delta-front deposits formed by alternation of parallel-bedded foresets and foresets with trough cross-bedding with chute channels and backset lamination, interpreted as deposited by deepwater (i.e., prograding into up to 100 m deep basin) delta (Nádaskay and Uličný 2014). Locality: Sloup near Nový Bor [WGS84 coordinates: N 50.7359475°, E 14.5811500°]. **(e)** Březno Fm. (lower–middle Coniacian): superposition of two units formed by quartzose sandstones, interpreted as highangle (ca. 24° dip) and low-angle (ca. 4° dip) delta foresets, respectively (e.g., Uličný 2001). Arrows indicate dip direction. Surface covering truncated top of the high-angle foreset package is interpreted as a maximum transgressive surface (MTS; Nádaskay and Uličný 2014). Locality: Údolí samoty near Radvanec [WGS84 coordinates: N 50.7665206°, E 14.6028308°]. **(f)** Březno Fm. (lower–middle Coniacian): close-up view on a bed of fine-grained sandstones in one of the youngest preserved Coniacian outcrops. Note the clay-coated *Ophiomorpha* burrows. Locality: roadcut north of Arnultovice near Nový Bor [WGS84 coordinates: N 50.7742594°, E 14.5660464°]. **(b)** Merboltice Fm. (Santonian): up to 2 m-thick beds of fine- to medium-grained sandstone with feldspar and clay admixture. Locality: disused sandpit Zubrnice [WGS84 coordinates: N 50.6495864°, E 14.2214200°].

Description of the studied samples

Twelve outcrops were sampled in a stratigraphic order, one of the Permian, two of the Jurassic, and the remaining nine of the Upper Cretaceous formations (Figs. 4). Two rock samples were taken from the same spot on each outcrop, one for the heavy mineral analysis (about up to 10 kg in weight) and one for the detrital zircon geochronology (about 30–40 kg in weight; except for sample Rs-28, which was over 50 kg in weight). The Permian sample is fine-grained red graywacke, the Jurassic samples are sandstone and limestones, samples from the Upper Cretaceous are exclusively sandstones (Fig. 5). Location, stratigraphic position, petrographic description of the samples, and other relevant details are given in Figs. 3, 4 and Tabs. 1, 2.

Heavy mineral analysis

Analytical methods

The samples were processed in the laboratories of the Czech Geological Survey, Prague: crushed, cleaned from clay matrix and sieved from medium- to coarse-grained sand fraction using the 0.5 mm sieves. Subsequently, the heavy minerals within the fraction below 0.5 mm (ca. 70 g
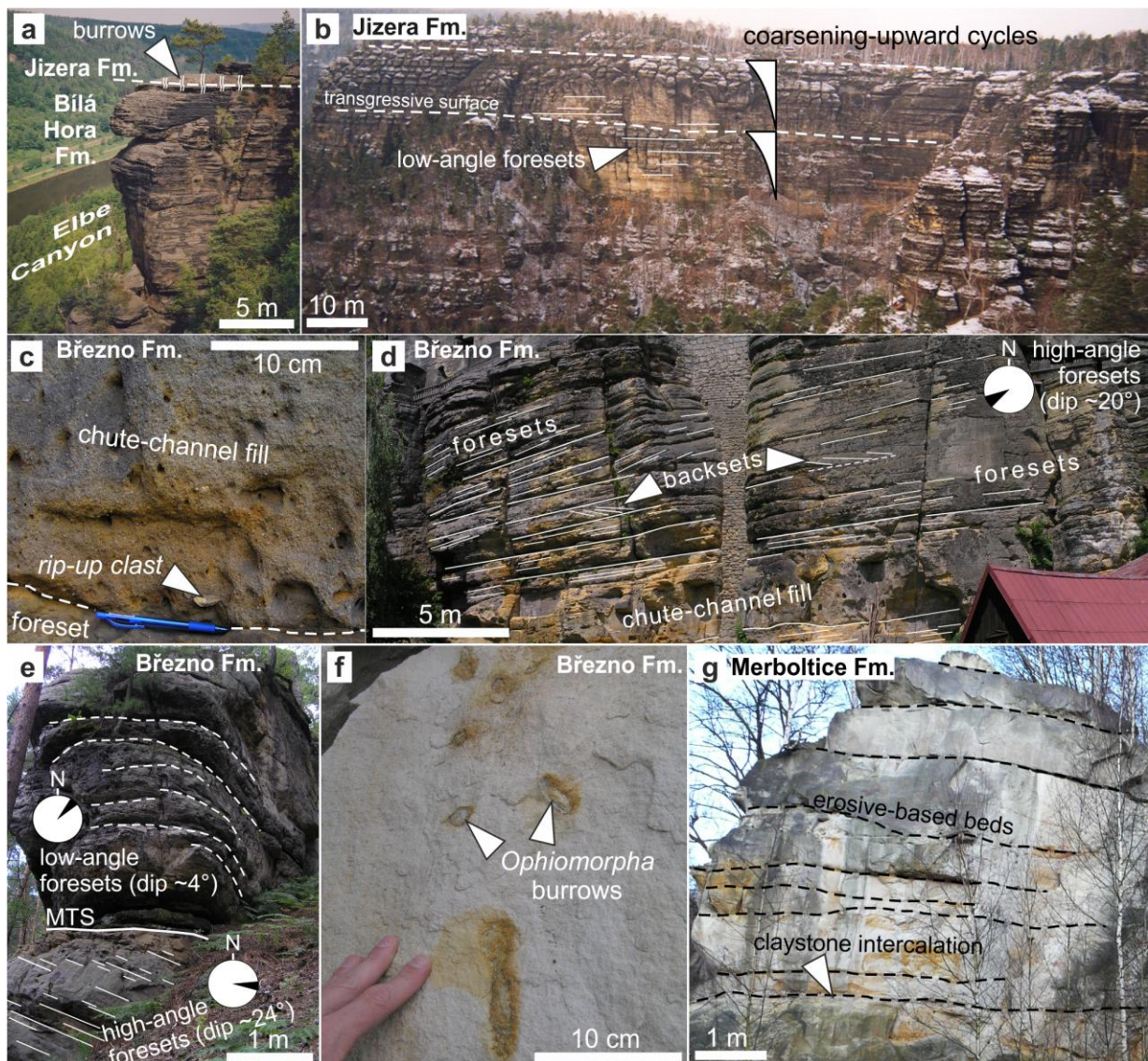
each sample) were separated from sand using heavy liquids (tetrabromoethane $C_2H_2Br_4$ with a density of 2.95 g/cm3). Mineral species were identified in the concentrates using a standard optical microscope.

Results: heavy mineral analysis

The main output of the analysis is a heavy mineral assemblage (HMA) identified in the individual samples (Fig. 6i–k, 7). The data are presented in a stratigraphic succession using selected heavy mineral indexes (Fig. 7): (1) the zircon–tourmaline–rutile (ZTR) index (Hubert 1962), which indicates mineralogical maturity of the studied rock; (2) the monazite–zircon (MZi) index (e.g., Morton and Hurst 1995), which reflects the relative significance of granitic material in the source; and (3) TiO_2-minerals–zircon (RZi) index (e.g., Morton and Hurst 1995), which reflects input of material derived from high-grade metamorphic rocks.

The following trends can be recognized in the HMA within the studied stratigraphic succession. The Permian sample (Rs-20) contains relatively uniform HMA, dominated by zircon

Table 1. Location of the geochronology samples (in a stratigraphic order).

Sample	Latitude (N) in degrees (WGS84)	Longitude (E) in degrees (WGS84)	Lithostratigraphic unit (formation)	Locality
Rs-25	50.681627	14.338959	Merboltice	Disused quarry near Merboltice
Rs-14	50.777242	14.361448	Březno	Disused sandpit near Markvartice
Rs-1	50.77437	14.567234	Březno	Roadcut N of Arnultovice, Nový Bor
Rs-27	50.725031	14.598179	Březno	Section Dědovy kameny, Sloup
Rs-18	50.853554	14.658004	Teplice	Disused quarry on the Sonnenberg hill, Waltersdorf
Rs-7	50.838209	14.432462	Teplice	Gorge NE of Lipnice
Rs-3	50.821715	14.673004	Jizera	Outcrops on the left bank of the Svitavka Creek, Juliovka
Rs-13	50.849361	14.221566	Bílá Hora	Outcrops on the left bank of the Elbe River, Belveder near Labská Stráň
Rs-12	50.831637	14.23002	Peruc–Korycany	Outcrops on the left bank of the Elbe River N of Děčín
Rs-28	50.896264	14.48128	Doubice	Disused quarries NE of Doubice
Rs-6	50.896002	14.481791	Brtníky	Disused quarries NE of Doubice
Rs-20	50.930720	14.452592	unnamed	Roadcut along a forest road near Vlčí Hora, NW of Krásná Lípa

Table 2. Description of the analyzed samples and their inferred depositional environment.

Sample	Lithology	Petrographic description and modal composition (vol. %)	Depositional geometries	Depositional environment
Rs-25	sandstone	Well-sorted, quartz *ca.* 85 %, up to 5–7 % of clay in the matrix, feldspar up to 7–8 % (incl. myrmekites), muscovite <1 %, quartzite clasts *ca.* 3 %; frequent rip-up clasts up to *ca.* 10 cm in size	Up to *ca.* 2 m thick beds, erosive-based	Gravity flows in a deltaic setting
Rs-14	sandstone	Moderately-sorted, quartz *ca.* 75 %, up to 15 % of clay in the matrix, feldspar up to 8 %, rare muscovite, coal fragments and fine plant debris *ca.* 1 % (coal clasts up to 1 cm in size), quartzite clasts *ca.* 3 %	Up to a few m thick beds, erosive-based, amalgamated sandstone beds	Gravity flows (possibly hyperpycnal), prodelta
Rs-1	quartzose sandstone	Well-sorted, quartz *ca.* 93 %, up to 5 % of clay in the matrix, feldspar *ca.* 1 %, muscovite <1 %, quartzite clasts *ca.* 2 %	Few tens of cm thick beds, massive, gently (ca. 2°) dipping	Shallow-water, proximal, prograding strandplain or low-angle delta-front
Rs-27	quartzose sandstone	Moderately-sorted to bimodal, quartz *ca.* 92 % (up to 0.8 mm in size), up to 5 % of clay and Fe-oxides in the matrix, feldspar <1 %, quartzite clasts *ca.* 2 %; quartz aggregates and rip-up	A few m thick sets, steeply dipping (up to *ca.* 25° dip), forming up to 80 m thick	Delta-front ('deepwater') foresets interbedded with chute-channel fills, gravity flows,

|				
		clasts up to 2 cm	bodies, coarse-grained interbeds	subsequent reworking by marine (tidal) currents
Rs-18	sandstone	Moderately-sorted, quartz *ca.* 75 %, up to 20 % of clay in the matrix, feldspar up to 8 % (incl. microcline), coal fragments and fine plant debris *ca.* 2 % (coal clasts up to 1 cm in size), quartzite clasts *ca.* 1 %, glauconite *ca.* 1 %, bioturbated	A few dm thick beds, subhorizontal, erosive-based interbeds	Shallow-water, proximal, reworking by marine (tidal) currents, occasional storm deposition
Rs-7	quartzose sandstone	Moderately-sorted, quartz *ca.* 90 % (up to 1.8 mm in size), up to 8 % of clay and Fe-oxides in the matrix, feldspar up to 2 %, quartzite clasts *ca.* 2 %, layers with coarse sand to granules	Up to a few m thick sets, gently (up to 5°) dipping	Prograding strandplain or shallow-water delta-front, reworking by marine (tidal) currents
Rs-3	sandstone	Poorly-sorted, quartz *ca.* 87 % (up to 1.4 mm in size), calcite cement (from leached shells), feldspar <1 %, quartzite clasts *ca.* 3 %, layers with coarse sand to granules, rare burrows	Up to a few m thick sets, subhorizontal	Prograding strandplain or shallow-water delta-front, reworking by marine (tidal) currents
Rs-13	quartzose sandstone	Poorly-sorted, quartz *ca.* 90 % (up to 1.6 mm), up to 7 % of clay and Fe-oxides in the matrix, quartzite clasts *ca.* 3 %, intensely silicified	Up to a few m thick sets, gently (up to 5°) dipping	Prograding strandplain or shallow-water delta-front, reworking by marine (tidal) currents
Rs-12	quartzose sandstone	Moderately- to poorly-sorted to bimodal, quartz *ca.* 93 % (up to 4.4 mm in size), up to 6 % of clay in the matrix, quartzite clasts <1 %, conglomeratic interbeds	Up to a few m thick sets, erosive-based in places	Shallow-water proximal, possibly prograding strandplain, reworking by marine (tidal) currents
Rs-28	dolomitic limestone	Sparritic dolomitic limestones, subordinately microsparitic dolomites (32–56 % $CaCO_3$, 27–36 % $MgCO_3$), admixture of sparry bioclasts (?echinoderms, molluscs), accessory siliciclastic grains (quartz, muscovite, *ca.* 1–3 %)	Beds up to a few dm thick, tectonically tilted and deformed	Shallow-marine, offshore
Rs-6	quartzose sandstone	Poorly-sorted, quartz *ca.* 92 % (up to 3.2 mm in size), quartz grains intensely fractured, up to 5 % of clay in the matrix, rare feldspar, quartzite clasts *ca.* 2 %	Up to dm to m thick alternating beds, tectonically tilted and deformed	Shallow-waters, proximal
Rs-20	lithic graywacke	Poorly-sorted, coarse-grained, matrix-supported, clay >20 %, dominated by lithic clasts (fine-grained metasedimentary rocks, shales), subordinate quartz grains (*ca.* 5 %)	Massive, thickness unknown	Gravity flows or fluvial

Thin sections
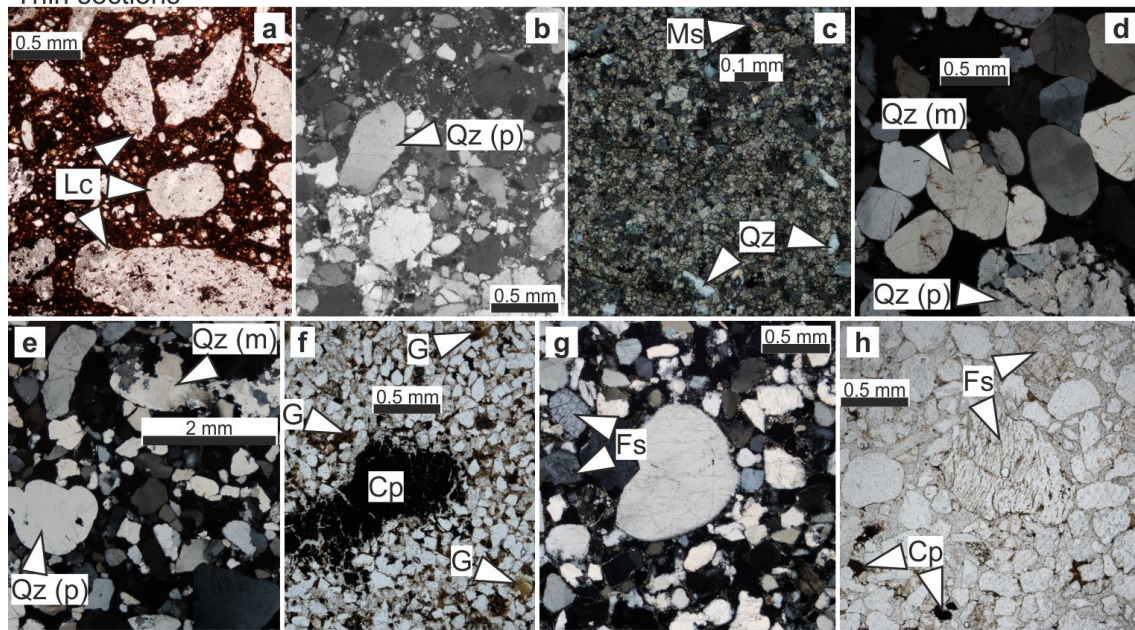
Heavy mineral concentrates
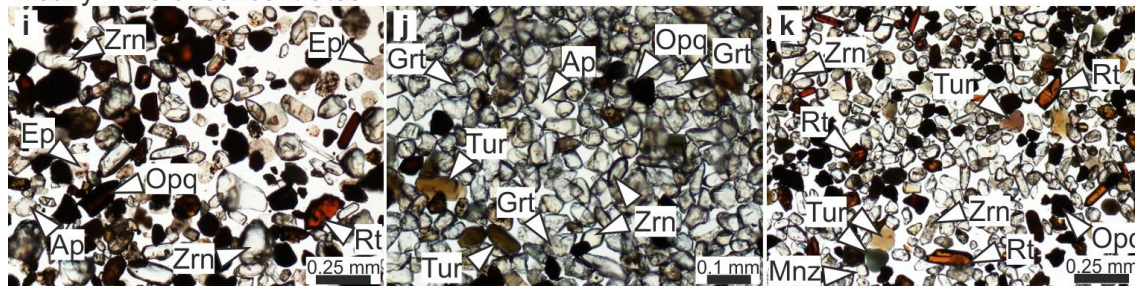
Figure 6. Photomicrographs of the studied samples. **(a)** Coarse-grained lithic graywacke with argillaceous matrix, sample Rs-20 (Permian); Lc – lithic clast. **(b)** Poorly sorted quartzose sandstone, sample Rs-6 (Jurassic); Qz (p) – igneous (plutonic) quartz. **(c)** Sparitic dolomitic limestone, sample Rs-28 (Jurassic); note accessory quartz (Qz) and micas (Ms). **(d)** Poorly sorted to bimodal quartzose sandstone, sample Rs-12 (Cenomanian); Qz (p) – igneous (plutonic) quartz, Qz (m) – metamorphic quartz (polycrystalline aggregate). **(e)** Poorly sorted sandstone, sample Rs-3 (upper Turonian); **(f)** Moderately sorted, slightly argillaceous sandstone with abundant coal fragments/coalified plant debris (Cp) and accessory glauconite (G), sample Rs-18 (lower Coniacian). **(g)** Moderately sorted, slightly argillaceous sandstone with abundant (up to 8%) feldspars (Fs), sample Rs-14 (upper Coniacian). **(h)** Well-sorted sandstone with abundant feldspars (Fs) and coal fragments (Cp), Sample Rs-21 (Santonian). **(i–k)** Photomicrographs of heavy mineral concentrates (Permian sample Rs-20, Jurassic sample Rs-28, lower Coniacian sample Rs-18, respectively). Mineral abbreviations after Whitney and Evans (2010). Detailed sample descriptions are given in Tab. 2.

(70 %), subordinate rutile (20 %), and a small proportion of other heavy minerals including apatite (Fig. 6i). Lower part of the Jurassic (sample Rs-6) is characterized by an abrupt increase in tourmaline (with almost equal proportion to zircon) and by a lower proportion of rutile and other heavy minerals as compared to the Permian sample (Fig. 7). The upper part of the Jurassic (sample Rs-28), containing rather fine-sand and silt-sized heavy mineral grains, differs significantly from all of the other stratigraphic units in the high proportion of garnet, reaching

70 % (Fig. 6j). Unlike the other analyzed samples, the Jurassic limestones contain carbonate, either dolomite or calcite, with an elevated content of Mg or Fe.

Again, the HMA abruptly changes between the Jurassic and the Upper Cretaceous samples (Fig. 7). The Cenomanian sample (Rs-12) is dominated by zircon (70 %), with subordinate rutile (20 %), and a minor proportion of tourmaline and epidote (both 4 %). The Turonian part of the succession differs from the Cenomanian in significant decrease of the zircon fraction down to 40–45 % and increase in the tourmaline (up to 35 %) and monazite fractions (Fig. 6k). The latter reaches maximum in lower Turonian (8 % in sample Rs-13), as indicated by the MZi index. In the remainder of the Upper Cretaceous succession, the proportion of monazite decreases again, varying between 1 % and 4 % (Fig. 7). The Turonian and Coniacian is then characterized by a variable proportion of zircon (45–60 %), except for sample Rs-27, where it decreases down to 30 %, being compensated by an increased proportion of tourmaline (25 %) and rutile (40 %). Moreover, rutile content gradually increases towards the upper Coniacian, as evidenced by the RZi index. The Santonian HMA is similar to the Coniacian assemblage, differing only in a slight decrease in the rutile content (15 %).
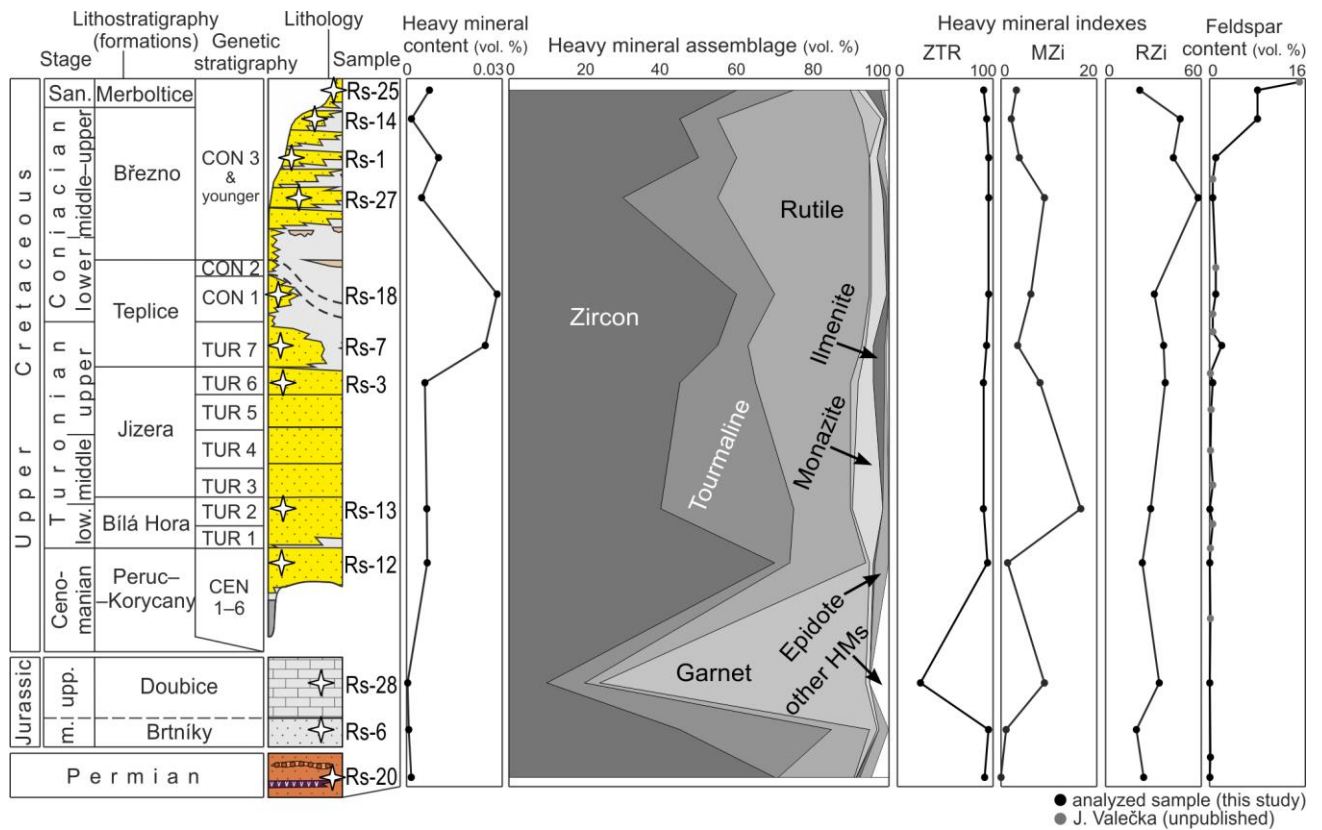

Figure 7. Diagram showing stratigraphic variations in the heavy mineral assemblages. ZTR zircon–tourmaline–rutile index, MZi monazite–zircon index, RZi rutile–zircon index. Feldspar content in individual samples was compiled from this study and unpublished data by J. Valečka.

Detrital zircon geochronology

Analytical methods

The geochronology samples were crushed, zircon grains were separated using the Wilfley shaking table and heavy liquids in the laboratories of the Czech Geological Survey, Prague, and finally mounted in epoxy-filled blocks and polished for subsequent cathodoluminescence (CL) imaging. From each sample, a random group of ca. 100–150 detrital zircon grains has been selected and mounted for analysis and, whenever possible, a group of euhedral, prismatic, and clear zircon crystals was preferentially picked and targeted to find the potentially youngest zircon age in the sample. The measured U–Pb zircon data and cathodoluminescence (CL) images are presented in Figs. 8 and 9 and in full in the online Supplementary Material.

A Thermo Scientific Element 2 sector field ICP-MS coupled to a 193 nm ArF excimer laser (Teledyne Cetac Analyte Excite laser) at the Institute of Geology of the Czech Academy of Sciences, Prague, Czech Republic, was used to measure the Pb/U and Pb isotopic ratios in zircons. The laser was fired at a repetition rate of 5 Hz and fluence of 3.17 J/cm^2 with 20 micron spot size. The He-carrier gas was flushed through the two-volume ablation cell at a flow rate of 0.75 L/min and mixed with 0.81 L/min Ar and 0.004 L/min N prior to introduction into the ICP. The in-house glass signal homogenizer (design of Tunheng and Hirata 2004) was used for mixing all the gases and aerosol resulting in smooth, spike-free signal. The signal was tuned for maximum sensitivity of Pb and U, Th/U ratio close to unity and low oxide level, commonly below 0.2 %. Typical acquisitions consisted of 15 second measurement of blank followed by measurement of U, Th, and Pb signals from the ablated zircon for another 35 seconds. The total of 420 mass scans data were acquired in time resolved – peak jumping – pulse counting/analog mode with 1 point measured per peak for masses ^{204}Pb + Hg, ^{206}Pb, ^{207}Pb, ^{208}Pb, ^{232}Th, ^{235}U, and ^{238}U. Due to a non-linear transition between the counting and analog acquisition modes of the ICP instrument, the raw data were pre-processed using a purpose-made Excel macro. As a result, the intensities of ^{238}U were left unchanged if measured in a counting mode and recalculated from ^{235}U intensities if the ^{238}U was acquired in analog mode. Data reduction was then carried out off-line using the Iolite data reduction package, version 3.4 with VizualAge utility (Petrus and Kamber 2012). Full details of the data reduction methodology can be found in Paton et al. (2010). The data reduction included correction for gas blank, laser-induced elemental fractionation of Pb and U and instrument mass bias. For the data presented here, blank intensities and instrumental bias were interpolated using an automatic spline function while down-hole inter-element fractionation was corrected using an exponential function. No common Pb correction was applied to the data due to the high Hg contamination of the commercially available He carrier gas, which precludes accurate correction of the interfering ^{204}Hg on the very small signal of ^{204}Pb
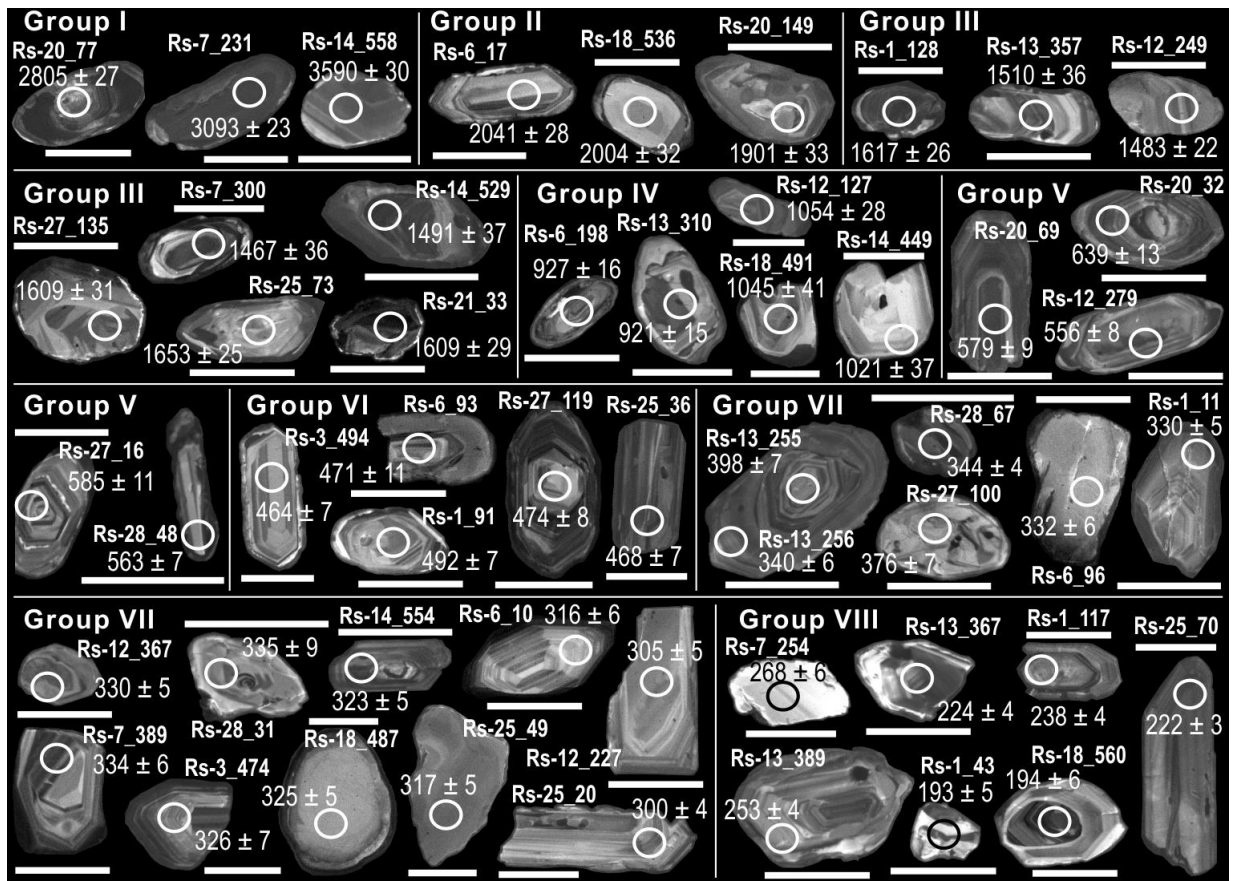
Figure 8. Representative cathodoluminescence images of the analyzed zircon grains. Laser-ablation ICP–MS analysis spots (20 µm in diameter, marked with concordant $^{206}Pb/^{238}U$ and $^{207}Pb/^{206}Pb$ ages, ± 2σ uncertainties). Scale bar is 100 µm.

(common lead). Primary concentrations of common Pb in zircon are considered very low and were controlled by observing the $^{206}Pb/^{204}Pb$ (radiogenic/common lead) ratio. Analyses with low values are examined (if present) in more detail.

Residual elemental fractionation and instrumental mass bias were corrected by normalization to the natural zircon reference material Plešovice (Sláma et al. 2008). Zircon reference materials GJ-1 (Jackson et al. 2004) and 91500 (Wiedenbeck et al. 1995) were periodically analysed during the measurement for quality control. The mean Concordia age values of 610 ± 4 Ma (2σ) for GJ-1 and 1065 ± 6 Ma (2σ) for 91500 obtained from analyses performed over two analytical sessions correspond perfectly and are less than 1 % within the published reference values (GJ-1: $^{207}Pb/^{206}Pb$ age of 608.53 ± 0.4 Ma, Jackson et al. 2004; 91500: $^{207}Pb/^{206}Pb$ age of 1065.4 ± 0.3 Ma, Wiedenbeck et al. 1995). For geological interpretation, the $^{206}Pb/^{238}U$ age was selected for zircons younger than 1.0 Ga and $^{207}Pb/^{206}Pb$ for those older than 1.0 Ga. The ages are presented as concordia and probability density plots generated using the ISOPLOT program version 3.70 (Ludwig 2008). The cumulative density plot of detrital zircon populations provides overview of similarity of zircon age spectra in the different stratigraphic units (Fig. 10).

Figure 9 (on the opposite page). U/Pb detrital $^{206}Pb/^{238}U$ and $^{207}Pb/^{206}Pb$ zircon concordia age distributions in the analyzed samples (arranged in a stratigraphic order from lower right to upper left). Only data less than 10 % discordant were used (see the methodology section for discordance calculation). Kernel density estimates (blue areas), frequency histograms (bin width of 15 Ma, bandwidth of 10 Ma), and probability density plots (dark blue) are used for data presentation.

Results: zircon U–Pb data

Eight distinct zircon age groups were identified in the obtained U–Pb age spectra (Fig. 9). From oldest to youngest, these groups are as follows. Group I is represented by Archean zircons (>2.5 Ga in age), Group II is represented by Paleoproterozoic zircons with ages around ca. 2.0–1.9 Ga, Group III are zircons with ages close to the Mesoproterozoic/Paleoproterozoic boundary (ca. 1.5 Ga), Group IV are zircons with Neoproterozoic ages around ca. 1 Ga, Group V are late Neoproterozoic (Ediacaran) to early Cambrian zircons dated at around 650–530 Ma ('Cadomian'), Group VI are Cambro–Ordovican ages at around 500–460 Ma, Group VII are Late Devonian to latest Carboniferous zircons ('Variscan', ca. 400–300 Ma), and Group VIII is represented by ages as young as late Permian, around 250 Ma ('post-Variscan').

Similar to the heavy mineral assemblages (Fig. 7), the relative contributions of the individual age groups vary across the studied stratigraphic succession and thus reveal important temporal variations in the age spectra (Figs. 8, 9). In particular, abrupt changes in the age spectra occur between the Permian and Jurassic, Jurassic and Cenomanian, in the upper Turonian between genetic sequences TUR 6 and 7 (sensu Uličný et al. 2009a), and between Coniacian and Santonian (Fig. 9).

The Permian sample (Rs-20) is dominated by Group V ages (Cadomian), followed by Group I (Archean) and II (Paleoproterozoic) ages, which show the highest proportion within the entire dataset, more than two times in comparison to the other samples. No detrital zircon ages younger than Cadomian were found in this sample.

The Jurassic samples are characterized by age spectra dominated by Variscan (Group VI) ages. These are twice as abundant in the sample from lower part of the succession (sandstone, Rs-6) than in the sample from the upper part (limestone, Rs-28). The limestone contains almost twice more zircon grains belonging to the Group V (Cadomian) and IV (Cambro–Ordovician).

Samples from the Cenomanian to the lower upper Turonian (TUR 6 sequence) contain a variable mixture of Variscan (ranging from 38 to 52.5 %), Cambro–Ordovician (10.7–15 %), and Cadomian ages (14.5–18.5 %). The most significant feature, however, is the stratigraphic (temporal) variation in age Groups III and IV. They are fairly abundant in the Cenomanian and lower Turonian samples Rs-12 and Rs-13 (14.5 % and 9 %, respectively), then decrease in the upper Turonian sample Rs-3 down to 1.7 %, and reappear from sample Rs-7 up the section,
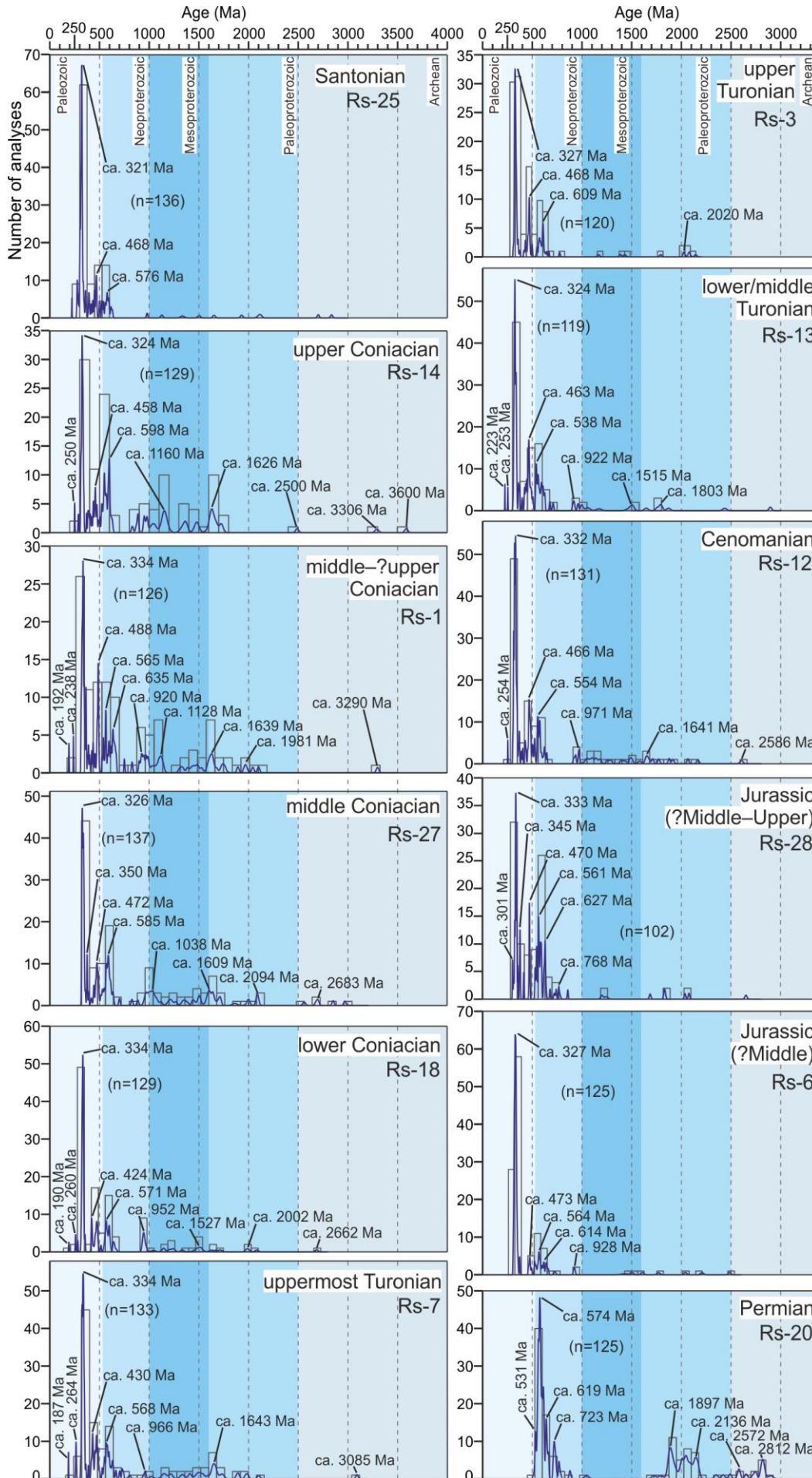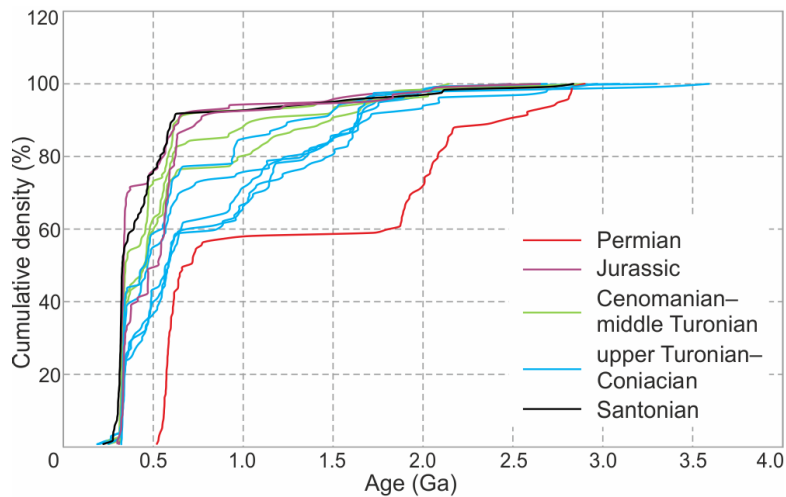
Figure 10. Cumulative density plot of random detrital zircon populations in the four samples of the Permian, Jurassic and Upper Cretaceous sedimentary rocks.

reaching maximum abundance in the middle–upper Coniacian sample Rs-14 (almost 25 %). The last abrupt change occurs in the Santonian (sample Rs-25), where the Group III and IV ages decrease in abundance down to less than 3 % while Variscan ages (Group VI) increase significantly (to 48.5 % from 23 % in Rs-14).

The post-Variscan ages (Group VIII) are present only in some of the Upper Cretaceous samples, the highest proportion of Group VIII is in the Santonian sample Rs-25 (ca. 7 %).

Unlike the pronounced temporal variations in the zircon age spectra (Figs. 9, 11), the analyzed samples do not show any systematic spatial variations over the study area. The exception are the four Coniacian samples representing different facies of a single depositional system (Fig. 11b). According to Nádaskay and Uličný (2014), the Coniacian interval could be characterized as uniform in terms of the depositional environment (nearshore to deltaic) and paleocurrent directions (to the S and SW). Sample Rs-18 represents the most proximal, nearshore part of the depositional system, sample Rs-1 represents a more distal setting, possibly shallow-water delta front, passing laterally into 'deep-water' delta front (sample Rs-27). The most distal part of the depositional system is represented by sample Rs-14, deposited in the prodelta setting. Zircon age spectra reflect this transition from proximal to distal facies by decrease in the proportion of Variscan-age zircon grains (Group VI) together with gradual increase in the proportion of zircon grains of Meso-/Neoproterozoic and Grenvillian ages (Groups III and IV).

Discussion

Interpretation of source areas

The eight distinct detrital zircon age groups (I–VIII) as defined above, together with their relative statistical importance in each sample and their stratigraphic distribution, reveal not only the diversity of source areas, but also provide an intriguing information on the development of sedimentary basins and intra-plate basement reactivation in the Alpine foreland from the Permian to Late Cretaceous times. Below, we first interpret the possible source areas for each age group

Figure 11. (a) Frequencies of the eight age groups (as defined in this study) in the analyzed samples plotted in a stratigraphic succession.

(b) Spatial variations in the measured detrital zircon ages over the study area (shown as pie charts summarizing proportion of the age groups in each sample). 'Nearshore', 'prodelta' and 'delta-front' facies refer to parts of the Coniacian depositional system.
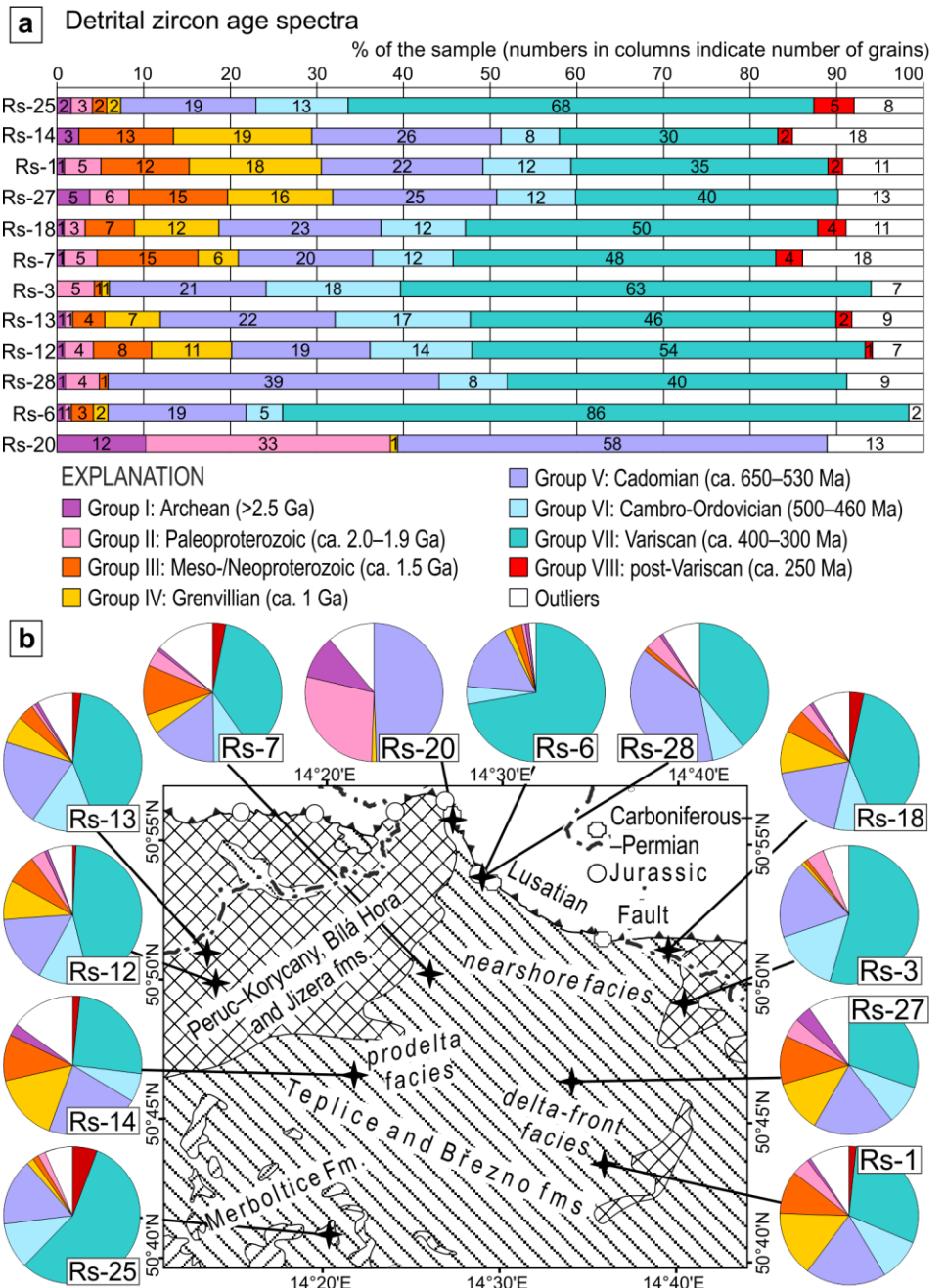
and then develop these interpretations into a broader tectonic model (see Fig. 12 for overview of the previously published models).

Although no Archean and Paleoproterozoic complexes occur in the Bohemian Massif and vicinity, the corresponding zircon ages are ubiquitous in its Cadomian basement and Lower Paleozoic overlap successions. These zircons were likely originally derived from the West African part of Gondwana and then multiply recycled into younger deposits (e.g., Linnemann et al. 2004; Drost et al. 2011; Meinhold et al. 2011; Košler et al. 2014; Hajná et al. 2017; Žák and Sláma 2018). Our age Groups I and II thus provide only limited provenance information, with no possibility to distinguish whether they come from the Saxothuringian, Teplá–Barrandian, or Moldanubian units.

In contrast, the ca. 1.5 and 1.0 Ga zircons (Groups III and IV) are typically absent or extremely rare in the Cadomian-derived crustal units of the Bohemian Massif (e.g., Linnemann et

al. 2004; Drost et al. 2011; see Meinhold et al. 2011 for discussion), but were detected in significant quantities in most of our samples (Figs. 9, 11a). We thus interpret Group III and IV ages as representing a distant source, most likely located along the southern margin of Baltica (e.g., Valverde-Vaquero et al. 2000; Bingen and Solli 2009; Lamminen et al. 2011; Jakob et al. 2016; Wiest et al. 2018).

The Cadomian ages (Group V) are no surprise as the nearby Lusatian Massif is composed of Neoproterozoic greywackes and early Cambrian granites (e.g., Linnemann and Romer 2002; Kemnitz 2007). Hence, the zircon ages of ca. 570–560 Ma, present in most of the samples, fit well the ages reported from the Lausitz Group graywackes or their correlatives (Linnemann et al. 2000; Żelaźniewicz et al. 2004, 2009), while less common zircon ages of ca. 540–530 Ma correspond to the Lusatian granites (e.g., Kröner et al. 1994, 2001; Gehmlich et al. 1997; Linnemann et al. 2000; Tichomirowa 2002). Older Cadomian zircons (>650 Ma) are from an unknown source and were most possibly also recycled from the greywackes (e.g., Białek et al. 2014). It should be noted, however, that despite the local (Lusatian) source for Group V is most likely, similar ages were frequently reported also from the Teplá–Barrandian unit (e.g., Drost et al. 2011; Hajná et al. 2017, 2018) and thus cannot be excluded from further interpretations.

The Cambro–Ordovician zircon grains (Group VI) may have been derived from the nearby granites (Václavice and Rumburk; 540–510 Ma, Białek et al. 2014; Zieger et al. 2018) however, as for the Cadomian zircons, Cambro–Ordovician (meta-)igneous complexes are a common component of the Saxothuringian, Teplá–Barrandian, and Moldanubian units (e.g., Dörr et al. 1998; see Pin et al. 2007 for overview) and thus they may also represent some distant source areas.

The Variscan zircons ages (Group VII) most typically fall within a narrow range of ca. 334–332 Ma (Viséan), corresponding to ages of early granitic pulses of the western and southwestern margin of the Bohemian Massif (e.g., Siebel et al. 1997; Klein et al. 2008). In addition, Group VII is also represented by a ca. 350–345 Ma zircon population (found in one sample, Rs-28, Jurassic in age), which is a distinct feature of continental margin arc granitoids straddling the Teplá–Barrandian/Moldanubian boundary (e.g., Holub et al. 1997; Janoušek et al. 2010). Less frequently, the Variscan age group also includes ca. 327–324 Ma (Serpukhovian) zircon ages, which fit well the emplacement ages of voluminous late-orogenic granites in the western and southwestern periphery of the Bohemian Massif (e.g., Klein et al. 2008; Siebel et al. 1999, 2003, 2008). The youngest Variscan ages determined at ca. 321 Ma could represent the easterly Krkonoše–Jizera plutonic complex (e.g., Awdankiewicz et al. 2010; Žák et al. 2013; Kryza et al. 2014).
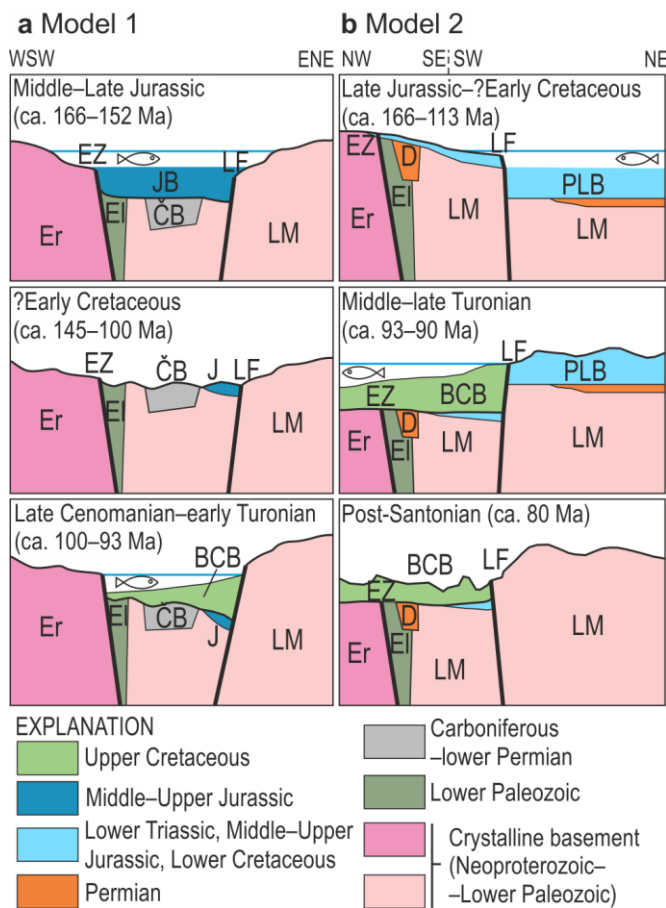
Figure 12. Summary of previous models of tectonosedimentary development of the northwestern Bohemian Cretaceous Basin and Lusatian Block (not to scale). **(a)** Sequence of events compiled from paleogeographic reconstructions (for the Jurassic by Bruder 1882; Svoboda 1964 and Eliáš 1981; for the Late Cretaceous by Uličný et al. 2009a). **(b)** A tectonic model modified from Voigt (1994, 2009) and Hofmann et al. (2018).

BCB – Bohemian Cretaceous Basin, ČB – Česká Kamenice Basin; D – Döhlen Basin, EI – Elbe Valley Slate Mountains, Er – Krušné hory/Erzgebirge, EZ – Elbe Fault Zone, J – Jurassic deposits, JB – a hypothetic Jurassic basin, LF – Lusatian Fault, LM – Lusatian Massif, PLB – Prignitz–Lausitz Basin (Jurassic–?Lower Cretaceous; sensu Voigt 2009). Not to scale.

The post-Variscan Group VIII includes zircon ages of ca. 271 Ma, which could be correlated with Permian dikes intruding the southern Moldanubian unit (Košler et al. 2001), but also includes age clusters at ca. 260–250 Ma (late Permian–Early Triassic), 220 Ma (Late Triassic), and 190 Ma (Early Jurassic). No such young igneous complexes are known from the Bohemian Massif. Searching for a possible source, the nearest relevant intrusions are found in the Northern Europe, namely the Oslo and North Atlantic rifts and the North Sea Dome (e.g., Ziegler 1990c; Underhill and Partington 1993; Andersen et al. 2011). Taking into account the large distance from the northern Bohemian Massif and Late Cretaceous paleogeography (e.g., Ziegler 1990a), direct transport of these zircons from source to the BCB is highly unlikely and possibly multiple redeposition during Triassic and Jurassic should be considered.

Temporal changes in sediment provenance and tectono-stratigraphic history

The Permian sample Rs-20 from the Česká Kamenice Basin contains zircons no younger than early Cambrian, while most of the analyzed zircon are of late Neoproterozoic age (Group V; Figs. 8, 9), suggesting that the basin was predominantly supplied from the Lusatian Massif at around ca. 295–290 Ma ('Saxonian', i.e. late Asselian–Sakmarian), although contribution from the westerly Saxothuringian unit cannot be excluded (Fig. 13a). The absence of Variscan zircons (Group VII) indicates that the sediment supply from the southern part of the Bohemian Massif

(e.g., Martínek and Štolfová 2009; Žák et al. 2018) was only active in the extensional basin system until early Permian (Asselian; Fig. 13a). Similar lithostratigraphic development of individual basins within this system (e.g., Pešek 2001) implies that they formed a single depositional space or were at least partially interconnected. Initiation of the extensional ('intermontane') grabens in the Bohemian Massif and their filling with large volumes of non-marine clastic deposits derived from the surrounding basement uplifts was an upper-crustal response to orogenic collapse of the Variscan belt (e.g., Burg et al. 1994; Ménard and Molnár 1988; Lorenz and Nichols 1976, 1984; Dörr and Zulauf 2010; Žák et al. 2018). From the late early Permian (late Asselian/Sakmarian) onwards, the gap in deposition points to a wide-scale tectonic uplift and inversion of the Carboniferous–Permian basins, associated with reactivation of the NW–SE-trending faults (Fig. 13b; e.g, Danišík et al. 2010; Berg 1938).

The Bohemian Massif remained a major topographic high until at least Late Jurassic (Fig. 12a, b; e.g., Ziegler 1990a; Paul et al. 2008, 2009; Vejbæk et al. 2010; Augustsson et al. 2018). This is well documented by our Middle and Late Jurassic samples (Rs-6 and Rs-28, respectively), which are the stratigraphically lowest to contain a significant proportion of Variscan zircons (Group VII; Fig. 11), in addition to Cadomian (Group V), Cambro–Ordovician (Group VI), and older zircons (Groups I–IV). The Variscan zircons suggest uplift of the southerly and westerly Variscan (and reworked Cadomian) basement blocks as major source areas; however, recycling of Group I–VI zircons from late Permian to Triassic deposits also cannot be excluded. Unlike the detrital zircon spectra, the heavy mineral spectra differ significantly in both samples (Fig. 7), perhaps due to high sensitivity of garnet (about 70 % of the limestone Rs-28 sample) to chemical weathering (e.g., Morton and Hallsworth 1999). We assume that calcite-cemented limestones prevented garnet grains from dissolution by diagenetic fluids. Another possibility could be hydrodynamic sorting (e.g., Morton and Hallsworth 1999) where very fine sand to silt fraction, deposited in a distal setting, was enriched in garnet rather than in zircon.

The Jurassic samples corroborate the long-term, Late Paleozoic to Mesozoic subsidence of the northern portion of the Bohemian Massif (Fig. 13b–e), perhaps as a result of far-field stress transfer from the North Atlantic Rift (e.g., Malkovský 1987; Ziegler 1990c; Doré 1991; Erratt et al. 1999). The subsidence generated a marine seaway connecting the Tethyan and Boreal realms (e.g., Bruder 1881, 1882; Svoboda 1964; Eliáš 1981; Ziegler 1975, 1990a). The seaway was presumably fault-controlled: the onset of deposition of the carbonate facies (Fig. 4; sample Rs-28) indicates locally transgressive conditions despite the global early Oxfordian sea-level fall (Norris and Hallam 1995), implying tectonically-driven subsidence of the basin-floor.

Following the Late Jurassic to Early Cretaceous depositional gap in the study area, a dramatic change in the source areas and tectonic regime is signaled by our Late Cretaceous
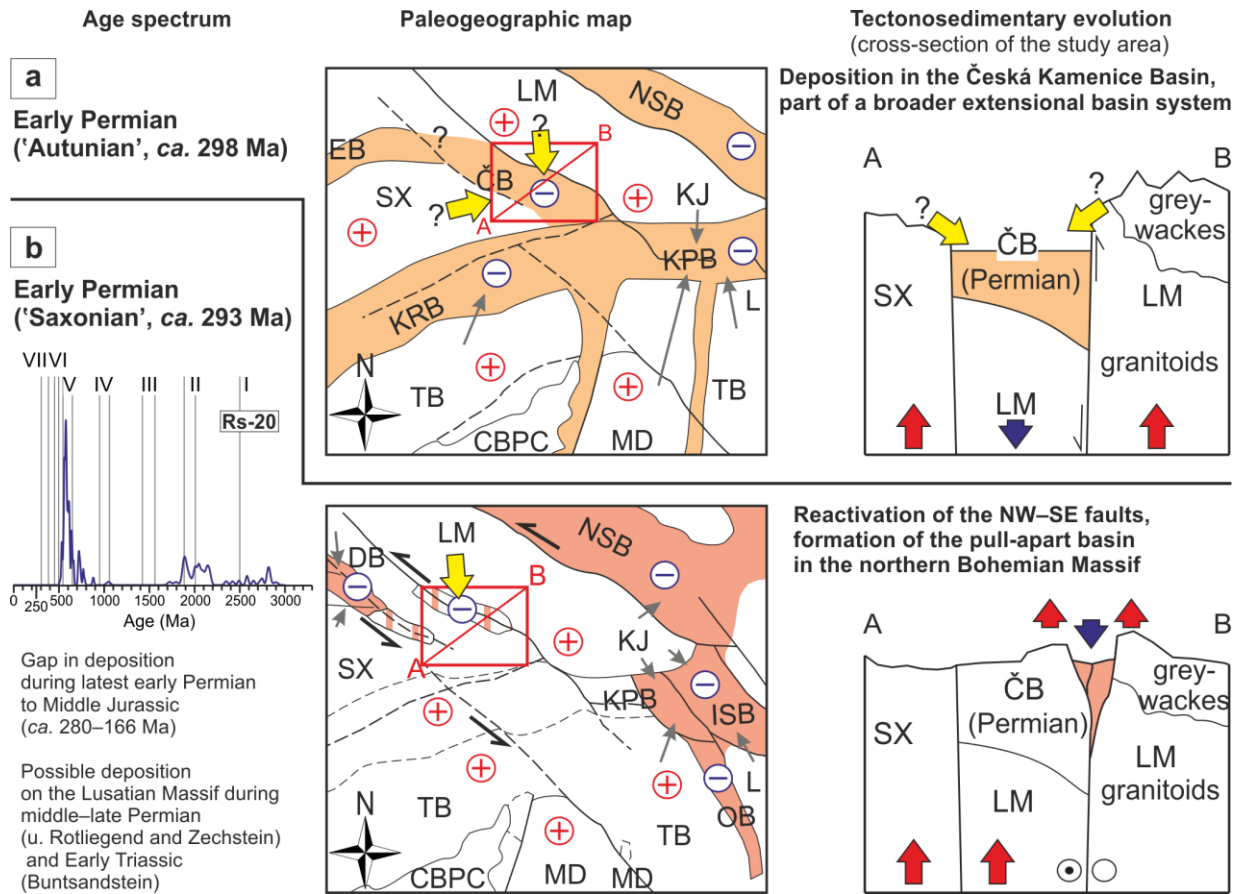
Figure 13 a–i. Schematic interpretive maps and cross-sections (along line A–B) summarizing the tectono sedimentary evolution of the northern Bohemian Massif as presented in this study from Permian to Late Cretaceous; see text for discussion. Arrows indicate the inferred direction of clastic supply; yellow—this study, gray—other sources, i.e., Martínek and Štolfová (2009); Martínek et al. (2012); Biernacka (2012a); Žák et al. (2018) for **(a)**; Berg (1938); Tásler (1979); Martínek and Uličný (2001); Lojka (2003); Zieger et al. (2019) for **(b)**; Voigt (1994); Uličný et al. (2009a); Biernacka and Józefiak (2009); Biernacka (2012b); Leszczyński (2018) for **(g)** and **(h)**. Brackets indicate that geological units were buried during the respective time interval. BCB – Bohemian Cretaceous Basin, CBPC – Central Bohemian Plutonic Complex, ČB – Česká Kamenice Basin, DB – Döhlen Basin, EB – Erzgebirge Basin, ESI – East Sudetic Island, ISB – Intra-Sudetic Basin, – KPB Krkonoše Piedmont Basin, KRB – Kladno–Rakovník Basin, KJ – Krkonoše–Jizera Metamorphic Complex, L – Lugian unit (eastern part), LM – Lusatian Massif, MD – Moldanubian unit, NSB – North Sudetic Basin, TB – Teplá–Barrandian unit, SX – Saxothuringian unit.

samples Rs-12 (late Cenomanian) to Rs-14 (middle to late Coniacian; Fig. 4). The most remarkable feature of their detrital zircon spectra is the abundance of ca. 1.5–1.0 Ga Baltica-derived zircons (Groups III and IV; Fig. 10). We find their direct input from source to the basin unlikely as the northern Bohemian Massif was separated from Baltica by an extensive marine realm, the hundreds of kilometers wide North German Basin (e.g., Voigt et al. 2008). Instead, the Baltica-derived zircons are interpreted here to record recycling of post-Oxfordian (sample Rs-28) to pre-Cenomanian (sample Rs-12), presumably Early Cretaceous deposits (Fig. 13e). This inference supports the hypothesis of Voigt (2009) and Hofmann et al. (2018), who assumed a Late Jurassic to Early Cretaceous basin of unknown thickness on top of the present-day Lusatian
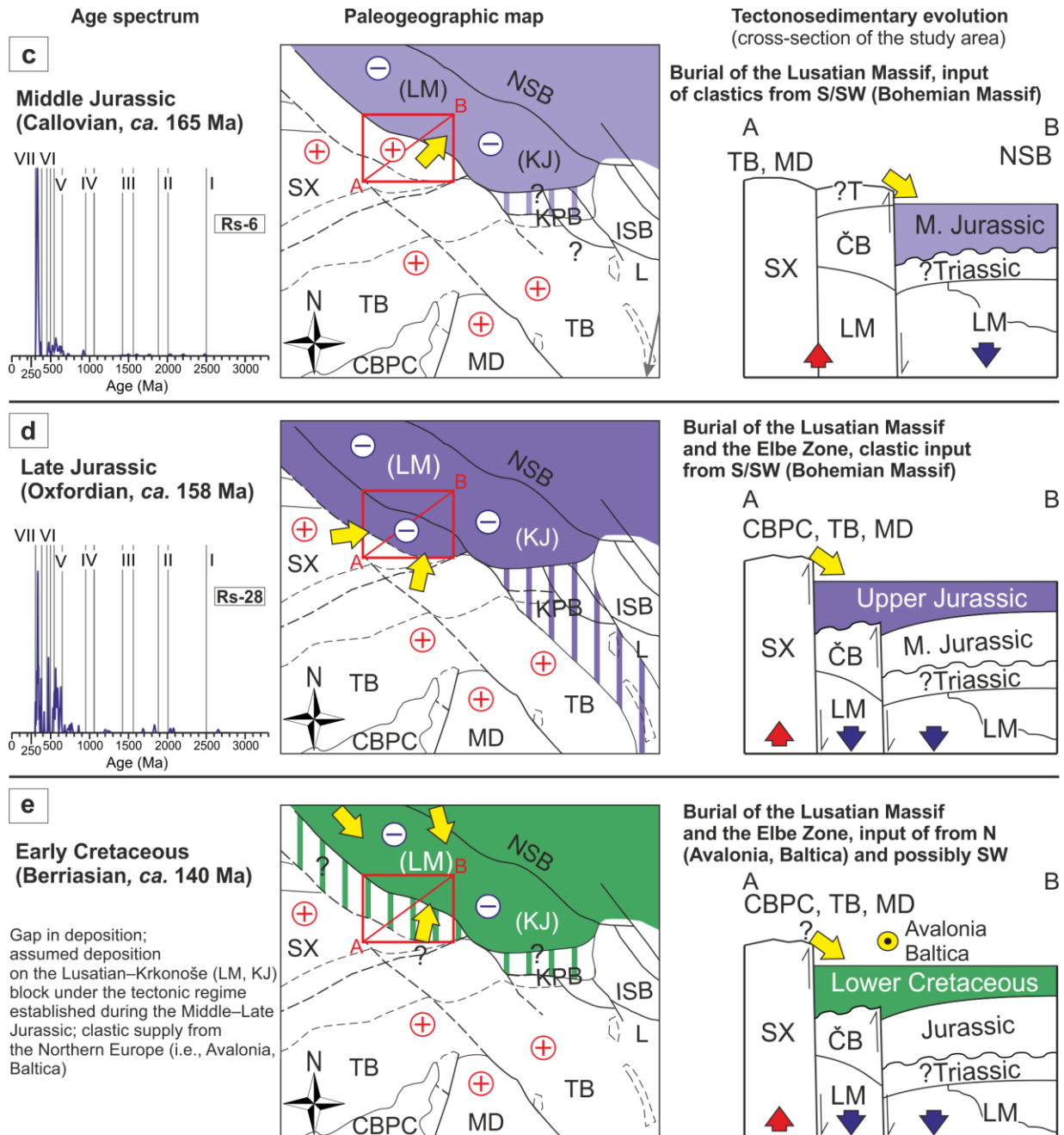
Figure 13 (continued),

Massif (see Fig. 11b) below referred to as the 'Lusatian Basin'. Vejbæk et al. (2010) and Mutterlose and Böckel (1998) showed that the area north and east of the Bohemian Massif was dominated by fluvial–lacustrine and deltaic to shallow-marine clastic depositional systems during Early Cretaceous, which may represent a favorable setting to deliver the Baltica-sourced zircons. Another supporting argument for the basin-scale recycling is the heavy mineral spectrum of the Rs-12 sample, exhibiting an anomalously high proportion of zircons (ca. 70 %; Fig. 7). Together with the mineralogical maturity and sorting of sandstones and general lack of material derived directly from granitic source rocks (micas, feldspar, lithic clasts), this also indicates a supply from older, mature sedimentary rocks, possibly in combination with further sorting by marine currents in a nearshore setting (e.g., Uličný 2001).
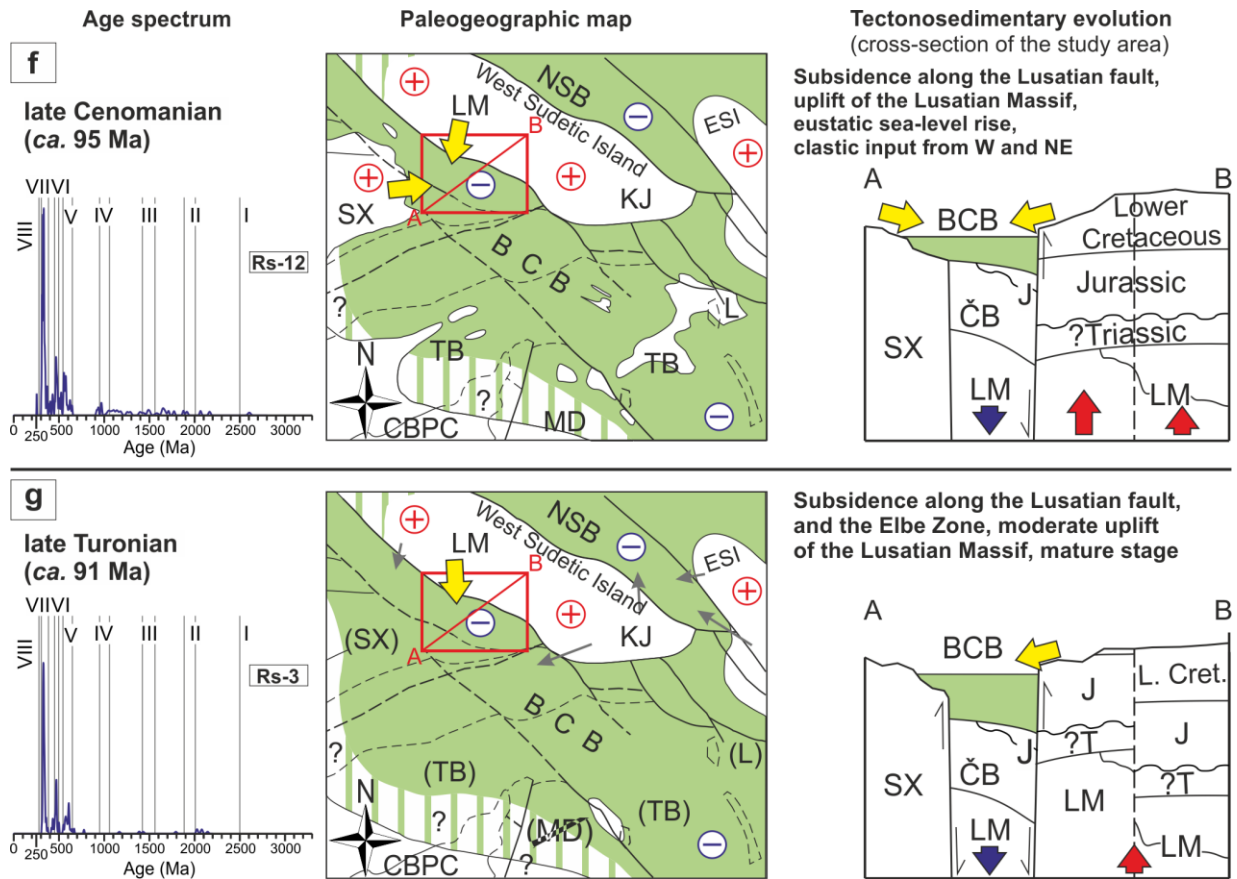
Figure 13 (continued),

Based on apatite fission-track and ZHe dating, Danišík et al. (2010) assumed that ca. 3.6–6 km of overburden was removed from the Krkonoše–Jizera Block since Permian, with maximum erosion (ca. 2.6–5 km) at around 100–75 Ma, a time interval roughly coinciding with the existence of the BCB. Part of its eroded overburden thus may have been represented by the Jurassic–Lower Cretaceous sedimentary fill of the Lusatian Basin. The end of deposition in the hypothetic Late Jurassic–Early Cretaceous basin may be constrained to end Albian from apatite fission-track ages, which indicate uplift of the Krkonoše–Jizera Block at around 97 Ma (Danišík et al. 2010). This event also marks onset of unroofing of the related Lusatian Block and its re-establishment as the source area (the West Sudetic Island; Fig. 13f–h) during late Cenomanian.

A further analysis of the detrital zircon spectra reveals an increased proportion of the Baltica-derived zircons at higher stratigraphic levels, reaching up to 25–30% per sample (Rs-27, Rs-1, Rs-14; Fig. 11). Provided this is not a sampling bias, we interpret abundant Baltica-derived zircons as reflecting accelerated uplift and intensified erosion/recycling of the Late Jurassic/Early Cretaceous basin fill during late Cenomanian–Coniacian (Fig. 13f–h). At this point, the detrital zircon spectra are remarkably consistent with the sedimentary record of tectonic reactivation and subsidence in the Bohemian Cretaceous Basin and coeval uplift of the West Sudetic Island since the latest Turonian (e.g., Uličný et al. 2009a; Nádaskay and Uličný 2014; Nádaskay et al. 2019).
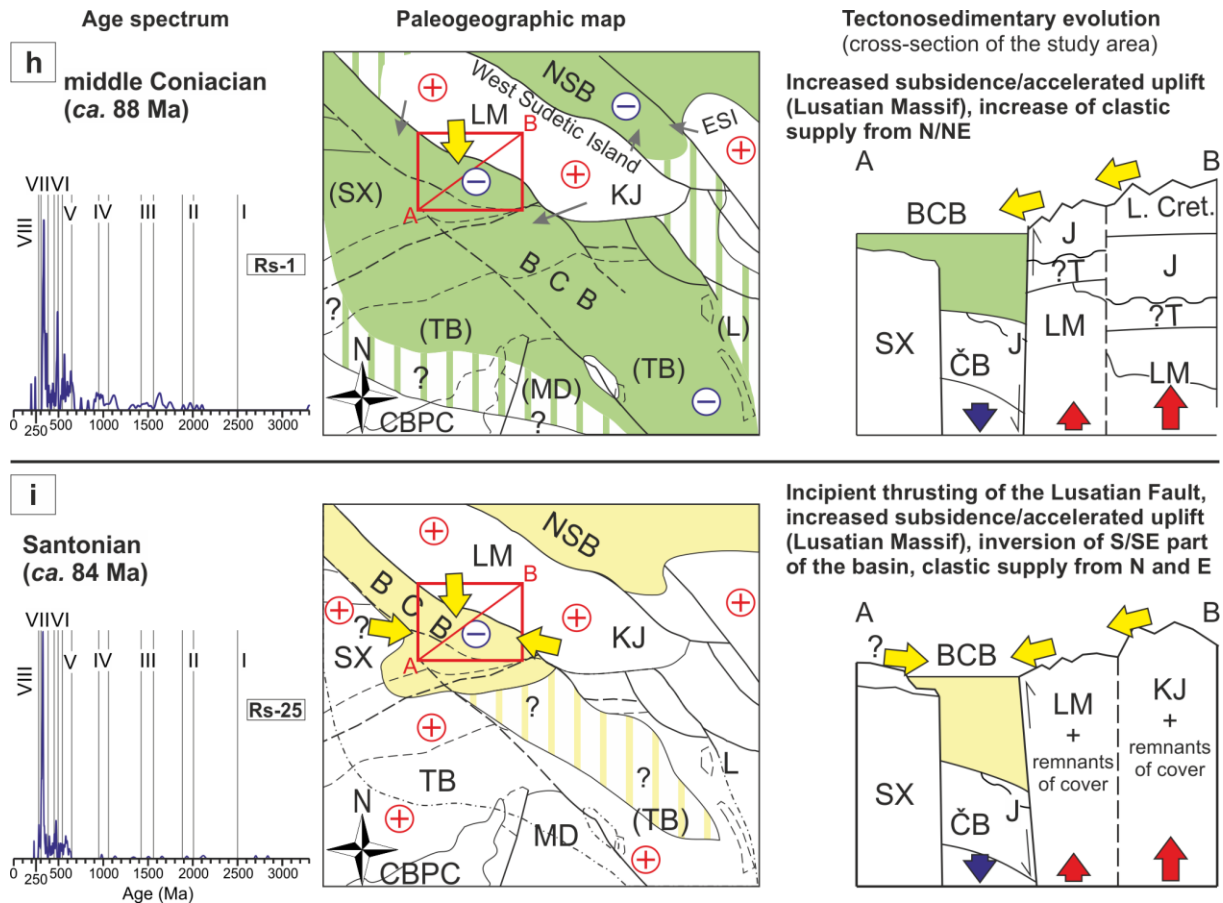
184

Figure 13 (continued),

In addition to the above, some further details can be inferred from stratigraphic variations in heavy mineral assemblages (Fig. 7), which indicate emergence of additional source areas (Fig. 9). For instance, an increasing proportion of tourmaline (up to 35 %) and monazite (up to 8 %) in the Turonian and Coniacian samples (Rs-13, Rs-3 and Rs-27, Rs-1, Rs-13, respectively; Fig. 7) point to a contribution from late-Variscan crustally-derived granites that occur in the Saxothuringian unit (Fig. 2). A proportion of rutile also increases up the section to as much as 35–40 % of the heavy mineral assemblage in the late Coniacian samples (Rs-27, Rs-1, RS-14; Fig. 7). These values are much higher than those in Jurassic and Cenomanian samples (Fig. 7). We interpret this pattern as indicating removal of the hypothetic Late Jurassic–Early Cretaceous Lusatian Basin from the source area where erosion of the West Sudetic Island reached pre-Jurassic rocks (e.g., Hofmann et al. 2018). Moreover, an increasing complexity of clay minerals in younger deposits (Štaffen 2002) may indicate contribution of diverse source rocks and could be interpreted in terms of accelerated differential uplift of individual fault-bounded blocks and variable fluvial incision within the West Sudetic Island from the latest Turonian onwards (Fig. 13h–i; see also Sobczyk et al. 2015).

Finally, the youngest major provenance change is recorded by the Santonian sample Rs-25 (Fig. 11). The abrupt disappearance of Baltica-sourced zircons is in agreement with the

complete erosion of remnants of the hypothetic Lusatian Basin (Fig. 13i). The Variscan Group VII dominates over Cambrian–Ordovician and Cadomian zircons (Groups IV and V, respectively) and could be explained by increased input from a granitic source; age peak at ca. 321 Ma (Fig. 8) corresponds to voluminous porphyritic granites within the easterly, rapidly uplifting Krkonoše–Jizera Block. A significant increase (up to 16 %) in proportion of feldspar grains in the sample supports this notion (Fig. 7). In a broader context, the sample Rs-25 marks the onset of regional basin inversion during the Santonian: the basin became substantially narrowed with the main depocenter shifted to near the Lusatian Fault, which was reactivated as a reverse fault, the seaway between the West and East Sudetic islands was closed, and deposition ended at around 86–85 Ma (Fig. 13i; Voigt et al. 2008; Leszczynski 2018). The end of deposition is also constrained by the emplacement of shallow-level dykes at ca. 77 Ma (early–middle Campanian; Pivec et al. 1998).

Paleogeographic and tectonic implications

The Jurassic period in Europe was marked by significant paleogeographic changes (e.g., Pieńkowski et al. 2008). The Early–Middle Jurassic uplift of the North Sea Dome and incipient extension in the area (e.g., Ziegler 1990c; Underhill and Partington 1993) significantly affected the North German Basin (e.g., Pieńkowski et al. 2008), but left no trace in the Bohemian Massif, a stable lithospheric block at that time. The emergence of individual islands on this block was previously assumed as being solely controlled by long-term sea-level fluctuations (e.g., Ziegler 1988; Pieńkowski et al. 2008). In contrast, our new detrital zircon ages may indicate significant Middle–Late Jurassic reactivation of major Variscan strike-slip faults (the NW–SE-trending Lusatian and Elbe fault zones) and accelerated subsidence and sediment supply during Early Cretaceous (Fig. 13c). To explain this event, far-field stress transfer from the initiating North Atlantic Rift may be considered as a possible geodynamic cause (e.g., Malkovský 1987).

We have shown that the Jurassic–Early Cretacous phase was followed by late Cenomanian inversion and uplift of the Lusatian Block, implying a major switch in kinematics and cause of the intra-plate deformation. This event led to the formation of a number of fault-related basins in Western and Central Europe, including the Bohemian Cretaceous Basin (e.g., Voigt et al. 2008; Uličný et al. 2009b). Gradual deformation of basin margins accompanied by basement-involved thrusting and deep erosion of uplifted flanks, similar processes as inferred above for the Bohemian Cretaceous Basin (Figs. 12f–i), were documented in the coeval Mid-Polish Trough and Subhercynian Basin (e.g., Gutowski et al. 2003; Krzywiec and Stachowska 2016; Krzywiec et al. 2018; Voigt et al. 2006; von Eynatten et al. 2008). We thus interpret that these intra-plate deformation processes were of regional scale and involved broader area of the

pre-Mesozoic basement in the Alpine foreland. The main phase of the Late Cretaceous intra-plate shortening is constrained between the latest Turonian and Campanian (ca. 86–70 Ma; e.g., Krzywiec 2006; Kockel 2003; Vejbæk and Andersen 2002; Voigt et al. 2004; Ziegler et al. 1995) and was interpreted as reflecting continental collision in the Alps (e.g., Marotta et al. 2001; Ziegler 1990a; Ziegler et al. 1995) or, alternatively, convergence of Africa–Iberia–Europe occurring at the same time (Kley and Voigt 2008).

Conclusions

1. The northern Bohemian Massif experienced a complex intra-plate tectonosedimentary evolution during Late Paleozoic to late Mesozoic that involved development of at least four generations of sedimentary basins in different settings: Permian intermontane red beds, Jurassic narrow marine seaway with tectonically-controlled transgression, Late Jurassic to Early Cretaceous, and Late Cretaceous marine transgression.

2. Combined U–Pb detrital zircon ages and heavy mineral analyses across this stratigraphic succession point to multiple, temporally evolving sources ranging from local (the Lusatian Block forming the West Sudetic Island) through more distant from elsewhere in the Bohemian Massif (Cadomian and Variscan basement) to exotic, likely derived from Baltica.

3. The Baltica-derived zircons are interpreted as a trace of now completely eroded Late Jurassic to Early Cretaceous basin that once covered the Lusatian Block and received Baltica-derived detritus from northerly fluvial and deltaic depositional systems. Fill of this hypothetic Lusatian Basin was then recycled into the Bohemian Cretaceous Basin during progressive unroofing of the West Sudetic Island.

4. A time-slice reconstruction of the paleogeographic and tectonosedimentary evolution of the northern Bohemian Massif shows that periods of basin development and deposition were interrupted by major depositional gaps (Middle Triassic–Early Jurassic, late Early Cretaceous, post-early Campanian). The Mesozoic depositional episodes resulted from reactivation of major NW–SE strike-slip fault zones due to stress transfer from the North Atlantic Rift during Jurassic to Early Cretaceous and were subsequently overridden by the far-field effect of convergence of Iberia, Africa, and Europe during Late Cretaceous.

References

Andersen, T., Saeed, A., Gabrielsen, R.H., Olaussen, S. (2011): Provenance characteristics of the Brumunddal sandstone in the Oslo Rift derived from U–Pb, Lu–Hf and trace element analyses of detrital zircons by laser ablation ICMPS. Norwegian Journal of Geology, 91, 1–19.

Arthaud, F., Matte, P. (1977): Late Paleozoic strike-slip faulting in southern Europe and northern Africa: result of a right-lateral shear zone between the Appalachians and the Urals. Geological Society of America Bulletin, 88, 1305–1320.

Asch, K. (2005): IGME 5000: 1:5 Million International Geological Map of Europe and Adjacent Areas – final version for the internet. Die Bundesanstalt für Geowissenschaften und Rohstoffe, Hannover.

Augustsson, C., Voigt, T., Bernhart, K., Kreißler, M., Gaupp, R., Gärtner, A., Hofmann, M., Linnemann, U. (2018): Zircon size-age sorting and source-area effect: the German Triassic Buntsandstein Group. Sedimentary Geology, 375, 218–231.

Awdankiewicz, M., Awdankiewicz, H., Kryza, R., Rodionov, N. (2010): SHRIMP zircon study of a micromonzodiorite dyke in the Karkonosze Granite, Sudetes (SW Poland): age constraints for late Variscan magmatism in Central Europe. Geological Magazine, 147, 77–85.

Betz, D., Führer, F., Greiner, G., Plein, E. (1987): Evolution of the Lower Saxony Basin. Tectonophysics, 137, 127–170.

Berg, G. (1938): Erläuterungen zu Blatt Landeshut. Lieferung 193. Preussische Geologische Landesanstalt, Berlin.

Bergerat, F. (1987): Stress fields in the European platform at the time of Africa–Eurasia collision. Tectonics, 6, 99–132.

Białek, D., Kryza, R., Oberc-Dziedzic, T., Pin, C. (2014): Cambrian Zawidów granodiorites in the Cadomian Lusatian Massif (Central European Variscides): What do the SHRIMP zircon ages mean? Journal of Geosciences, 59, 313–326.

Biernacka, J. (2012a): Detritus from Variscan lower crust in rotliegend sandstones of the intra-Sudetic Basin, SW Poland, revealed by detrital high-pyrope garnet. Annales Societatis Geologorum Poloniae, 82, 127–138.

Biernacka, J. (2012b): Provenance of Upper Cretaceous quartz-rich sandstones from the North Sudetic Synclinorium, SW Poland: constraints from detrital tourmaline. Geological Quarterly, 56, 315–332.

Biernacka, J., Józefiak, M. (2009): The Eastern Sudetic Island in the Early-to-Middle Turonian: evidence from heavy minerals in the Jerzmanice sandstones, SW Poland. Acta Geologica Polonica, 59, 545–565.

Bingen, B., Solli, A. (2009): Geochronology of magmatism in the Caledonian and Sveconorwegian belts of Baltica: synopsis for detrital zircon provenance studies. Norwegian Journal of Geology, 89, 267–290.

Brink, H.J., Dürschner, H., Trappe, H. (1992): Some aspects of the late and post-Variscan development of the northwestern German Basin. Tectonophysics, 207, 65–95.

Bruder, G. (1881): Zur Kenntnis der Juraablagerungen von Sternberg bei Zeidler in Böhmen. Sitzungsberichte der Akademie der Wissenschaften, 83, 47–49.

Bruder, G. (1882): Neue Beitrage zur Kenntnis der Juraablagerungen im nördlich Böhmen I. Sitzungsberichte der Akademie der Wissenschaften, 85, 450–490.

Burg, J.P., van den Driessche, J., Brun, J.P. (1994): Syn- to post-thickening extension in the Variscan Belt of Western Europe: modes and structural consequences. Géologie de la France, 3, 33–51.

Čech, S. (2011): Palaeogeography and stratigraphy of the Bohemian Cretaceous Basin (Czech Republic) – An overview. Geologické výzkumy na Moravě a ve Slezsku, 18, 18–21.

Čech, S., Klein, V., Kříž, J., Valečka, J. (1980): Revision of the Upper Cretaceous stratigraphy of the Bohemian Cretaceous Basin. Věstník Ústředního ústavu geologického, 55, 277–296.

Cloetingh, S. (1986): Intraplate stresses: a new tectonic mechanism for fluctuations of relative sea level. Geology, 14, 617–620.

Cloetingh, S., McQueen, H., Lambeck, K. (1985): On a tectonic mechanism for regional sea level variations. Earth and Planetary Science Letters, 75, 157–166.

Cloetingh, S., Ziegler, P.A., Bogaard, P.J.F., Andriessen, P.A.M., Artemieva, I.M., Bada, G., van Balen, R.T., Beekman, F., Ben-Avraham, Z., Brun, J.P., Bunge, H.P., Burov, E.B., Carbonell, R., Faccenna, C., Friedrich, A., Gallart, J., Green, A.G., Heidbach, O., Jones, A.G., Matenco, L., Mosar, J., Oncken, O., Pascal, C., Peters, G., Sliaupa, S., Soesoo, A., Spakman, W., Stephenson, R.A., Thybo, H., Torsvik, T., de Vicente, G., Wenzel, F., Wortel, M.J.R. (2007): TOPO-EUROPE: the geoscience of coupled deep Earth-surface processes. Global and Planetary Change, 58, 1–118.

Coubal, M. (1990): Compression along faults: example from the Bohemian Cretaceous Basin. Mineralia Slovaca, 22, 139–144.

Coubal, M., Adamovič, J., Málek, J., Prouza, V. (2014): Architecture of thrust faults with alongstrike variations in fault-plane dip: anatomy of the Lusatian Fault, Bohemian Massif. Journal of Geosciences, 59, 183–208.

Coubal, M., Málek, J., Adamovič, J., Štěpančíková, P. (2015): Late Cretaceous and Cenozoic dynamics of the Bohemian Massif inferred from the paleostress history of the Lusatian Fault Belt. Journal of Geodynamics, 87, 26–49.

Cháb, J., Stráník, Z., Eliáš, M. (2007): Geological map of the Czech Republic 1:500 000. Czech Geological Survey, Prague.

Dallmeyer, R.D., Franke, W., Weber, K. (1995): Pre-Permian Geology of Central and Eastern Europe. Springer, Berlin.

Danišík, M., Migoń, P., Kuhlemann, J., Evans, N.J., Dunkl, I., Frisch, W. (2010): Thermochronological constraints on the long-term erosional history of the Karkonosze Mts., Central Europe. Geomorphology, 117, 78–89.

Dewey, J.F., Helman, M.L., Turco, E., Hutton, D.H.W., Knott, S.D. (1989): Kinematics of the western Mediterranean. In: Coward, M.P., Dietrich, D., Park, R.G. (eds.): Alpine tectonics. Geological Society, London, Special Publications, 45, p. 265–283.

Doré, A.G. (1991): The structural foundation and evolution of Mesozoic seaways between Europe and the Arctic. Palaeogeography, Palaeoclimatology, Palaeoecology, 87, 441–492.

Dörr, W., Fiala, J., Vejnar, Z., Zulauf, G. (1998): U–Pb zircon ages and structural development of metagranitoids of the Teplá crystalline complex: evidence for pervasive Cambrian plutonism within the Bohemian massif (Czech Republic). Geologische Rundschau, 87, 135–149.

Dörr, W., Zulauf, G. (2010): Elevator tectonics and orogenic collapse of a Tibetan-style plateau in the European Variscides: the role of the Bohemian shear zone. International Journal of Earth Sciences, 99, 299–325.

Drost, K., Gerdes, A., Jeffries, T., Linnemann, U., Storey, C. (2011): Provenance of Neoproterozoic and early Paleozoic siliciclastic rocks of the Teplá–Barrandian unit (Bohemian Massif): evidence from U–Pb detrital zircon ages. Gondwana Research, 19, 213–231.

Edel, J.B., Weber, K. (1995): Cadomian terranes, wrench faulting and thrusting in the central Europe Variscides: geophysical and geological evidence. Geologische Rundschau, 84, 412–432.

Eliáš, M. (1981): Facies and paleogeography of the Jurassic of the Bohemian Massif. Sborník geologických věd, Geologie, 35, 75–144.

Erratt, D., Thomas, G.M., Wall, G.R.T. (1999): The evolution of the Central North Sea Rift. Geological Society, London, Petroleum Geology Conference Series, 5, 63–82.

Fediuk, F., Losert, J., Röhlich, P., Šilar, J. (1958): Geologické poměry území podél lužické poruchy ve Šluknovském výběžku. Rozpravy Československé akademie věd, Řada matematicko-přírodovědná, 68, 1–42.

Franke, W. (2000): The mid-European segment of the Variscides: tectonostratigraphic units, terrane boundaries and plate tectonic evolution. In: Franke, W., Haak, V., Oncken, O., Tanner, D. (eds.): Orogenic Processes: Quantification and Modelling in the Variscan Belt. Geological Society, London, Special Publications, 179, p. 35–61.

Franke, W. (2006): The Variscan orogen in Central Europe: construction and collapse. In: Gee, D.G., Stephenson, R.A. (eds.): European Lithosphere Dynamics. Geological Society, London, Memoirs, 32, p. 333–343.

Gehmlich, M., Linnemann, U., Tichomirowa, M., Lützner, H., Bombach, K. (1997): Die Bestimmung des Sedimentationsalters cadomischer Krustenfragmente im Saxothuringikum durch die Einzelzirkon Evaporatisationsmethode. Terra Nostra, 5, 46–49.

Golonka, J., Oszczypko, N., Ślączka, A. (2000): Late Carboniferous–Neogene geodynamic evolution and palaeogeography of the Circum-Carpathian region and adjacent areas. Annales Societatis Geologorum Poloniae, 70, 107–136.

Guiraud, R., Bosworth, W. (1999): Phanerozoic geodynamic evolution of northeastern Africa and the northwestern Arabian platform. Tectonophysics, 315, 73–108.

Gutowski, J., Krzywiec, P., Pożaryski, W. (2003): From extension to inversion: sedimentary record of Mesozoic tectonic evolution within the Marginal Fault Zone, SE Mid-Polish Trough. Geolines, 16, 38–39.

Hajná, J., Žák, J., Dörr, W. (2017): Time scales and mechanisms of growth of active margins of Gondwana: a model based on detrital zircon ages from the Neoproterozoic to Cambrian Blovice accretionary complex, Bohemian Massif. Gondwana Research, 42, 63–83.

Hajná, J., Žák, J., Dörr, W., Kachlík, V., Sláma, J. (2018): New constraints from detrital zircon ages on prolonged, multiphase transition from the Cadomian accretionary orogen to a passive margin of Gondwana. Precambrian Research, 317, 159–178.

Hayward, A.B., Graham, R.H. (1989): Some geometrical characteristic of inversion. In: Cooper, M.A., Williams, G.D. (eds.): Inversion tectonics. Geological Society, London, Special Publications, 44, p. 17–39.

Hecht, L., Vigneresse, J.L., Morteani, G. (1997): Constraints on the origin of zonation of the granite complexes in the Fichtelgebirge (Germany and Czech Republic): evidence from a gravity and geochemical study. Geologische Rundschau, 86, 93–109.

Herčík, F., Herrmann, Z., Valečka, J. (2003): Hydrogeology of the Bohemian Cretaceous Basin. Czech Geological Survey, Prague.

Hofmann, M., Linnemann, U., Voigt, T. (2013): The Upper Cretaceous section at Schmilka in Saxony (Elbsandsteingebirge, Germany): syntectonic sedimentation and inverted zircon age populations revealed by LA-ICP-MS U/Pb data. Geologica Saxonica, 59, 101–130.

Hofmann, M., Voigt, T., Bittner, L., Gärtner, A., Zieger, J., Linnemann, U. (2018): Reworked Middle Jurassic sandstones as a marker for Upper Cretaceous basin inversion in Central Europe – a case study for the U–Pb detrital zircon record of the Upper Cretaceous Schmilka section and their implication for the sedimentary cover of the Lausitz. International Journal of Earth Sciences, 107, 913–932.

Holcová, K., Holcová, M. (2016): Calcareous nannoplankton in the Upper Jurassic marine deposits of the Bohemian Massif: new data concerning the Boreal–Tethyan communication corridor. Geological Quarterly, 60, 624–636.

Holub, F.V., Cocherie, A., Rossi, P. (1997): Radiometric dating of granitic rocks from the Central Bohemian Plutonic Complex: constraints on the chronology of thermal and tectonic events along the Barrandian–Moldanubian boundary. Comptes Rendus de l Académie des Sciences, Series IIA, Earth and Planetary Science, 325, 19–26.

Hrbek, J. (2014): The Systematics and paleobiogeographic significance of sub-Boreal and Boreal ammonites (Aulacostephanidae and Cardioceratidae) from the Upper Jurassic of the Bohemian Massif. Geologica Carpathica, 65, 375–386.

Hubert, J.F. (1962): A zircon–tourmaline–rutile maturity index and the interdependence of the composition of heavy mineral assamblages with the gross composition and texture of sandstones. Journal of Sedimentary Petrology, 32, 440–450.

Illies, H. (1975): Intraplate tectonics in stable Europe as related to plate tectonics in the Alpine system. Geologische Rundschau, 64, 677–699.

Jackson, S.E., Pearson, N.J., Griffin, W.L., Belousova, E.A. (2004): The application of laser ablation-inductively coupled plasma-mass spectrometry to in situ U–Pb zircon geochronology. Chemical Geology, 211, 47–69.

Jakob, J., Alsaif, M., Corfu, F., Andersen, T.B. (2017): Age and origin of thin discontinuous gneiss sheets in the distal domain of the magma-poor hyperextended pre-Caledonian margin of Baltica, southern Norway. Journal of the Geological Society, 174, 557–571.

Janetschke, N., Wilmsen, M. (2014): Sequence stratigraphy of the lower Upper Cretaceous Elbtal Group (Cenomanian–Turonian of Saxony, Germany). Zeitschrift der Deutschen Gesellschaft für Geowissenschaften, 165, 179–207.

Janoušek, V., Wiegand, B.A., Žák, J. (2010): Dating the onset of Variscan crustal exhumation in the core of the Bohemian Massif: new U–Pb single zircon ages from the high-K calc-alkaline granodiorites of the Blatná suite, Central Bohemian Plutonic Complex. Journal of the Geological Society, 167, 347–360.

Kemnitz, H. (2007): The Lausitz graywackes, Saxo-Thuringia, Germany: witness to the Cadomian Orogeny. In: Linnemann, U., Nance, R.D., Kraft, P., Zulauf, G. (eds.): The Evolution of the Rheic Ocean: From Avalonian-Cadomian Active Margin to Alleghenian-Variscan Collision. Geological Society of America Special Papers, 423, p. 97–141.

Klein, T., Kiehm, S, Siebel, W., Shang, C.K., Rohrmüller, J., Dörr, W., Zulauf, G. (2008): Age and emplacement of late-Variscan granites of the western Bohemian Massif with main focus on the Hauzenberg granitoids (European Variscides, Germany). Lithos, 102, 478–507.

Klein, V. (1966): Stratigrafie a litologie svrchní křídy mezi Jizerou a Labem. Sborník geologických věd, Geologie, 11, 49–76.

Klein, V., Müller, V., Valečka, J. (1979): Lithofazielle und Paläogeographische Entwicklung des Böhmischen Kreidebeckens. In. Wiedmann, J. (ed.): Aspekte Des Kreide Europas. IUGS Series A, 6, p. 435–446.

Kley, J., Voigt T. (2008): Late Cretaceous intraplate thrusting in Central Europe: Effect of Africa-Iberia-Europe convergence, not alpine collision. Geology, 36, 839–842.

Kockel, F. (1986): Upper Cretaceous biostratigraphy – the key to the understanding of inversion tectonics in NW-Germany. Annales de la Société géologique de Belgique, 109, 357–361.

Kockel, F. (2003): Inversion structures in Central Europe: expressions and reasons, an open discussion. Netherlands Journal of Geosciences, 82, 351–366.

Košler, J., Kelley, S., Vrána, S. (2001): ^{40}Ar/^{39}Ar hornblende dating of a microgranodiorite dyke: implications for early Permian extension in the Moldanubian Zone of the Bohemian Massif. International Journal of Earth Sciences, 90, 379–385.

Košler, J., Konopásek, J., Sláma, J., Vrána, S. (2014): U–Pb zircon provenance of Moldanubian metasediments in the Bohemian Massif. Journal of the Geological Society, 171, 83–95.

Kröner, A., Hegner, E., Hammer, J., Haase, G., Bielicki, K.H., Krauss, M., Eidam, J. (1994): Geochronology and Nd–Sr systematics of Lusatian granitoids, significance for the evolution of the Variscan orogen in east–central Europe. Geologische Rundschau, 83, 357–376.

Kröner, A., Jaeckel, P., Hegner, E., Opletal, M. (2001): Single zircon ages and whole rock Nd isotopic systematics of early Palaeozoic granitoid gneisses from the Czech and Polish Sudetes (Jizerské hory, Krkonoše Mountains and Orlice–Sněžník Complex). International Journal of Earth Sciences, 90, 304–324.

Kroner, U., Romer, R.L. (2013): Two plates — many subduction zones: the Variscan orogeny reconsidered. Gondwana Research, 24, 298–329.

Kryza, R., Pin, C., Oberc-Dziedzic, T., Crowley, Q.G., Larionov, A. (2014): Deciphering the geochronology of a large granitoid pluton (Karkonosze Granite, SW Poland): an assessment of U–Pb Zircon SIMS and Rb–Sr whole-rock dates relative to U–Pb Zircon CA-ID-TIMS. International Geology Review, 56, 756–782.

Krzywiec, P. (2006): Structural inversion of the Pomeranian and Kuiavian segments of the Mid-Polish Trough: lateral variations in timing and structural style. Geological Quarterly, 51, 151–168.

Krzywiec, P., Stachowska, A. (2016): Late Cretaceous inversion of the NW segment of the Mid-Polish Trough: how marginal troughs were formed, and does it matter at all? Zeitschrift der Deutschen Gesellschaft für Geowissenschaften, 167, 107–119.

Krzywiec, P., Stachowska, A., Stypa, A. (2018): The only way is up – On Mesozoic uplifts and basin inversion events in SE Poland. In: Kilhams, B., Kukla, P.A., Mazur, S., McKie, T., Mijnlieff, H.F., van Oijk, K. (eds.): Mesozoic Resource Potential in the Southern Permian Basin. Geological Society, London, Special Publications, 469, p. 33–57.

Kučera, M., Pešek, J. (1982): Geology of the Česká Kamenice Basin and vicinity. Acta Universitatis Carolinae Geologica, 3, 285–295.

Lake, S.D., Karner, G.D. (1987): The structure and evolution of the Wessex Basin, southern England: an example of inversion tectonics. Tectonophysics, 137, 347–378.

Lamminen, J., Andersen, T., Nystuen, J.P. (2011): Zircon U–Pb ages and Lu–Hf isotopes from basement rocks associated with Neoproterozoic sedimentary successions in the Sparagmite region and adjacent areas, south Norway: the crustal architecture of western Baltica. Norwegian Journal of Geology, 91, 35–55

Laurin, J., Uličný, D. (2004): Controls on a shallow-water hemipelagic carbonate system adjacent to a siliciclastic margin: Example from late Turonian of Central Europe. Journal of Sedimentary Research, 74, 697–717.

Le Pichon, X., Bergerat, F., Roulet, M.J. (1988): Plate kinematics and tectonics leading to the Alpine belt formation: a new analysis. In: Clark, S.P., Burchfiel, B.C., Suppe, J. (eds.): Processes in Continental Lithospheric Deformation. Geological Society of America Special Papers, 218, p. 111–131.

Leszczyński, S. (2018): Integrated sedimentological and ichnological study of the Coniacian sedimentation in North Sudetic Basin, SW Poland. Geological Quarterly, 62, 767–816.

Liboriussen, J., Ashton, P., Tygesen, T. (1987): The tectonic evolution of the Fennoscandian border zone in Denmark. Tectonophysics, 137, 21–29.

Linnemann, U., Gehmlich, M., Tichomirowa, M., Buschmann, B., Nasdala, L., Jonas, P., Lützner, H., Bomback, K. (2000): From Cadomian subduction to Early Paleozoic rifting: the evolution of Saxo-Thuringia at the margin of Gondwana in the light of single zircon geochronology and basin development (Central European Variscides, Germany). In: Franke, W., Haak, V., Oncken, O., Tanner, D. (eds.): Orogenic Processes: Quantification and Modelling in the Variscan Belt. Geological Society, London, Special Publications, 179, 131–153.

Linnemann, U., McNaughton, N.J., Romer, R., Gehmlich, M., Drost, K., Tonk, C. (2004): West African provenance for Saxo-Thuringia (Bohemian Massif): did Armorica ever leave pre-Pangean Gondwana? U/Pb-SHRIMP zircon evidence and the Nd-isotopic record. International Journal of Earth Sciences, 93, 683–705.

Linnemann, U., Romer, R. (2002): The Cadomian Orogeny in Saxo-Thuringia, Germany: geochemical and Nd–Sr–Pb isotopic characterization of marginal basins with constraints to geotectonic setting and provenance. Tectonophysics, 352, 33–64.

Lojka, R. (2003): Sedimentologie aluviálních uloženin a původ klastického materiálu trutnovského souvrství ve vnitrosudetské pánvi (spodní perm, Čechy). MSc. thesis, Charles University, Prague.

Lorenz, V., Nicholls, I.A. (1976): The Permocarboniferous Basin and Range Province of Europe. An application of plate tectonics. In: Falke, H. (ed.): The Continental Permian in Central, West, and South Europe. D. Reidel Publishing Company, Dordrecht, p. 313–342.

Lorenz, V, Nicholls, I.A. (1984): Plate and intraplate processes of Hercynian Europe during the Late Paleozoic. Tectonophysics, 107, 25–56.

Ludwig, K.R. (2008): Isoplot/Ex 3.70. A Geochronological Toolkit for Microsoft Excel. Berkeley Geochronological Center, Special Publication 4, Berkeley.

Malkovský, M. (1987): The Mesozoic and Tertiary basins of the Bohemian Massif and their evolution. Tectonophysics, 137, 31–42.

Marotta, A.M., Bayer, U., Scheck, M., Thybo, H. (2001): The stress field below the NE German basin: effects induced by the Alpine collision. Geophysical Journal International, 144, 8–12.

Martínek, K., Blecha, M., Daněk, V., Franců, J., Hladíková, J., Johnová, R., Uličný, D. (2006): Record of palaeoenvironmental changes in a Lower Permian organic-rich lacustrine succession: integrated sedimentological and geochemical study of the Rudník Member, Krkonoše Piedmont Basin, Czech Republic. Palaeogeography, Palaeoclimatology, Palaeoecology, 230, 85–128.

Martínek, K., Štolfová, K. (2009): Provenance study of Permian non-marine sandstones and conglomerates of the Krkonoše Piedmont Basin (Czech Republic): exotic marine limestone pebbles, heavy minerals and garnet composition. Bulletin of Geosciences, 84, 555–568.

Martínek, K., Uličný, D. (2001): Depositional Processes in a Low-Sinuosity Fluvial System: Facies and Depositional Geometries of the Permian Havlovice Member, Krkonoše Piedmont Basin. Geolines, 13, 89–90.

Martínek, K., Verner, K., Buriánek, D., Žáček, V. (2012): Zdrojové horniny detritických biotitů spodněpermských pískovců severního okraje podkrkonošské pánve. Zprávy o geologických výzkumech, 46, 45–50.

Marshak, S., Paulsen, T. (1996): Midcontinent U.S. fault and fold zones: a legacy of Proterozoic intracratonic extensional tectonism? Geology, 24, 151–154.

Massari, F. (1996): Upper-flow-regime stratification types on steep-face, coarse-grained, Gilbert-type progradational wedges (Pleistocene, Southern Italy). Journal of Sedimentary Research, 66, 364–375.

Massari, F. (2017): Supercritical-flow structures (Backset-bedded sets and sediment waves) on high-gradient clinoform systems influenced by shallow-marine hydrodynamics. Sedimentary Geology, 360, 73–95.

Mattern, F. (2001): Permo-Silesian movements between Baltica and Western Europe: tectonics and 'basin families'. Terra Nova, 13, 368–375.

Meier, T., Soomro, R.A., Viereck, L., Lebedev, S., Behrmann, J.H., Weidle, C., Cristiano, L., Hanemann, R. (2016): Mesozoic and Cenozoic evolution of the Central European lithosphere. Tectonophysics, 692, 58–73.

Meinhold, G., Morton, A.C., Fanning, C.M., Frei, D., Howard, J.P., Phillips, R.J., Strogen, D., Whitham, A.G. (2011): Evidence from detrital zircons for recycling of Mesoproterozoic and Neoproterozoic crust recorded in Paleozoic and Mesozoic sandstones of southern Libya. Earth and Planetary Science Letters, 312, 164–175.

Ménard, G., Molnar, P. (1988): Collapse of a Hercynian Tibetan Plateau into a late Palaeozoic European Basin and Range province. Nature, 334, 235–237.

Mlčoch, B., Krentz, O., Nádaskay, R., Valečka, J., Mrázová, Š., Junge, R., Reinhardt, S., Pohle, M. (2018): Geologische Karte des Sächsisch–Böhmischen Kreidebeckens. Geologická mapa sasko-české křídové pánve. 1:100 000. Česká geologická služba, Praha, Sächsische Landesamt für Umwelt, Landwirtschaft und Geologie, Freiberg.

Mortimore, R.N. (1986): Controls on Upper Cretaceous sedimentation in the South Downs with particular reference to flint distribution. In: Sieveking, G. de G., Hart, M.B. (eds.): The Scientific Study of Flint and Chert. Cambridge University Press, p. 21–42.

Mortimore, R.N. (2018): Late Cretaceous tectonosedimentary events in NW Europe. Proceedings of the Geologists' Association, 129, 392–420.

Mortimore, R.N., Pomerol, B. (1997): Upper Cretaceous tectonic phases and end Cretaceous inversion in the Chalk of the Anglo-Paris Basin. Proceedings of the Geologists' Association, 108, 231–255.

Mortimore, R.N., Wood, C.J., Pomerol, B., Ernst, G. (1998): Dating the phases of the Subhercynian tectonic epoch: Late Cretaceous tectonics and eustatics in the Cretaceous Basins of Northern Germany compared with the Anglo-Paris Basin. Zentralblatt für Geologie und Paläontologie, Teil I, 1996, 1349–1401.

Morton, A.C., Hallsworth, C.R. (1999): Processes controlling the composition of heavy mineral assemblages in sandstones. Sedimentary Geology, 124, 3–29.

Morton, A.C., Hurst, A. (1995): Correlation of sandstones using heavy minerals: an example from the Statfjord Formation of the Snorre field, northern North Sea. In: Dunay, R.E., Hailwood, E.A. (eds.): Non-biostratighraphical Methods of Dating and Correlation. Geological Society, London, Special Publications, 89, p. 3–22.

Mutterlose, J., Böckel, B. (1998): The Barremian–Aptian interval in NW Germany: a review. Cretaceous Research, 19, 539–568.

Nádaskay, R., Uličný, D. (2014): Genetic stratigraphy of Coniacian deltaic deposits of the northwestern part of the Bohemian Cretaceous Basin. Zeitschrift der Deutschen Gesellschaft für Geowissenschaften, 165, 547–575.

Nádaskay, R., Kochergina, Y.V., Čech, S., Švábenická, L., Valečka, J., Erban, V., Halodová, P., Čejková, B. (2019): Integrated stratigraphy of an offshore succession influenced by intense siliciclastic supply: Implications for Coniacian tectonosedimentary evolution of the West Sudetic area (NW Bohemian Cretaceous Basin, Czech Republic). Cretaceous Research, 102, 127–159.

Nance, R.D., Gutierréz-Alonso, G., Keppie, J.D., Linnemann, U., Murphy, J.B., Quesada, C., Strachan, R.A., Woodcock, N.H. (2010): Evolution of the Rheic Ocean. Gondwana Research, 17, 194–222.

Niebuhr, B., Baldschuhn, R., Ernst, G., Walaszczyk, I., Weiss, W., Wood, C.J. (1999): The Upper Cretaceous succession (Cenomanian–Santonian) of the Staffhorst shaft, Lower Saxony, northern Germany: Integrated biostratigraphic, lithostratigraphic and downhole geophysical log data. Acta Geologica Polonica, 49, 175–213.

Nielsen, S.B., Stephenson, R., Thomsen, E. (2007): Dynamics of mid-Palaeocene North Atlantic rifting linked with European intra-plate deformations. Nature, 450, 1071–1074.

Nielsen, S.B., Thomsen, E., Hansen, D.L., Clausen, O.R. (2005): Plate-wide stress relaxation explains European Palaeocene Basin inversions. Nature, 435, 195–198.

Norling, E., Bergström, J. (1987): Mesozoic and Cenozoic tectonic evolution of Scania, southern Sweden. Tectonophysics, 137, 7–19.

Norris, M.S., Hallam, A. (1995): Facies variations across the Middle–Upper Jurassic boundary in Western Europe and the relationship to sea-level changes. Palaeogeography, Palaeoclimatology, Palaeoecology, 116, 189–245.

Opluštil, S., Schmitz, M., Kachlík, V., Štamberg, S. (2016): Re-assesment of lithostratigraphy, biostratigraphy and volcanic activity of the Late Paleozoic Intra-Sudetic, Krkonoše-Piedmont and Mnichovo Hradiště basins (Czech Republic) based on new U-Pb CA-ID-TIMS ages. Bulletin of Geosciences, 91, 399–432.

Pastor-Galán, D., Groenewegen, T., Brouwer, D., Krijgsman, W., Dekkers, M.J. (2015): One or two oroclines in the Variscan Orogen of Iberia? Implications for Pangea amalgamation. Geology, 43, 527–530.

Paul, J., Wemmer, K., Ahrendt, H. (2008): Provenance of siliciclastic sediments (Permian to Jurassic) in the Central European Basin. Zeitschrift der Deutschen Gesellschaft für Geowissenschaften, 159, 641–650.

Paul, J., Wemmer, K., Wetzel, F. (2009): Keuper (Late Triassic) sediments in Germany: indicators of rapid uplift of Caledonian rocks in southern Norway. Norwegian Journal of Geology, 89, 193–202.

Pešek, J. (2001): Geologie a ložiska svrchnopaleozoickych limnickych pánví České Republiky. Český geologický ústav, Praha.

Petrus, J.A., Kamber, B.S. (2012): VizualAge: a novel approach to laser ablation ICP-MS U–Pb geochronology data reduction. Geostandards and Geoanalytical Research, 36, 247–270.

Pieńkowski, G., Schudack, M., Bosák, P., Enay, R., Feldman-Olszewska, A., Golonka, J., Gutowski, J., Herngreen, J.G.F.W., Jordan. P., Krobicki, M., Lathuiliere, B., Leinfelder, R., Michalík, J., Mönnig, E., Noe-Nygaard, N., Pálfy, J., Pint, A., Rasser, M.W., Reisdorf, A.G., Schmid, D.U., Schweigert, G., Surlyk, F., Wetzel, A., Wong, T.E. (2008): Jurassic. In: McCann, T. (ed.): Geology of Central Europe, Volume 2: Mesozoic and Cenozoic. Geological Society, London, p. 823–922.

Pin, C., Kryza, R., Oberc-Dziedzic, T., Mazur, S., Turniak, K., Waldhausrová, J. (2007): The diversity and geodynamic significance of Late Cambrian (ca. 500 Ma) felsic anorogenic magmatism in the northern part of the Bohemian Massif: a review based on Sm–Nd isotope and geochemical data. In: Linnemann, U., Nance, R.D., Kraft, P., Zulauf, G. (eds.): The Evolution of the Rheic Ocean: From Avalonian-Cadomian Active Margin to Alleghenian-Variscan Collision. Geological Society of America Special Papers, 423, p. 209–229.

Pivec, E., Ulrych, J., Höhndorf, A., Rutšek, J. (1998): Melilititic rocks from northern Bohemia: geochemistry and mineralogy. Neues Jahrbuch für Mineralogie - Abhandlungen, 1998, 312–339.

Reicherter, K., Froitzheim, N., Jarosiński, M., Badura, J., Franzke, H.J., Hansen, M., Hübscher, C., Müller, R., Stackebrandt, W., Voigt, T., von Eynatten, H., Zuchiewicz, W. (2008): Alpine tectonics north of the Alps. In: McCann, T. (ed.): Geology of Central Europe, Volume 2: Mesozoic and Cenozoic. Geological Society, London, p. 999–1030.

Scupin, H. (1936): Zur Palaeographie des sudetischen Kreidemeeres. Zeitschrift der Deutschen Gesellschaft für Geowissenschaften, 88, 309–325.

Scheck, M., Bayer, U. (1999): Evolution of the northeast German Basin: inferences from a 3D structural model and subsidence analysis. Tectonophysics, 313, 145–169.

Scheck-Wenderoth, M., Krzywiec, P., Zühlke, R., Maystrenko, Y., Froitzheim, N. (2008): Permian to Cretaceous tectonics. In: McCann, T. (ed.): Geology of Central Europe, Volume 2: Mesozoic and Cenozoic. Geological Society, London, p. 999–1030.

Schmid, S.M., Bernoulli, D., Fügenschuh, B., Matenco, L., Schefer, S., Schuster, R., Tischler, M., Ustaszewski, K. (2008) The Alpine–Carpathian–Dinaridic orogenic system: correlation and evolution of tectonic units. Swiss Journal of Geosciences, 101, 139–183.

Schulmann, K., Konopásek, J., Janoušek, V., Lexa, O., Lardeaux, J.M., Edel, J.B., Štípská, P., Ulrich, S. (2009): An Andean type Palaeozoic convergence in the Bohemian Massif. Comptes Rendus - Géoscience, 341, 266–286.

Siebel, W., Breiter, K., Wendt, I., Höhndorf, A., Henjes-Kunst, F., René, M. (1999): Petrogenesis of contrasting granitoid plutons in western Bohemia (Czech Republic). Mineralogy and Petrology, 65, 207–235.

Siebel, W., Chen, F., Satir, M. (2003): Late-Variscan magmatism revisited: new implications from Pb-evaporation zircon ages on the emplacement of redwitzites and granites in NE Bavaria. International Journal of Earth Sciences, 92, 36–53.

Siebel, W., Shang, C.K., Reitter, E., Rohrmüller, J., Breiter, K. (2008): Two distinctive granite suites in the SW Bohemian Massif and their record of emplacement: constraints from geochemistry and zircon $^{207}Pb/^{206}Pb$ chronology. Journal of Petrology, 49, 1853–1872.

Siebel, W., Trzebski, R., Stettner, G., Hecht, L., Casten, U., Hohndorf, A., Muller, P. (1997): Granitoid magmatism of the NW Bohemian massif revealed: gravity data, composition, age relations and phase concept. Geologische Rundschau, 86, 45–63.

Skoček, V., Valečka, J. (1983): Paleogeography of the Late Cretaceous Quadersandstein of Central Europe. Palaeogeography, Palaeoclimatology, Palaeoecology, 44, 71–92.

Sláma, J., Košler, J., Condon, D.J., Crowley, J.L., Gerdes, A., Hanchar, J.M., Horstwood, M.S.A., Morris, G.A., Nasdala, L., Norberg, N., Schaltegger, U., Schoene, B., Tubrett, M.N., Whitehouse, M.J. (2008): Plešovice zircon: a new natural reference material for U–Pb and Hf isotopic microanalysis. Chemical Geology, 249, 1–35.

Sobczyk, A., Danišík, M., Aleksandrowski, P., Anczkiewicz, A. (2015): Post-Variscan cooling history of the central Western Sudetes (NE Bohemian Massif, Poland) constrained by apatite fission-track and zircon (U–Th)/He thermochronology. Tectonophysics, 649, 47–57.

Stampfli, G.M., von Raumer, J.F., Borel, G.D. (2002): Paleozoic evolution of pre-Variscan terranes: from Gondwana to the Variscan collision. Geological Society of America Special Papers, 364, 263–280.

Štaffen, Z. (2002): Chemostratigraphic determination of equivalent strata and formations in Bohemian Cretaceous Basin. Acta Montana, Seria A, 21, 77–109.

Štolfová, K. (2004): Architectural element analysis of fluvial sandstones, Vrchlabí formation, Krkonoše Piedmont Basin, NE Czech Republic: Tectonic and climate controls. Unpublished MSc. thesis, Charles University, Prague.

Svoboda, J. (1964): Regionální geologie ČSSR I/2. Ústřední ústav geologický, Praha.

Tásler, R. (1979): Geologie české části vnitrosudetské pánve. Academia/Ústřední ústav geologický, Praha.

Tichomirowa, M. (2002): Zircon inheritance in diatexite granodiorites and its consequence on geochronology: a case study in Lusatia and Erzgebirge (Saxo-Thuringia, eastern Germany). Chemical Geology, 191, 209–224.

Tucker, R.M., Arter, G. (1987): The tectonic evolution of the North Celtic Sea and Cardigan Bay Basins with special reference to basin inversion. Tectonophysics, 137, 291–307.

Tunheng, A., Hirata, T. (2004): Development of signal smoothing device for precise elemental analysis using laser ablation-ICP-mass spectrometry. Journal of Analytical Atomic Spectrometry, 19, 932–934.

Uličný, D. 2001. Depositional systems and sequence stratigraphy of coarse-grained deltas in a shallow-marine, strike-slip setting: The Bohemian Cretaceous Basin, Czech Republic. Sedimentology, 48, 599–628.

Uličný, D., Jarvis, I., Gröcke, D.R., Čech, S., Laurin, J., Olde, K., Trabucho-Alexandre, J.P., Švábenická, L., Pedentchouk, N. (2014): A high-resolution carbon-isotope record of the Turonian stage correlated to a siliciclastic basin fill: Implications for mid-Cretaceous sea-level change. Palaeogeography, Palaeoclimatology, Palaeoecology, 405, 42–58.

Uličný, D., Laurin, J., Čech, S. (2009a): Controls on clastic sequence geometries in a shallow-marine, transtensional basin: The Bohemian Cretaceous Basin, Czech Republic. Sedimentology, 56, 1077–1114.

Uličný, D., Martínek, K., Grygar, R. (2002): Syndepositional geometry and post-depositional deformation of the Krkonoše Piedmont Basin: a preliminary model. Geolines, 14, 101–102.

Uličný, D., Špicáková, L., Grygar, R., Svobodová, M., Čech, S., Laurin, J. (2009b) Palaeodrainage systems at the basal unconformity of the Bohemian Cretaceous Basin: Roles of inherited fault systems and basement lithology during the onset of basin filling. Bulletin of Geosciences, 84, 577–610.

Underhill, J.R., Partington, M.A. (1993): Jurassic thermal doming and deflation in the North Sea: implications of the sequence stratigraphic evidence. Geological Society, London, Petroleum Geology Conference Series, 4, 337–345.

Valečka, J. (1975): Litologie, cyklická stavba a geneze bazálních svrchnokřídových sedimentů západně od Děčína. Časopis pro mineralogii a geologii, 20, 409–416.

Valečka, J. (1979): Paleogeografie a litofaciální vývoj severozápadní části české křídové pánve. Sborník geologických věd, Geologie, 33, 47–81.

Valečka, J. (1989): Sedimentology, stratigraphy and cyclicity of the Jizera Formation (Middle–Upper Turonian) in the Děčín area (N. Bohemia). Věstník Ústředního ústavu geologického, 64, 77–90.

Valečka, J. (1994): Litologické změny v nejvyšší části jizerského souvrství v ssv. okolí České Kamenice a jejich vztah k paleoproudovému režimu. Zprávy o geologických výzkumech, 1993, 96–97.

Valečka J. et al. (2000): Vysvětlivky k základní geologické mapě České republiky 1:25 000, list 02-242 Dolní Podluží. Česká geologická služba. Praha.

Valečka, J. (2015): Říční sedimenty peruckých vrstev české křídové pánve u Benešova nad Ploučnicí. Zprávy o geologických výzkumech, 48, 31–36.

Valečka, J., Rejchrt, M. (1973): Litologie a geneze tzv. flyšoidní facie coniaku ve východní části Českého středohoří. Časopis pro mineralogii a geologii, 18, 379–391.

Valečka, J., Skoček, V. (1991): Late Cretaceous lithoevents in the Bohemian Cretaceous Basin, Czechoslovakia. Cretaceous Research, 12, 561–577.

Valečka J., Slavík. J. (1985): Litologický a sedimentologický vývoj na křídových stratotypových lokalitách Sutiny a Merboltice. Unpublished report. Czech Geological Survey, Prague.

Valverde-Vaquero, P., Dörr, W., Belka, Z., Franke, W., Wiszniewska, J., Schastok, J. (2000) U–Pb single-grain dating of detrital zircon in the Cambrian of central Poland: implications for Gondwana versus Baltica provenance studies. Earth and Planetary Science Letters, 184, 225–240.

van der Pluijm, B.A., Craddock, J.P., Graham, B.R., Harris, J.H. (1997): Paleostress in cratonic North America: implications for deformation of continental interiors. Science, 277, 794–796.

van Wijhe, D.H. (1987): Structural evolution of inverted basins in the Dutch offshore. Tectonophysics, 137, 171–219.

Vejbæk, O.V., Andersen, C. (2002): Post mid-cretaceous inversion tectonics in the Danish Central Graben: regionally synchronous tectonic events? Bulletin of the Geological Society of Denmark, 49, 129–144.

Vejbæk, O.V., Andersen, C., Dusa, M., Herngreen, W., Krabbe, H., Leszczynski, K., Lott, G.K., Mutterlose, J., van der Molen, A.S. (2010): Cretaceous. In: Doornenbal, H., Stevenson, A. (eds.): Petroleum Geological Atlas of the Southern Permian Basin Area. EAGE Publications, Houten, p. 195–209.

Ventura, B., Lisker, F. (2003): Long-term landscape evolution of the northeastern margin of the Bohemian Massif: apatite fission-track data from the Erzgebirge (Germany). International Journal of Earth Sciences, 92, 961–700.

Whitney, D.L., Evans, B.W. (2010): Abbreviations for names of rock-forming minerals. American Mineralogist, 95, 185–187.

Voigt, S., Wagreich, M., Surlyk, F., Walaszczyk, I., Uličný, D., Čech, S., Voigt T., Wiese, F., Wilmsen, M., Niebuhr, B., Reich, M., Funk, H., Michalík, J., Jagt., J.W.M., Felder, P.J., Schulp, A.S. (2008): Cretaceous. In: McCann, T. (ed.): Geology of Central Europe, Volume 2: Mesozoic and Cenozoic. Geological Society, London, p. 923–997.

Voigt, T. (1994): Faziesentwicklung und Ablagerungssequenzen am Rand eines Epikontinentalmeeres – Die Sedimentationsgeschichte der Sächsischen Kreide. Unpublished PhD. thesis, TU Bergakademie Freiberg.

Voigt, T. (1998): Entwicklung und Architektur einer fluviatilen Talfüllung: die Niederschöna Formation im Sächsischen Kreidebecken. Abhandlungen des Staatlichen Museums für Mineralogie und Geologie zu Dresden, 43–44, 121–139.

Voigt, T. (2009) Die Lausitzer-Riesengebirgs-Antiklinalzone als kreidezeitliche inversionsstruktur: geologische Hinweise aus den umgebenden Kreidebecken. Zeitschrift für Geologische Wissenschaften, 37, 15–39.

Voigt, T., von Eynatten, H., Franzke, H.J. (2004): Late Cretaceous unconformities in the Subhercynian Cretaceous Basin (Germany). Acta Geologica Polonica, 54, 673–694.

Voigt, T., Wiese, F., von Eynatten, H., Franzke, H.J., Gaupp, R. (2006): Facies evolution of syntectonic Upper Cretaceous deposits in the Subhercynian Cretaceous Basin and adjoining areas (Germany). Zeitschrift der Deutschen Gesellschaft für Geowissenschaften, 157, 203–243.

von Eynatten, H., Voigt, T., Meier, A., Franzke, H.-J., Gaupp, R. (2008): Provenance of Cretaceous clastics in the Subhercynian Basin: Constraints to exhumation of the Harz Mountains and timing of inversion tectonics in Central Europe. International Journal of Earth Sciences, 97, 1315–1330.

Wiedenbeck, M., Allé, P., Corfu, F., Griffin, W.L., Meier, M., Oberli, F., von Quadt, A., Roddick, J.C., Spiegel, W. (1995) Three natural zircon standards for U–Th–Pb, Lu–Hf, trace element and REE analyses. Geostandards Newsletter, 19, 1–23.

Wiest, J.D., Jacobs, J., Ksienzyk, A.K., Fossen, H. (2018): Sveconorwegian vs. Caledonian orogenesis in the Eastern Øygarden Complex, SW Norway: geochronology, structural constraints and tectonic implications. Precambrian Research, 305, 1–18.

Wilmsen, M., Niebuhr, B., Chellouche, P., Pürner, T., Kling, M. (2010): Facies pattern and sea-level dynamics of the early Late Cretaceous transgression: a case study from the lower Danubian Cretaceous Group (Bavaria, southern Germany). Facies, 56, 483–507.

Winchester, J.A., Pharaoh, T.C., Verniers, J., Ioane, D., Seghedi, A. (2006): Palaeozoic accretion of Gondwana-derived terranes to the East European Craton: recognition of detached terrane fragments dispersed after collision with promontories. In: Gee, D.G., Stephenson, R.A. (eds.): European Lithosphere Dynamics. Geological Society, London, Memoirs, 32, 232–332.

Žák, J., Svojtka, M., Opluštil, S. (2018): Topographic inversion and changes in the sediment routing systems in the Variscan orogenic belt as revealed by detrital zircon and monazite U–Pb geochronology in post-collisional continental basins. Sedimentary Geology, 377, 63–81.

Žák, J., Sláma, J. (2018): How far did the Cadomian 'terranes' travel from Gondwana during early Palaeozoic? A critical reappraisal based on detrital zircon geochronology. International Geology Review, 60, 319–338.

Žák, J., Verner, K., Finger, F., Faryad, S.W., Chlupáčová, M., Veselovský, F. (2011): The generation of voluminous S-type granites in the Moldanubian unit, Bohemian Massif, by rapid isothermal exhumation of the metapelitic middle crust. Lithos, 121, 25–40.

Žák, J., Verner, K., Sláma, J., Kachlík, V., Chlupáčová, M. (2013): Multistage magma emplacement and progressive strain accumulation in the shallow-level Krkonoše–Jizera plutonic complex, Bohemian Massif. Tectonics, 32, 1493–1512.

Żelaźniewicz, A., Dörr, W., Bylina, P., Franke, W., Haack, U., Heinisch, H., Schastok, J., Grandmontagne, K., Kulicki, C. (2004): The eastern continuation of the Cadomian orogeny: U–Pb zircon evidence from Saxo-Thuringian granitoids in south-western Poland and northern Czech Republic. International Journal of Earth Sciences, 93, 773–781.

Żelaźniewicz, A., Fanning, C.M., Achramowicz, S. (2009): Refining the granite, gneiss and schist interrelationships within the Lusatian–Izera Massif, West Sudetes, using SHRIMP U–Pb zircon analyses and new geologic data. Geologica Sudetica, 41, 67–84.

Zieger, J., Linnemann, U., Hofmann, M., Gärtner, A., Marko, L., Gerdes, A. (2018): A new U–Pb LA-ICP-MS age of the Rumburk Granite (Lausitz Block, Saxo-Thuringian Zone): constraints for a magmatic event in the Upper Cambrian. International Journal of Earth Sciences, 107, 933–953.

Zieger, J., Bittner, L., Gärtner, A., Hofmann, M., Gerdes, A., Marko, L., Linnemann, U. (2019): U–Pb ages of magmatic and detrital zircon of the Döhlen Basin: geological history of a Permian strike-slip basin in the Elbe Zone (Germany). International Journal of Earth Sciences, 108, 887–910.

Ziegler, P.A. (1988): Evolution of the Arctic-North Atlantic and the western Tethys. AAPG Memoir, 43.

Ziegler, P.A. (1975): The geological evolution of the North Sea area in the tectonic framework of North Western Europe. Norges geologiske undersøkelse Bulletin, 316, 1–27.

Ziegler, P.A. (1989): Evolution of Laurassia, a Study of Late Paleozoic Plate Tectonics. Kluwer, Dordrecht.

Ziegler, P.A. (1990a): Geological Atlas of Western and Central Europe. 2nd edition. Shell International Petroleum Maatschappij B.V., The Hague.

Ziegler, P.A. (1990b) Collision related intra-plate compression deformations in Western and Central Europe. Journal of Geodynamics, 11, 357–388.

Ziegler, P.A. (1990c): Tectonic and palaeogeographic development of the North Sea rift system. In: Blundell, D.J., Gibbs, A.D. (eds.): Tectonic evolution of the North Sea rifts. Oxford University Press, Oxford, p. 1–36.

Ziegler, P.A., Cloetingh, S., van Wees, J.D. (1995): Dynamics of intra-plate compressional deformation: the Alpine Foreland and other examples. Tectonophysics, 252, 7–59.

Ziegler, P.A., Dèzes, P. (2007): Cenozoic uplift of Variscan massifs in the Alpine Foreland: timing and controlling mechanisms. Global and Planetary Change, 58, 237–269.

Ziegler, P.A., van Wees, J.D., Cloetingh, S. (1998): Mechanical controls on collision-related compressional intraplate deformation. Tectonophysics, 300. 103–129.

Concluding remarks

During the Late Paleozoic–late Mesozoic, the Bohemian Massif experienced a complex intraplate tectonosedimentary evolution that, in its N/NE part, involved development of several generations of sedimentary basins in different settings. An approach that combined analysis of depositional controls (creation of accommodation space, sediment supply, eustatic sea-level changes) with analysis of sediment provenance (heavy mineral analysis, detrital zircon geochronology), allowed for deciphering processes generated by tectonic reactivation of basement faults that exerted control on depositional record. The episodes of tectonic reactivation were correlated with events that are recorded in the vicinity of Bohemian Massif in central Europe, and interpreted in a broader geodynamic context – from early post-Variscan extension related to 'orogenic collapse', through distant signal of the Uralian Orogeny during the late Pennsylvanian–Permian, to Mesozoic far-field stress transfer related to uplift of North Sea Dome, opening of the North Atlantic and later early ('Laramide') phase of the Alpine Orogeny.

The evolution of fluvio-lacustrine system of the Vrchlabí Fm., Krkonoše Piedmont Basin (KPB; an element of the W–E-oriented, intermontane basin complex between W Bohemia and central Silesia) revealed that interaction of fluvial system (Stará Paka and Čistá sandstones) prograding into the extensive Rudník lake was a result of tectonic basin-floor subsidence and climate variations. The former generated initial accommodation split into two parallel sub-basins adjacent to W–E principal faults, of which one, the northern, became dominant over time. This led to subsidence of intrabasinal high and merging of both depocenters. Gradual progradation of the fluvial system and subsequent filling of the basin reflects deceleration of tectonic subsidence over time. After the initial, tectonic-dominated phase, the A/S ratio was controlled by climate – creation of accommodation space was driven by pulses of lake expansion and retreat, compensated by fluvial sediment supply.

The extensional phase of the Pilsen–Trutnov Basin Complex, during which Vrchlabí Fm. was deposited, was punctuated by the late–middle Permian phases of strike-slip reactivation of the NW–SE-oriented faults (e.g., the Lusatian Fault). First of them, letf-lateral, took place in the Asselian. This phase is recorded by formation of unnamed basin now preserved as remnants at the Lusatian Fault near Varnsdorf (N Bohemia); its stratigraphic counterpart is the Döhlen Basin in Saxony and, arguably, Chotěvice Fm. of the KPB. Subsequent reactivation in right-lateral regime occurred during the late early–middle Permian ('Saxonian'), when Trutnov–Náchod sub-basin (eastern KPB) was formed discordantly to inverted W–E extensional grabens. As discussed by this thesis, the Late Paleozoic tectonosedimentary evolution of the Bohemian Massif as a whole is more complex than expected.

Another phase of tectonic reactivation took place at the Middle/Late Jurassic transition. This phase is cryptic and has been deciphered from the provenance record of the Upper Cretaceous. The U–Pb dating revealed presence of 'exotic' population of detrital zircons, Paleo-/Mesoproterozoic in age, likely derived from Baltica. It is interpreted as a trace of now completely eroded Late Jurassic to Early Cretaceous basin that once covered the Lusatian Block. Presumably, it was fed by N–S-directed fluvial drainage capable of redeposition of Baltica-derived material during the Early Cretaceous, the only period of the Mesozoic when paleogeography favored such transport. The onset of inversion of this hypothetic Lusatian Basin is assumed at the latest Jurassic, with acceleration of subsidence and accummulation of clastic material during the Early Cretaceous and termination presumably during the Aptian–Albian, as suggested by coeval gaps in deposition in surrounding basins (Lower Saxony Basin, Mid-Polish Trough).

The formation of Bohemian Cretaceous Basin (BCB) reflects the mid-Cretaceous reactivation of basement faults all over central Europe. During the late Turonian–Coniacian, the sedimentary processes and stratigraphic architectures markedly changed compared to previous, late Cenomanian–middle Turonian phase, as evidenced by progradation of high-angle (Gilbert-type) deltas into the Lužice–Jizera sub-basin. However, at the same time, stacking pattern of these deltaic wedges reflect increase in A/S ratio. This is interpreted as recording acceleration of tectonic processes related to incipient inversion of the BCB. This phase of intensified tectonic activity is recorded within practically all the basins surrounding the Bohemian Massif. However, new data suggest that this phase does not mark the onset of inversion, only its acceleration. The onset of inversion in central Europe has been recetnly placed to late Cenomanian, as suggested by provenance data presented in this thesis. In terms of driving mechanism of its formation, the BCB is briefly compared to the Subhercynian Basin, recently interpreted as an 'intraplate foreland basin'. Combination of elastic flexure and rigid tilting of tectonically partitioned crust is likely a driving mechanism behind formation of the BCB. On the contratry, various arguments are provided to disprove the transtensional/strike-slip nature of the basin formation.

At last, the presented time-slice reconstruction of the paleogeographic and tectonosedimentary evolution of the northern Bohemian Massif shows that periods of basin development and deposition were interrupted by major depositional gaps (Middle Triassic–Early Jurassic, late Early Cretaceous, post-early Campanian). The Mesozoic depositional episodes resulted from reactivation of major NW–SE fault zones due to stress transfer from the North Atlantic Rift during Jurassic to Early Cretaceous and were subsequently overridden by the far-field effect the Alpine Orogeny, or convergence of Iberia, Africa, and Europe during the Late Cretaceous.